RESTRAINED SHRINKAGE BEHAVIOUR OF CONCRETE WITH RECYCLED MATERIALS

A thesis submitted for the degree of
Doctor of Philosophy

By
Khaleel Hassan Younis
(BSc, MSc)

Centre for Cement and Concrete
Department of Civil and Structural Engineering
The University of Sheffield

Sheffield
March 2014

To my wife ***Shelan*** , my sustainable and renewable source of encouragement and love

ABSTRACT

The construction industry is responsible for some of the most serious sustainability and environmental issues the world is currently facing. Recycled materials such as recycled aggregate (RA) -generated from processed construction waste- and recycled tyre steel fibres (RTSF) -extracted from post-consumer tyres- in new constructions can potentially conserve natural aggregates (NA), eliminate unnecessary consumption of limited landfill areas and reduce energy consumption. However, the variability in the characteristics of recycled materilas, and the low density, high water absorption and porosity of RA, can lead to poor quality concrete and shrinkage cracks, particularly under restrained conditions. This study aims to examine the use of recycled materials such as RA and RTSF in the production of structural concrete and in particular to contribute towards understanding the shrinkage behaviour of NA concrete (NAC) and RA concrete (RAC) under restrained conditions.

An extensive experimental study to characterise the properties of both NA and RA and identify the effect of various key parameters on the performance of RAC is undertaken. Approaches to improve the properties of RA and RAC are explored. A new restraining frame for restrained shrinkage test and a procedure to quantify the post-shrinkage mechanical properties (compressive and flexural strength and flexural elastic modulus) of concrete are developed and assessed. The mechanical performance of concrete mixes incorporating RA and RTSF, as well as mixes with NA and industrial steel fibres (ISF), is examined under free and restrained conditions.

It is shown that the compressive strength of RAC can be predicted using a predictive model that takes into account: particle density, LA value, water absorption and RA content. Surface treatment of RA using reactive and non-reactive microfillers, as well as the utilization of RTSF, helped improve the compressive strength of RAC by up to 30%.

For unrestrained specimens, it is shown that there is a significant difference in shrinkage strains with depth, resulting in significant shrinkage curvatures. Under restrained conditions, stress history, which depends on the rate of development of stiffness and shrinkage, plays a key role in governing the failure of concrete. Shrinkage induced cracks can reduce the compressive strength, flexural strength and flexural elastic modulus of plain concrete by up to 14%, 24% and 29%, respectively.

The addition of RTSF and surface treatment of RA resulted in better flexural performance of RAC compared to that of NAC without fibres and comparable to that of NAC with fibres.

It is shown that whilst ISF do not affect shrinkage strains, RTSF increase initial shrinkage strains due to higher air content. Despite that, it is concluded that RTSF control well shrinkage induced microcracking, enhance tensile relaxation and promote auto-healing of microcracks, leading to an overall better flexural performance even when using RAC.

ACKNOWLEDGEMENTS

I would like to express my sincere gratitude and appreciation to my main supervisor, Professor Kypros Pilakoutas, for his precious time, continuous support, directive guidance, valuable comments and helpful suggestions that helped greatly in completion of this work. Thank you Kypros for keeping my hopes up throughout the difficult years.

I also would like to thank my second supervisor(s) Dr. Kyriacos Neocleous (for the first year) and Dr Cyril Lynsdale (for the second and third year) for their support and assistance.

I acknowledge the financial support of the Iraqi's Ministry of Higher Education and Scientific Research (MHESR) during the period of this research.

Great thanks to all technicians in the Heavy Structures Laboratory for their continuous assistance. Special thanks to Kieran Nash, Paul Blackburn and David Hobart for their collaboration and continuous support.

I am also grateful to all my friends and colleagues in the Construction Innovations Group, especially Kamaran Ismail for his assistance in FE-Analysis and Harris Angelakopoulos for the valuable discussions and suggestions.

Finally, and in no sense the least, my deepest thanks to my wife, *Shelan* and children *Ari, Arya and Saya* to whom I am indebted for their encouragement, understanding and patience over the years.

TABLE OF CONTENTS

LIST OF FIGURES

LIST OF TABLES

LIST OF SYMBOLS AND ABBREVIATIONS

ρ	Particle density of aggregate
ρ_{rd}	Particle density of aggregate (oven dry)
ρ_a	Particle density of aggregate (apparent)
ρ_{ssd}	Particle density of aggregate (saturated surface dry)
Δ_{T-B}	Ratio between the strains developed at the top and at the bottom surfaces
Δ_{T-S}	Ratio between the strains developed at the top and at the side surfaces
$\mu\varepsilon$	Microstrain
AASHTO	American Association of State Highway and Transportation Officials
ACI	American Concrete Institute
ASTM	American Society for Testing and Materials
BS	British Standard
CDW	Construction and demolition waste
C-S-H	Calcium Silicate Hydrate
E	Modulus of elasticity
E_c	Modulus of elasticity
E_{flex}	Flexural elastic modulus of concrete at any load
E_{fmax}	Maximum value of flexural elastic modulus (E_{flex}) in the range of 30% to 60% of the ultimate bending load
ε_{free}	Free shrinkage strain (strain measured on the free specimen)
ε_R	Restrained shrinkage strain = shrinkage strain measured on the free specimen - shrinkage strain measured on the restrained specimen.
F	Free (shrinkage)
FA	Fly ash
F_c or F_{rig}	Tensile force due to restrained shrinkage
f_{cu}	Mean compressive strength (cube)
FEA	Finite Element Analysis
fl_{LOP}	Flexural strength at the limit of proportionality

fl_{ult}	Ultimate flexural strength (at ultimate bending load)
FRC	Fiber reinforced concrete
FRC-NAC	Natural aggregate concrete reinforced with steel fibre
FRC-RAC	Recycled aggregate concrete reinforced with steel fibre
GGBS	Ground granulated blast slag
I	Second moment of area
ISF	Industrial steel Fibres
ITZ	Interfacial transition zone
K	Stiffness ratio between concrete and restraining rig
k_A	Average shrinkage curvature
k_{S-B}	Shrinkage curvature between sides bottom surfaces
k_{T-S}	Shrinkage curvature between top and sides
LA	Los Angeles
LOP	Limit of proportionality
LP	Lime stone powder
LVDT	Linear variable displacement tranducer
NA	Natural aggregate
NAC	Natural aggregate concrete
NCM	New cement mortar
OCM	Old cement mortar
OPC	Ordinary portland cement
P	Usually Porosity or Load
PMT	Pre-mixing technique
R	Restrained (shrinkage)
RA	Recycled aggregate
RA-B	Coarse recycled brick aggregate from construction and demolition waste
RAC	Recycled aggregate concrete

RA-C	Coarse recycled concrete aggregate from construction and demolition waste
RA-C1	Coarse recycled concrete aggregate produced by crushing old laboratory concrete samples
RAm	Recycled aggregate from CDW
RA-M	Coarse recycled mixed aggregate from construction and demolition waste
RC	Reinforced concrete
RCA	Recycled concrete aggregate
RF	Restraint Factor
RH	Relative humidity
RILEM	Reunion Internationale des Laboratoires et Experts des Materiaux, Systemes de Construction et Ouvrages (International Union of Laboratories and Experts
RTSF	Recycled tyre steel fibres
RTSFRC	Recycled tyre steel fibre reinforced concrete
SF	Silica fume
SSD	Saturated surface dry
TSMA	Two- stage mixing approach
$TSMA_{sc}$	Two- stage mixing approach with silica fume
w/c	Water to cement ratio
WA	Water absorption
WMT	Within-mixing technique
δ	Vertical displacement at the centre of the spam
ν	Poisson's ratio

Chapter 1

Introduction

1 Introduction

1.1 Motivation

Over the last century, urbanization has expanded enormously worldwide as a result of population growth and industrialization. This has generated a demand for the construction of more infrastructure including housing, buildings, roads, bridges and tunnels. Concrete is the dominant structural material used by the construction industry to accommodate this demand. The global consumption rate of natural aggregates (NA) is estimated at 8-12 billion tonnes per year [1], equivalent to 4000 km^2 of 1 meter deep quarries, about the combined area of both Greater London and Paris, leaving enormous scars on the landscape.

The large consumption of natural resources and consequent generation of massive quantities of construction and demolition waste (CDW) make the construction industry responsible for some of the most serious sustainability and environmental issues the world is currently facing. In the UK alone, construction waste amounts to roughly 110 million tonnes per year, corresponding to 60% of total waste [2]. However, the construction industry is capable of mitigating environmental problems through the utilization of waste materials in the production of concrete.

The use of recycled aggregates (RA), generated from processed CDW, in new constructions can potentially conserve the non-renewable natural resource of virgin aggregates, eliminate unnecessary consumption of limited landfill areas and reduce energy consumption. However, the variability in the characteristics of RA and recycled aggregate concrete (RAC) is the main engineering concern that hinders the widespread use of RA. Low density and high water absorption and porosity, mainly caused by the heterogeneous nature of RA, can lead to poor quality concrete (low compressive, tensile and flexural strength). As a result, current standards and specifications [3-6] impose limitations on the use of RA in new concrete and particularly in structural concrete. In general, only 20-30% of NA can be replaced by RA in new structural concrete [3]. Therefore, more research in this field is necessary to understand the effect of the various key parameters and explore approaches to improve the properties of RA and RAC. This will help drive the use of RA as a viable alternative to NA.

Other critical issues with RAC are high shrinkage and creep. Due to higher water absorption and porosity of RA, RAC exhibits significantly higher shrinkage and creep than natural aggregate concrete (NAC) [7]. Shrinkage in particular can increase the cracking tendency of

RAC and create more obstacles to the use of RAC. Therefore, it is vital to examine the phenomenon of RAC shrinkage, with particular emphasis on restrained shrinkage and associated cracking. Understanding the factors that influence restrained shrinkage, effects of restrained shrinkage on the behaviour of concrete, assessment methods and crack mitigation techniques are also crucial.

1.2 Background of Research Problem

1.2.1 Recycled Aggregates : Concerns and the Need for Improvement

RA are a by-product of crushing debris obtained from demolished concrete and masonry structures and asphalt concrete pavements. RA may contain only concrete or a mixture of concrete and masonry rubble or even asphalt, and can be produced as fine or coarse aggregates. Due to their heterogeneous nature, RA possess high variability in their properties and lower quality than NA. RA derived from CDW often suffer from a porous and weak surface, mainly due to old mortar or inferior materials such as low strength bricks. When RA are used in concrete, the high variability and low quality in their properties reflects on the properties of RAC. Therefore it is recommended to always characterise RA before use in concrete applications [4].

Studies in this field reveal that RA have lower particle density (up to 30% of that of NA) [7, 8] and higher water absorption (up to 10 times or more for RA contains crushed brick) [9, 10]. This is mainly attributed to the nature of RA and the porous and cracked nature of attached mortar of recycled concrete aggregate. This has an adverse effect on density and mechanical properties of concrete. In comparison to NAC, RAC shows lower: density (up to 15%), compressive strength (up to 40%), tensile strength (up to 15%) [1, 7, 11], flexural strength (up to 10%) [7, 8] and modulus of elasticity (up to 40%) [12, 13]. RAC also exhibits higher shrinkage (up to 100% after 28 days of drying) [7, 14, 15] and creep (up to 60%) [7, 15, 16] than NAC. These losses are due to the heterogeneous composition, high porosity, high water absorption and low internal restraint of RA. Large shrinkage strains can increase cracking tendency, in particular when concrete is restrained. On the other hand, the higher creep of RAC [7, 17] and its lower elastic modulus can play a mitigating role in reducing the effects of shrinkage induced tensile stresses. Very limited work can be found in the literature on the shrinkage behaviour of RAC under restrained conditions.

RA could be improved before use in concrete to mitigate the repercussions of high variability in its characteristics on the properties of RAC. One possible solution is to

strengthen weaknesses on the surface of RA using fine reactive [18, 19] and non-reactive powders.

1.2.2 Shrinkage

1.2.2.1 General

Concrete shrinkage leads to a reduction in the volume of concrete. Concrete shrinks in response to moisture loss, temperature reduction and chemical reactions (hydration). Concrete may experience shrinkage at different times (early ages -hours after casting- and long term -many years) and under a variety of conditions. Generally, there are several types of concrete shrinkage: plastic, autogenous, drying, thermal and carbonation shrinkage. They can contribute to cracking in structural concrete elements to differing degrees [20-22]. The types of shrinkage and their consequences are described further in Appendix A.

1.2.2.2 Restrained Shrinkage

Shrinkage induced deformations only lead to stresses and cracking if they are restrained. However, in real life, all concrete elements are restrained to some degree, since some restraint always exists and can be provided by supporting elements or from the different parts of the element itself. Degree of restraint or restraint factor (RF) is one of the factors that determines the magnitude of developed tensile stresses and cracking [23, 24]. In general, there are two types of restraints: external and internal as described further in Appendix B. Experimental procedures and tests for restrained shrinkage are vital to quantify the restrained shrinkage behaviour of RAC.

1.2.2.3 Assessment of Restrained Shrinkage

Shrinkage of concrete can be assessed in two conditions free and restrained. Free shrinkage tests can provide information on factors affecting shrinkage such as concrete composition, environmental conditions, and size and shape of the concrete element being assessed. However, they cannot provide information on the cracking behaviour of concrete under restrained conditions [25-28]. Restrained shrinkage tests are the only way to assess: a) the cracking tendency and ability of materials to withstand tensile stresses, and b) the effects of shrinkage induced cracks on structural and durability performance of concrete [24, 29, 30].

The shrinkage tests available in the literature are presented briefly below and more extensively in Appendix B.

Although attempts in assessing (testing) shrinkage of concrete under restrained conditions started in the early decades of last century [29], it is only in the last decade when the American Society for Testing and Materials (ASTM in 2004) and the American Association of State Highway and Transportation Officials (AASHTO in 2008) adopted a test (the ring test) as a standard test for restrained drying shrinkage of concrete.

The ring test was developed during WWII by Carlson [31] (cited in [24]). The fact that it took more than 70 years for this test to be adopted highlights the difficulties associated with quantifying restrained shrinkage. For a given drying environment, the ring test can provide information on the cracking time and the width of crack and its rate of increase with time. Hence, the ring test is considered as a qualitative method of comparing the cracking tendency of different concrete mixes [24, 28, 32]. However, the test cannot quantify the effect of shrinkage induced cracks on the residual strength of cracked concrete.

Several other test methods for restrained shrinkage have been developed. These can be classified into plate or linear [33] by the shape of the specimen. These tests can provide information on different properties of concrete such as: shrinkage restrained strains and stresses, cracking (age and width), creep strains and rate of tensile stress development. However, from a practical point of view, when many parameters are needed to be examined, the setting up of such tests and their instrumentation can be complicated and expensive. Automatic crack width measurements are also difficult since cracking positions are not known a-priori. The small dimensions of the specimens used in some of these tests, mainly to reduce costs and accelerate drying, is also another issue since they limit the use of normal size coarse aggregates.

None of these tests allows dismounting of concrete specimen after exposure to restrained shrinkage without destroying the specimen. As a result, restrained shrinkage tests are avoided in common quality control testing and large-scale parametric investigations [24, 34-36].

Therefore, it is crucial to develop a test procedure and a simple and economical rig for restrained shrinkage assessment that enables dismounting of the specimen. This would facilitate bending and compression tests to quantify the effect of shrinkage induced cracks on residual mechanical properties.

1.2.2.4 Shrinkage Crack Control

Reinforcing bars are commonly used to control concrete cracking in concrete structures and pavements. Fiber reinforced concrete (FRC) is also used to increase toughness, fatigue and flexural strength of concrete, and to reduce the cost and increase the speed of the process of construction. Different materials are used as fibres in structural and non-structural applications. Non-metalic fibres are in general used for non-structural applications. Randomly distributed steel fibres, due to their high modulus of elasticity, can control crack propagation and hence enhance the post cracking behaviour of structural concrete. It has been reported [26, 37-39] that the addition of steel fibres can also decrease free shrinkage in concrete. This was attributed [40] to a physical restraining effect (similar to aggregate restraining effect) which develops due to the interfacial bond strength between the fibres and the matrix. Some studies [34, 39, 41, 42] have reported that the addition of low contents of steel fibres (less than 1% by volume) does not alter the shrinkage behaviour of concrete. Others [43, 44] have reported that fibres may be responsible for an increase in the porosity of concrete resulting in higher free shrinkage strains. Therefore, it appears that there is no general agreement on the effect of fibres on the free shrinkage behaviour of concrete.

Undoubtedly, the most significant effect of fibres in concrete is their ability to control crack width and propagation after matrix failure. Fibres can play three significant roles: 1) encourage the development of fine smeared cracks rather than a big single crack, 2) transfer tensile stresses across cracks, 3) enable healing/(sealing) of cracks in the long-term [45, 46].

The random distribution of fibres in concrete means that to achieve the same flexural performance as conventional reinforced concrete, larger volumes (than rebar) are required. This, sometimes makes the use of fibres, particularly industrial steel fibres (ISF), uneconomical. Therefore, recycled tyre steel fibres (RTSF) extracted from post-consumer tyres have been put forward as a cheaper alternative to ISF. The first investigations on the mechanical properties of recycled tyre steel fibre reinforced concrete (RTSFRC) mixes to examine their structural performance were started at the University of Sheffield in early 2000 [47-49]. Utilizing RTSF in concrete has considerable environmental benefits since only a small fraction of the energy needed to make steel wire is used in their production. Only two experimental studies on the free shrinkage behaviour of these fibres were found in the literature. Both studies were conducted under the EU project "Ecolanes" [50]. The shrinkage behaviour of RTSF concrete under restrained conditions has not been explored.

The use of RTSF coupled with the use of RA in concrete could lead to a more sustainable construction solution. The addition of RTSF can enhance both the mechanical properties and shrinkage behaviour of RAC. Before utilizing any new type of fibre in real life applications, it is of utmost importance to investigate its behaviour, especially under the effects of restrained shrinkage. Apart from the work undertaken by Wang et al. (2000) which was done using short fibres and NA, there are no studies on the restrained shrinkage behaviour of concrete with recycled fibres. Thus, there is a vital need to assess the ability of RTSF to control shrinkage cracks.

1.3 Aims and Objectives

This work is part of a wider set of projects at the University of Sheffield which aim to facilitate the use of recycled materials such as RA and RTSF in the production of structural concrete to reduce the sustainability and environmental issues associated with concrete. The study aims in particular to contribute towards understanding the shrinkage behaviour of NAC and RAC under restrained conditions. The objectives of this research are to:

On RA

- Understand the effect of the various key parameters on the properties of different types of RA through conducting an experimental study to characterise the properties of RA.

- Characterise the rheological and mechanical properties of RAC through an experimental study.

- Identify and quantify the parameters of RA that most affect the behaviour of RAC.

- If possible, develop a strength predictive model for RAC.

- Explore approaches to improve the behaviour of RA and the properties of RAC.

- Develop a rig for restrained shrinkage testing and a procedure to quantitatively assess the impact of shrinkage induced cracks due to external restraints on the mechanical properties (compressive strength, flexural strength and flexural modulus of elasticity) of concrete.

- Conduct a parametric study to quantify the post-restrained shrinkage mechanical properties of mixes with different w/c ratios and assess the effectiveness of the developed restraining frame.

- Examine the shrinkage effects on RAC under restrained conditions.

- Assess the use of RTSF as a mitigation method to reduce the negative effects of restrained shrinkage induced cracking on the behaviour of NAC and RAC.

1.4 Thesis Presentation

This thesis is presented in a non-conventional manner and two types of chapters: chapters written following normal thesis format (chapters 1, introduction and 7, conclusions), and chapters consisting of "stand-alone" journal papers (2 to 6). Literature on the common types of concrete shrinkage and their main driving mechanisms can be found in Appendix A. Information on the effect of the shrinkage induced cracks on the behaviour of concrete is explained in Appendix B. Appendix B also includes literature and a discussion on the types of the restraint and the available tests and experimental procedures for restrained shrinkage. A brief description of each chapter is given below:

Chapter Two is based on Younis K. and K. Pilakoutas [51] and examines the effect of various parameters on the performance of RAC and proposes a strength prediction model. Three types of coarse aggregate: NA, RA originating from processing CDW and RA produced by crushing old laboratory concrete samples were used. An extensive experimental study was conducted and presented to characterise the properties of both NA and RA.

Utilizing multi-linear and non-linear regression analysis, relationships that link the properties of RA to the strength of RAC are developed. To enhance the compressive strength of RAC, the effect of surface treatment of RA using small quantities of reactive and non-reactive microfillers is also investigated. The effectiveness of two mixing methods and the addition of RTSF on the compressive strength of RAC are also examined. Based on the obtained results it is shown that, the utilization of RTSF as well as reactive and non-reactive microfillers can improve the strength of RAC.

Chapter Three is based on Younis K. and K. Pilakoutas [52] (submitted paper) and proposes a test rig for restrained shrinkage and associated procedures to assess the post-shrinkage mechanical properties (compressive and flexural strength) of concrete. Free and restrained shrinkage tests are conducted and the change of apparent restraint factor (RF) with time is determined. A simple finite element analysis is performed to quantify the theoretical RF and the results are compared to the apparent RF. According to the results, the RF of the proposed rig is dependent on the time and the stiffness of the concrete. Results of residual mechanical properties show that restrained shrinkage induced cracks can affect the mechanical behaviour (flexural and compressive strength and stiffness) of concrete.

Chapter Four is based on Younis K. and K. Pilakoutas [53] (submitted paper) and aims at assessing the post-restrained shrinkage behaviour of concrete. This chapter deals with a new restraining frame for restrained shrinkage test of concrete. A parametric experimental study is performed to examine the effectiveness of the proposed restraining frame. In this chapter, the development of the restraining frame is presented. Also, results of free shrinkage, mass loss and mass loss vs shrinkage of three concrete mixes with different water/cement (w/c) ratios are presented and discussed. The results show that, for unrestrained specimens, there is a significant difference in shrinkage strains with depth, resulting in significant curvature deformations.

Chapter Five is based on Younis K. and K. Pilakoutas [54] (submitted paper) and attempts to quantify the post-restrained behaviour of concrete. In chapter 4, a new restrained shrinkage test is presented and experimental parametric study was undertaken using three mixes with w/c ratios of 0.3, 0.4 and 0.5. Also, in chapter 4, free shrinkage test results are discussed. This chapter presents experimental results and discusses the behaviour of the concrete mixes under restrained conditions, including variations in shrinkage strains, the evolution of RF, failure of restrained concrete and the post-restrained mechanical behaviour. The obtained results show that stress history, which depends on the rate of development of stiffness and shrinkage, plays a key role in governing the failure of restrained concrete.

Shrinkage induced cracks reduced significantly the compressive strength, flexural strength and flexural elastic modulus of concrete. Creep is identified as the possible mechanism for the loss of the stiffness.

Chapter Six is based on Younis K., K. Pilakoutas and K. Neocleous (to be submitted) and examines the restrained shrinkage behaviour of concrete mixes incorporating recycled materials such as recycled tyre steel fibre RTSF -extracted from post consumer tyres- and recycled aggregates RA -from construction and demolition waste-. For comparison purposes, the experimental work in this chapter also includes mixes with industrial steel fibres ISF and natural aggregates NA. The restraining frame and procedure to quantify the post-restrained shrinkage behaviour of concrete, developed in chapter 4 are employed. Four NAC mixes (one plain and three with fibres) and two RAC mixes (one plain and one with RTSF) are investigated. Experiments performed include: free and restrained shrinkage, loss of mass, compressive strength, flexural strength and flexural elastic modulus.

Chapter Seven includes a summary of the research work and general conclusions as well as recommendations for future work.

Finally, The current status (26/03/2014) of the chapters (papers) mentioned previously are as follows:

Chapter two: published in Construction and Building Materials.

Chapter three: submitted to ACI Materials Journal.

Chapter four: submitted to Cement and Concrete Composites.

Chapter five: submitted to Cement and Concrete Composites.

Chapter six: to be submitted to Cement and Concrete Composites.

References

1. Li, Y.J., et al., *Study on the workability and mechanical properties of recycled aggregate concrete containing ultra-fine fly ash.* Environmental Ecology and Technology of Concrete, 2006. **302-303**: p. 314-320.
2. WRAP, *Perfomance Related Approach to Use Recycled Aggregates*. 2007, Waste and Resources Action Programme: Oxon.
3. BS 8500-2, *Concrete complementary British Standard to BS EN 206 part 1 -Part 2: Specification for constituent materials and concrete*, in. 2006, British Standard Institiution: London.
4. BS EN 12620 :2002 +A1, *Aggregates for concrete.* 2008, British Standards Institution, London.
5. DIN- 4226. *Aggregate for Mortar and Concrete , Part 100: Recycled Aggregates* 2002, DIN: Berlin.
6. WBTC No. 12/2002, *Specifications Facilitating the Use of Recycled Aggregates.* 2002, Works Bureau Technical Circular: Hong Kong.
7. Hansen, T.C., *Recycled of Demolished Concrete and Masonry* 1992, London: E & FN SPON.
8. Tam, W.W.V.C.M., *Recycled Aggregate from Concrete Waste for Higher Grades of Concrete Construction , PhD thesis*, in *Department of Building and Construction*. 2005, City University of Hung Kong: Hung Kong.
9. Zega, C., Y. Villagrán-Zaccardi, and A. Di Maio, *Effect of natural coarse aggregate type on the physical and mechanical properties of recycled coarse aggregates.* Materials and Structures, 2010. **43**(1): p. 195-202.
10. Katz, A., *Properties of concrete made with recycled aggregate from partially hydrated old concrete.* Cement and Concrete Research, 2003. **33**(5): p. 703-711.
11. Soutsos, M.N., K. Tang, and S.G. Millard, *Concrete building blocks made with recycled demolition aggregate.* Construction and Building Materials, 2011. **25**(2): p. 726-735.
12. Kou, S.C., C. Poon, and D. Chan., *Properties of Steam Cured Recycled Aggreagte Fly Ash Concrete*, in *Conference on the Use of Recycled Materials In Building and Structures*, 2004: Bareclona , Spain.
13. Kou, S., C. Poon, and D. Chan, *Influence of fly ash as a cement addition on the hardened properties of recycled aggregate concrete.* Materials and Structures, 2008. **41**(7): p. 1191-1201.
14. Hansen, T.C. and E. Boegh, *Elasticity and Drying Shrinkage of Recycled-Aggregate Concrete*. Journal of the American Concrete Institute, 1985. **82**(5): p. 648-652.
15. Fan, Y., J. Xiao, and V.W.Y. Tam, *Effect of old adhered mortar on creep of recycled aggregate concrete.* Structural Concrete, 2013: p. n/a-n/a.
16. Ravindrarajah, R.S. and C.T. Tam, *Methods of Improving the Quality of Recycled Aggregate Concrete*. Demolition and Reuse of Concrete and Masonry, Vols 1-2, 1988: p. 575-584.

17. Ajdukiewicz, A. and A. Kliszczewicz, *Influence of recycled aggregates on mechanical properties of HS/HPC.* Cement & Concrete Composites, 2002. **24**(2): p. 269-279.

18. Tam, V.W.Y. and C.M. Tam, *Diversifying two-stage mixing approach (TSMA) for recycled aggregate concrete: TSMA(s) and TSMA(sc).* Construction and Building Materials, 2008. **22**(10): p. 2068-2077.

19. Katz, A., *Treatments for the improvement of recycled aggregate.* Journal of Materials in Civil Engineering, 2004. **16**(6): p. 597-603.

20. Concrete Society TR 22 *Non – Structural Cracks in Concrete*. 2010, Concrete Society. : Surrey, UK.

21. Gribniak, V., G. Kaklauskas, and D. Bacinskas, *Shrinkage in Reinforced Concrete Structures: A Computational Aspect.* Journal of Civil Engineering and Management, 2008. **14**(1): p. 49-60.

22. Qiao, P., McLean, D. and Zhuang, J.,, *Mitigation Strategies for Early-Age Shrinkage Cracking in Bridge decks*. 2010, Department of Civil and Environmental Engineering , Washington State University: Pullman, Washington. .

23. Bisschop Jan, *Drying Shrinkage Microcracking in Cement-based Materials*, in *Civil engineering and Geoscience*. 2002, Delft University of Technoloy: Delft, Netherlands.

24. ACI 231R-10, *Report on Early-Age Cracking: Causes, Measurement, and Mitigation*, in *ACI Committee 231*. 2010, American Concrete Institute: Farmington Hills, U.S.A.

25. Weiss, W.J., W. Yang, and S.P. Shah, *Shrinkage cracking of restrained concrete slabs.* Journal of Engineering Mechanics-Asce, 1998. **124**(7): p. 765-774.

26. Swamy, R.N. and H. Stavrides, *Influence of Fiber Reinforcement on Restrained Shrinkage and Cracking.* Journal of the American Concrete Institute, 1979. **76**(3): p. 443-460.

27. Grzybowski, M. and S.P. Shah, *Shrinkage Cracking of Fibre Reinforced Concrete.* ACI Materials Journal, 1990. **87**(2).

28. Carlsward J. , *Shrinkage Cracking of Steel Fibre Reinforced self compacting Concrete Overlays*, in *Department of civil and Environmental Engineering*. 2006, Lulea University of Technology: Lulea,Sweden.

29. Carlson, R.W., *Attempts to Measure the Cracking Tendency of Concrete* ACI, 1940. **36**: p. 533-537.

30. Altoubat, S.A., *Early age stresses and creep-shrinkage interaction of restrained concrete*. 2000.

31. Carlson, R.W., *Cracking of Concrete.* The Boston Society of Civil Engineers, 1942. **29**(2): p. 98-109.

32. Banthia, N., C. Yan, and S. Mindess, *Restrained shrinkage cracking in fiber reinforced concrete: A novel test technique.* Cement and Concrete Research, 1996. **26**(1): p. 9-14.

33. Bentur, A. and K. Kovler, *Evaluation of early age cracking characteristics in cementitious systems.* Materials and Structures, 2003. **36**(3): p. 183-190.

34. Altoubat, S.A. and D.A. Lange, *Creep, shrinkage, and cracking of restrained concrete at early age.* Aci Materials Journal, 2001. **98**(4): p. 323-331.

35. Tongaroonsri, S. and S. Tangtermsirikul, *Influence of mixture condition and moisture on tensile strain capacity of concrete.* ScienceAsia, 2008. **34**(1): p. 59-68.

36. Hossain, A.B., and Weiss, W. J., , *Assessing Residual Stress Development and Stress Relaxation in Restrained Concrete Ring Specimens.* Cement and Concrete Composites, 2004. **26**: p. 531-540.

37. Chern, J.-C. and C.-H. Young, *Compressive creep and shrinkage of steel fibre reinforced concrete.* International Journal of Cement Composites and Lightweight Concrete, 1989. **11**(4): p. 205-214.

38. Tan, K. and P. Paramasivam, *Creep and Shrinkage Deflections of RC Beams with Steel Fibers.* Journal of Materials in Civil Engineering, 1994. **6**(4): p. 474-494.

39. Zhang, J. and V.C. Li, *Influence of Fibres on Drying Shrinkage of Fibre-Reinforced Cementitious Composite.* Journal of Engineering Mechanics, ASCE, 2001. **127**(1): p. 37-44.

40. Mangat, P.S. and M.M. Azari, *A Theory for the Free Shrinkage of Steel Fibre Reinforced Cement Matrices.* Journal of Material Science 1984. **19** (7): p. 2183-2194.

41. Li, Z., M.A. Perez Lara, and J.E. Bolander, *Restraining effects of fibers during non-uniform drying of cement composites.* Cement and Concrete Research, 2006. **36**(9): p. 1643-1652.

42. Grzybowski, M. and S.P. Shah, *Model to Predict Cracking in Fiber Reinforced-Concrete Due to Restrained Shrinkage*. Magazine of Concrete Research, 1989. **41**(148): p. 125-135.

43. Wang, K., S.P. Shah, and P. Phuaksuk, *Plastic Shrinkage Cracking in Concrete Materials- Influence of Fly Ash and Fibres.* ACI Materilas Journal, 2001. **98**(6): p. 458-464.

44. Aly, T., J.G. Sanjayan, and F. Collins, *Effect of polypropylene fibers on shrinkage and cracking of concretes.* Materials and Structures 2008. **41**: p. 1741–1753.

45. Hoff, G.C., *Durability of fiber reinforced concrete in a severe marine environment.* ACI Special Publication, 1987. **100**.

46. ACI 544.1R-96, *State-of-the-Art Report on Fiber Reinforced Concrete* 1996, ACI: Detroit. p. 1-66.

47. Pilakoutas, K., K. Neocleous, and H. Tlemat, *Reuse of steel fibres as concrete reinforcement.* Engineering Sustainability,, 2004. **157**(ES3): p. 131-138.

48. Tlemat H., *Steel fibres from waste tyres to concrete: testing, modelling and design*, in *Department of Civil and Structural Engineering*. 2004, The University of Sheffield: Sheffield UK.

49. Pilakoutas, K. and R. Strube. *Re-use of Tyres Fibres in Concrete*. in *Proceedings of the International Symposium on Recycling and Reuse of Used Tyres*. 2001: Thomas Telford, University of Dundee, Dundee, UK.

50. Neocleous, K., et al. (2011) *Fibre-reinforced roller-compacted concrete transport pavements*. Proceedings of the ICE - Transport **164**, 97-109.

51. Younis, K.H. and K. Pilakoutas, *Strength prediction model and methods for improving recycled aggregate concrete.* Construction and Building Materials, 2013. **49**(0): p. 688-701.

52. Younis, K.H. and K. Pilakoutas, *Assessment of Post-Restrained Shrinkage Mechanical Properties of Concrete* ACI Materials, 2014. **Submitted for publication**.

53. Younis, K.H. and K. Pilakoutas, *New Restrained Shrinkage Test to Assess Post-Shrinkage Behaviour of Concrete - Part I: Development of Test and Free Shrinkage Results.* Cement and Concrete Composites, 2014. **Submitted for publication**

54. Younis, K.H. and K. Pilakoutas, *New Restrained Shrinkage Test to Assess Post-Shrinkage Behaviour of Concrete - Part II: Restrained and Post-Restrained Test Results.* Cement and Concrete Composites, 2014. **Submitted for publication**.

Chapter 2

Strength Prediction Model and Methods for Improving Recycled Aggregate Concrete

Younis, K.H. and K. Pilakoutas, *Strength prediction model and methods for improving recycled aggregate concrete*. Construction and Building Materials, 2013. **49**(0): p. 688-701.

This chapter examines the effect of various parameters on the performance of recycled aggregate concrete (RAC) and proposes a strength prediction model. Relations that link the properties of recycled aggregate (RA) to the strength of RAC are developed using multi-linear and non-linear regressing analysis. To enhance the compressive strength of RAC, the effect of surface treatment of RA using small quantities of reactive and non-reactive microfillers is examined. For the same purpose, two mixing methods and the addition of recycled tyres steel fibres (RTSF) are also investigated. The results show that RTSF as well as reactive and non-reactive microfillers can enhance the strength of RAC by 30%. Furthermore, density separation can be used to produce high quality RA from construction and demolition waste (CDW).

This chapter consists of a "stand alone" journal paper and includes relevant bibliography at the end of the chapter. Additional information and further test results are presented in Appendix C.

2.1 Introduction

Large quantities of construction and demolition waste (CDW) materials arise annually worldwide. In the UK alone, this waste amounts to roughly 110 million tonnes per year which corresponds to 60% of total waste[1]. Only 40% of this amount is reused or recycled. At the same time, large quantities of natural aggregates are extracted for construction every year. The utilization of recycled aggregates (RA) in concrete production can potentially conserve the non-renewable natural resource of virgin aggregates, eliminate unnecessary consumption of limited landfill areas and reduce energy consumption. However, the variability in the characteristics of RA and recycled aggregate concrete (RAC) are the main engineering concern which hinders the use of RA. Low density and high water absorption and porosity, mainly caused by the heterogeneous nature of RA, can lead to low quality concrete (low compressive, tensile and flexural strength as well as high creep and shrinkage). For example, the use of recycled concrete aggregate (RCA) can lead to reduction of up to 40% in compressive strength [1-3]. As a result, current standards and specifications [4-7] impose limitations on the use of RA in new concrete and particularly in structural concrete. With limitations, such as only 20-30% of NA can be replaced by RA in new structural concrete being common. Therefore, more research in this field is necessary to understand the effect of the various key parameters and explore approaches to improve the properties of RA and RAC.

Different approaches have been adopted by researchers to improve the characteristics of RA and RAC. Some of these approaches deal with how to improve the RA itself while others focus on concrete production technology. Examples include, detaching the attached cement mortar from the aggregate through mechanical means (ball milling) [8], through immersing the RA in chemical solvents (acids) [9], through heating and rubbing [10, 11] , heating using microwaves [12], and through ultrasonic cleaning methods [13]. Although some of these approaches helped improve some of the properties of RA, they have shortcomings such as high costs, environmental pollution, energy consumption or compromising durability.

A possible better solution is surface treatment of RA with silica fume (SF) in liquid form. Katz [13] showed that this improved both the compressive strength (15% increase at 28 day) and the microstructure of the interfacial transition zone (ITZ). However, since the treatment was applied before mixing, it may not prove cost-effective in practice, due to the additional costs of this operation.

Cement treatment during mixing was also examined by others; for example, Tam et al [14-17] developed a "two-stage mixing approach" (TSMA) aiming at coating the RCA with a layer of cement paste during the mixing procedure and reported strength and durability improvements. However, since cement particles are not small enough to penetrate and fill all microcracks, Tam and Tam [18] and Li et al [19] tried to use the same technique, but with utilizing reactive micro-fillers (pozzolans) such as SF , fly ash (FA) and ground granulated blast furnace slag (GGBS). Kong et al [20] used a triple mixing method to coat RCA (derived from crushing laboratory concrete samples with strength of 40 MPa) with first a layer of either FA or GGBS and then with a layer of cement paste. An improvement of 29% in compressive strength (at 28 day with 100% RCA) was obtained when RCA was coated with GGBS. This was attributed to the enhancement of the microstructure of the ITZ. The amount of cement replacement used (20% cement mass) was enough to provide a coating layer around the RA with a thickness ranging between 500- 800 µm [19], which covered, not only the ITZ but also, the cement paste around the ITZ. However, improving the cement paste is known to improve the concrete properties irrespective of the aggregate used and if possible should be eliminated in comparative studies. For this reason, the current study attempts to exclude the effect of enhancing the cement paste by using small enough quantities of coating materials that only provide a thin coating layer to cover the ITZ. Since only few studies explored the effect of reactive micro-fillers on the properties of RAC and nothing was found in the literature on the use of nonreactive micro-fillers, the influence of reactive micro-fillers (SF, FA and GGBS) and non-reactive micro-fillers such as lime stone powder (LP) are studied in this paper. Two techniques are used to coat the RA, pre-mixing technique (PMT) and within mixing technique (WMT).The PMT is similar to the procedure used by Katz [13]and the WMT is proposed as an improvement to the TSMA and $TSMA_{sc}$ developed by Tam and Tam [18] as explained in section 2.7.1.The effect of fine recycled tyres steel fibres (RTSF) is also examined as they were shown in previous studies [21] to control microcracks propagation.

2.2 Materials

2.2.1 Cementitious Materials

Portland Cement CEM I 52.5 N, meeting the requirements of BS EN 197 [22] was used in this research. The full chemical analysis of the cement is shown in Table 2.1. Table 2.2 presents the physical and mechanical properties of the cement, reactive micro-fillers (FA, GGBS, SF) and non-reactive micro-fillers (LP) used in this study.

Table 2. 1 Chemical analysis of OPC.

SiO_2	Al_2O_3	Fe_2O_3	CaO	MgO	SO_3	Na_2O	K_2O	Na_2O_{eq}
20.99	4.98	2.9	65.88	0.79	2.8	0.24	0.44	0.52

Table 2. 2 Physical and mechanical properties of OPC, PFA, GGBS, SF and LP.

Property	OPC	FA	GGBS	SF	LP
Initial setting time (min)	110	-	-	-	-
Fineness (m^2/kg)	445	370	481	22300	640
Loss on ignition (%)	2.07	4.7	-	2.5	43.6
Compressive strength (MPa)	68.1	-	-	-	-
Density (Mg/m^3)	3.15	2.15	2.9	2.2	2.65
Activity Index (28 day) %	-	86	96	107	-

2.2.2 Aggregates

The fine aggregate used throughout this study was natural sand with a maximum size of 5mm, whereas two types of coarse aggregates were used, natural and recycled. The natural gravel was river aggregate with a maximum size of 20 mm. Two types of coarse RA were used; a) construction and demolition waste CDW and b) recycled concrete aggregate RCA produced by crushing old laboratory concrete specimens. The RCA from lab specimens can be considered as high quality RCA, since it is not contaminated and has no impurities and foreign matter.

The RA used originated from CDW and contained crushed concrete, masonry (brick) and asphalt. It was crushed by a jaw crusher (primary crusher) and a cone crusher (secondary crusher).The supplier could not provide information regarding the composition and properties of the RA. This is also true in general practice, as it is hard to track the properties or composition of rubble delivered to recycling plants from various demolition sites. Figure 2.1a shows the RA used in this study, as received from the supplier.

Figure 2. 1a Recycled Aggregates from CDW.

Methodologies described and published in the current (BS and EN) standards were employed to conduct the characterization of all aggregates used (see Table 2.3). The purpose of the characterization was firstly to assess their suitability for use in concrete, in particular of that of RA, and secondly to determine the required mix design parameters.

Table 2. 3 Standard tests for RA characterization

Test	Standard
Classification of coarse RA	BS EN 933-11:2009 [23]
Physical	
Gradation (particle size distribution)	BS EN 933-1:1997 + A1:2005 [24]
Particle densities and water absorption	BS EN 1097-6:2000 +A1 :2005 [25]
Porosity	BS EN 1936:2006 [26]
Surface texture and shape	BS EN 812-102:1989 [27]
Shape Index (SI)	BS EN 933-4:2008 [28]
Bulk density and voids ratio	BS EN 1097-3:1998 [29]
Mechanical	
Resistance to fragmentation :Los Angeles (LA)	BS EN 1097-2 +A1:2006 [30]

Since one of the objectives of this study was to examine the effect of density of RA on concrete strength, the first step taken was to separate the mixed CDW into different types.

This process started with the separation of RA by size (three fraction of sizes 14-20 , 10-14 and 5-10 mm) and then by type using visual inspection and hand sorting. Based on the colours of the RA three distinct types of RA were identified:

- RA- Concrete (white or grey)

- RA- Brick (red)

- RA- Asphalt (black)

Since the quantity of the third type (black) was very low, it was excluded from the study. Therefore, the characterisation of the RA was conducted on the following types:

- NA (coarse and fine).
- RA-C (Coarse RA-Concrete from CDW).
- RA-B (Coarse RA-brick from CDW).
- RA-M (Coarse RA-Mixed from CDW).
- RA-C1 (Coarse RA-produced by crushing old laboratory concrete samples).

2.2.3 Recycled Tyres Steel Fibre (RTSF)

The RTSF used in this research is derived from the mechanical processing (e.g. shredding and granulation) of post-consumer tyres [31]. The RTSF used had an average diameter of (0.1-0.2) mm and tensile strength of around 2000 MPa [32]. The RTSF comes in variable lengths ranging from 3-30 mm (5% of the fibres had length shorter than 3 mm and 5% longer than 30 mm). The length distribution determined is shown in Figure 2.1b.

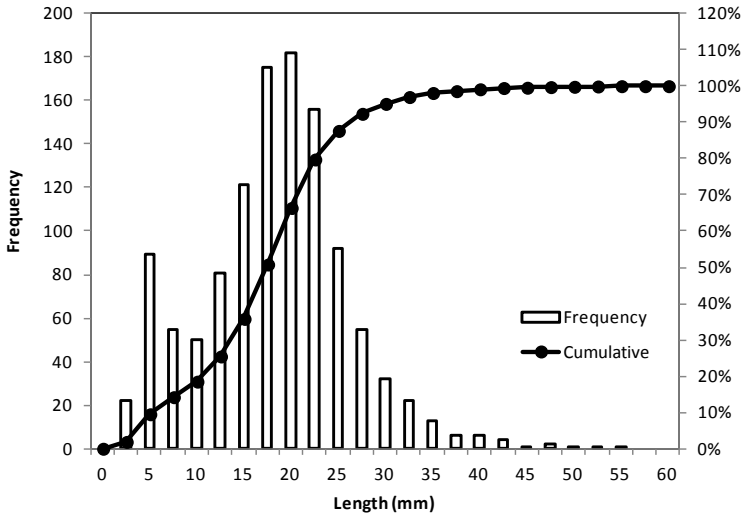

Figure 2. 1b Length distribution of RTSF.

2.2.4 Superplasticizer and Air Entraining Admixture

An aqueous solution containing polycarboxylate ether (PCE) polymers was used as superplasticizer. The air entraining admixture AEA used was Microair 103; both superplasticizer and AEA comply with EN 934-2 .

2.3 Aggregate Characterization

2.3.1 Composition

Figure 2.2 illustrates the composition of all types of (5-20) mm coarse RA, while the quantities of the constituent materials of RA is shown in Table C-1 in Appendix C. To identify the category for each type of RA based on its composition (see Table 2.4), the results were compared with categories described in (BS EN 12620+A1:2008) [5]. Although around 80% of RA-M consists of concrete and unbound aggregate, it is classified as RA [4] [5] (Table 2.5) similar to RA-B. Both RA-C and RA-C1 are classified as RCA.

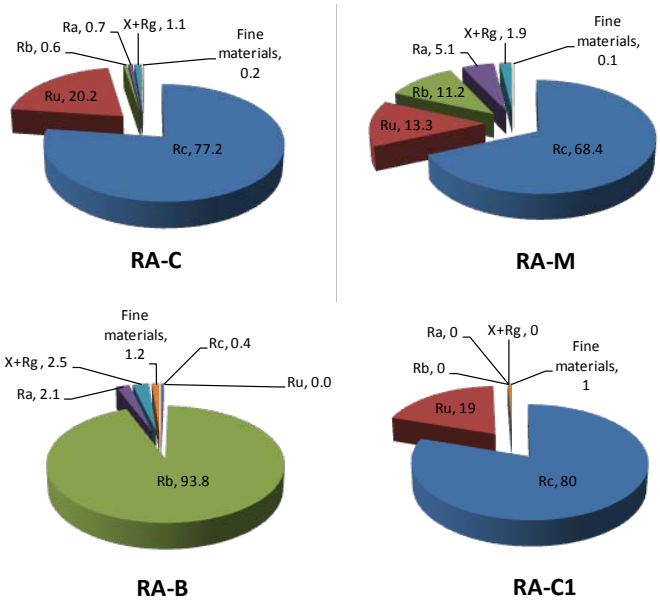

Figure 2. 2 Composition of RA for sizes between (5-20 mm).

Table 2. 4 Identified categories of RA according to BS EN 12620+A1:2008 [5] for recycled aggregate.

Type of RA	Category					
	Constituents (BS EN 12620:2008)					
	Rc	**Rc+Ru**	**Rb**	**Ra**	**X+Rg**	**FL**
RA-C	Rc_{70}	Rcu_{95}	Rb_{10-}	Ra_{1-}	XRg_{1-}	$FL_{0.2-}$
RA-M	Rc_{50}	Rcu_{70}	Rb_{30-}	Ra_{10-}	XRg_{2-}	FL_{2-}
RA-B	Rc_{1}	Rcu_{1}	Rb_{95-}	Ra_{5-}	XRg_{2-}	FL_{2-}
RA-C1	Rc_{80}	Rcu_{95}	-	-	-	-

Table 2. 5 Rrequirements of BS EN 12620:2002+A1:2008 for both RA* and RCA.**

	Rc	**Rc+Ru**	**Rb**	**Ra**	**X+Rg**	**FL**
RA*	not defined	Rcu_{50}	Rb_{50-}	Ra_{10-}	XRg_{1-}	FL_{2-}
RCA**	Rc_{80}	not defined	Rb_{10-}	Ra_{5-}	XRg_{1-}	FL_{2-}

* RA is described in BS 8500-2 as recycled aggregates with high content of masonry.

** RCA is described in BS 8500-2 as recycled aggregates with high content of concrete.

2.3.2 Size Distribution

The results of the size distribution of both NA and RA (5-20 mm) are illustrated in Figure 2.3. For each type of RA, a mix of aggregate of size 5-20 mm from the three fractions of size was obtained in a way that ensured their size distribution lies within the upper and lower limit curves of the current standard [5]. The same standard was used to assess the gradation of fine NA. The results are shown in Table 2.6.

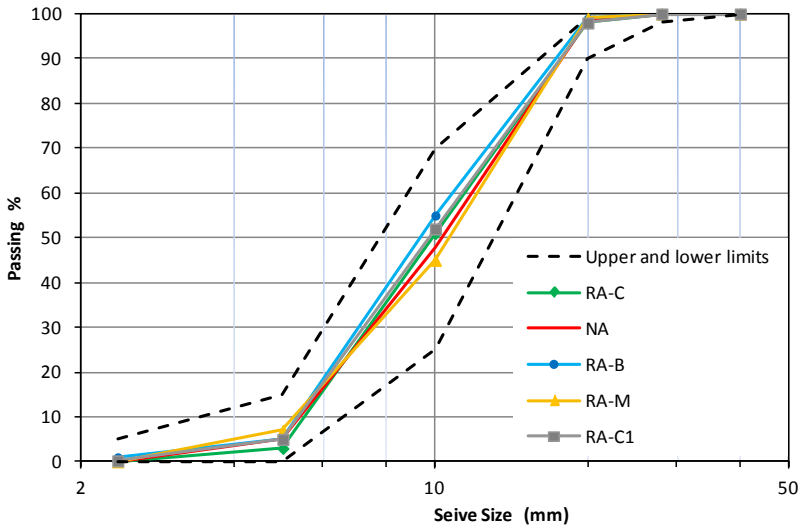

Figure 2. 3 Size distribution curves of coarse NA and RA.

Table 2. 6 Particle size distribution of fine aggregate.

Sieve size mm	8	6.3	4	1.18	0.6	0.3
% Passing	100	100	96.9	84.1	71.1	35.6

The results of the physical and mechanical properties of aggregate are shown in Table 2.7. As a result of the crushing process, the RA had an angular and irregular shape with rough surface while the NA had a rounded and irregular shape with smooth surface.

Table 2. 7 Physical and mechanical properties of NA and RA.

Physical and Mechanical Properties		Type of Aggregate						
		Size fraction mm	NA	RA-C	RA-M	RA-B	RA-C1	Sand
Shape(Visual)		All	Rounded-irregular	Angular-irregular	Angular-irregular	Angular-irregular	Angular-irregular	Rounded
Surface Texture		All	Smooth	Rough	Rough	Rough	Rough	Smooth
Shape Index %		14-20	11	7	11	15	6	
		10-14	9	12	10	9	10	
		5-10	9	7	10	9	7	
		5-20	11	8	11	12	7	
Particle density Mg/m^3 (ρ)	ρ_{rd} (oven dried)	14-20	-	2.36	2.3	1.87	2.41	2.65
		10-14	-	2.35	2.4	1.89	2.40	
		5-10	-	2.33	2.22	1.84	2.37	
		5-20	2.61	2.35	2.25	1.87	2.40	
	ρ_{ssd} (saturated surface dry)	14-20	-	2.45	2.41	2.11	2.50	2.66
		10-14	-	2.44	2.37	2.12	2.49	
		5-10	-	2.43	2.36	2.07	2.48	
		5-20	2.63	2.45	2.37	2.1	2.50	
	ρ_a (apparent)	14-20	-	2.59	2.58	2.45	2.64	2.68
		10-14	-	2.62	2.53	2.48	2.63	
		5-10	-	2.6	2.58	2.41	2.64	
		5-20	2.68	2.61	2.57	2.46	2.64	
Bulk density kg/m^3		14-20	1646	1310	1212	1027	1318	1646
		10-14	1585	1283	1171	1038	1293	
		5-10	1603	1257	1184	1026	1287	
		5-20	1668	1338	1234	1042	1352	
Voids %		5-20	36	43	45	44	42	38
Water absorption (WA) %		14-20	1	3.6	4.8	12.6	3.1	0.5
		10-14	1	4.5	5.1	12.7	3.9	
		5-10	1	4.8	6.4	12.7	4.4	
		5-20	1	4.2	5.5	12.7	4.0	
Porosity %		5-20	2.6	11.0	12.9	29.1	10.2	-
LA %		10-14	23	33	35	43	30	-

2.3.3 Density

Overall, the RA had lower densities than those of NA. For example, for size range 5-20 mm, the ρ_{ssd} for RA-C1, RA-C, RA-M and RA-B are less than that of NA by 5%, 7%, 10% and 20%, respectively. RA-C1 has the highest density (SSD); this is expected as RA-C1 is very clean crushed RCA. Also, as their size decreases, the SSD density of RA-C1, RA-C and RA-M decreases, whereas this is not always true in the case of RA-B. This reduction in SSD density is a consequence of mortar attached to the surface of the particles. The smaller the size of the RA is, the higher the amount of attached mortar on the RA surface. In fact, some of the small particles of RA were entirely mortar. However, this is not applicable for RA-B as its particles were free of attached mortar, but the brick itself was of low density.

Higher bulk density was observed for NA in comparison to RA. The lower particle density of RA is partly responsible for its lower loose bulk density when compared to NA. Shape also affects bulk density; usually rounded particles increase packing capacity. Since all aggregates had almost the same gradation, it appears that the shape of the particles is the main factor responsible for the fact that RA has higher void ratio than NA.

2.3.4 Water Absorption

The rate of WA for RA was obtained by measuring WA at 10 minutes, ½ hr, 1 hr, 2 hr, 9hr, and 24 hr for three samples (see Figure 2.4). Approximately around 70% of the 24hr water absorption capacity for all types occurred within the first 10 min. After that, the rate of absorption decreased and about 97-100 % of the final absorption took place by the end of 2hr. Between 9hr and 24hr, no further absorption was observed.

As expected, higher values of WA were measured for RA than for NA. For example, for size 5-20 mm WA of 4.2 % was measured for RA-C, as compared to 1% for NA. The results of RA-C1 show only slightly less WA than that for RA-C. The WA for RA-M and RA-B were 5.5 % and 12.7 % respectively. These results are in line with results reported elsewhere [1, 33]. Again the attached mortar on the RA surface and the inherent high porosity of RA-B are considered responsible for their high WA. It is clear from table 2.7 that for RA-C, RA-C1 and RA-M, the smaller the aggregate size the higher the WA, mainly due to the higher content of attached mortar as discussed earlier. However, this trend was not true for RA-B as its particles were relatively free of attached mortar.

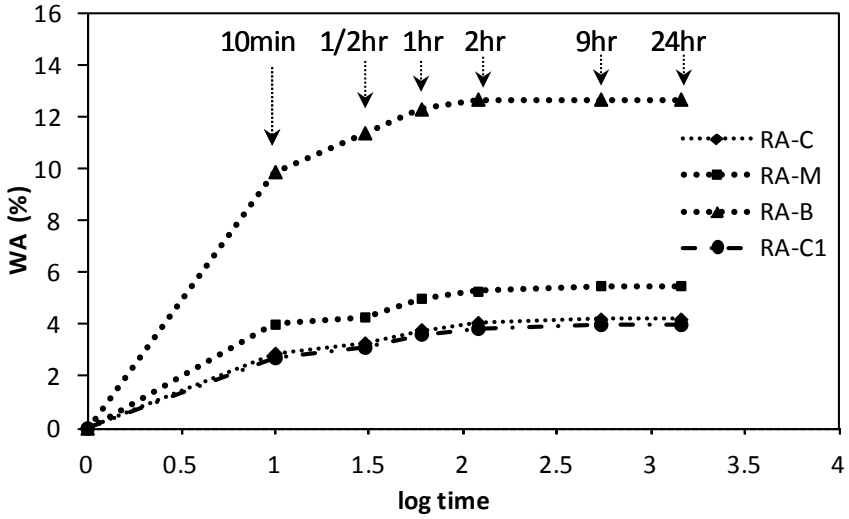

Figure 2. 4 Rate of WA of different types of RA.

2.3.5 Porosity and LA

The porosity of coarse RA (all types) is also higher than that of NA due to the open structure of attached mortar and brick. Similar results were reported by others [2, 3, 34, 35].

The lowest value of LA (greatest resistance to fragmentation) was observed for NA and the highest for RA-B. Although all types of RA exhibited lower mechanical performance than that of NA, their LA values (apart from RA-B) still comply with the limit (≤ 40%) of BS 8500 for use in structural applications of concrete such as concrete for heavy duty pavements. Similar results were reported by WRAP[1]. The high resistance to fragmentation exhibited by RA-C1 can be attributed to the type of the NA (high quality granite) used in the old concrete specimens. This was also found by Zega et al [36] who studied the effect of type of natural coarse aggregate on the properties of RA. According to the categories proposed by BS EN 12620:2002 [5] for LA, the NA and RA-C1 correspond to categories LA_{25} and LA_{30}, respectively, while both RA-C and RA-M correspond to LA_{35} and RA-B to LA_{50}.

2.4 Mix proportioning

The relative densities and WA of aggregates are used for mix proportioning. Various coarse RA contents 20%, 50%, 75% and 100 % were examined in this study and the NA was replaced by RA volumetrically. The mix proportions for NAC were: 340 kg/m^3 of cement , w/c=0.47, coarse aggregate =1275 kg/m^3, fine aggregate =556 kg/m^3. The same mix

proportions were used for RAC except from the quantity of coarse aggregate which is given in Table 2.8 and the water which is adjusted based on the moisture content of the aggregate.

Table 2. 8 Quantities of coarse RA used in production of RAC.

% RA	Coarse aggregate kg/m^3											
	RA-C	NA	Total	RA-M	NA	Total	RA-B	NA	Total	RA-C1	NA	Total
0	0	1275	1275	0	1275	1275	0	1275	1275	0	1275	1275
20	238	1020	1259	231	1020	1251	204	1020	1225	243	1020	1263
50	596	638	1234	577	638	1214	511	638	1149	608	638	1246
75	894	319	1213	865	319	1184	767	319	1085	912	319	1231
100	1192	0	1192	1154	0	1154	1022	0	1022	1216	0	1216

2.5 Concrete production

In concrete containing porous aggregates such as lightweight aggregate or RA (used in this study), the absorption or moisture condition of the aggregate plays a key role in controlling the microstructure of the ITZ. The moisture condition of the aggregates can be controlled during the production of concrete [37]. Highly porous aggregates tend to absorb significant amounts of water from the concrete mix and this can result in a dense structure of ITZ and indeed benefit from some diffusion of fine cement grains into the outermost layer of the aggregate. Therefore, introducing porous aggregates to the concrete mixer in a pre-wetted condition could result in a poorer structure of ITZ [38, 39] and, hence, lower quality concrete. Pre-wetting could also lead to accumulation of excessive water around aggregate particles , thus increasing the micro bleeding effect on the ITZ structure[38].

It is strongly recommended to introduce the RA into the mixer in SSD condition to reduce the impact of its high water absorption on concrete workability and to maintain the desired w/c ratio required for strength. This can be done by pre-soaking the RA [2, 3]. However, in practice, it is difficult to achieve the SSD condition.

Another approach was used in this study to overcome introducing excessive water around the aggregate particles. The aggregates were added to the mixer in the dry condition and mixed with half of the total water (w/c + water to account for the absorption of aggregates) required for the mix. The aggregates were then left in the mixer for 10 minutes to achieve a partially saturated condition. This period of time was selected based on the results of the absorption tests on RA.

Slump tests were conducted to assess the workability of the fresh concrete by following the procedure in BS EN 12350-2 [40]. The concrete was placed in moulds and compacted using a vibrating table. After 24hr, the specimens were demoulded and coded. Specimens were water cured at 20 ± 2 ^{o}C.

The density of hardened concrete cubes (100mm in dimension) was measured using BS EN 12390-7 [41]. The compressive strength of 100mm cubes was obtained using BS EN 12390-3 [42].

2.6 Properties of NAC and RAC

2.6.1 Workability, Air voids and Density

Table 2.9 shows workability, air voids and density of concrete. The results show that the incorporation of RA (except RA-M) had little effect on the workability of concrete. This shows that the pre-mixing procedure worked. The slump values of the RAC incorporating RA-M with 75% and 100% RA content were 30mm (lower than the 50mm target); therefore superplastisizer was added to enhance workability.

Table 2. 9 Properties concrete: workability, air content and density.

Property	RA %	Type of coarse Aggregate				
		NA	RA-C	RA-M	RA-B	RA-C1
Slump	0	60	-	-	-	-
	20	-	65	55	80	65
	50	-	60	50	60	60
	75	-	55	85*	60	60
	100	-	55	65**	55	55
Air content %	100	3.5	4	5.5	5.5	4
Density kg/m^3 (Normalised)	0	2378 (1)	-	-	-	-
	20	-	2336 (0.98)	2348 (0.98)	2256 (0.95)	2351 (0.99)
	50	-	2315 (0.97)	2275 (0.96)	2229 (0.94)	2334 (0.98)
	75	-	2295 (0.96)	2242 (0.94)	2150 (0.90)	2309 (0.97)
	100	-	2273 (0.95)	2205 (0.93)	2102 (0.88)	2285 (0.96)

* SP was added (0.32 % of cement mass). ** SP was added (0.16 % of cement mass).

The dosage of the AEA to achieve the required air entrained voids content (min 3.5 %) was established at 0.11 of the cement mass. The air content of RAC was found to be only slightly higher than that of NAC.

As expected, the RAC had lower density than NAC. Similar results were found by others [2, 3, 33, 43]. Since both had the same gradation and were compacted in the same way, any reduction in density can be attributed to aggregate density and shape.

2.6.2 Compressive Strength Results

The results of the compressive strength (average of 3 samples) at 7 and 28 days are shown in Table 2.10. Figure 2.5 shows the normalized compressive strength at 28 days ($f_{cu,28,RA}$ / $f_{cu,28,NA}$) versus RA content. RAC made of RA from CDW had lower compressive strength than that of NAC regardless of the type of RA. In addition, as expected, increasing RA content decreases strength.

Table 2. 10 Compressive strength of NAC and RAC.

RA content %	Compressive Strength MPa									
	7 days					28 days				
	NA	RA-C	RA-M	RA-B	RA-C1	NA	RA-C	RA-M	RA-B	RA-C1
0	43.6	-	-	-	-	53.1	-	-	-	-
20	-	41.9	41.2	33.9	44.1	-	50.0	48.0	40.0	53.2
50	-	37.9	36.3	30.5	45.2	-	45.3	41.7	37.0	54.0
75	-	37.5	33.1	28.8	46.7	-	44.0	39.5	33.1	55.8
100	-	35.4	30.8	27.6	47.3	-	41.6	38.1	31.5	58.3

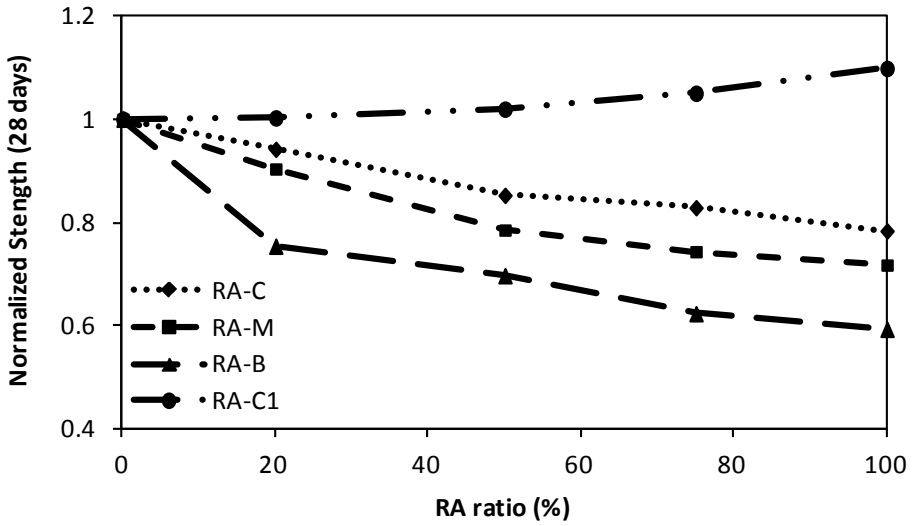

Figure 2. 5 Normalized compressive strength of RAC at different RA content.

The behaviour of RAC made of RA-C1 was much better than that of RAC using RA from CDW. For all contents, the compressive strength at both 7 and 28 days were higher than those of NAC.

2.6.3 Effect of particle density on properties of RA and RAC

Figure 2.6 shows the effect of aggregate particle density on aggregate strength (LA %). Unlike observations elsewhere [1], the particle density of RA had a clear relationship and strong correlation with its mechanical behaviour (LA). The high values of LA for RA (29-35%), which mean low resistance to fragmentation (low strength), are caused by low density loose, porous and weak layers of mortar present on the surface of coarse RA.

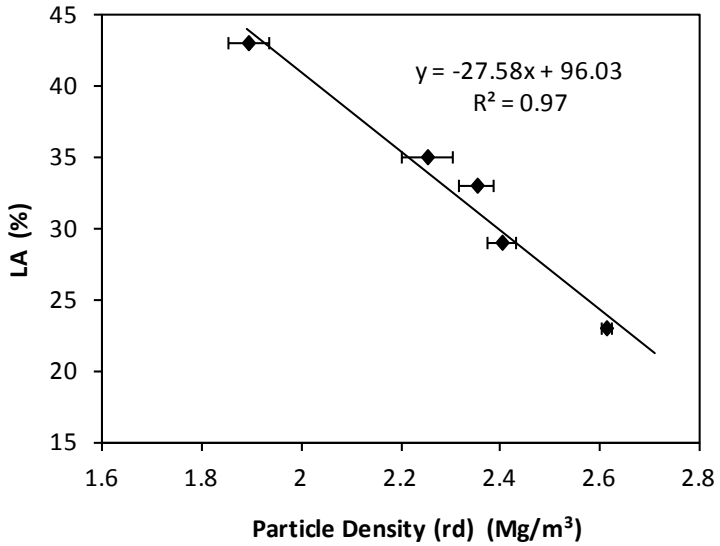

Figure 2. 6 Effect of particle density of RA on its strength.

The attached mortar and the porosity of the brick also cause problems in terms of WA and porosity of RA, as can be seen in Figure 2.7. For a particle density (ssd) decrease of 10%, the WA increases by about 6% and porosity increases by around 12%.

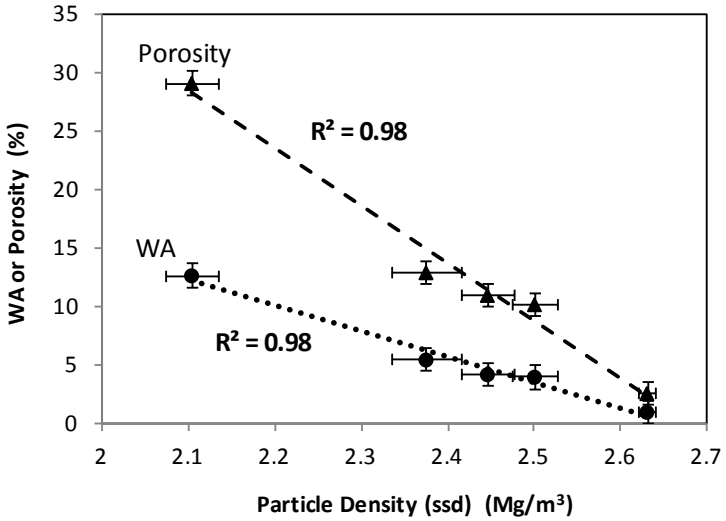

Figure 2. 7 Effect of particle density of RA on its WA and porosity.

As expected, there is a linear correlation between density (ssd) of RA and normalized density of RAC as can be seen in Figure 2.8. Figure 2.8 also shows the theoretical curve of the normalized density of concrete which is calculated based on the particle density of the aggregate and the mix proportions.

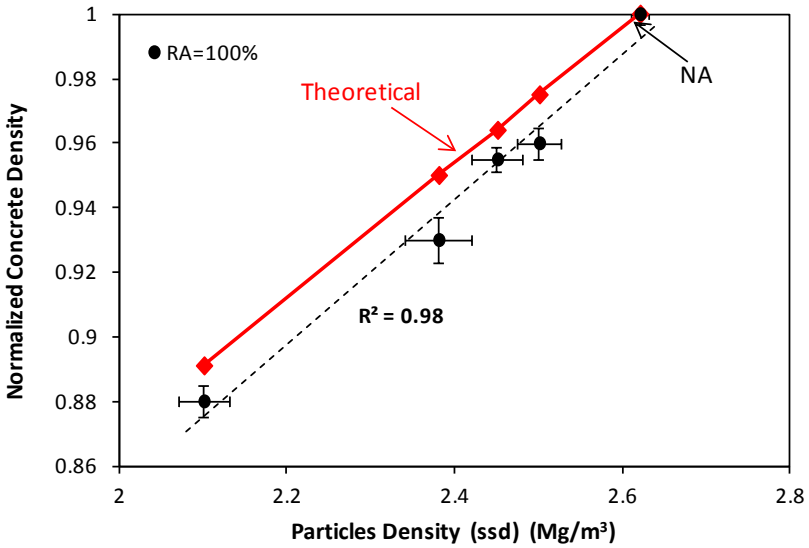

Figure 2. 8 Effect of particle density on the normalised density of RAC.

Figure 2.9 shows the effect of particle density on the normalized strength of RAC at 28 days for different RA contents. A strong relationship with relatively good correlation appears to exist between the particle density and the strength of RAC. It can be seen that an 8% increase in particle density approximately leads to a 10 % increase in concrete strength regardless the RA content.

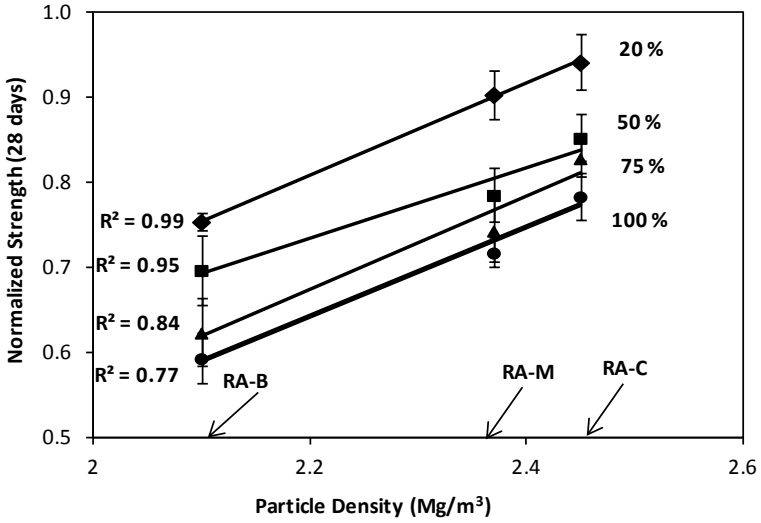

Figure 2. 9 Effect of particle density of RA on normalized strength of RAC.

2.6.4 Parameters affecting Strength of RAC

Figure 2.10 shows the effect of normalized density of RAC containing RA from CDW on its normalized compressive strength at 28 days. There appears to be a strong relationship between the density of RAC and its strength with a good correlation (R^2 =0.94). It can be seen that when the density of concrete increases by 10%, its compressive strength increases by 40%. A similar relationship was reported by Xiao et al. [44], who reviewed the results of many published experimental studies. However, RAC made with RA-C1 does not support this trend as although it has a similar concrete density to that containing RA-C and RA-M , its strength is substantially higher. Hence , it is clear that another parameter also affects the strength of RAC. The obvious candidate to consider is the strength of RA (e.g. LA value) and this is examined in Figure 2.11. A good correlation can be identified between LA of RA and the normalized strength of RAC in Figure 2.11. Therefore, it is proposed that both LA and particle density should be used to determine the effect of RA on the strength of RAC using statistical analysis.

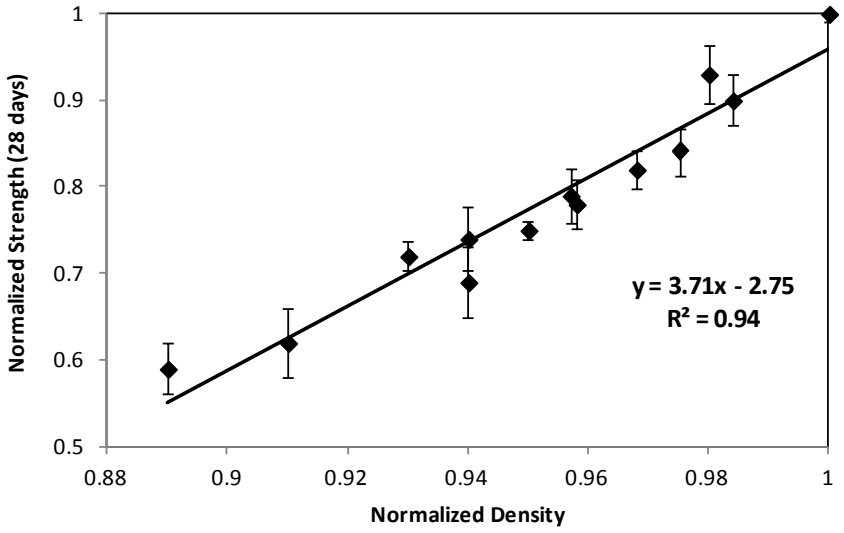

Figure 2. 10 Relation between normalized density and normalised strength of RAC.

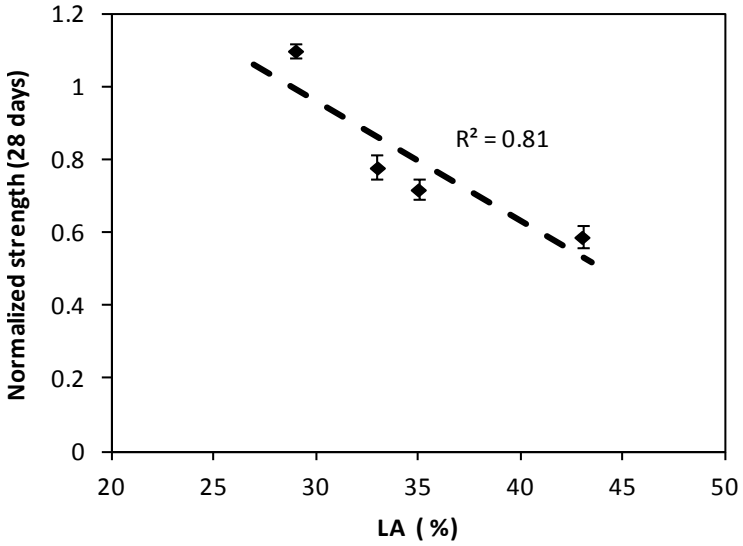

Figure 2. 11 Effect of LA of RA on normalized strength of RAC.

2.6.5 Strength Prediction Equations

A multi-linear regression analysis was used to develop a multi-variable model to predict the compressive strength of RAC. In this study the dependent variable is the compressive strength of RAC while the independent variables are particle density (dry), LA, WA and RA (ratio). The normalized form for all variables is used.

Three models were developed, as shown below: two linear models, eq. 1 and 2 and one non-linear, eq. 3

$$f_{cu,RA} = \left[13.7\frac{\rho_{\mathrm{rd,RA}}}{\rho_{\mathrm{rd,NA}}} + 2.47\frac{LA_{\mathrm{RA}}}{LA_{\mathrm{NA}}} - 0.2\frac{WA_{\mathrm{RA}}}{WA_{\mathrm{NA}}} - 0.12RA - 10.35 \right] \times f_{cu,NA} \quad R^2 = 0.89 \quad (1)$$

$$f_{cu,RA} = \left[-1.245\frac{\rho_{\mathrm{rd,RA}}}{\rho_{\mathrm{rd,NA}}} + 3.22\frac{LA_{\mathrm{NA}}}{LA_{\mathrm{RA}}} - 0.99\frac{WA_{\mathrm{NA}}}{WA_{\mathrm{RA}}} - 0.13RA \right] \times f_{cu,NA} \quad R^2 = 0.85 \quad (2)$$

$$f_{cu,RA} = \left[f_{cu,RA} \times \left(\frac{\rho_{\mathrm{rd,RA}}}{\rho_{\mathrm{rd,NA}}}\right)^{-0.15} \times \left(\frac{LA_{\mathrm{RA}}}{LA_{\mathrm{NA}}}\right)^{-3.6} \times \left(\frac{WA_{\mathrm{RA}}}{WA_{\mathrm{NA}}}\right)^{0.65} \right] / (RA+1)^{0.12} \quad R^2 = 0.87 \quad (3)$$

The difference between eq. 1 and 2 is that in the latter (LA_{NA}/ LA_{RA}) and (WA_{NA}/ WA_{RA}) were used instead of (LA_{RA}/ LA_{NA}) and (WA_{RA}/ WA_{NA}). Figure 2.12 (a, b and c) examines the accuracy of the developed models. It can be seen that all models can predict the f_{cu} of RAC reasonably well.

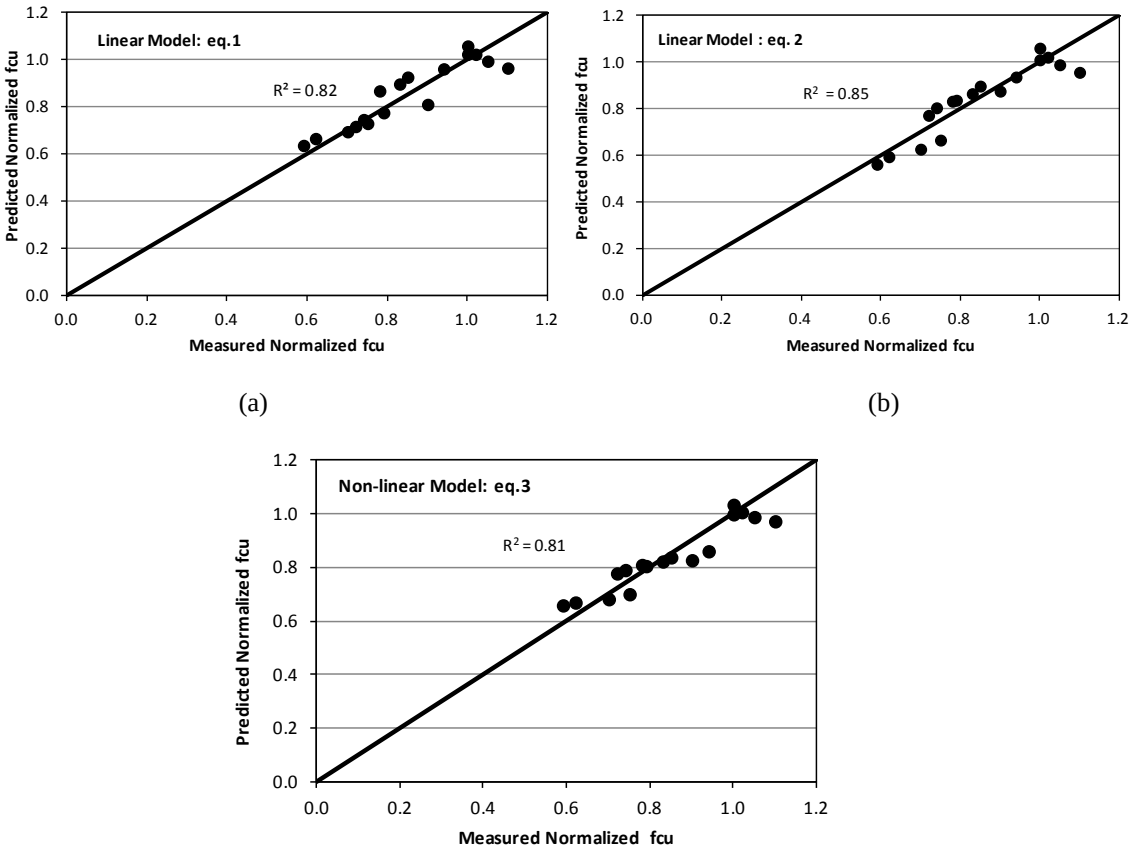

Figure 2. 12 Predictive models for f_{cu} of RAC, (a) linear model eq.1, (b) linear model eq.2, (c) non-linear model eq. 3.

To check the validity of the developed models, worldwide experimental results found in the literature [1, 2, 39, 45-49] were examined. The results are shown in Figure 2.13 (a, b and c). It can be seen that the linear model (eq. 2) can predict the compressive strength of RAC better than the other two models. For the results of (Tam [15], Kou et al [20], Xiao et al [45] and Brendt [48]) the values of LA were not given, so the equation shown in Figure 2.6 was used to determine the value of LA.

Discussion

Although equation 2 has a negative value on the density ratio coefficient which could be taken as that an increase in aggregate density can decrease strength, it should be remembered that LA is also a function of the density and that causes this abnormality. The value of LA is the sole indicator of RAC strength, but LA is not a property that can be controlled. Density, on the other hand, can be controlled by using different separation techniques (such as centrifugal force or floatation) that could be developed industrially. Hence, it is clear that the development of density separation techniques can help produce RA of different strengths, some of which could be used for high quality concrete.

The other main parameter that may be able to be controlled is WA, which may help improve the concrete ITZ.

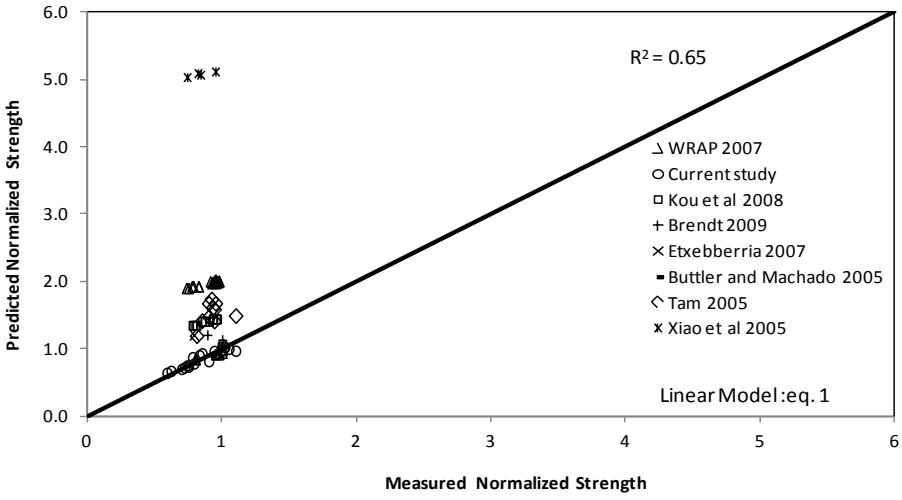

(a)

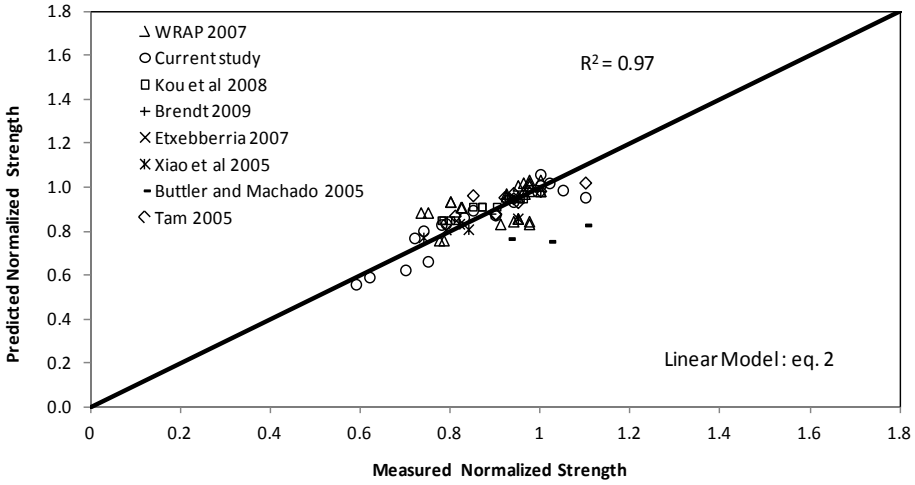

(b)

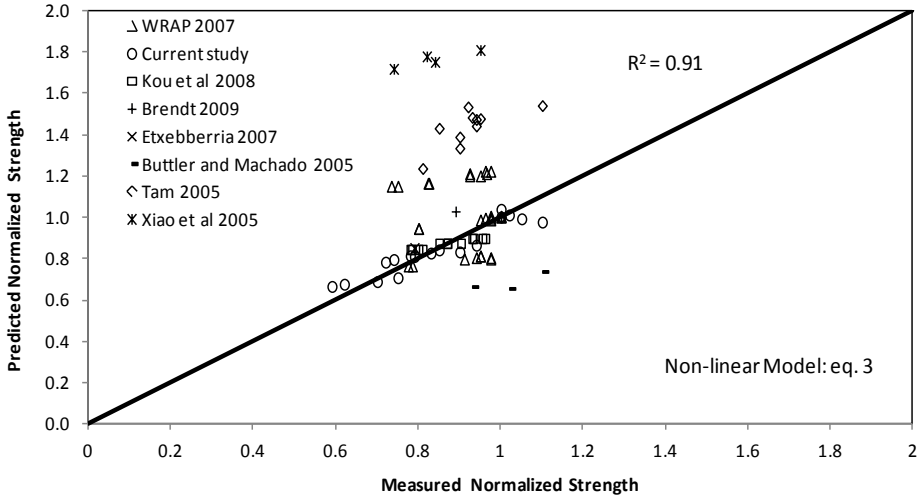

(c)

Figure 2. 13 Validity of the predictive models for f_{cu} of RAC: a- linear model eq.1, b- linear model eq. 2, c-non-linear model eq.3

2.7 Surface Treatment of RA

As already mentioned RA often suffers from a weak and porous surface, mainly due to old mortar or inferior materials such as low strength bricks. The cracked, loose, porous and weak surface of RA may be strengthened by: (1) filling the cracks, (2) increasing the bond between the loose particles and the surface, (3) decreasing the porosity of this layer. Minimizing the effects of these weaknesses and densifying the surface of RA can enhance the strength of RAC. Modifying the microstructure of the ITZ by incorporating mineral admixtures is not uncommon [13]. This improvement is usually achieved through two mechanisms: physical and chemical. The former is due to the ability of the mineral admixtures to act as micro-fillers to fill micro-pores in the ITZ, whereas the latter is due to the pozzolanic reaction between the SiO_2 in the mineral admixtures and the CH existing in the ITZ, in the presence of water to produce C-S-H. For porous aggregates such as lightweight aggregate and RA, the ITZ is not limited to the vicinity of the aggregate surface, rather it goes beyond that reaching a certain distance inside the RA through the attached old mortar. Coating the RA with a layer of mineral admixtures facilitates the penetration of micro-particles into the porous and cracked surface of RA.

In this study, an attempt was made to improve the surface properties of RA by coating with very fine materials. Different types of materials were used to treat the RA including reactive micro-fillers (mineral admixtures such as FA, GGBS and SF) and non-reactive micro-fillers (LP). RA-M was selected to undertake the surface treatment utilizing two coating techniques; pre-mixing treatment (PMT) and within-mixing treatment (WMT).

2.7.1 Methodology for Surface Treatment

In PMT, RA was immersed in a solution containing microfillers to apply a coating layer on the surface of the RA. A liquid form of several fillers (SF, GGBS, LP, FA) was prepared by using a mixing ratio (by mass) of 1 powder : 10 water. Superplastisizer was added (1% of the mass of powder) to ensure dispersion of the powder particles in the water. The RA was soaked in the solution in oven dry conditions. They were left in the solution for 24 hr. They were then transferred to a tray and placed in the oven for 24hr.The mass of the RA was measured before and after treatment (in dry condition) to calculate the mass of the powder absorbed by the RA.

In the WMT, the treatment was undertaken during the mixing process as shown in

Figure 2.14. This differs from the $TSMA_s$ and $TSMA_{sc}$ developed by Tam and Tam [18] in that no cement is added at the first stage and after the first stage, there is a 10 minute resting period, during which moisture is allowed to penetrate to the RA and, pull-in some of the fines, to block pores.

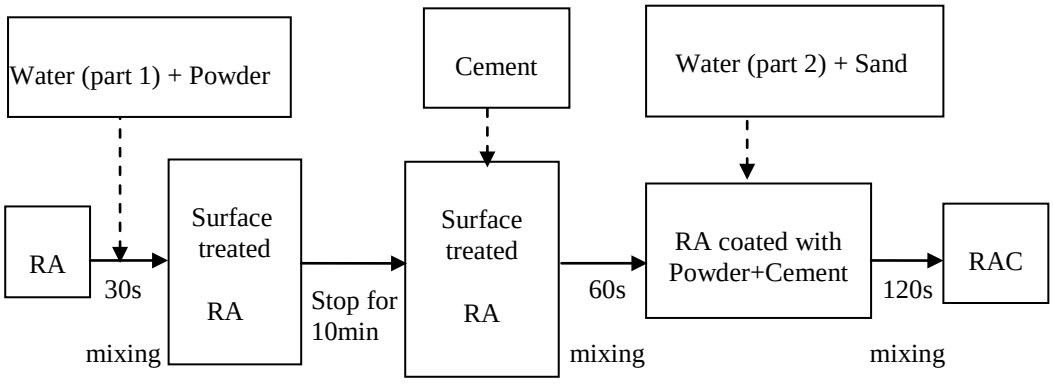

Figure 2. 14 Mixing steps of WMT

The same mix proportions as adopted earlier were used to produce -RAC made with treated RA-M (100% content). Examinations on powder uptake, workability, density of concrete and compressive strength were undertaken. The results are presented in Table 2.11.

Table 2. 11 Properties of RAC made with treated RA-M (%RA=100 %).

Powder Type	Uptake % (by mass of RA)	Uptake % (by mass of cement)	Slump mm		Density kg/m^3		Compressive Strength MPa (SD)*		Normalized Strength	
			PMT	WMT	PMT	WMT	PMT	WMT	PMT	WMT
None	-	-	65		2205		38.1 (1.2)		1	
LP	2.6	4.6	65	70	2222	2217	40.8 (1.4)	41.2 (1.0)	1.07	1.08
SF	1.1	1.9	65	65	2221	2228	43.6 (1.1)	44.6 (1.1)	1.15	1.17
GGBS	2.1	3.8	65	70	2230	2224	40.1 (1.1)	40.4 (1.2)	1.05	1.06
FA	0.6	1.1	70	70	2207	2213	37.6 (1.0)	38.0 (2.0)	0.99	1.0
SF-RSF			-	60**	-		-	49.7 (1.2)	-	1.30

* Standard deviation. ** SP was added (0.1 % of cement mass).

2.7.2 Results of the Treatment Techniques

2.7.2.1 Uptake of RA and workability

The results show that very small amounts of FA and SF were absorbed by the RA, whereas larger amounts of LP and GGBS were absorbed.

The workability, in general, was better than that of NAC (60 mm) and equal (or higher) to that of RAC of untreated RA-M (65 mm) which was achieved using superplasticizers. This was expected as it is well known that mineral admixtures usually enhance the workability of concrete.

2.7.2.2 Density and compressive strength

Regardless of the material and technique used for treatment of RA, concrete density (average of three samples) was similar or slightly higher than without treatment (2205 kg/m^3). This indicates that the treatment process does not penetrate much into the RA and, hence, does not improve much the density of concrete.

Regardless of the treatment method, comparable strength to that of untreated RA was observed for RA coated with FA. As can be seen in Table 2.11 coating with FA did not help the strength. One possible explanation for this result may be that the size of FA particles was not small enough (as can be seen from its fineness Table 2.1) to effectively fill the micro cracks on the surface of the RA. This view is also supported by the fact that the amount of FA uptake (see table 2.11) is the lowest amongst the micro-fillers used. SEM scanning undertaken by Kong et al [20] on RCA treated with FA shows that some un-reacted particles of FA were present even after 28 days of curing leaving a large amount of CH crystals around its particles. This may explain why the FA treatment resulted in lower strength than the untreated RA.

Strength improvements of 6%, 17% and 8% were obtained when RA was coated with GGBS, SF and LP, respectively. GGBS seems to perform better than FA and this can be attributed mainly to the fact that GGBS used in this study had higher fineness than FA. This enhanced the ability of GGBS particles to fill the voids on the RA and the much higher uptake confirms this. GGBS also tends to be more uniform in chemical composition and physical properties [50, 51] and as a result may have had less problems with reactivity.

Significant strength improvement was achieved with SF. The ability of SF particles to act as micro-fillers (high fineness, see Table 2.1) and their high reactivity are well known [13, 18,

51]. The treatment with SF not only improves the ITZ, but it can also increase the mechanical strength of the RA by: a) filling the cracks on the surface of RA, b) reacting with the CH accumulated on the mortar attached to the RA and c) reducing the effect of the loose particles on the strength of RA by effectively bonding them to the surface of the RA [13].

A strength improvement was seen when coating RA with LP. This again can be attributed to the small size of the particles which resulted in the highest uptake. This was also found by Goldman and Bentur [52] who showed that nonreactive micro-fillers (e.g. carbon black) can strengthen the ITZ and improve the composite behaviour of concrete leading to strength improvements as large as that obtained from the pozzolanic effect of SF. To a lesser extent, a chemical mechanism may contribute to the strength enhancement by the formation of calcium mono-carboaluminates when LP is used as a filler [53]. This strength improvement can also be attributed to the nucleation effect, as the introduction of many nucleation sites may homogenise the distribution of C-S-H and hence densify the pore-structure of cement paste [54-56], in particular at the ITZ.

The use of WMT exhibited better strength improvement than PMT though the difference is insignificant. The slight difference observed could be due to the fact that in WMT all the microfiller used to coat the RA remained in the concrete mixtures, while in PMT some of the microfillers came off when the dried and treated RA was transferred to the mixer as some of the microfillers were seen in the drying tray. From a practical prospective, WMT is preferred as it saves time and effort.

2.7.3 Effect of ITZ on the Strength of RAC

At the macroscopic level, concrete appears as a two phase material (aggregate particles surrounded by cement matrix). However, at the microscopic level, a third phase, known as ITZ, can be distinguished as a film of 10-50 microns thickness at the interface between aggregate and cement matrix. ITZ possesses different properties and microstructure than aggregate and cement paste and is responsible for many strength and durability behavioural aspects of concrete. ITZ is in general weaker than the other two phases and is characterised by high porosity caused by the 'wall effect' and internal bleeding [51]. The inclusion of RA in concrete increases the complexity of the structure of concrete and whilst in NAC only one type of ITZ exists, in RAC, three types can be identified (see Figure 2.15): a) ITZ1 between old cement (attached) mortar (OCM) and the NA , b) ITZ2 between OCM part of RA and the new cement mortar (NCM), c) ITZ3 between the NA part of RA and NCM. Since the

mix proportions and the properties of the old and new cement mortars in RAC are usually different, the properties and microstructure of these ITZs are also expected to differ.

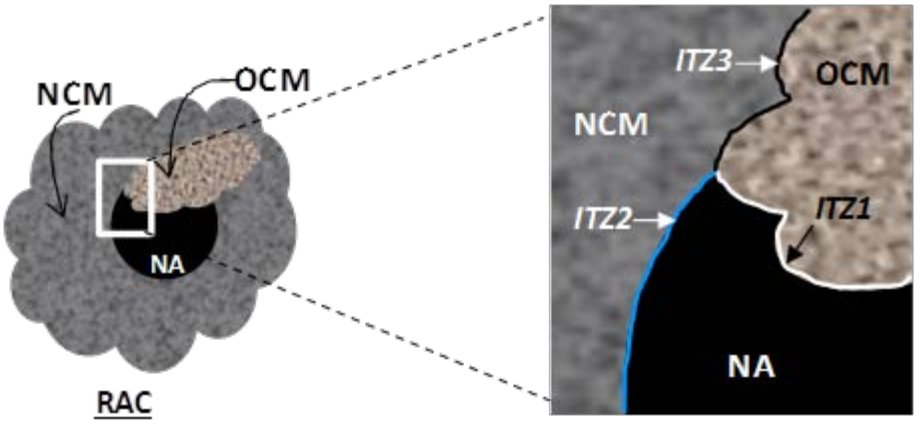

Figure 2. 15 Schematic representation of ITZs in RAC.

For this reason, SEM (Scanning Electron Microscope) tests were conducted on RAC samples. Three different ITZs can be identified in Figure 2.16 (a, b, c, d and e). Better bond between the NCM and the OCM can be identified (as there is no clear boundary between them), whereas clear lines can be seen between the OCM and the NA and between the NCM and the NA (ITZ1and ITZ2). It appears that the process of preparing the samples may have affected the ITZ1 and the ITZ2 (mortar separated from NA), but this is not clear in ITZ3 and this can confirm the better bond between the OCM and NCM in ITZ3.

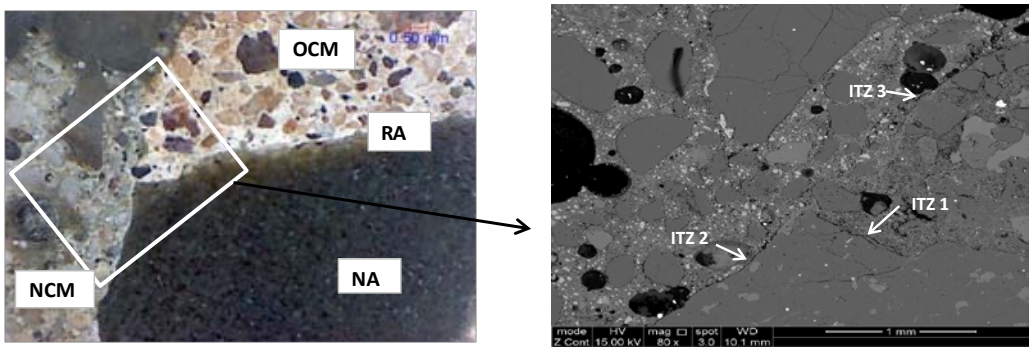

(a) Microscope image of RAC (b) SEM image of RAC

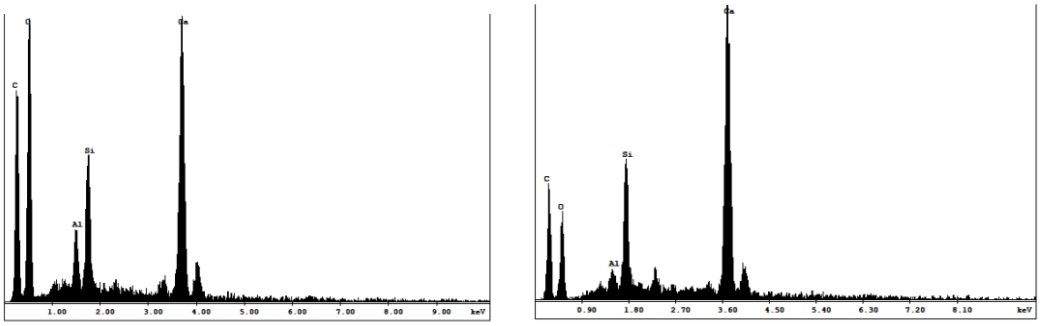

(c) EDAX of a point in ITZ1 (d) EDAX of a point in ITZ2

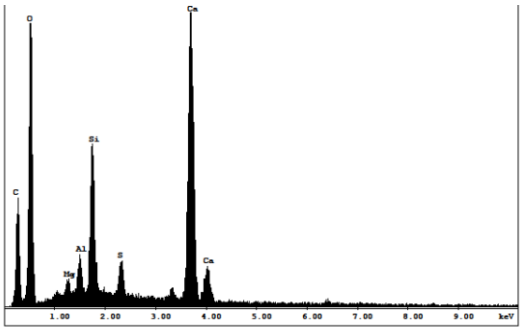

(e) EDAX of a point in ITZ3

Figure 2. 16 Microscope and SEM images and EDAX of RAC.

It is reported [13, 18, 38, 57] that the surface of RA is characterised by a weak layer of loose crumbs (particles) and macro and micro cracks caused by the crushing process in the production of RA. These weaknesses can further diminish the quality of RAC at the ITZ and increase the absorption of RA, causing an increase of the w/c ratio at the new ITZs (ITZ2 and ITZ3) which in turn can lead to the formation of large calcium hydroxide (CH) crystals and increase the porosity in this zone [13, 15, 20] .

Figure 2.17 a and b show microscope and SEM images of RAC samples with RA treated with SF. Evidence of damage on ITZ1 and ITZ2 can be easily seen, however it is absent from ITZ3. This can be attributed to the role of SF in reacting with CH on the surface of OCM of RA enhancing the bond between OCM and NCM.

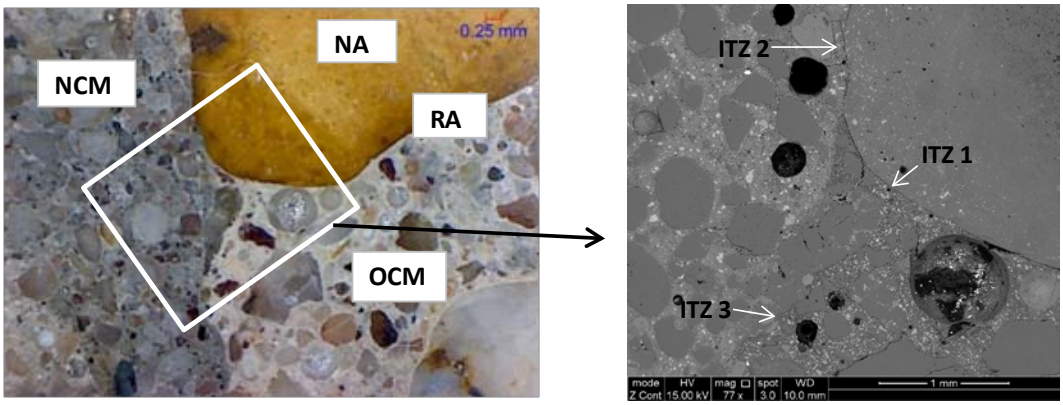

(a) (b)

Figure 2. 17 Microscope and SEM images of RAC with SF treated RA.

2.8 Effect of RTSF on Strength of RAC

RTSF had a positive effect on the compressive strength of RAC (see Table 2.11). When RAC containing RA coated with SF (1.9% of cement mass) was reinforced with 2% by mass (48 kg/m^3) of RTSF, strength improvement of 11% was achieved (from 44.6 to 49.7 MPa). In comparison to plain RAC (containing untreated RA), the treatment of RA with SF and the addition of RSF led to a 30% strength improvement (from 38.1 to 49.7 MPa). The strength enhancement resulted in RAC with 94% of the strength of NAC (53.1 MPa).

The positive effect of RTSF on compressive strength is in line with other studies which used industrial steel fibres (ISF). It is reported [32, 58, 59] that the addition of ISF (up to a certain content e.g. 3% by mass) can increase the compressive strength of concrete in the range of 6-25 %, though strength reductions were reported by others [60-62]. On the other hand, very few studies investigated the behaviour of RTSF reinforced concrete under compressive loading [21, 32, 63]. Strength increases of 6%, 10% and 25% were reported by [21], [32] and [63] respectively for contents up to 3-4 % (by mass). The failure mechanism of concrete under compression initiates with the development of micro-cracks, due to tensile stresses normal to the direction of the compressive stresses, which coalescence to form macro-

cracks. The short RTSF appear to prevent/delay the propagation of micro-cracks and , hence, help increase the compressive strength [21].

2.9 Conclusions

- Four types of RA conforming to BSI requirements [4] for RA and RCA were examined. According to the British standards [4, 5], RA-C and RA-M can be classified as RCA, whilst RA-B is classified as RA.

- The evolution of WA of RA shows that more than 70% of the 24hr WA capacity of all types of RA can be achieved when immersing them in water for 10 min. For this reason, to overcome the issue of high absorption, it is recommended to leave the RA in the mixer with half of the mixing water for 10 minute.

- The particle density of RA has a clear relationship with its strength (LA), WA and porosity. When the particle density decreases, its strength decreases while its WA and porosity increases.

- A strong relationship with very good correlation appears to exist between the particle density and the strength of RAC. It was found that an 8% increase in particle density leads to an increase of approximately 10 % in concrete strength, regardless of RA content. Therefore, just as in NA, the particle density of RA seems to be predominantly responsible for the density of RAC. Also, the density of RA appears to directly affect the strength of RAC. Hence, density separation is proposed to produce high quality of RA from CDW.

- A good correlation was identified between LA of RA and the normalized strength of RAC. It is proposed that the use of LA coefficient alongside the particle density is used to determine the effect of RA on the strength of RAC.

- A strength predictive model is proposed that takes into account the most important parameters (ρ_{rd}, LA, WA and RA content) that affect the performance of RAC.

- Two techniques were used to treat the surface of RA-M (coating with reactive and non-reactive microfillers), PMT and WMT. WMT leads to slightly better results, since all the microfiller used to coat the RA remains in the concrete mixtures. Reactive microfillers such as GGBS and SF led to an increase in compressive strength of RAC by 6% and 17% respectively (using WMT). FA did not result in any strength improvement possibly due to

the large size of FA particles. Treatment with non-reactive (LP) enhanced the compressive strength by 8%. SF gave the best results and is recommended for surface treatment of RA.

- Short RTSF delay the propagation of microcracks and enhance the compressive strength. The inclusion of 2% (by mass) RTSF helps improve the compressive strength of RAC.

References

1. WRAP, *Perfomance Related Approach to Use Recycled Aggregates*. 2007, Waste and Resources Action Programme: Oxon.
2. Tam, W.W.V.C.M., *Recycled Aggregate from Concrete Waste for Higher Grades of Concrete Construction , PhD thesis*, in *Department of Building and Construction*. 2005, City University of Hung Kong: Hung Kong.
3. Hansen, T.C., *Recycled of Demolished Concrete and Masonry* 1992, London: E & FN SPON.
4. BS 8500-2, *Concrete complementary British Standard to BS EN 206 part 1 -Part 2: Specification for constituent materials and concrete*, in. 2006, British Standard Institiution: London.
5. BS EN 12620 :2002 +A1, *Aggregates for concrete.* 2008, British Standards Institution London.
6. RILEM TC 121-DRG, *Specifications for concrete with recycled aggregates.* Materials and Structures, 1994. **27**(9): p. 557-559.
7. WBTC No. 12/2002, *Specifications Facilitating the Use of Recycled Aggregates*. 2002, Works Bureau Technical Circular: Hong Kong.
8. Montgomery, D.G., *Workability and compressive strength properties of concrete containing recycled concrete aggregate.* Proc. Sustainable Construction: Use of Recycled Concrete Aggregate, 1998: p. 289-296.
9. Tam, V.W.Y., C.M. Tam, and K.N. Le, *Removal of cement mortar remains from recycled aggregate using pre-soaking approaches.* Resources Conservation and Recycling, 2007. **50**(1): p. 82-101.
10. Tateyashiki, H., et al., *Properties of concrete with high quality recycled aggregate by heat and rubbing method.* Proceedings of JCI, 2001. **23**(2): p. 61-66.
11. Muller, H.A. and E. Linss, *Processing of Concrete With High oerformance Sonic Impulses*, in *Conference on the Use of Recycled Materials In Building and Structures* 2004: Barcelona, Spain
12. Akbarnezhad, A., et al., *Microwave-assisted beneficiation of recycled concrete aggregates.* Construction and Building Materials, 2011. **25**(8): p. 3469-3479.
13. Katz, A., *Treatments for the improvement of recycled aggregate*. Journal of Materials in Civil Engineering, 2004. **16**(6): p. 597-603.
14. Tam, V.W.Y., X.F. Gao, and C.M. Tam, *Comparing performance of modified two-stage mixing approach for producing recycled aggregate concrete.* Magazine of Concrete Research, 2006. **58**(7): p. 477-484.
15. Tam, V.W.Y., X.F. Gao, and C.M. Tam, *Microstructural analysis of recycled aggregate concrete produced from two-stage mixing approach.* Cement and Concrete Research, 2005. **35**(6): p. 1195-1203.
16. Tam, V.W.Y. and C.M. Tam, *Assessment of durability of recycled aggregate concrete produced by two-stage mixing approach.* Journal of Materials Science, 2007. **42**(10): p. 3592-3602.
17. Tam, V.W.Y., C.M. Tam, and Y. Wang, *Optimization on proportion for recycled aggregate in concrete using two-stage mixing approach.* Construction and Building Materials, 2007. **21**(10): p. 1928-1939.

18. Tam, V.W.Y. and C.M. Tam, *Diversifying two-stage mixing approach (TSMA) for recycled aggregate concrete: TSMA(s) and TSMA(sc).* Construction and Building Materials, 2008. **22**(10): p. 2068-2077.

19. Li, J., H. Xiao, and Y. Zhou, *Influence of coating recycled aggregate surface with pozzolanic powder on properties of recycled aggregate concrete.* Construction and Building Materials, 2009. **23**(3): p. 1287-1291.

20. Kong, D., et al., *Effect and mechanism of surface-coating pozzalanics materials around aggregate on properties and ITZ microstructure of recycled aggregate concrete.* Construction and Building Materials, 2010. **24**(5): p. 701-708.

21. Graeff, A.G., et al., *Fatigue resistance and cracking mechanism of concrete pavements reinforced with recycled steel fibres recovered from post-consumer tyres.* Engineering Structures, 2012. **45**(0): p. 385-395.

22. BS EN 197-1:2011, *Cement. Composition, specifications and conformity criteria for common cements*. 2011, British Standard Institution: London, UK.

23. BS EN 933-11:2009, *Tests for geometrical properties of aggregates -Part 11: Classification test for the constituents of coarse recycled aggregate*. 2010, British Standard Institution: London.

24. BS EN 933-1:1997, *Tests for geometrical properties of aggregates -Part 1: Determination of particle size distribution — Sieving method*. 2006, British Standard Institution: London.

25. BS EN 1097-6:2000, *Tests for mechanical and physical properties of aggregates — Part 6: Determination of particle density and water absorption*. 2005, British Standard Institution: London.

26. BS EN 1936:2006, *Natural stone test methods — Determination of real density and apparent density, and of total and open porosity*. 2007, British Standard Institution: London.

27. BS 812-102:1989, *Testing aggregates. Methods for sampling*. 1989, British Standard Institution: London-UK. p. 12.

28. BS EN 933-4:2008, *Tests for geometrical properties of aggregates Part 4: Determination of particle shape — Shape index*. 2009, British Standard Institution: London.

29. BS EN 1097-3:1998, *Tests for mechanical and physical properties of aggregates - Part 3: Determination of loose bulk density and voids*. 1998, British Standard Institution: London.

30. BS EN 1097-2:1998, *Tests for mechanical and physical properties of aggregates- Part 2: Methods for the determination of resistance to fragmentation*. 2006, British Standards Institution: London.

31. Musacchi, E., P. Iacobucci, and M. Pierfelice, *Potential Process for Cleaning and Sorting of the recycled fibres, Deliverable report 13, FB6 STREP Project Ecolanes (031530)*. 2008.

32. Tlemat H., *Steel fibres from waste tyres to concrete: testing, modelling and design*, in *Department of Civil and Structural Engineering*. 2004, The University of Sheffield: Sheffield UK.

33. Soutsos, M.N., K. Tang, and S.G. Millard, *Concrete building blocks made with recycled demolition aggregate.* Construction and Building Materials, 2011. **25**(2): p. 726-735.

34. Tam, V.W.Y., K. Wang, and C.M. Tam, *Assessing relationships among properties of demolished concrete, recycled aggregate and recycled aggregate concrete using regression analysis.* Journal of Hazardous Materials, 2008. **152**(2): p. 703-714.

35. Angulo, S., et al., *On the classification of mixed construction and demolition waste aggregate by porosity and its impact on the mechanical performance of concrete.* Materials and Structures, 2010. **43**(4): p. 519-528.

36. Zega, C., Y. Villagrán-Zaccardi, and A. Di Maio, *Effect of natural coarse aggregate type on the physical and mechanical properties of recycled coarse aggregates.* Materials and Structures, 2010. **43**(1): p. 195-202.

37. Katz, A., A. Bentur, and K.O. Kjellesen, *Normal and high strength concrete with lightwieght aggregates,* in *Engineering and Transport Properties of the Interfacial Transition Zone in Cementitious Composites*, M.G. Alexander, et al., Editors. 1999, RILEM Report 20: France. p. 71-88.

38. Punkki, J. and O.E. Grov. *Effect of water absorption by aggregate on properties of high-strength light weight concrete*. in *Int. Symposium on Structural Lightwieght Aggregate Concrete*. 1995. Sardefjord, Norway: Norwegian Concrete Association.

39. Etxeberria, M., et al., *Influence of amount of recycled coarse aggregates and production process on properties of recycled aggregate concrete.* Cement and Concrete Research, 2007. **37**(5): p. 735-742.

40. BS EN 12350-2, *Testing fresh concrete – Part 2: Slump test.* . 2009, British Standards Institution: London

41. BS EN 12390-7:2009, *Testing hardened concrete Part 7: Density of hardened concrete*. 2009, British Standards Institution: London.

42. BS EN 12390-3:2009, *Testing hardened concrete Part 3: Compressive strength of test specimens*. 2009, British Standards Institution: London.

43. Katz, A., *Properties of concrete made with recycled aggregate from partially hydrated old concrete.* Cement and Concrete Research, 2003. **33**(5): p. 703-711.

44. Xiao, J.Z., J.B. Li, and C. Zhang, *On relationships between the mechanical properties of recycled aggregate concrete: An overview.* Materials and Structures, 2006. **39**(6): p. 655-664.

45. Xiao, J.Z., J.B. Li, and C. Zhang, *Mechanical properties of recycled aggregate concrete under uniaxial loading.* Cement and Concrete Research, 2005. **35**(6): p. 1187-1194.

46. Kou, S., C. Poon, and D. Chan, *Influence of fly ash as a cement addition on the hardened properties of recycled aggregate concrete.* Materials and Structures, 2008. **41**(7): p. 1191-1201.

47. Gonzalez-Fonteboa, B. and F. Martinez-Abella, *Concretes with aggregates from demolition waste and silica fume. Materials and mechanical properties.* Building and Environment, 2008. **43**(4): p. 429-437.

48. Berndt, M.L., *Properties of sustainable concrete containing fly ash, slag and recycled concrete aggregate.* Construction and Building Materials, 2009. **23**(7): p. 2606-2613.

49. Buttler, A.M. and J.E.F. Machado, *Properties of Concrete with Recycled Concrete Coarse Aggregates,* Special publication Aci Materials Journal, 2005. **229**: p. 497-510.

50. Neville, A.M., *Properties of concrete*. 1995, Harlow: Longman Group.

51. Mehta, P.K. and P.J.M. Monteiro, *Concrete: Microstructure, Properties, and Materials*. 2006, New York: McGraw-Hill.

52. Goldman, A. and A. Bentur, *The Influence of Microstructures on Enhancement of Concrete Strength.* Cement and Concrete Research, 1993. **23**: p. 962-972.

53. Newman, J. and B.S. Choo, *Advanced Concrete Technology: Constituent Materials*. 2003, London: Elsevier Ltd.

54. Sellevold, E.J., *Silica Fume - Cement Paste: Hydration and Pore Structure* 1982, Report BML 82.610 Norwegian Institute of Technologhy: Trondheim, Norway. p. 19-50.

55. Peter Hawkins, Paul Tennis, and R. Detwiler, *The use of limestone in the Portland Cement: A State-of-the-Art reveiw*. 2003, PCA, Portland Cement Association Skokie,Illinois, USA.

56. Moosberg-Bustnes, H., B. Lagerblad, and E. Forssberg, *The function of fillers in concrete.* Materials and Structures, 2004. **37**(2): p. 74-81.

57. Soutsos, M.N., K. Tang, and S.G. Millard, *The use of recycled demolition aggregate in precast concrete products – Phase III: Concrete pavement flags.* Construction and Building Materials, 2012. **36**(0): p. 674-680.

58. Pilakoutas, K., K. Neocleous, and H. Tlemat, *Reuse of steel fibres as concrete reinforcement.* Engineering Sustainability,, 2004. **157**(ES3): p. 131-138.

59. Graeff A., *Long-Term Performance of Recycled Steel Fibre Reinforced Concrete for Pavement Application*, in *Department of civil and Structural Engineering*. 2011, The University of Sheffield: Sheffield, UK.

60. Lee, M.K. and B.I.G. Barr, *An overview of the fatigue behaviour of plain and fibre reinforced concrete.* Cement and Concrete Composites, 2004. **26**(4): p. 299-305.

61. Altun, F., T. Haktanir, and K. Ari, *Effects of steel fiber addition on mechanical properties of concrete and RC beams.* Construction and Building Materials, 2007. **21**(3): p. 654-661.

62. Boulekbache, B., et al., *Flowability of fibre-reinforced concrete and its effect on the mechanical properties of the material.* Construction and Building Materials, 2010. **24**(9): p. 1664-1671.

63. Centonze, G., M. Leone, and M.A. Aiello, *Steel fibers from waste tires as reinforcement in concrete: A mechanical characterization.* Construction and Building Materials, 2012. **36**(0): p. 46-57.

Chapter 3

Assessment of Post-Restrained Shrinkage Mechanical Properties of Concrete- Pilot Study

Younis, K.H. and K. Pilakoutas, *Assessment of post-restrained shrinkage mechanical properties of concrete using a new test.* ACI Materials journal, 2014.***Submitted***.

This chapter proposes a simple and economical test rig for restrained shrinkage and associated procedures to assess the post-shrinkage mechanical properties (compressive and flexural strength) of concrete. Free and restrained shrinkage tests were conducted and the change of apparent restraint factor (RF) with time was determined. A simple finite element analysis was performed to quantify the theoretical RF and the results were compared to the apparent RF. The results show that the restraining factor of the proposed rig is dependent on the time and the stiffness of the concrete. Results of residual mechanical properties show that restrained shrinkage induced cracks can affect the mechanical behaviour (flexural and compressive strength and stiffness) of concrete by up to 21%.

This chapter consists of a "stand alone" journal paper and includes relevant bibliography at the end of the chapter. Typical results are presented in this chapter and Appendix D provides more test results.

3.1 Introduction

Due to chemical, thermal and physical changes, concrete develops unavoidable complex volume changes which lead to time-dependent internally induced deformations. Drying and autogenous shrinkage are the results of such changes. Restraint against these internally induced deformations results in stress development [1], which can lead to cracking, if such stresses exceed the instantaneous tensile strength of concrete [2]. Cracks, induced by restrained shrinkage, can cause issues with serviceability and structural integrity. Shrinkage induced cracks can also compromise durability by affecting properties such as permeability, diffusivity and sorptivity, enhancing the ingress of detrimental substances, freeze-thaw damage, corrosion of steel reinforcement and spalling. All these premature deteriorations and structural deficiencies often occur prior to the application of external loads. Therefore, the excessive development of concrete cracks should be controlled at early ages [3, 4].

If there is no restraint against volume changes, no significant cracks are expected to develop. However, all concrete elements are practically restrained to some degree, since some internal or external restraint always exists [5]. External restraint may result from supporting elements (e.g. walls and columns), contact with adjacent elements, and (in the case of concrete pavements or slabs on grade) applied loads and base friction [1, 6]. Internal restraint sources comprise of aggregates and reinforcement [7, 8]. Internal restraint can also be caused by non-uniform drying shrinkage, which is usually caused by either moisture or temperature gradients [1].

The best way to mitigate the effect of shrinkage deformations is to prevent the loss of moisture and protect the concrete from rapid cooling. Nonetheless, from a practical perspective, the complete elimination of internal deformations is impossible. Hence, it is important to find ways of quantifying restrained strains and associated stresses so as to account for them at the design process.

Restrained shrinkage is a major design issue for concrete pavements. Technical report No.34 of Concrete Society [9] identifies the need for shrinkage induced stresses to be included in the design procedures of concrete industrial floors and slabs on grade. However, due to lack of advanced knowledge and design models, in the calculation of the hogging moment capacity of the slabs, a fixed value of restrained flexural tensile stress is subtracted from the flexural tensile strength of the concrete irrespective of the material properties and geometry of the element. This restrained tensile stress is calculated using free shrinkage strains.

Nonetheless, TR34 does identify that the interaction between shrinkage induced stresses and those caused by external loading need further research.

Free shrinkage tests can provide information on the shrinkage behaviour of different concrete mixtures, based on the environmental conditions, and size and shape of concrete elements being assessed. However, such tests cannot provide information on the post-cracking behaviour of concrete under restrained conditions [10-14]. Restrained shrinkage tests help in the assessment of cracking tendencies and the ability of concrete to withstand shrinkage induced tensile stresses [1, 2, 15].

There is no standardized test to assess the post shrinkage behaviour of concrete under restrained conditions [10, 14, 15]. However, both the American Association of State Highway and Transportation Officials (AASHTO in 2008) and the American Society for Testing and Materials (ASTM in 2004) adopted the ring test [16] (see Fig. 3.1) as a standard test for restrained drying shrinkage. Simplicity and versatility, are the main features of this test. For a given drying environment, the ring test can provide information on the age at cracking, the width and rate of crack width increase with time. This information can be used to compare the cracking sensitivity of different concrete mixtures or to assess the efficiency of materials such as fibres in controlling crack width [1, 13]. However, the test has the following drawbacks:

a- The test does not simulate and cannot predict concrete cracking in actual service life, and rather reflects the relative cracking tendency of concrete mixtures [13, 17, 18],

b- The strains used to calculate the elastic stresses are not measured directly from the concrete; instead they are measured on the outer face of the steel ring (see Fig. 3.1), assuming a linear stress distribution throughout the steel ring [1],

c- The restrained shrinkage strain obtained from the ring test cannot be compared directly with the free shrinkage strain of prismatic specimens [19],

d- The test cannot quantify the residual strength of cracked concrete.

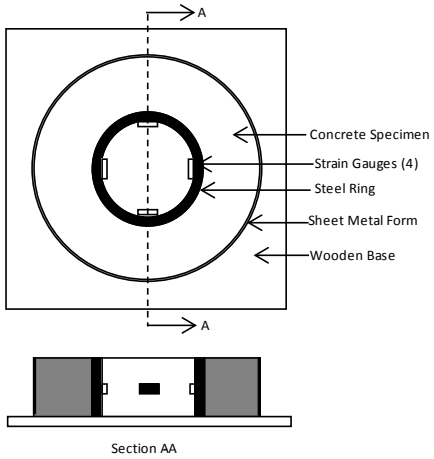

Figure 3. 1 Ring test apparatus.

Several other test methods for restrained shrinkage have been proposed [20]. These can be classified by the shape of the specimen into plate or linear tests [21], with the former providing biaxial restraint, whereas the latter providing uniaxial restraint. In linear tests, the ideal configuration to provide full restraint against shrinkage strains is to rigidly fix the concrete specimen at its ends (see Fig. 2a). This is practically impossible since an infinitely stiff reaction frame and fixity/gripping system is required. Therefore, other more practical solutions have been attempted using 'passive' (Fig. 2b) and 'active' restraint control (Fig. 2c) [20].

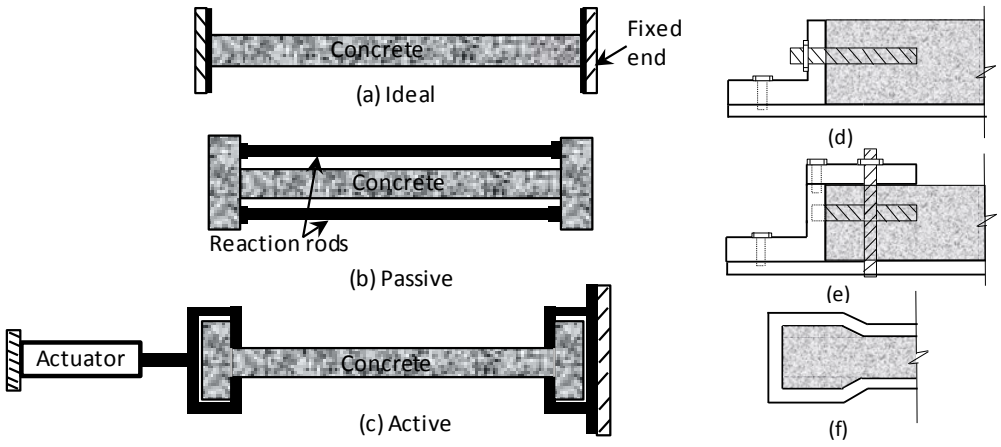

Figure 3. 2 (a-c) Schematics of previously attempted configurations to simulate restrained shrinkage, (d-f) End gripping arrangements.

In linear-passive tests (e.g. RILEM test [22]), the restraint is provided by stiff steel sections or by embedding restraining steel reinforcement bars in the specimen ends (the bar being

debonded in the middle part only) [2, 23, 24]. Passive tests usually provide partial, often unknown, level of restraint. In linear-active tests, one end is fixed (restrained) and the other is left free [20]. The free end is either manually adjusted using a screw [25, 26] or using an actuator [27], but these can be fully/actively computer controlled to simulate full fixity [28] (provided the gripping system is rigid). This method has the merit of quantifying tensile creep strains and is used by others [15, 29, 30].

Different mechanisms can be used to grip the ends of the concrete specimen. These mechanisms include:

1- bolt anchors using a number of steel threaded bars at the end of the concrete specimen (see Fig. 2d) [31, 32],

2- lateral clamping utilizing steel plates and threaded bars at the ends of the specimen to clamp the ends against the reaction frame (see Fig. 2e) [14],

3- fixity using enlarged end specimen to fit into steel grip reaction at the ends (e.g. dog-bone, see Fig. 2f) [22, 28].

4- epoxy to bond the concrete specimen to end supports and the reaction rig [33].

From linear tests, a variety of concrete properties can be obtained such as: shrinkage (drying and autogenous) strain and stress, age of cracking, crack width, creep strain of concrete, development of tensile stress with time and degree of restraint. From a practical point of view when many parameters are needed to be examined, the setting up of such tests and their instrumentation can be complicated and expensive. Automatic strain measurements are also difficult since cracking positions are not known a-priori. The small dimensions of the specimens used in some of these tests, mainly to reduce costs, is also another issue, since they limit the use of normal size coarse aggregates. In fact, in some of these tests no coarse aggregate is used at all [18]. Another issue to consider is how to dismount the concrete specimen at the end of the drying exposure time without destroying it. As a result of these difficulties, such tests are avoided in common quality control testing and large-scale parametric study investigations [1, 19, 34].

The impact of shrinkage induced cracks due to external restraints on the mechanical properties (compressive strength, flexural strength and stiffness) of concrete is not well studied and in fact, there is no standard experimental procedure to quantify the effect of shrinkage cracks on these properties. Nonetheless, these are the most important properties

needed to design restrained concrete elements, such as slabs on grade. For this reason, the current study attempts to develop a simple and economical test rig for restrained shrinkage and a procedure that can quantify the post-shrinkage residual mechanical properties of concrete.

The proposed rig is presented next followed by details of the experimental procedure used to evaluate its effectiveness. These are followed by a critical discussion of the results and recommendations for improvements.

3.1.1 Research Significance

Cracking due to restrained shrinkage is a major concern for both serviceability and durability of concrete. To account for such issues at the design process, quantifying restrained strains and associated stresses are crucial. The absence of a standard or a practice test to quantify the effect of shrinkage induced cracks on the mechanical properties of concrete complicates the issue. This study is an attempt to develop a new restrained shrinkage test and a procedure to quantify the post-shrinkage residual mechanical properties.

3.2 Proposed Restrained Shrinkage Test Rig

For a restrained shrinkage test, a suitable starting point was found in the configuration used by Weiss *et al*, [14] that aimed at developing a test method for assessing the shrinkage cracking potential of normal and high strength concrete (with and without fibres) for pavement applications (see Fig. 3.3). Nonetheless, the section size used by Weiss *et al* was only 25 mm and hence, a deeper specimen is required to: 1) enable the use of coarse aggregate (20 mm), 2) to allow the specimens to be used for flexural tests (e.g the ASTM C1018-97). However, the increase in depth requires more effective end restraint conditions. Furthermore, the test-rig should allow the demoulding of the concrete specimens at an early stage and the demounting at the end of the restraining period.

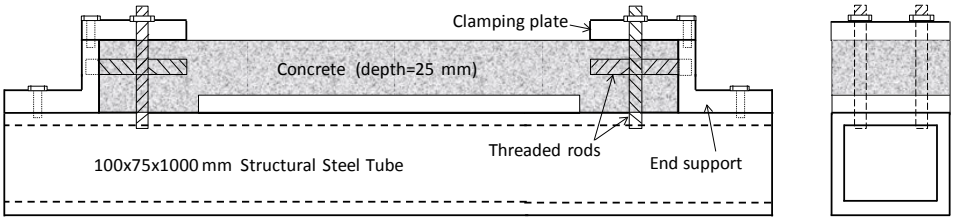

Figure 3. 3 Geometry of the restraining rig used by Weiss et al.[14]

Fig. 3.4 shows the general layout of the developed rig. Fig. 3.5 shows a photo of the rig and mould during the assembly stage.

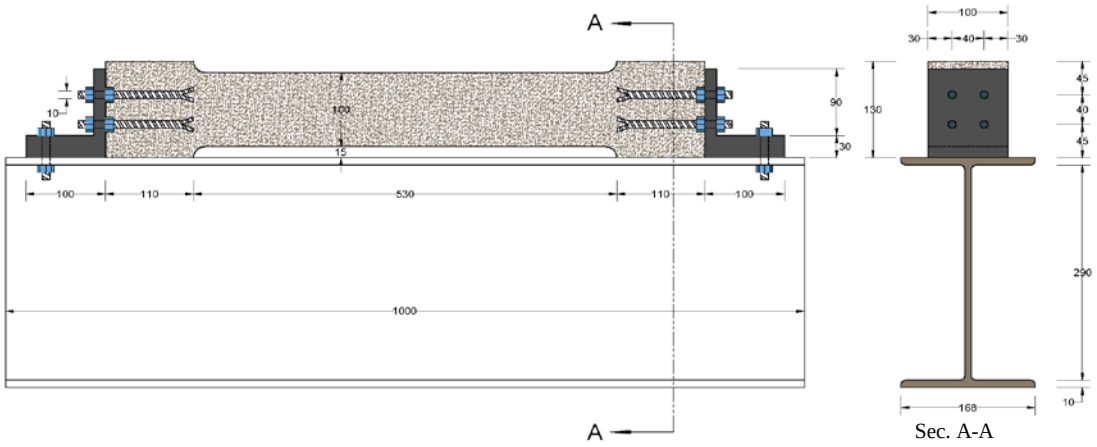

Figure 3. 4 Front view of the developed rig for restrained shrinkage test.

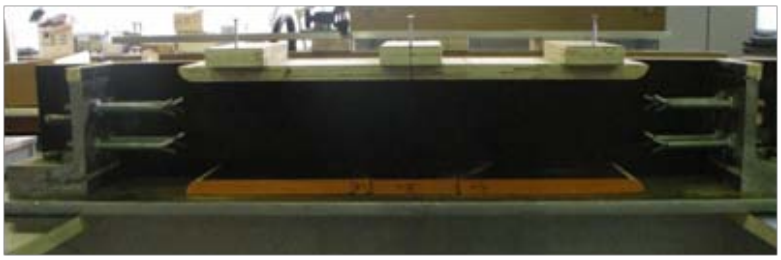

Figure 3. 5 The developed rig after manufacturing.

The new set up consists of a reaction beam (I-section) with sufficient dimensions to provide enough stiffness (at least 4 times the stiffness of hardened concrete) to resist axial shortening. The reaction beam is 1m long with its upper flange polished to provide a smooth and slippery surface to ensure that the restraint only develops at the ends. Two L-shaped steel supports are bolted to the flange to provide restraint at the ends of the concrete specimen. The concrete ends are fixed to the steel angles by four bolts split at the ends to increase their ability to grip the concrete. These bolts will enable easy dismounting of the concrete specimen after the completion of the drying period.

The concrete section is reduced from 130 mm to 100 mm away from the supports to avoid crack formation at the anchorage zone. Furthermore, to achieve a more uniform drying condition around the concrete section, removable framework is used to separate the bottom of the concrete surface from the steel surface. To achieve this, a timber plate (15 mm thick

and 530 mm long with curved ends) cut into three parts with a wedge at the mid-section is used to ensure easy removal (24h) after casting the concrete specimen. A similar plate is used on the top face.

The proposed rig was used in trial tests described below to assess its effectiveness in quantifying the post-shrinkage residual mechanical properties of concrete.

3.3 Materials and Experimental Procedure

3.3.1 Materials and specimen preparation

Portland Cement CEM I 52.5 N, meeting the requirements of BS EN 197:2009 [35] was used in this research. The fine aggregate used in this study was sand with a maximum size of 5 mm. The coarse aggregate was river aggregate with maximum size of 20 mm.

The mix proportion was cement: water: sand: gravel= 390:176:560:1111 (kg/m^3) with w/c ratio 0.45.

In the moulds, the concrete was cast in three layers, and each layer was compacted using the vibrating table. The specimens were then covered by plastic sheet and allowed to cure for 24 hours before being demoulded. A slightly shorter (500 mm long) control prism was stored in water and a second control prism (750×100×100 mm) for free shrinkage test was stored next to the restrained specimen at 22 ±2 ^{o}C and RH of 45 ±5 %. Furthermore, 15 cubes (100 mm) were cast to determine the compressive strength at different times.

Immediately after demoulding, Demec gauge points were fixed to the concrete surface at 50 mm spacing (see Fig. 3.6) using a rapid-hardening adhesive on the top and side surfaces.

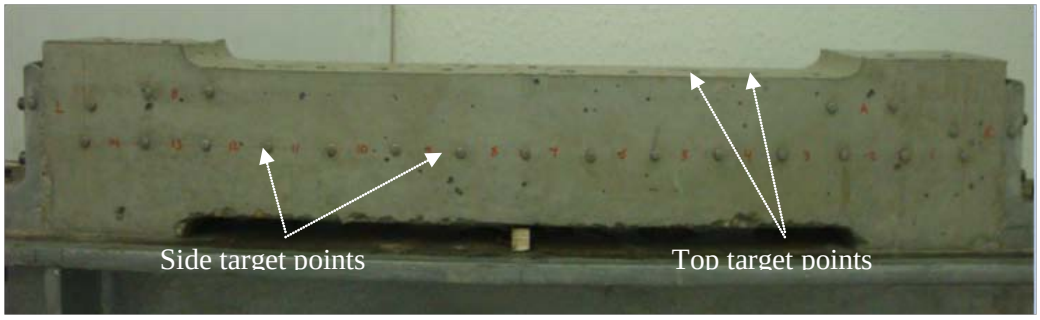

Figure 3. 6 Distribution of Demec points for restrained specimen.

3.3.2 Tests

3.3.2.1 Free and Restrained Shrinkage

Three Demec gauges were used to measure strains having lengths of (50, 100 and 300 mm and precision of 20, 16 and 5.2 με. The first shrinkage strains were measured at 24 h (soon after the adhesive hardened) and at 24 h intervals for the first week, followed by measurements at 10,14, 21 and 28 days. Two or three readings were taken for each gauge length, and the average values calculated.

According to ACI 207.2R-95 [36] the degree of restraint or restraint factor (RF) is given as the ratio of actual stress induced by the restrained volume change to the stress which would develop if the specimen was fully restrained. In other words, it is a ratio between the amount of strain that is restrained to the free shrinkage strain [37, 38]. Assuming the modulus of elasticity is constant, equation 3-1 can be used to calculate the RF:

$$\mathrm{RF} = \frac{\varepsilon_R}{\varepsilon_{free}} \qquad (3\text{-}1)$$

where:

ε_R Restrained shrinkage strain = shrinkage strain measured on the free specimen - shrinkage strain measured on the restrained specimen.

ε_{free} Free shrinkage strain (strain measured on the free specimen).

CRACK DETECTION

Regular daily checks for cracks were performed using an optical microscope with a magnification factor of 40x and a precision of 20 μm and a digital microscope with a magnification up to 200x and a precision of 10 μm. The crack width reported here is the crack opening at its widest, normally at the edge of the specimen.

There is no clear definition of what is a microcrack in the literature. RILEM committee (TC-122-MLC on "Microcracking and life time performance of concrete", cited in [39]) uses width of less than 10 microns to define microcracks. Others [39-41] adopt 50 microns. In this study 20 microns or less was used to define the microcracks, as it was found that cracks with width larger than 20 microns are visible to the naked eye when properly illuminated.

3.3.2.2 Loss of Mass (loss of moisture)

The loss of mass for the free shrinkage specimen was determined using a balance with the precision of 0.1 g. The first reading, which is considered as the initial mass, was measured at 24 h, after the Demec points were bonded. Thereafter, the readings were obtained at the same time intervals as for the free shrinkage measurements.

3.3.2.3 Compressive Strength

The compressive strength was obtained at 1, 3, 7, 28 and 75 days using the (100 mm cubes) and BS EN 12390-3 [42]. The compressive strength was also obtained from the two prisms (free and restrained) tested in bending, by following the recommendations of BS 1881-119 [43].

3.3.2.4 Flexural tests

All prisms were tested in four-point loading over a length of 300 mm following the recommendations of the ASTM C1018 (1997) [44] using a universal testing machine in displacement control. A yoke was used to mount the deflection transducers and to eliminate errors from support displacement and torsion. The central deflections were determined from the average of two linear variable displacement transducers (LVDTs) placed on opposite sides of the specimen. From the load versus-deflection curve, the flexural strength and stiffness were calculated. Equation 3-2 was used to determine the flexural modulus of elasticity E_{flex} (GPa) from the stiffness, based on the theory of classical elasticity.

$$E_{\text{flex}}(GPa) = \frac{23P}{1296\delta}.\frac{L^3}{I}\left[1+\frac{216}{115}\left(\frac{h}{L}\right)^2(1+\nu)\right] \qquad (3\text{-}2)$$

where :

P/δ is the slope of the linear elastic part of the load-deflection curve (kN/mm); L is the supported span of the prism (mm); I is the second moment of area of the cross-section (mm^4); b is the width of the cross-section (mm); h is the height of the cross-section (mm); and ν is the Poisson's ratio. The flexural elastic modulus of concrete (E_{fmax}) was determined as the maximum value of E_{flex} in the range of 30% to 60% of the ultimate bending load (see Appendix D).

3.4 Experimental Results and Discussion

3.4.1 Free Shrinkage Strains

Fig. 3.7 and Fig. 3.8 show the results of free shrinkage strain using the three gauge lengths 50, 100 and 300 mm taken from the side and top surfaces, respectively. As expected the shrinkage rate is high at the early age slowing down with time; the shrinkage strain after one week was almost 40% of that measured at 75 days. Fig. 3.7 and Fig. 3.8, also show that the measured strains using the different gauge lengths are similar.

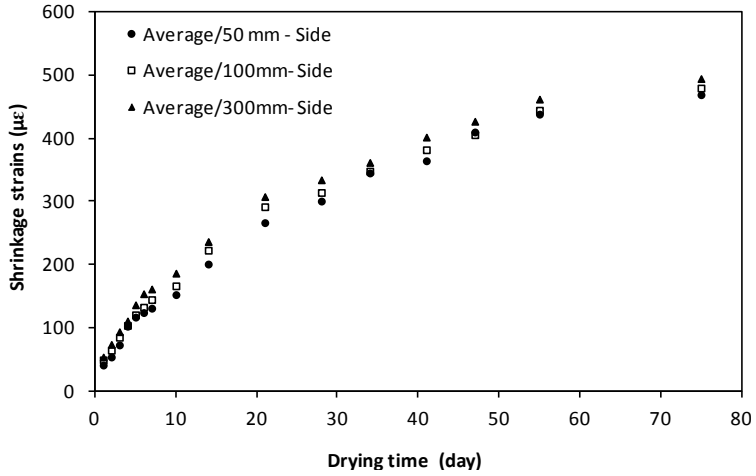

Figure 3. 7 Free shrinkage strains of the side surface

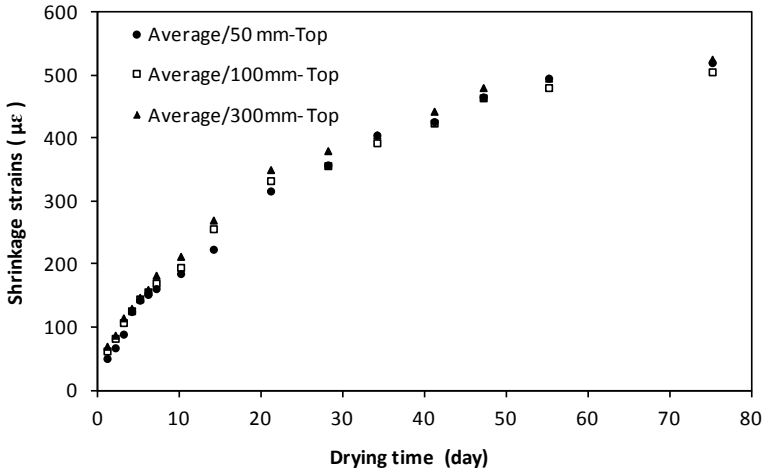

Figure 3. 8 Free shrinkage strain of the top surface.

The shrinkage strains measured on the top surface of the concrete specimen are slightly higher than those measured on the side surface. This may be due to concrete bleeding which usually happens at the top (trowelled) surface altering the microstructure of this surface and possibly resulting in slightly higher porosity which in turn causes more shrinkage.

Furthermore, concrete is better compacted at bigger depths resulting in more dense concrete, which tends to shrink less.

3.4.2 Restrained Shrinkage Strains, RF and Characterisation of Cracks

The shrinkage strains measured on the side of the concrete specimen are shown in Fig. 3.9 (for 50 mm gauge length) and in Fig. 3.10 (for the 300 mm gauge length). Fig. 3.10 represents the average shrinkage strains that occurred over time for 14 individual distances. The development of large strains on the restrained sample indicates that the developed rig only provides partial restraint.

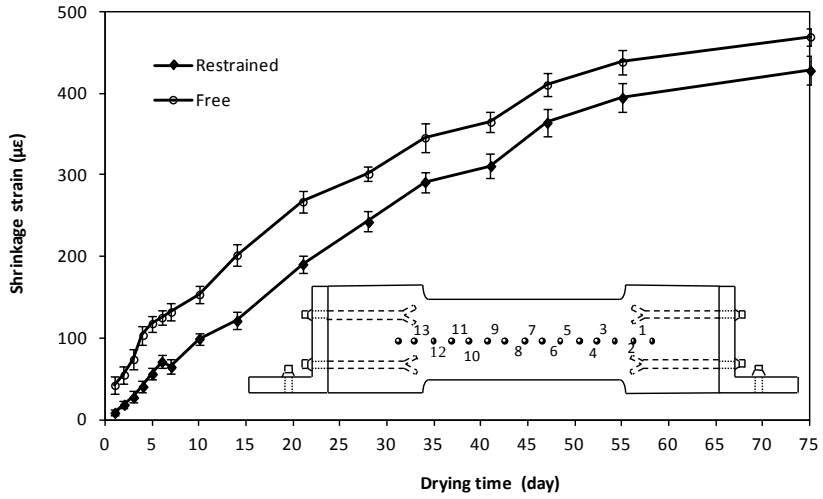

Figure 3. 9 Shrinkage strains of the restrained specimen using 50 mm gauge length.

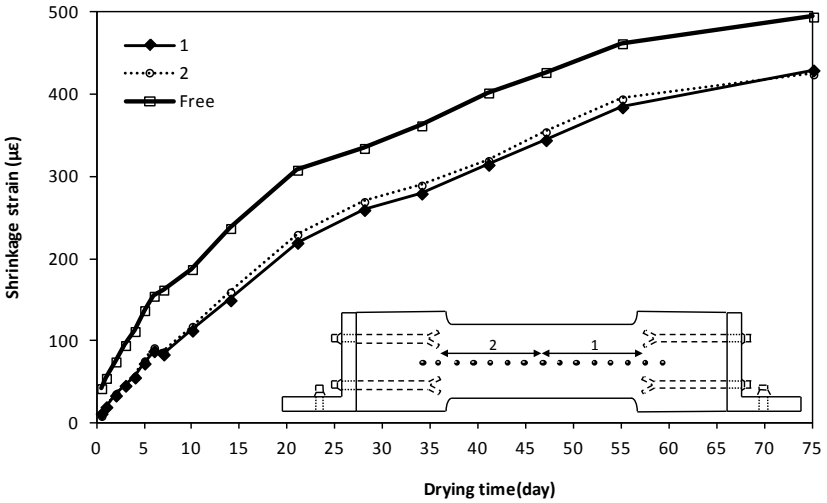

Figure 3. 10 Shrinkage strains of the restrained specimen using 300 mm gauge length.

Fig. 3.11 shows that the RF was 64% on the first day. After 5 days of drying, it decreased to almost 46%. Thereafter, it decreased to 21% at 28 days and around 14% at 75 days.

Microcracks occurring at the ends of the sample also reduce the restraint efficiency, resulting in a lower degree of apparent restraint.

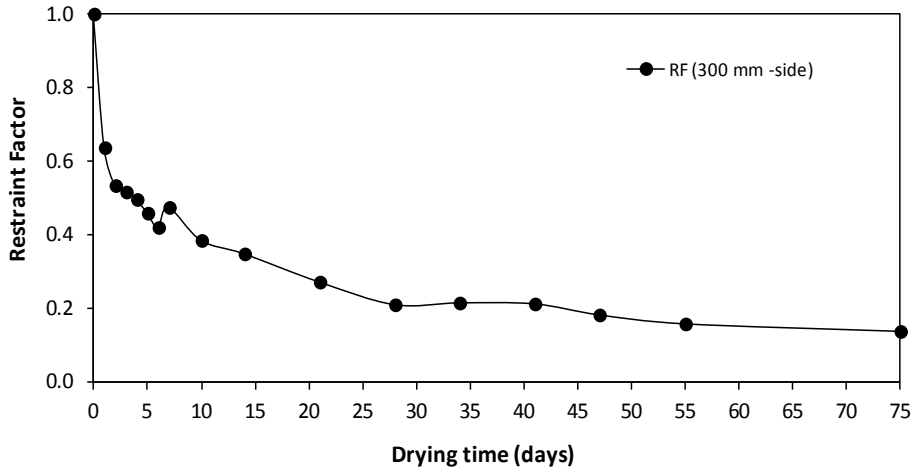

Figure 3. 11 RF calculated from the strains measured (on the side of the specimen) using 300mm gauge length.

After 1 day of drying, the first microcracks were detected at several positions using the digital micro-scope. A slight reduction in the shrinkage strain was observed (see Fig. 3.11) after 7 days of drying, though no visible cracks were observed. Such a reduction can only be due to cracks developing further. After 9 days of drying few visible cracks were recorded at the top edges of the specimen. The width of the visible cracks were in the range of (0.025-0.035) mm when first detected. Similar observations were reported by Grzbowski and Shah [10] and Weiss *et al* [14] during the monitoring of restrained concrete specimens (ring type), as they noticed a decrease in the strain measured on the steel ring prior to the detection of cracks. Many microcracks were detected by the microscopes, but only 10 visible cracks were observed. Details on the visible cracks at 75 days are summarized in Table 3.1.

Table 3. 1 Cracking time and width and length of cracks (Note: 1mm = 0.04in).

Crack code	Drying time (day)*	Crack width (mm)		Crack length (mm)	
		Initial	Final **	Initial	Final ***
1	9	0.025	0.055	15	43
2	9	0.025	0.035	12	32
3	9	0.025	0.045	10	35
4	9	0.025	0.04	12	30
5	10	0.035	0.045	11	38
6	11	0.025	0.04	11	25
7	11	0.025	0.04	12	28
8	11	0.025	0.045	12	30
9	11	0.02	0.04	12	33
10	11	0.02	0.04	11	30

* Drying time when the crack is visible. ** Crack width at age 75 days. *** Crack length at age 75 days.

Crack growth was very slow (see Table 3.1). The maximum crack width measured was 55μm (crack 1) at the age of 75 days. Although visible cracks developed on both sides of the restrained specimen, none of them propagated and turned into a through crack. This can be attributed to the following reasons: a- the cracks that formed at the ends of the specimen may have reduced the degree of restraint, b- the slow rate of shrinkage strain development after the first week of exposure, c- the effect of tensile creep which can serve to relax shrinkage stresses.

The distribution of the cracks at age 75 day is shown in Fig. 3.12.

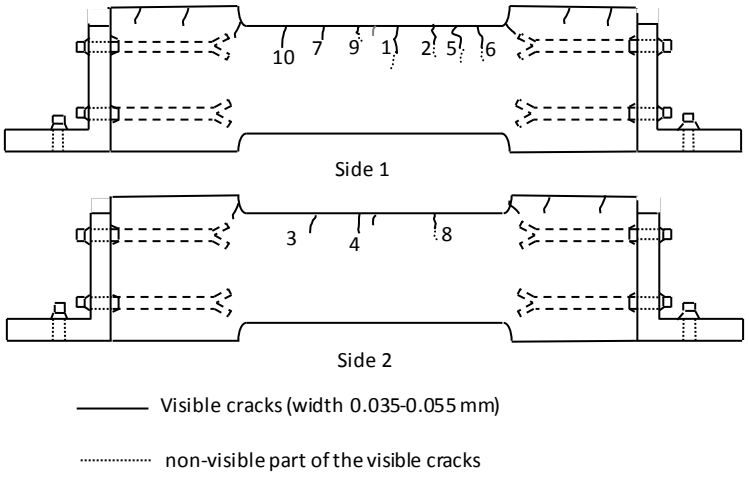

Figure 3. 12 Crack distribution at day 75 on the sides of the restrained specimen.

Microcracks were also observed on the surfaces of the free shrinkage specimens. These randomly distributed discontinuous cracks had a net shape and developed at different areas on the surfaces of the concrete. The larger crack width at day 75 was 0.02 mm. The main cause of such cracks is internal restraint (differential drying) caused by moisture gradient.

3.4.3 Mass Loss

Mass loss versus time is presented in Fig. 3.13a. It can be seen that mass loss is faster at the early stages, behaving in the same way as shrinkage. Nonetheless, when shrinkage strain is plotted against mass loss (see Fig. 3.13b), a different trend can be seen as the initial rate of mass loss is much faster than the shrinkage strain rate. This may be due to the fact that during the first week, though moisture is lost at a higher rate, this moisture is being lost from coarse pores, resulting in relatively low shrinkage due to low capillary pressures. With further drying, finer pores start to lose moisture, causing higher capillary pressure, thus resulting in higher shrinkage for a smaller mass loss.

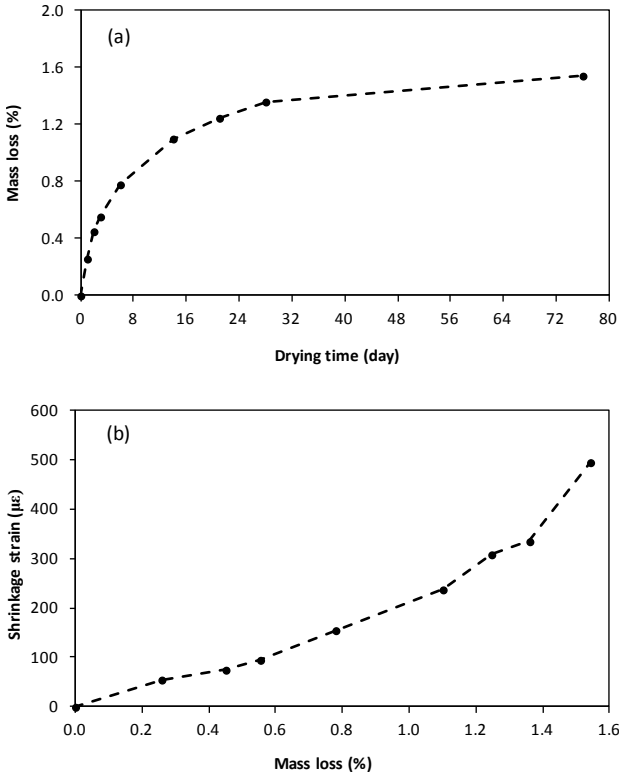

Figure 3. 13 a-Evolution of mass loss of the free sample, b- Mass loss against shrinkage strain

3.4.4 Effect of strain loss on RF and cracking development

It is evident from the recorded strain loss on the prisms that the rig only offers partial restraint. Strain loss may occur due to deformations of the restraining beam (bending and contraction) and the end supports (L-shape) caused by the tensile force applied by the restrained concrete (see Fig. 3.14). Finite element elastic analysis (Fig. 3.15) shows that the greatest part of strain loss is caused by the deformation of the end supports. For example, the magnitude of the expected tensile force resulting from a 100 με shrinkage strain (E_c=26 GPa), will lead to a strain loss of 20 με due to shortening and 43 με due to beam bending. The same force would also pull-in the end supports with a corresponding strain loss of 200 με. Part of these elastic strain losses will be counteracted by the creep effect.

Figure 3. 14 Schematic representation the deformations of the rig caused by the restrained shrinkage of concrete.

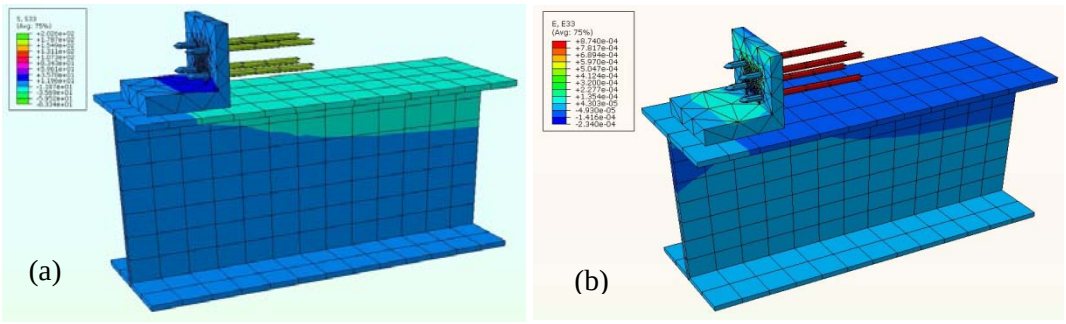

Figure 3. 15 Finite element analysis a-stresses , b- strains.

To estimate the variation of the RF over time and compare it with the apparent (measured) RF (Fig. 3.11), the ratio between the stiffness of the concrete and the rig must be known. This can be determined by using equilibrium and compatibility conditions. Equation 3-3 represents the equilibrium equation of the forces that develop in the concrete (tensile force, F_c or F_{rig}) due to restrained shrinkage.

$$F_c = F_{rig} \tag{3-3}$$

$$E_c A_c \varepsilon_c = E_{rig} A_{rig} \varepsilon_{rig} \tag{3-4}$$

where:

E_c, E_{rig} = elastic modulus of concrete and rig, respectively.

A_c, A_{rig} = cross-sectional area of concrete and rig, respectively .

ε_c = restrained shrinkage strain.

ε_{rig} = strain developed in the rig due to shrinkage induced forces.

$$\frac{E_c A_c}{E_{rig} A_{rig}} = \frac{\varepsilon_{rig}}{\varepsilon_c} \tag{3-5}$$

$$\text{if} \quad K = \frac{E_c A_c}{E_{rig} A_{rig}} \tag{3-6}$$

$$\text{then} \quad K = \frac{\varepsilon_{rig}}{\varepsilon_c} \tag{3-7}$$

Hence, the stiffness ratio (K) between the concrete and the restraining rig is equal to the ratio of the restrained shrinkage strain of concrete (ε_c or ε_R), which results in developing a tensile force inside the concrete, to the strain of the rig (strain loss, ε_{rig}) caused by the same force (see Fig. 3.16).

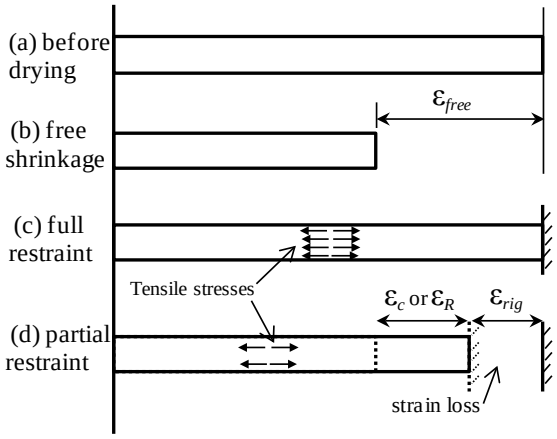

Figure 3. 16 Shrinkage induced strains (deformations) in concrete and rig.

From Fig. 3.16, the strain compatibility equation can be developed as follows:

$$\varepsilon_c + \varepsilon_{rig} = \varepsilon_{free} \tag{3-8}$$

From equation (3-7):

$$\varepsilon_{rig} = K\varepsilon_c \tag{3-9}$$

Then: $$\varepsilon_c + K\varepsilon_c = \varepsilon_{free} \tag{3-10}$$

$$\varepsilon_c or \varepsilon_R = \frac{\varepsilon_{free}}{1+K} \tag{3-11}$$

Since, $$RF = \frac{\varepsilon_R}{\varepsilon_{free}} \quad \text{(eq. 3-1)}$$

Then, the estimated RF is: $$RF = \frac{1}{1+K} \tag{3-12}$$

Equation 3-12 can be used to assess the effect of E_c on the estimated RF. By using the same previous example for E_c =26 GPa, K is 2.63 and the estimated RF at this particular concrete stiffness is 0.28. Fig. 3.17 shows the effect of the E_c on the estimated RF by substituting

different values of E_c in equation (3-12). The trend of the curve in the Fig. 3.17 is natural, as an increase in E_c results in a higher restraining force and higher strain loss; hence decreasing the RF.

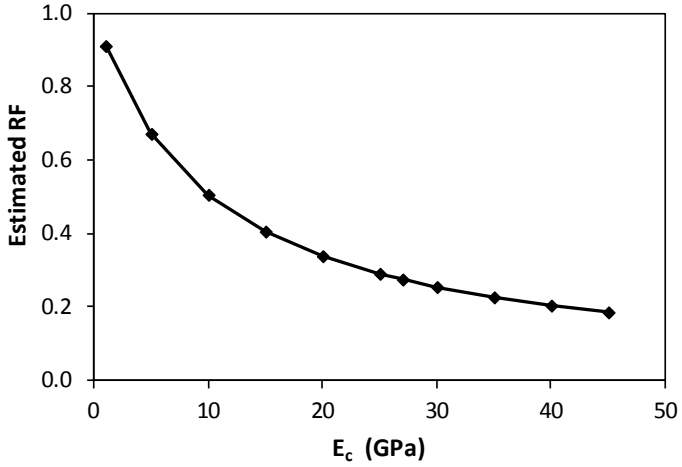

Figure 3. 17 Effect of elastic modulus of concrete (E_c) on the estimated RF (Note: 1 GPa = 145 ksi).

The above relationship can be used to determine the variation of the estimated RF over time. This can be done if the development of E_c over time is known. E_c can be linked to compressive strength by using equations such as those given by Eurocode-2 [45] and the development of the compressive strength with time is known from the measurements, as shown in Fig. 3.18.

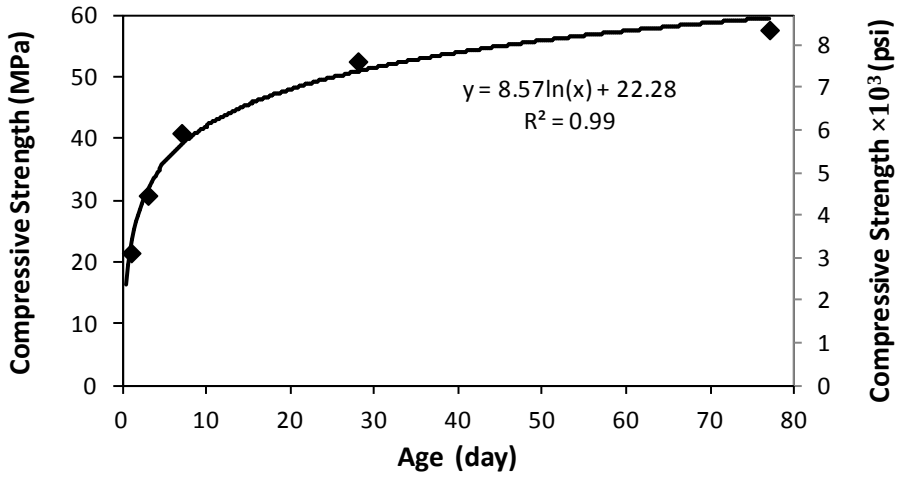

Figure 3. 18 Development of compressive strength (Note: 1 MPa = 145 psi).

Fig. 3.19 shows the variation of the estimated and apparent RF over time. It can be seen that the apparent RF is higher than the estimated RF (up to 25days). This may be attributed to the fact that the estimated RF does not include the effect of tensile creep/relaxation which reduces the tensile stress, resulting in a lower stain loss and consequently higher RF. Once the concrete cracks, the concrete stiffness is reduced and the apparent RF increases temporarily as a consequence.

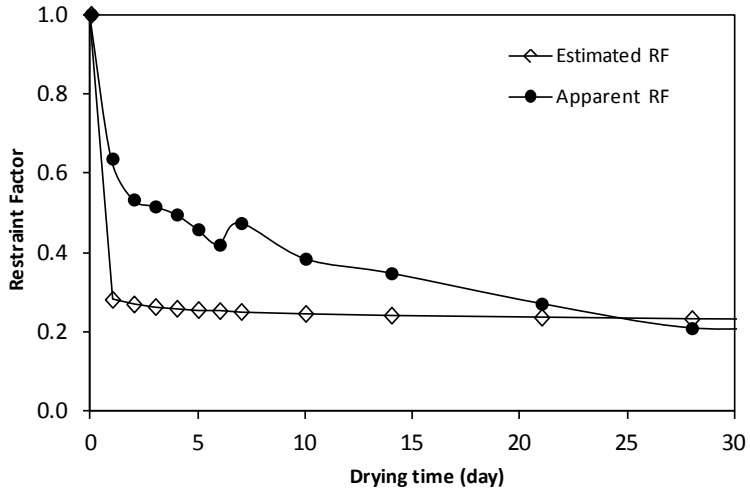

Figure 3. 19 Variation of estimated and measured RF over time.

Fig. 3.20 shows the variation over time of the ratio of the estimated elastic tensile stress to the instantaneous predicted tensile strength of concrete. The predicted tensile strength is obtained using Eurocode 2 model for development of compressive strength [45]. The tensile stress developed in the concrete is calculated based on the RF, free shrinkage and E_c (product of: RF× ε_{free} × E_c). It can be seen that the developed stress using the estimated RF leads to a lower stress/strength ratio than that of apparent (measured) RF. This may again be attributed to creep effects. A high stress/ strength ratio (around 0.75) can also be seen developing at early stages of drying and, this ratio increased to 0.98 at 7 days. This predicts very well the time of development of the first crack, which became visible after 9 days of drying.

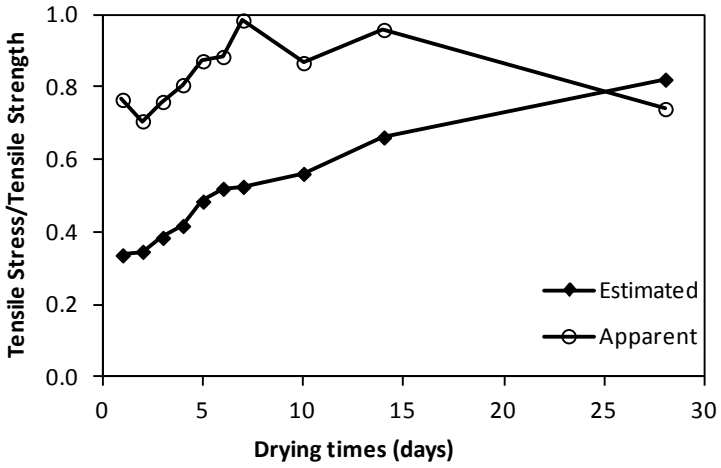

Figure 3. 20 Variation of stress/strength ratio over time.

3.4.5 Compressive Strength

Almost all previous studies utilized uniaxial compression strength to quantify the effect of drying on concrete mechanical properties. The results of the compressive strength for the water cured cubes (WC/cubes) and portions of tested prisms (WC/prism) and the residual compressive strength of the free and restrained specimens at 77 days, are shown in Fig. 3.21. The result is the average of 3 samples for the cubes and 2 samples for the prisms. The compressive strength (cubes) at 28 days was 52.5 MPa. It can be seen that the compressive strength of the concrete exposed to restrained shrinkage reduced by 19% in comparison to that of WC/prisms and 14% in comparison to the free specimen.

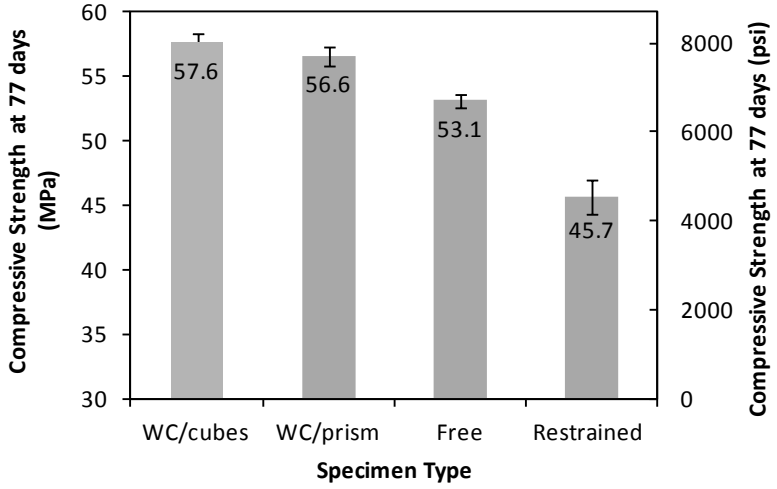

Figure 3. 21 Results of compressive strength. (Note: 1 MPa = 145 psi).

The mechanical properties (strength and stiffness) of concrete may be affected by the drying shrinkage (without external restraint) in two ways. On the one hand, the strength increases as a result of an increase in capillary pressure (which acts as isotropic pressure) on the C-S-H particles when the saturation decreases. This can lead to a stiffening effect by increasing the bonding between the C-S-H particles [46] [47] [48] . On the other hand, the strength and the stiffness decrease due to the formation of microcracks (which develop due to non-uniform shrinkage, enhanced by local restraint by the aggregates) [46]. In these tests it is clear that shrinkage cracks were dominant in reducing the compressive strength.

3.4.6 Flexural Strength and Flexural Elastic Modulus

The load-deflection curves of water cured (control) specimen, free specimen and restrained shrinkage specimen are shown in Fig. 3.22. The unrestrained air and water cured specimens behave in a similar manner having similar flexural stiffness (around 40GPa) and similar strength (air 5.94 MPa and water 6.21 MPa). The restrained specimen only reached around 82% (4.89 MPa) of that of unrestrained specimen. This means that the restrained shrinkage induced cracks caused a reduction of around 18% in its flexural strength. These cracks not only affected the strength, but also reduced the initial stiffness (flexural modulus of elasticity). Fig. 3.23 shows the estimated flexural modulus of elasticity (E_{flex}) against the bending load. The E_{fmax} is normally determined in the range of 30-60 % of the ultimate bending load (linear part of the load-deflection curve where E_{flex} is almost constant). The E_{fmax} of the restrained specimen (31.6 GPa) is lower than that of both the free shrinkage (40.5 GPa) and the control specimen (40.0 GPa). Restrained shrinkage induced cracks led to around 21% loss in flexural stiffness affecting the stiffness in exactly the same way as the strength.

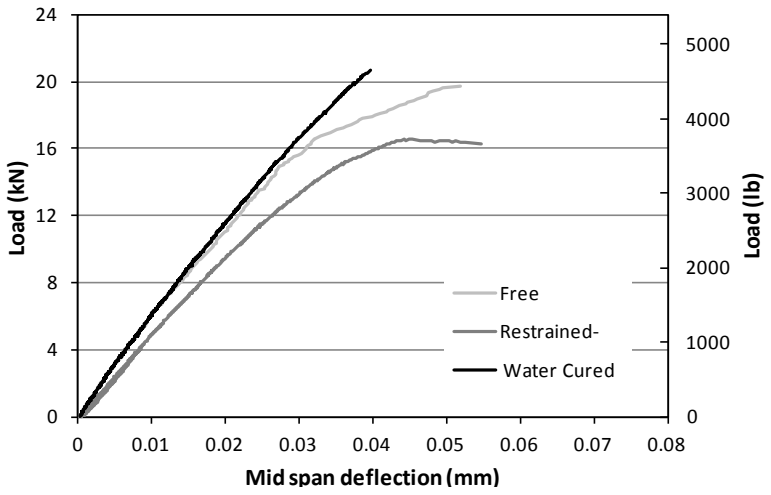

Figure 3. 22 Mid -span deflection versus bending load (Note: 1 kN=224.8 lb).

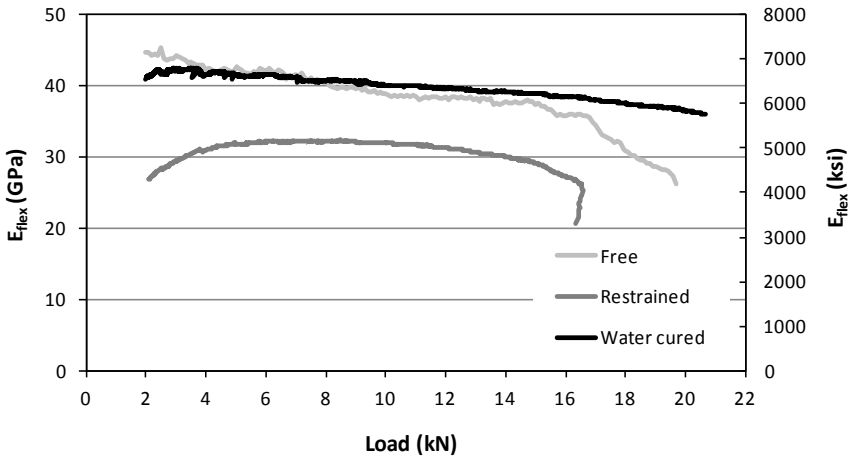

Figure 3. 23 Flexural elastic modulus (E_{flex}) versus bending load (Note 1 GPa= 145 ksi).

3.4.7 General Discussion

The proposed rig for restraining concrete only provided a variable RF which started for around 0.64 and ended up at around 0.2. The drop of RF with time can be explained by the development of the concrete stiffness. The rig managed to provide enough restrain to lead to concrete cracking due to exceedance of the flexural strength around 7 days. More restraint will help, but it is unlikely that the effect on residual stiffness will be great since it is clear that concrete autoheals. Nonetheless, most of the strain loss is a result of rig deformations and an improved rig needs to be developed. To counteract the change in RF with time, the rig could be prestressed before concrete casting and the stress released as the concrete hardens.

3.5 Conclusions

This paper proposes a new rig and a test procedure to assess the post shrinkage cracking mechanical behaviour of concrete. Results from bending and compression tests showed that restrained shrinkage induced cracks can affect the mechanical behaviour (flexural and compressive strength and flexural stiffness) of concrete by up to 21%. However, this was a very limited proof-of-concept study and more tests are required to validate this conclusion. The proposed rig only provided partial restraint and proposals for improvements are made. The RF was shown to vary with time due to the concrete strength/stiffness evolution and crack development.

References

1. ACI 231R-10, *Report on Early-Age Cracking: Causes, Measurement, and Mitigation*, in *ACI Committee 231*. 2010, American Concrete Institute: Farmington Hills, U.S.A.
2. Carlson, R.W., *Attempts to Measure the Cracking Tendency of Concrete* ACI, 1940. **36**: p. 533-537.
3. Hughes, B.P., *A new look at rigid concrete pavement design.* Proceedings of the Institution of Civil Engineers-Transport, 2003. **156**(1): p. 29-36.
4. Bishop J., *The early age Behaviour of Concrete Industrial Ground Floor Slabs*. 2001, loughborough University: loughborough, UK
5. ACI 207.2R, *Report on Thermal and Volume Change Effects on Cracking of Mass Concrete*, A.C. 207, Editor. 2002, American Concrete Institute: Farmington Hills, U.S.A.
6. Banthia, N. and R. Gupta, *Influence of polypropylene fiber geometry on plastic shrinkage cracking in concrete.* Cement and Concrete Research, 2006. **36**(7): p. 1263-1267.
7. Mehta, P.K. and P.J.M. Monteiro, *Concrete: Microstructure, Properties, and Materials*. 2006, New York: McGraw-Hill.
8. Bisschop, J. and J.G.M. Van Mier, *Effect of aggregates on drying shrinkage microcracking in cement-based composites.* Materials and Structures/Materiaux et Constructions, 2002. **35**(252 SPEC.): p. 453-461.
9. Concrete Society TR 34, *Concrete Industrial Ground Floors - A Guide to their Design and Construction*. 2003, Concrete Society. : Surrey,UK
10. Grzybowski, M. and S.P. Shah, *Model to Predict Cracking in Fiber Reinforced-Concrete Due to Restrained Shrinkage.* Magazine of Concrete Research, 1989. **41**(148): p. 125-135.
11. Swamy, R.N. and H. Stavrides, *Influence of Fiber Reinforcement on Restrained Shrinkage and Cracking.* Journal of the American Concrete Institute, 1979. **76**(3): p. 443-460.
12. Tritsch, N., Darwin, D. and Browning, J.A. , *Evaluating shrinkage and cracking behaviour of concrete using restrained ring and free shrinkage tests*. 2005, Structural Engineering and Engineering Materials,The University of Kansas Center for Research Inc.: Lawrence, Kansas.
13. Carlsward J. , *Shrinkage Cracking of Steel Fibre Reinforced self compacting Concrete Overlays*, in *Department of civil and Environmental Engineering*. 2006, Lulea University of Technology: Lulea,Sweden.
14. Weiss, W.J., W. Yang, and S.P. Shah, *Shrinkage cracking of restrained concrete slabs.* Journal of Engineering Mechanics-Asce, 1998. **124**(7): p. 765-774.
15. Altoubat, S.A. and D.A. Lange, *Creep, shrinkage, and cracking of restrained concrete at early age.* ACI Materials Journal/ SP, 2001. **98**(4): p. 323-331.
16. Carlson, R.W., *Cracking of Concrete.* The Boston Society of Civil Engineers, 1942. **29**(2): p. 98-109.

17. Banthia, N., C. Yan, and S. Mindess, *Restrained shrinkage cracking in fiber reinforced concrete: A novel test technique.* Cement and Concrete Research, 1996. **26**(1): p. 9-14.

18. Qiao, P., McLean, D. and Zhuang, J.,, *Mitigation Strategies for Early-Age Shrinkage Cracking in Bridge decks*. 2010, Department of Civil and Environmental Engineering , Washington State University: Pullman, Washington. .

19. Tongaroonsri, S. and S. Tangtermsirikul, *Effect of mineral admixtures and curing periods on shrinkage and cracking age under restrained condition.* Construction and Building Materials, 2009. **23**(2): p. 1050-1056.

20. Bentur, A. and K. Kovler, *Evaluation of early age cracking characteristics in cementitious systems.* Materials and Structures, 2003. **36**(3): p. 183-190.

21. Bentur, A., *Early Age Cracking Tests*, in *Early Age Cracking in Cementitious Systems - Report of RILEM Technical Committee 181-EAS - Early age shrinkage induced stresses and cracking in cementitious systems*, A. Bentur, Editor. 2003, RELIM. p. 241-255.

22. Springenschmid, R., Breitenbucher, R., Mangold, R.,. *Development of the cracking frame temperature-stress testing machine,* . in *Thermal Cracking in Concrete at Early Ages* 1994. Proceedings RILEM Symposium E&FN SPON.

23. JCI, *Committee Report: Technical Committee on Autogenous Shrinkage of Concrete* in *AUTOSHRINK'98, Worshop on Autogenous Shrinkage of Cocncrete*, E. Tazawa, Editor. 1998, Japan Concrete Institute Japan. p. 5-66.

24. Collins, F. and J.G. Sanjayan, *Cracking tendency of alkali-activated slag concrete subjected to restrained shrinkage*. Cement and Concrete Research, 2000. **30**(5): p. 791-798.

25. Bloom, R. and A. Bentur, *Free and Restrained Shrinkage of Normal and High-Strength Concretes.* Aci Materials Journal, 1995. **92**(2): p. 211-217.

26. Springenschmidt, R., *Prevention of Thermal Cracking in Concrete at Early Ages—State of the Art Report*. 1998, London: E&FN Spon.

27. Paillere A. M., B.M., Serrano J. J. ,, *Effect of Fiber Addition on the Autogenous Shrinkage of Silica Fume*. ACI Materials Journal, 1989. **86**(2): p. 6.

28. Kovler, K., *Testing System for Determining the Mechanical-Behavior of Early Age Concrete under Restrained and Free Uniaxial Shrinkage.* Materials and Structures, 1994. **27**(170): p. 324-330.

29. Igarashi, S., A. Bentur, and K. Kovler, *Stresses and creep relaxation induced in restrained autogenous shrinkage of high-strength pastes and concretes.* Advances in Cement Research, 1999. **11**(4): p. 169-177.

30. Igarashi, S., A. Bentur, and K. Kovler, *Autogenous shrinkage and induced restraining stresses in high-strength concretes.* Cement and Concrete Research, 2000. **30**(11): p. 1701-1707.

31. Carlsward, J., *Shrinkage Cracking of Steel Fibre Reinforced self compacting Concrete Overlays*, in *Department of civil and Environmental Engineering*. 2006, Lulea University of Technology: Lulea,Sweden.

32. Banthia, N., M. Azzabi, and M. Pigeon, *Restrained Shrinkage Cracking in Fiber-Reinforced Cementitious Composites.* Materials and Structures, 1993. **26**(161): p. 405-413.

33. Leung, C.K.Y., et al., *A new testing configuration for shrinkage cracking of shotcrete and fiber reinforced shotcrete.* Cement and Concrete Research, 2006. **36**(4): p. 740-748.

34. Hossain, A.B., and Weiss, W. J., , *Assessing Residual Stress Development and Stress Relaxation in Restrained Concrete Ring Specimens.* Cement and Concrete Composites, 2004. **26**: p. 531-540.

35. BS EN 197-1:2011, *Cement. Composition, specifications and conformity criteria for common cements*. 2011, British Standard Institution: London, UK.

36. ACI 207.2R-95, *Effect of Restraint, Volume Change, and Reinforcement on Cracking of Mass Concrete*, A.C. 207, Editor. 1995, American Concrete Institute: Farmington hills, MI, USA. p. 47.

37. Leung, C., A. Lee, and R. Lai, *New Testing Procedure for Shrinkage Cracking of Fiber-Reinforced Shotcrete.* Journal of Materials in Civil Engineering, 2007. **19**(3): p. 214-218.

38. Abbasnia, R., P. Godossi, and J. Ahmadi, *Prediction of restrained shrinkage based on restraint factors in patching repair mortar.* Cement and Concrete Research, 2005. **35**(10): p. 1909-1913.

39. Idiart, A.E., *Coupled analysis of degradation processes in concrete specimens at the meso-level*, in *Geotechnical Engineerin and Geosciences*. 2009, Polytechnic University of Catalunya: Barcelona.

40. Bisschop Jan, *Drying Shrinkage Microcracking in Cement-based Materials*, in *Civil engineering and Geoscience*. 2002, Delft University of Technoloy: Delft, Netherlands.

41. Shiotani, T., J. Bisschop, and J.G.M. Van Mier, *Temporal and spatial development of drying shrinkage cracking in cement-based materials.* Engineering Fracture Mechanics, 2003. **70**(12): p. 1509-1525.

42. BS EN 12390-3:2009, *Testing hardened concrete Part 3: Compressive strength of test specimens*. 2009, British Standards Institution: London.

43. BS 1881-119:2011, *Testing concrete. Method for determination of compressive strength using portions of beams broken in flexure (equivalent cube method)*. 2011, BSI: London-UK. p. 12.

44. ASTM-C1018-97, *Standard Test Method for Flexural Toughness and First-Crack Strength of Fiber-Reinforced Concrete (Using Beam With Third-Point Loading)*. 1997, ASTM International.

45. BS EN 1992-1-1:2004, *Eurocode 2: Design of concrete structures — Part 1-1: General rules and rules for buildings* 2004, British Standard Institution: London, UK.

46. Yurtdas, I., et al., *Influences of water by cement ratio on mechanical properties of mortars submitted to drying.* Cement and Concrete Research, 2006. **36**(7): p. 1286-1293.

47. Kanna, V., R.A. Olson, and H.M. Jennings, *Effect of shrinkage and moisture content on the physical characteristics of blended cement mortars.* Cement and Concrete Research, 1998. **28**(10): p. 1467-1477.

48. Pihlajavaara, S.E., *A review of some of the main results of a research on the ageing phenomena of concrete: Effect of moisture conditions on strength, shrinkage and creep of mature concrete.* Cement and Concrete Research, 1974. **4**(5): p. 761-771.

Chapter 4

Assessment of Post-Restrained Shrinkage Mechanical Properties of Concrete- Parametric Study (Part I)

Younis, K.H. and K. Pilakoutas, *New Restrained Test to Assess Post-Shrinkage Behaviour of Concrete-Part I: Development of Test and Free Shrinkage Results.* Cement and Concrete Composites, 2014. ***Submitted***.

This chapter deals with a new test for restrained shrinkage of concrete and aims at assessing the post-restrained shrinkage behaviour of concrete. To examine the effectiveness of the proposed restraining frame, a parametric experimental study was conducted. The development of the restraining frame and results of free shrinkage, mass loss and mass loss vs shrinkage of three concrete mixes with different water/cement (w/c) ratios are presented and discussed in part I. Part II deals with the behaviour of the concrete mixes under restrained conditions including: shrinkage strains, restrained factor (RF), failure of restrained concrete and the post-restrained mechanical behaviour. The results of Part I show that, for unrestrained specimens there is a significant variation in shrinkage strains with depth, resulting in significant curvature deformations. In early ages, free shrinkage strains and their rate of development in mixes with low w/c are larger than those with higher w/c whereas, for later ages, the opposite applies.

This chapter consists of a "stand alone" journal paper and therefore, relevant bibliography is presented at the end of the chapter. Appendix E includes additional information and further test results.

4.1 Introduction

Over time concrete undergoes unavoidable complex chemical, physical and thermal volume related changes known as autogenous, drying and thermal shrinkage. The existence of restraint against these volume changes leads to internal stress development resulting in cracks when the instantaneous tensile strength of concrete is exceeded [1]. Cracks, induced by restrained shrinkage, can lead to issues with serviceability and structural integrity. Shrinkage cracks can also result in durability issues by affecting permeability, diffusivity and sorptivity of concrete, thus causing deteriorations such as freeze-thaw damage, corrosion of steel reinforcement and spalling. Such cracks and premature deterioration can start even before the application of external loads. As a result, cracking potential, stress evaluation and effect of cracks on concrete properties have received considerable attention by the concrete community [1-4].

Preventing the rapid loss of moisture and temperature at an early age is the best practical way to mitigate the effect of shrinkage deformations. However, the complete elimination of these deformations is practically impossible. Hence, finding ways of quantifying restrained strains and associated stresses is crucial to account for them during the design process.

Commonly used free shrinkage tests can provide information on shrinkage behaviour of different concrete mixtures, environmental conditions, and size and shape of concrete elements being assessed. However, they cannot provide information on the post-cracking behaviour of concrete under restrained conditions [5-8]. On the other hand, restrained shrinkage tests can help in the assessment of cracking tendencies and the ability of concrete to withstand shrinkage induced tensile stresses [9]. There are different types of the restrained shrinkage tests; for example the ring test, the linear passive and active tests and the plate test [1, 10] .

The impact of shrinkage induced cracks due to external restraints on the mechanical properties of concrete is still largely unknown and to date there is no standard experimental procedure to quantify the effect of such cracks on these properties. For this reason, the authors have recently developed a new linear rig test [11] (see Figure 4.1) and a procedure to assess the post-shrinkage mechanical properties of concrete. It was found that the test rig provided a variable partial restraining factor (RF) and improvements were proposed for the restraining element and supports [11]. The current research aims to enhance the RF of the restraining elements, integrate them into a frame for multi-specimen testing and to examine the effectiveness of the developed frame through an experimental parametric study. The

results and findings of the research are presented in two parts. Part I (the current paper) will present the development of the restraining frame, describe the experimental procedures and discuss the free shrinkage behaviour, mass loss and mass loss vs shrinkage of the three concrete mixes of very different w/c ratios. Part II (second paper) will present the results and discuss the behaviour of the concrete mixes under restrained conditions, including shrinkage strains, RF, failure of restrained concrete and the post-restrained mechanical behaviour of the three concrete mixes.

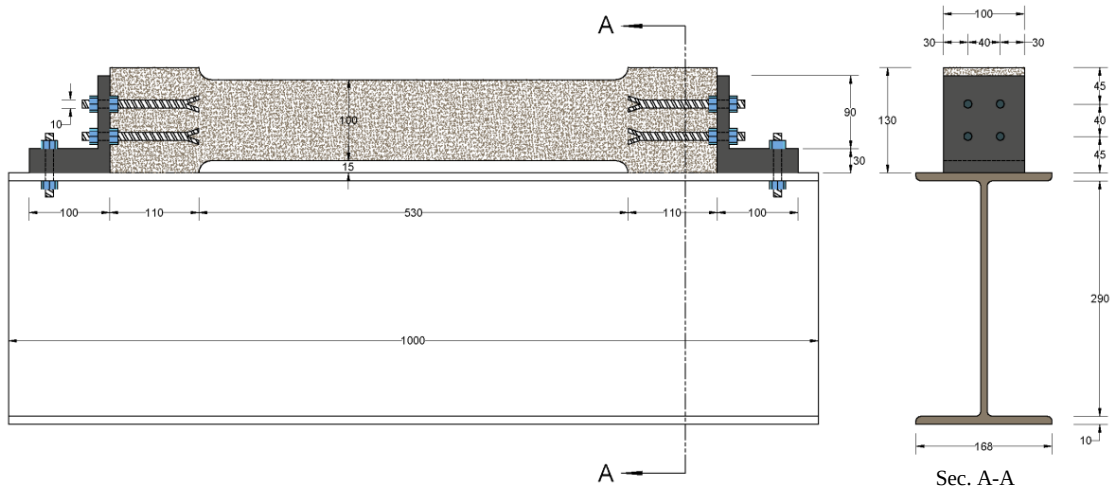

Figure 4. 1 Front view of the developed rig for restrained shrinkage test [11] (dimensions in mm).

4.2 Experimental Programme

4.2.1 Development of New Restraining Frame

Due to strain loss caused by the deformations of the supports (ends) and restraining beam, the degree of the restraint achieved using the rig in Figure 4.1, was not enough to allow potential through cracks to develop. Therefore, it was proposed to modify the concept of the developed rig to: 1- provide higher restraint, and 2- examine 3 specimens at the same time, to enable parametric investigations.

The new restraining frame (see Figure 4.2) consists of three horizontally positioned beams made of a 120×120×10 mm steel square hollow box sections (SHS) (as shown in Figures 4.2a and 4.2b). The beams are held by two channel sections (CS) columns (C150×75, flange length =75mm, web length=150mm, thickness of flange = thickness of web= 10mm). For ease of assembly, the three beams are welded onto one of the columns. To connect the two columns, three pairs (one pair per beam) of threaded M16 steel rods (length × diameter =1000×16 mm) were used. Each pair of steel rods passes through the length of the SHS and is prestressed onto the columns using torque wrench (utilising 80% of the rod capacity). The function of these rods is to keep all parts (beams and columns) together to form a rigid frame. Another function of these rods is to enable the modification of the degree of restraint during exposure to drying conditions. This could be done by releasing the prestressing force when required. Steel plates stiffeners (120×120×10 mm) were welded onto the columns to stiffen further the contact area with the beams.

Results from the previous study (chapter 3) carried out by the authors [11] indicated that most loss of RF was due to bending of the gripping device (end supports). Therefore, a much stiffer restraint with less freedom to rotate is required to minimise bending. Hence, rather than using steel angles, the new rig utilises a channel section CS to connect the concrete specimen onto the reaction beam through bolts. To provide continuity, the CS runs height wise to create a three-specimen rig. To develop some ability to compensate for some of the strain imposed on the restraining beams by the shrinking concrete specimens, prestressed rods are also utilised.

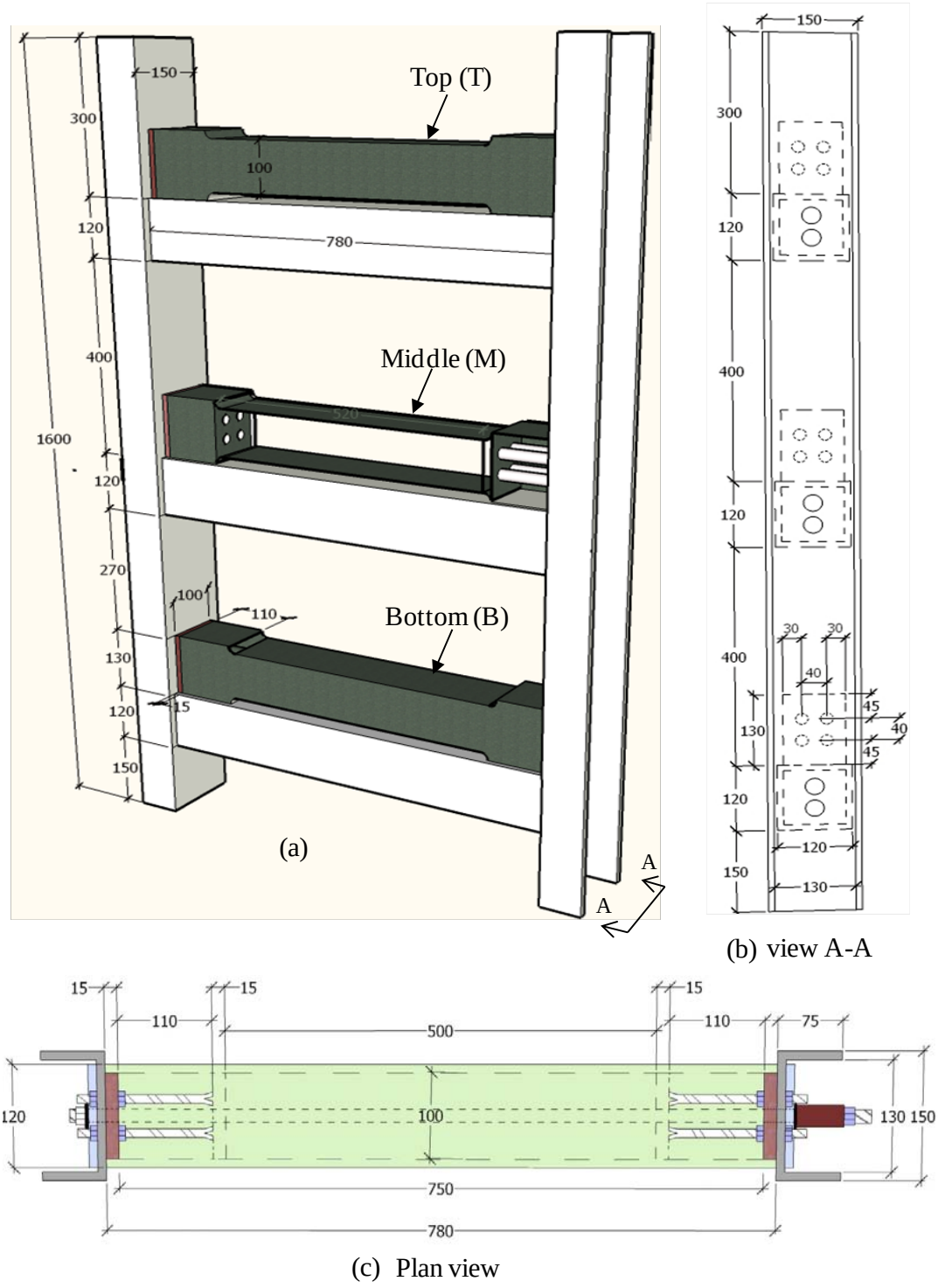

Figure 4. 2 New restraining frame (dimensions in mm).

Details of the frame after manufacturing are shown in Figures 4.3(a-f). Each specimen is provided with 4 anchor bolts at each end made of M10 steel threaded rods (see Figures 4.2a and 4.3e). The rods are bolted to the columns for easy dismounting of the concrete specimen at the end of the test. Two steel plates (100×130×15 mm) were welded to the inner side of the columns for each beam to strengthen this area (see Figure 4.3e).

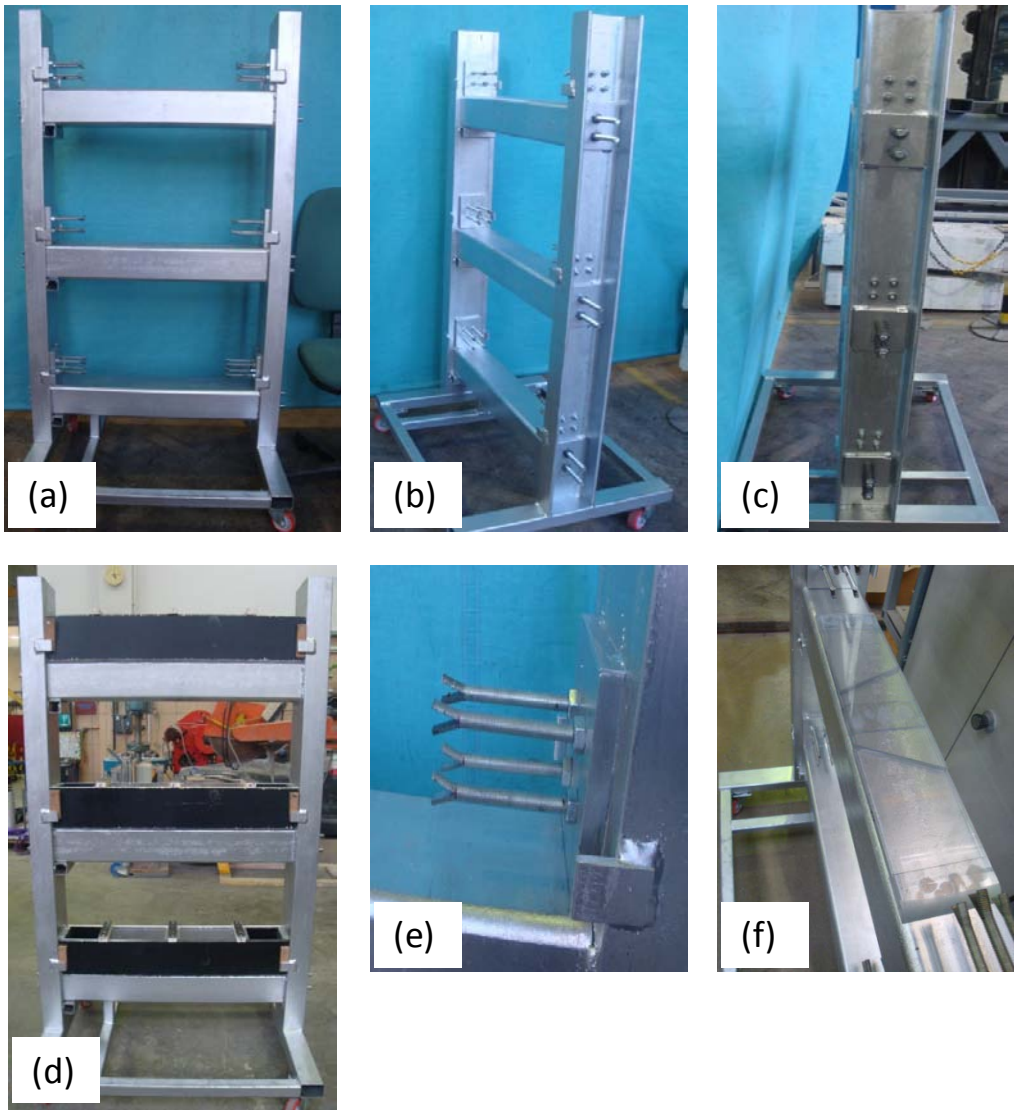

Figure 4. 3 New restraining frame after manufacturing: a and b- general view c- side view d- frame with the timber sides and the top perspex cover in place. e- details of the end f- rectangular prespex piece with curved ends used to provide space at the bottom of each prism.

Rectangular timber pieces were initially tried at the top and bottom of the concrete specimen in the rig, but were later replaced by two perspex pieces of the same dimensions (see Figure 4.3d and f) to ensure easy removal during demoulding. Timber plates with dimensions of 780×130×15 mm were used as side shutters (see Figure 4.3d).

The rig is mounted on a braced rectangular base with four wheels (see Figure 4.3a). This facilitates movement inside the conditioning room.

4.2.2 Materials, Mix Proportions and Geometry and Preparation of Specimens

In this study, Ordinary Portland Cement (OPC) CEM I 52.5 N, complying with BS EN 197-1:2011 [12] was used. Table 4.1 presents the chemical analysis of the cement (as given by the supplier). The aggregates used in this study were sand (maximum size of 5mm) as fine aggregate and river gravel (maximum size of 20 mm) as coarse aggregate.

Table 4. 1 Chemical composition of OPC .

SiO_2	Al_2O_3	Fe_2O_3	CaO	MgO	SO_3	Na_2O	K_2O	Na_2O_{eq}
21.0	5.0	2.9	65.9	0.80	2.8	0.24	0.44	0.52

The mix proportions of the three mixes investigated in this study are presented in Table 4.2.

Table 4. 2 Mix proportions (kg/m^3)

Mix Code	w/c	C	CA	FA	SP
NA30	0.3	430	1203	659	0.64*
NA40	0.4	375	1147	715	0.32*
NA50	0.5	330	1109	752	0.07*

w/c: water to cement ratio. C: cement. CA: coarse aggregate. FA: fine aggregate. * % of cement mass.

The following specimens were cast for each mix: 12 of 100 mm cubes, 3 control prisms 100×100×500 mm, 3 prisms 100×100×750 mm for free shrinkage test, and 3 prisms (in one frame) for restrained shrinkage. The concrete was compacted on a vibrating table in two layers [13]. The concrete specimens in the restraining frame were compacted by clamping the frame to the vibrating table using a steel bar, as shown in Figure 4.4.

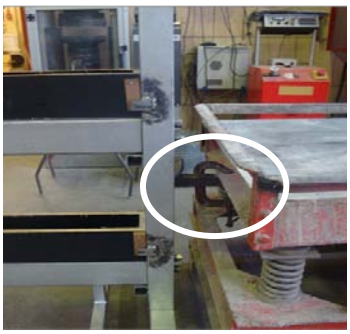

Figure 4. 4 Restraining frame clamped to vibrating table.

After compaction and levelling of the surface of the prisms, a rectangular perspex piece (which was part of the mould) was placed on the top surface of each specimen in the restraining frame. The specimens were then covered with plastic sheets to prevent moisture loss before being demoulded at 24h. After demoulding, Demec gauge points were bonded to the concrete surface at 300 and 500 mm spacing using a rapid-hardening adhesive (as explained in next the section). The control prisms were then stored in water while the specimens in the restraining frame and the prisms for free shrinkage were maintained in a laboratory environment at 22 ±2 ^{o}C and RH of 45 ±5 %.

4.2.3 Shrinkage and Mass Loss Measurements

Two Demec gauges (seen in Figure 4.5a) were used to measure shrinkage strains having length of 300 and 500 mm and precision of 5.2 με and 3.2 με, respectively. The location of the Demec points for the free shrinkage specimens is shown in Figure 4.5a. At the centre of each surface of the concrete prisms, four demec points are used to obtain one reading over a length of 500 mm and two readings over a 300 mm length.

Figure 4. 5 Location of Demec points for: a and c-free shrinkage specimens, b-restrained shrinkage specimens (all presented values are in mm).

For the restrained specimens, Demec points were fixed to the sides and top of each specimen as can be seen in Figure 4.5b. In some cases, and to examine the distribution of the shrinkage across the depth of the concrete specimen, Demec points were attached on the side surfaces at three depths from the troweled surface (5 mm (top A), 50 mm (middle B), and 95 mm (bottom C)), see Figures 4.5b and c. The first shrinkage strains were measured at 24h (immediately after the adhesive hardened) and at 24 hours intervals for the first week,

followed by measurements at 10,14, 21 and 28 days. Two or three readings were taken for each gauge length, and the average values calculated.

The loss of mass for the free shrinkage specimens was determined at regular intervals starting at 24 h soon after the Demec points were bonded.

4.3 Results and Discussion

4.3.1 Free Shrinkage Strains

4.3.1.1 Effect of gauge length

Figures 4.6, 4.7 and 4.8 show the results of free shrinkage strains (average of three specimens) for the three mixes investigated in this study. Each figure presents the shrinkage strains on the top (T) (troweled surface), sides (S) and bottom (B) surfaces. Generally, it can be seen that there is insignificant difference between the results of the two gauges, with a maximum difference of around 10%. Since gauge length had insignificant effect on shrinkage strains, only strains measured using the 300 mm gauge length will be used in the discussions and when considering other parameters in the next sections.

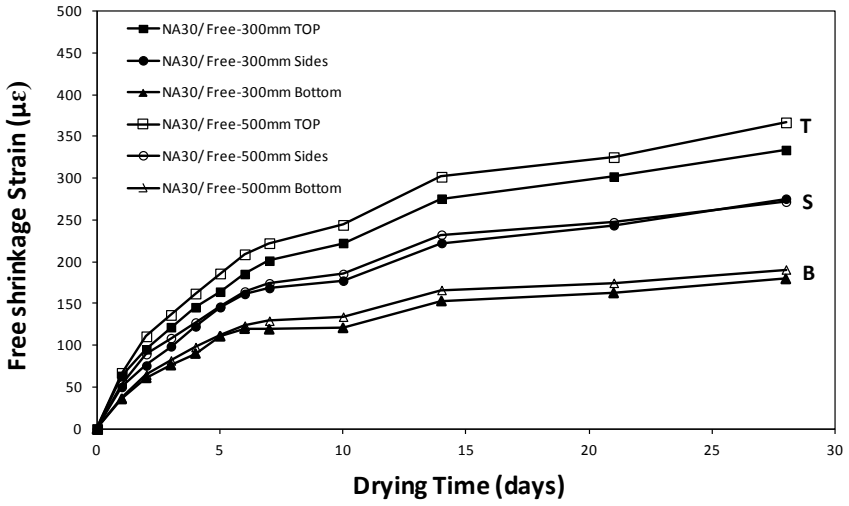

Figure 4. 6 Free shrinkage strains measured on top, sides and bottom surfaces for mix NA30.

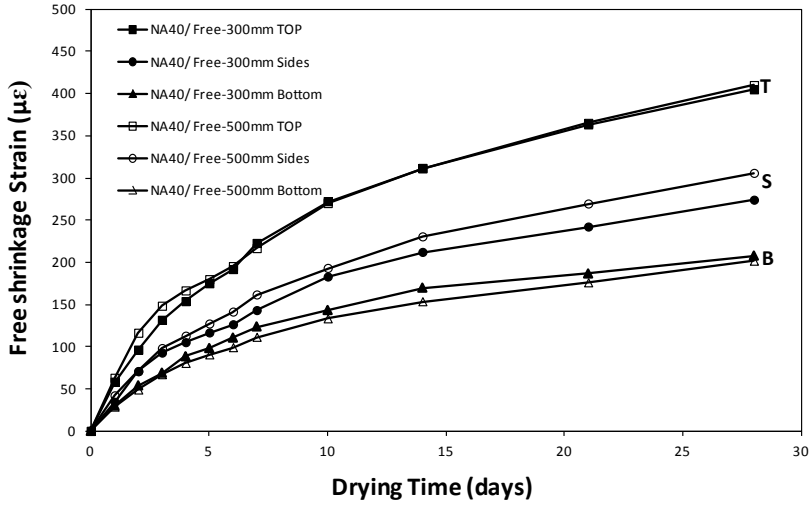

Figure 4. 7 Free shrinkage strains measured on top, sides and bottom surfaces for mix NA40.

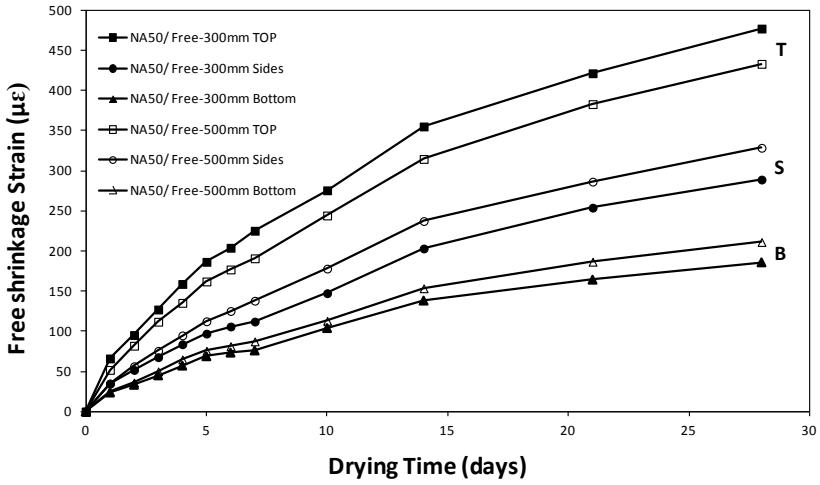

Figure 4. 8 Free shrinkage strains measured on top, sides and bottom surfaces for mix NA50.

4.3.1.2 Effect of surface (top, sides and bottom)

The shrinkage strains measured on these surfaces were different for each mix. Highest shrinkage strains were observed at the top surface and lowest at the bottom; strains on the sides were about the average of the two other faces (see Figures 4.6, 4.7 and 4.8). For example, after 28 days of drying, the shrinkage strain developed at the top of the specimens of mix NA40 (410 με) is twice that developed at the bottom surface (202 με) and higher than that developed at the sides of the specimen (274 με) by 136 με. This may be due to concrete bleeding which usually happens at the top (troweled) surface altering the microstructure of this surface and possibly resulting in slightly higher porosity which in turn causes more shrinkage. Furthermore, concrete is better compacted at greater depths resulting in more dense concrete, which tends to shrink less. This difference in shrinkage strains between

different surfaces indicates that upon drying the concrete will also bend due to curvature (see section 4.3.1.4).

To assess the effect of w/c ratio on the variation in shrinkage on the different surfaces, the ratio between the strains developed at the top and at the bottom (Δ_{T-B}) and side surfaces (Δ_{T-S}) were calculated and shown in Figures 9 and 10. It can be seen that the ratio of strains reduces with the decrease in w/c ratio. It can also be seen that though the ratios Δ_{T-B} and Δ_{T-S} (for w/c = 0.4 and 0.5) are variable at the early ages (up to 7 days), there is a general trend for an increase in the first few days followed by a decrease and then stabilization. Nonetheless, for w/c ratio 0.3, strain ratios (Δ_{T-B} and Δ_{T-S}) appear to increase slightly with time.

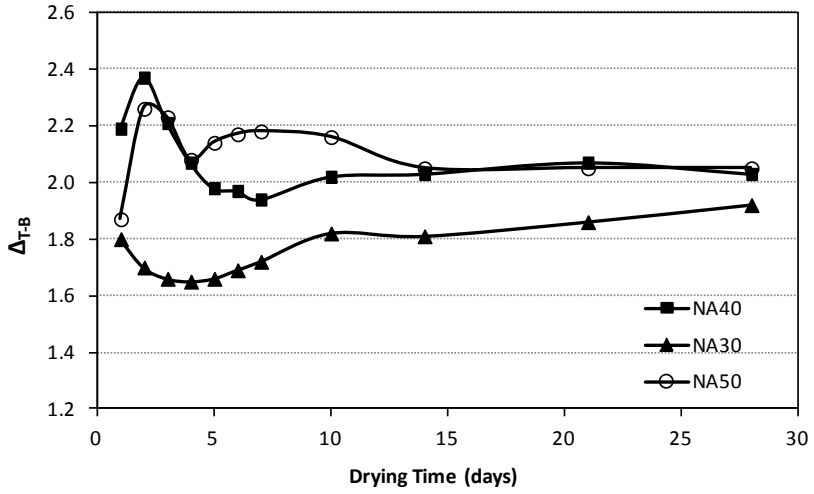

Figure 4. 9 Difference in the strains between top and bottom surfaces.

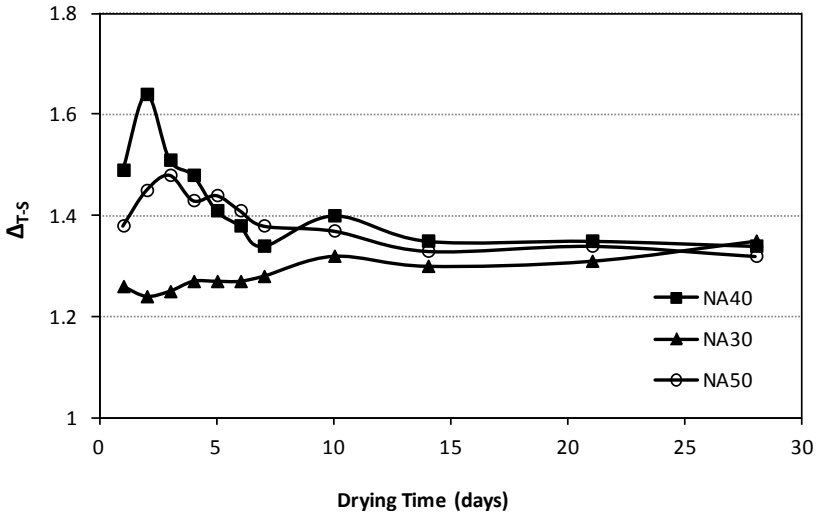

Figure 4. 10 Difference in the strains between top and side surfaces.

4.3.1.3 Effect of depth (variation of shrinkage over specimen depth)

Figures 4.11, 4.12 and 4.13 show the shrinkage strains (average of two specimen for each mix) at the middle part of the sides at three different depths: 5mm (top-T), 50 mm (centre-C), 95 mm (bottom-B) from the troweled face of the specimen (see Figure 4.5c). Regardless of the w/c ratios, it is clear that there is significant difference between the shrinkage measured at the top (upper edge) and bottom (lower edge) of the side face. For example, this difference (at 28 days) is equal to 204 με, 162 με and 218 με, which corresponds to around 122%, 89% and 76% of the strains developed at the lower edge for the mixes NA30, NA40 and NA50, respectively. These results indicate that there is differential (non-uniform) shrinkage over the depth of the concrete specimens. This variation in shrinkage strains causes curvature as discussed in the next subsection. Furthermore, this may increase the intensity of the tensile stress, that develops due to non-uniform shrinkage (differences in the moisture between surface and core), at the upper edges.

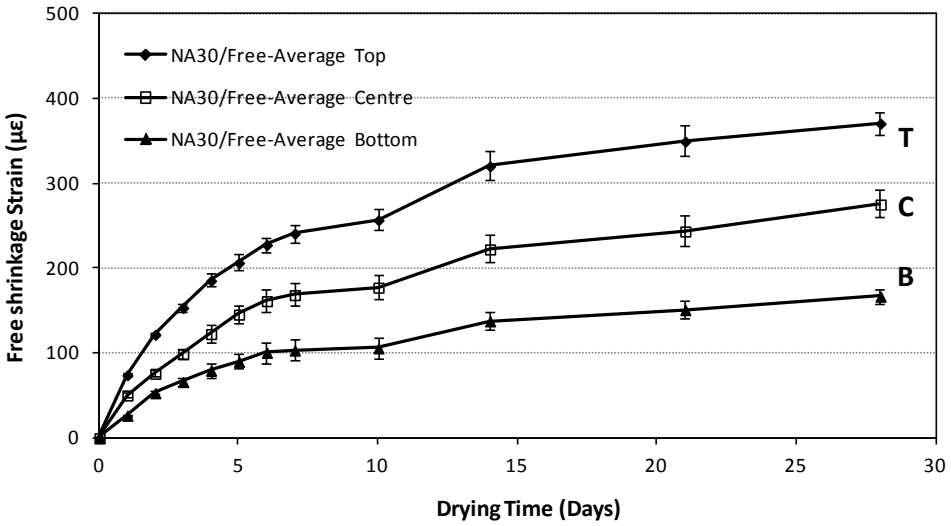

Figure 4. 11 Shrinkage strains at upper edge, centre and lower edge of the side face of mix NA30.

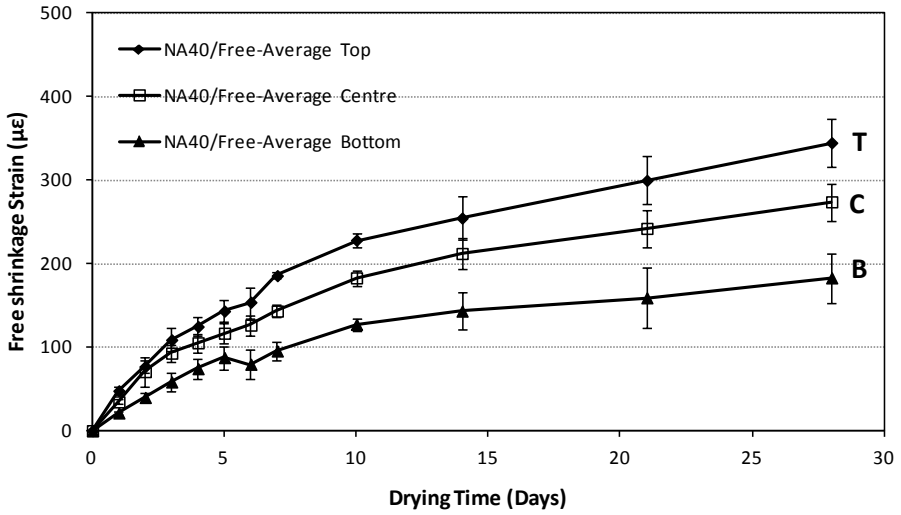

Figure 4. 12 Shrinkage strains at upper edge, centre and lower edge of the side face of mix NA40.

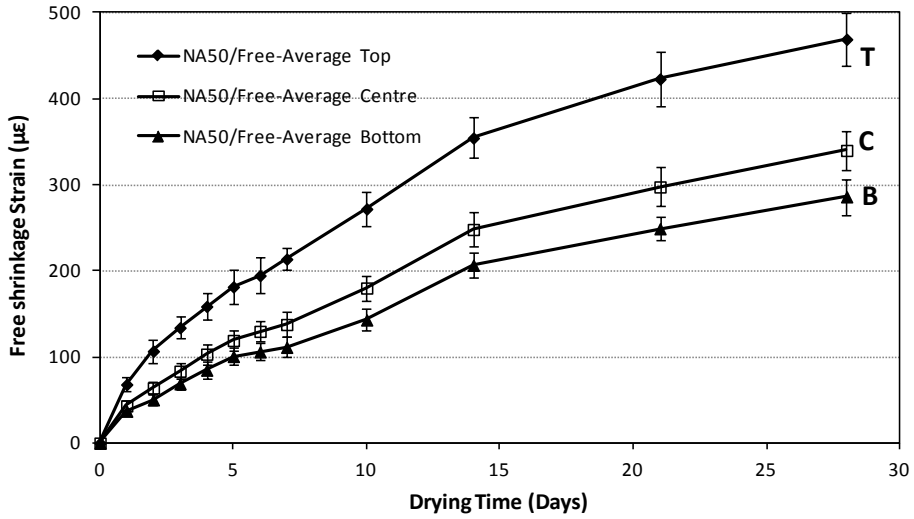

Figure 4. 13 Shrinkage strains at upper edge, centre and lower edge of the side face of mix NA50.

Figures 4.14 a-c show the distribution of the shrinkage strains over the depth at different time intervals for mixes NA30, NA40 and NA50, respectively.

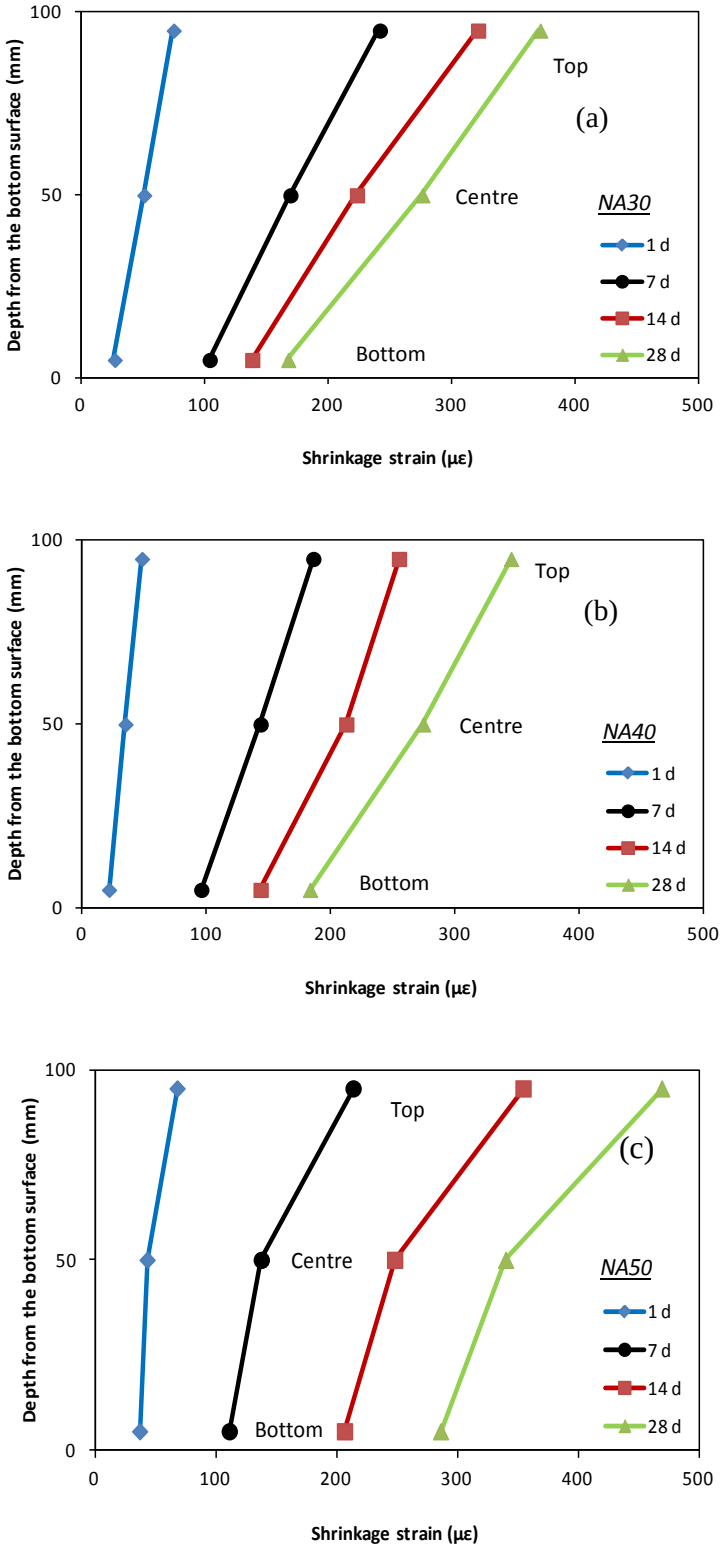

Figure 4. 14 Variation of shrinkage strains over the depth of the concrete specimen (a) mix NA30, (b) mix NA40, (c) mix NA50.

4.3.1.4 Shrinkage curvature

Figures 4.15 (a-c) show the development of curvature over time for all mixes. Curvature is shown as calculated between top and sides (k_{T-S}), sides and bottom (k_{S-B}) surfaces and average (kA) (average of three specimens) for all mixes. It can be seen that curvature increases overall with an increase in w/c. For NA40 and NA50 the curvature of the upper half of the concrete specimens is higher than the lower half, whereas, for NA30, it is uniform for the first few days and after that the curvature of the lower half is higher than that of the upper half. This may be due to the high amount of microcracks observed on the surface of specimens of mix NA30 which can cause relaxation of the top surface.

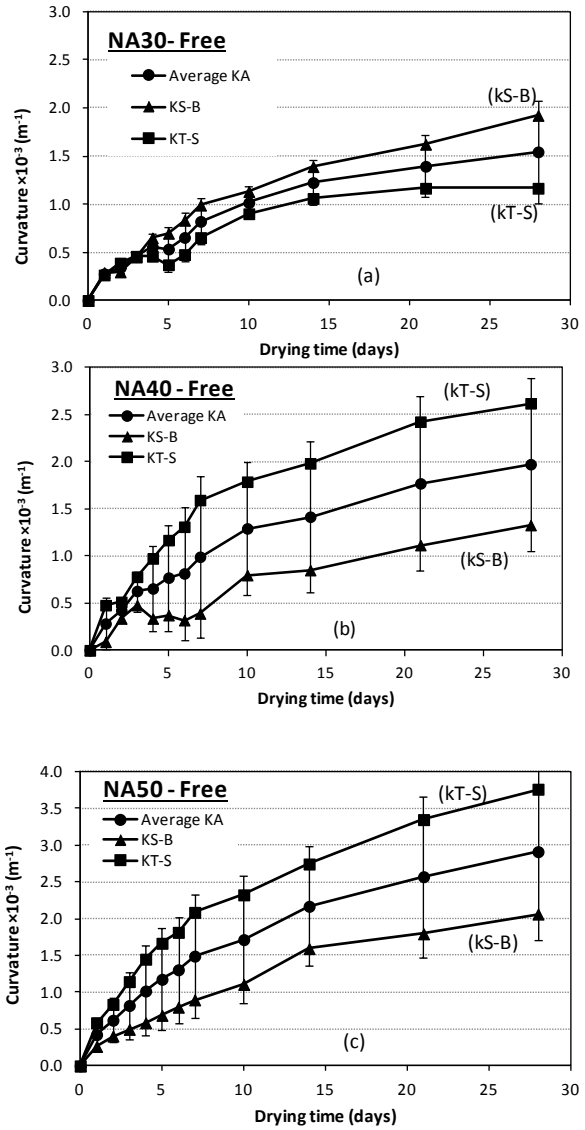

Figure 4. 15 Shrinkage curvature developed on the free specimens, (a) mix NA30, (b) mix NA40, (c) mix NA50.

4.3.1.5 Effect of w/c

Shrinkage strains developed at the sides of the specimens versus time for all mixes are shown in Figure 4.16.

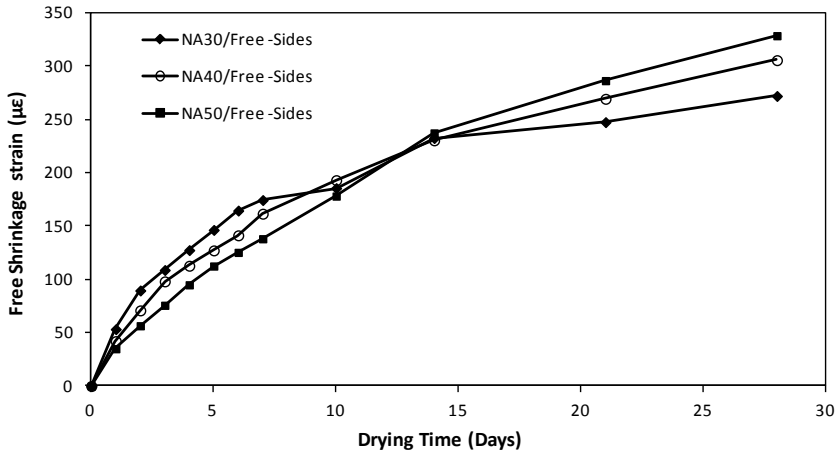

Figure 4. 16 Shrinkage strains development for all mixes.

The figure shows that, in the early ages, shrinkage strains increase faster for the lower w/c ratios. This can be attributed to the influence of the autogenous shrinkage which is more pronounced in low w/c ratio mixes. Similar results were reported by Altoubat and Lange [9]. After 7-15 days, however, for the mixes with lower w/c ratios shrinkage development slows down faster. This may be due to the fact that for the lower w/c mixes there is less moisture that can be lost upon drying due to their denser (finer) microstructure.

4.3.2 Mass Loss

Mass loss versus time for the three mixes is shown in Figure 4.17. As, expected, it is clear that the w/c has significant influence on mass loss, with the higher w/c ratio mixes having much higher mass loss, especially at the early ages.

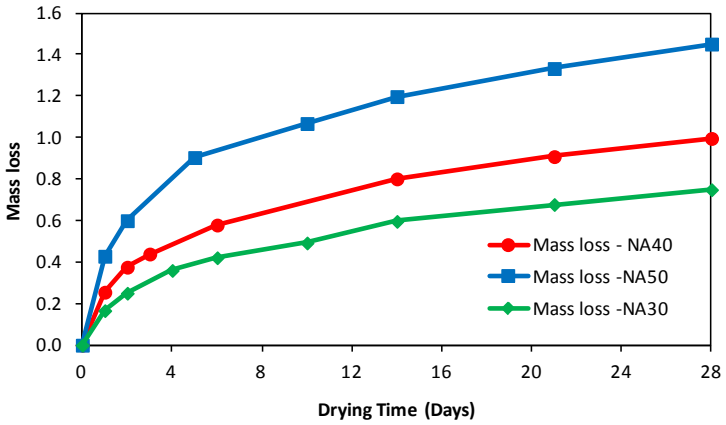

Figure 4. 17 Mass loss versus time.

4.3.3 Mass Loss vs Free Shrinkage Strains

The mass loss versus shrinkage strains for all mixes is shown in Figure 4.18. Regardless of the w/c ratio, the mass loss- shrinkage strain curve is characterised by a two stage behaviour. Initially, the rate of shrinkage strain per mass loss decreases with increasing w/c ratio. This rate appears to be influenced partly by autogenous shrinkage and partly by the pore structures of the mixes. In the second stage, the effect of the w/c on the rate of shrinkage strain per mass loss appears to be negligible as all three curves have the same gradient. This may be attributed to the slow-down of autogenous shrinkage and also to the fact that the majority of coarse pores are dry and the drying causes moisture loss from the finer capillary pores. Similar results were reported by Powers 1959 [14] (cited in [15]), who specifically examined the effect of different porosity mixtures having different aggregate contents. It is argued that water is initially lost from large capillary pores with little shrinkage thus contributing mainly to the rapid loss of mass.

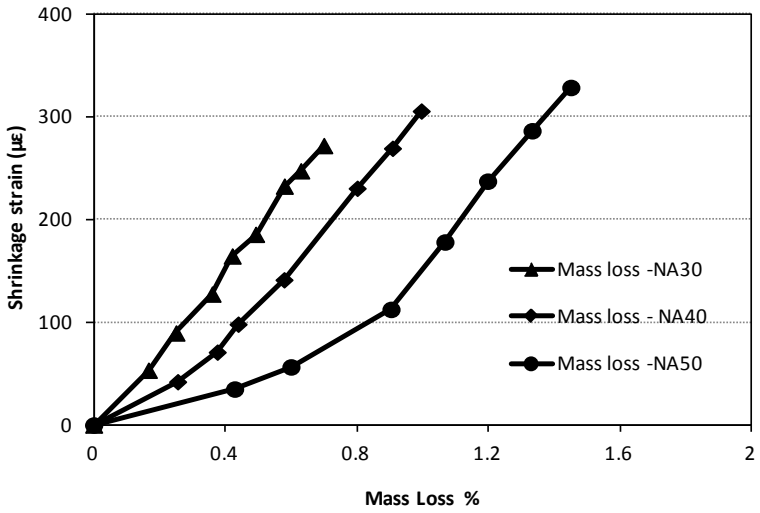

Figure 4. 18 Mass loss-shrinkage strains curves.

The smoothed behaviour of shrinkage strain-mass loss curves are shown in Figure 4.19.

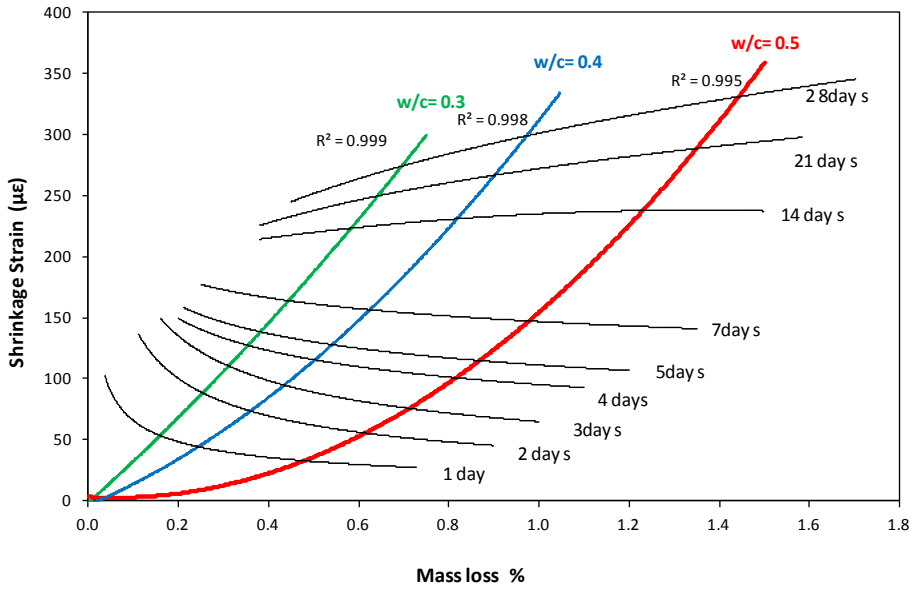

Figure 4. 19 Shrinkage strain-mass loss curves at different times of drying.

4.4 Conclusions

This study proposes a new test for restrained shrinkage to assess the post-restrained shrinkage mechanical behaviour of concrete. This chapter dealt with the development of the restraining frame and discussed results on free shrinkage. Chapter 5 (Part II) will deal with the post-restrained behaviour of concrete. The main findings of this chapter are:

For unrestrained specimens, the shrinkage strains on the top surface of the concrete are higher than those on the sides and the bottom surface by up to 100% after 28 days drying. The variation in strains is higher at an early age and more pronounced in mixes with high w/c ratios, possibly due to their higher porosity and better compaction of the lower layer of the concrete. As a result, this paper quantifies that free shrinkage specimens develop curvatures due to differences in shrinkage strains along the depth. Differential shrinkage can also develop between the surfaces and core of the specimens, which can lead to surface tensile stresses which can amplify the effects of restrained shrinkage. This issue requires further investigation.

In early ages, for the low w/c mix (NA30), the free shrinkage strains and their rate of development are higher than those for higher w/c mixes (NA40 and NA50) due to higher autogenous shrinkage. For later ages, the development of the shrinkage strains of low w/c mixes slows down faster than for higher w/c mixes, possibly due to the fact that there is less

moisture that can be lost upon drying due to their denser microstructure. High w/c ratios mixes initially lose mass faster, due to moisture loss from large capillary pores and this results in relatively low initial shrinkage strain.

References

1. ACI 231R-10, *Report on Early-Age Cracking: Causes, Measurement, and Mitigation*, in *ACI Committee 231*. 2010, American Concrete Institute: Farmington Hills, U.S.A.
2. Banthia, N., C. Yan, and S. Mindess, *Restrained shrinkage cracking in fiber reinforced concrete: A novel test technique.* Cement and Concrete Research, 1996. **26**(1): p. 9-14.
3. Banthia, N. and R. Gupta, *Influence of polypropylene fiber geometry on plastic shrinkage cracking in concrete.* Cement and Concrete Research, 2006. **36**(7): p. 1263-1267.
4. Bishop J., *The early age Behaviour of Concrete Industrial Ground Floor Slabs*. 2001, loughborough University: loughborough, UK
5. Swamy, R.N. and H. Stavrides, *Influence of Fiber Reinforcement on Restrained Shrinkage and Cracking.* Journal of the American Concrete Institute, 1979. **76**(3): p. 443-460.
6. Weiss, W.J., W. Yang, and S.P. Shah, *Shrinkage cracking of restrained concrete slabs.* Journal of Engineering Mechanics-Asce, 1998. **124**(7): p. 765-774.
7. Carlsward J. , *Shrinkage Cracking of Steel Fibre Reinforced self compacting Concrete Overlays*, in *Department of civil and Environmental Engineering*. 2006, Lulea University of Technology: Lulea,Sweden.
8. Grzybowski, M. and S.P. Shah, *Shrinkage Cracking of Fibre Reinforced Concrete.* ACI Materials Journal, 1990. **87**(2).
9. Altoubat, S.A. and D.A. Lange, *Creep, shrinkage, and cracking of restrained concrete at early age.* ACI Materials Journal/ SP, 2001. **98**(4): p. 323-331.
10. Bentur, A., *Early Age Cracking Tests*, in *Early Age Cracking in Cementitious Systems - Report of RILEM Technical Committee 181-EAS - Early age shrinkage induced stresses and cracking in cementitious systems*, A. Bentur, Editor. 2003, RELIM. p. 241-255.
11. Younis, K.H. and K. Pilakoutas, *Assessment of Post-Restrained Shrinkage Mechanical Properties of Concrete* ACI Materials, 2014. **Submitted for publication**.
12. BS EN 197-1:2011, *Cement. Composition, specifications and conformity criteria for common cements*. 2011, British Standard Institution: London, UK.
13. BS EN 12390-2:2009, *Testing hardened concrete Part 2: Making and curing specimens for strength tests.* 2009, British Standards Institution: London.
14. Powers, T.C., *Causes and Control of Volume Change.* PCA Research and Development Laboratories, 1959. **1**(1): p. 29-39.
15. Johnston, C.D. and E.H. Sidewell, *Influence of Drying on Strength of Concrete Specimens.* ACI, 1969. **66-63**: p. 748-755.

Chapter 5

Assessment of Post-Restrained Shrinkage Mechanical Properties of Concrete- Parametric Study (Part II)

Younis, K.H. and K. Pilakoutas, *New Restrained Test to Assess Post-Shrinkage Behaviour of Concrete-Part II: Restrained and Post-Restrained Test Results.* Cement and Concrete Composites, 2014.***Submitted***.

This chapter attempts to quantify the restrained and post-restrained shrinkage behaviour of concrete. In Part I (chapter 4) a new restrained shrinkage test was presented and free shrinkage test results were discussed. The experimental parametric study undertaken included three mixes with w/c ratios of 0.3, 0.4 and 0.5. This part (Part II, chapter 5) presents experimental results and discusses the behaviour of the similar concrete mixes under restrained conditions, including variations in shrinkage strains, the evolution of restraint factor (RF), failure of restrained concrete and the post-restrained mechanical behaviour. The results reveal that stress history, which depends on the rate of development of stiffness and shrinkage, is an important factor that governs the failure of restrained concrete. Shrinkage induced cracks reduce the compressive strength, flexural strength and flexural elastic modulus of concrete by up to 14%, 24% and 29% respectively. Mixes with high w/c ratios lose more elastic modulus but less strength. Creep is identified as the possible mechanism for the loss of the stiffness. Mixes with low w/c ratios benefit less from creep and tend to mature and crack earlier, losing relatively more strength than high w/c mixes.

This chapter consists of a "stand alone" journal paper and includes relevant bibliography at the end of the chapter. Further test results are included in Appendix F.

5.1 Introduction

Restrained shrinkage induced cracks can adversely affect the mechanical properties of concrete, in particular flexural strength and flexural rigidity (flexural modulus of elasticity), and can lead to unacceptable serviceability performance. In the first part (Part I-chapter 4) a restrained shrinkage test was developed which is used in this chapter to get better understanding of the post-restrained behaviour of concrete. The experimental parametric study undertaken uses three mixes with w/c ratios of 0.3, 0.4 and 0.5. Details on the materials used, mix proportions, geometry and preparation of specimens, shrinkage strains and mass loss measurements were presented in chapter 4.

Drying of concrete takes place by nonlinear diffusion of moisture [1], which leads to non-uniform distribution of moisture and makes differential shrinkage between the surface and core inevitable [2, 3]. Differential shrinkage leads to tensile stresses which can result in surface microcracking. Nonetheless, it was also found in chapter 4, that free shrinkage strains on the top surface are higher than those on the sides and the bottom surface of the prisms examined. This was confirmed by strains measured on the sides of the concrete specimens. The variation was found to be higher at early ages and more pronounced in mixes with high w/c ratios. This variation in shrinkage strain causes curvature of the unrestrained specimens. This may cause additional stress under restrained conditions. It may also lead to restraint factor (RF) variation between the different surfaces of the concrete and over its depth.

Restrained shrinkage cracking depends on the rates of development of shrinkage strains, tensile strength, elastic modulus (E_c) and creep (tensile relaxation). The results in chapter 4 indicated that shrinkage strains are also a function of w/c ratio. It was also found that, at early ages, the low w/c ratio mixes exhibites higher rate of shrinkage than high w/c mixes and the opposite applies for later ages. This may affect the failure or cracking tendency of such mixes. However, the interaction of these time-dependent material properties in the presence of external or internal restraint governs the initiation of cracking [3]. Creep, due to its role in relaxing shrinkage induced tensile stresses, is considered a beneficial relaxation mechanism reducing the crack potential of restrained concrete [3, 4]. Altoubat and Lange [3] studied the interaction of shrinkage and creep of restrained concrete at early ages and concluded that tensile creep relaxes the shrinkage induced tensile stresses by up to 50 %.

In general, dried beams (under free condition) tested in bending show lower flexural strength in comparison to saturated specimens [5]. A reduction of up to 30% was reported by Nielsen [6] and between 30-40% by Yurtdas *et al* [7].

Very limited work has been undertaken on the effect of external restraint on the mechanical properties of concrete, in particular the flexural strength of concrete. The interactions between the development of strength and stiffness versus the development of shrinkage (autogenous and drying) and creep strains are also not well understood.

This chapter (Part II) presents experimental results and discusses the behaviour of the concrete mixes under restrained conditions, including: shrinkage strains, restraint factor (RF), failure of restrained concrete and the post-restrained mechanical behaviour.

5.2 Test procedures and Measurements

This section introduces briefly the test procedures and measurements taken during and after the restraining period.

Crack Detection

Regular checks for cracks were performed using an optical microscope with a magnification factor of 40x and a precision of 20 μm and a digital microscope with a magnification up to 200x and a precision of 10 μm. The crack width reported is the crack opening at its widest, normally at the edges of the specimens.

In the literature there is no clear definition of what defines a microcrack. RILEM committee (TC-122-MLC), (on Microcracking and Life Time Performance of Concrete) uses widths of less than 10 micron to define microcracks. Others [8-10] adopt 50 microns. In this study 20 microns or less was used to define microcracks, as it was found that cracks with width larger than 20 microns are visible to the naked eye when properly illuminated.

Restraint Factor (RF)

Shrinkage strains were measured using two Demec gauges having lengths of 300 and 500 mm and precision of 5.2 μm and 3.2 μm, respectively. For the free shrinkage tests, readings were taken at the centre of each surface of the prisms to obtain one strain measurement over a length of 500 mm and two over a 300 mm length. For the restrained shrinkage specimens, strains were measured over a gauge length of 300 mm, on the sides and top of each specimen. The variation of shrinkage strains across the depth of concrete specimen was

examined (in some cases) by measuring strains on the side surfaces at three depths from the troweled surface (5 mm (top A), 50 mm (middle B), and 95 mm (bottom C)). The first readings of shrinkage strains were taken at 24h, soon after the adhesive hardened, and at 24 hours intervals for the first week, followed by measurements at 10,14, 21 and 28 days. Two or three readings were taken for each gauge length, and the average values determined.

The extent of restraint (degree of restraint or restraint factor) plays a significance role in the development of tensile stresses inside the concrete. Bentur [11] mentioned that the degree of restraint can be defined as the ratio of the stiffness of the restraining member and the shrinking element and when the two are equal the degree of restraint is 50%. According to ACI 207.2R [12] the restraint factor is the ratio of actual stress induced by the restrained volume change to the stress that would develop if the specimen was fully restrained. In other words, it is a ratio between the amount of strain that is restrained to the free shrinkage strain [13]. Therefore, assuming that the modulus of elasticity is constant, equation 1 can be used to calculate RF:

$$\mathrm{RF} = \frac{\varepsilon_R}{\varepsilon_{free}} \tag{5-1}$$

where:

ε_R Restrained shrinkage strain = shrinkage strain measured on the free specimen-shrinkage strain measured on the restrained specimen.

ε_{free} Free shrinkage strain (strain measured on the free specimen).

5.2.1 Compressive Strength

The compressive strength was obtained at 1, 3, 7 and 28 days using the 100 mm cubes and BS EN 12390-3 [14]. The compressive strength was also obtained from the prisms (free and restrained specimens) tested in bending, by following the recommendations of BS 1881-119 [15]. The compressive strength test for prisms was conducted one or two days after testing the prisms in bending.

5.2.2 Bending Tests (Flexural strength and Modulus of Elasticity)

Specimens were tested following the recommendations of the ASTM C1018 [16] in four-point flexural loading over a length of 300 mm. A yoke [17] was used to mount the deflection transducers to eliminate errors from support displacement and torsion. Central deflections were taken as the average of two displacements measured on opposite sides of the specimen. The flexural strength and stiffness (flexural modulus of elasticity) were determined using the load versus-deflection and load versus flexural modulus of elasticity E_{flex} (GPa) curves (determined based on the theory of classical elasticity) [18]. The flexural elastic modulus of concrete (E_{fmax}) was determined as the maximum value of E_{flex} in the range of 30% to 60% of the ultimate bending load.

5.3 Results and Discussion

5.3.1 Crack Characterization

Microcracks were detected on all surfaces (sides and top) of the specimens from the first day of drying. The width of these microcracks was in the range of 10-20 μm when first detected. Most of the microcracks were developed on the upper edges of both sides since shrinkage on these regions is higher than other regions as also observed during the free shrinkage tests. Some of these microcracks propagated and coalesced into macrocracks (cracks with width of more than or equal to 20 μm and up to 50 μm, visible if properly illuminated), while others turned first into a through crack (crack along the entire top surface) and then propagated to a full-depth crack. Figure 5.1 (a-c) shows the distribution of the macro and full depth cracks for all mixes at the end of the exposure time. Solid lines represent the visible part of the macro cracks or the through cracks and the dotted lines are the non-visible part (width less than 20 μm) of these cracks. It can be seen that high strength concrete (NA30) shows a higher intensity of macro-cracking.

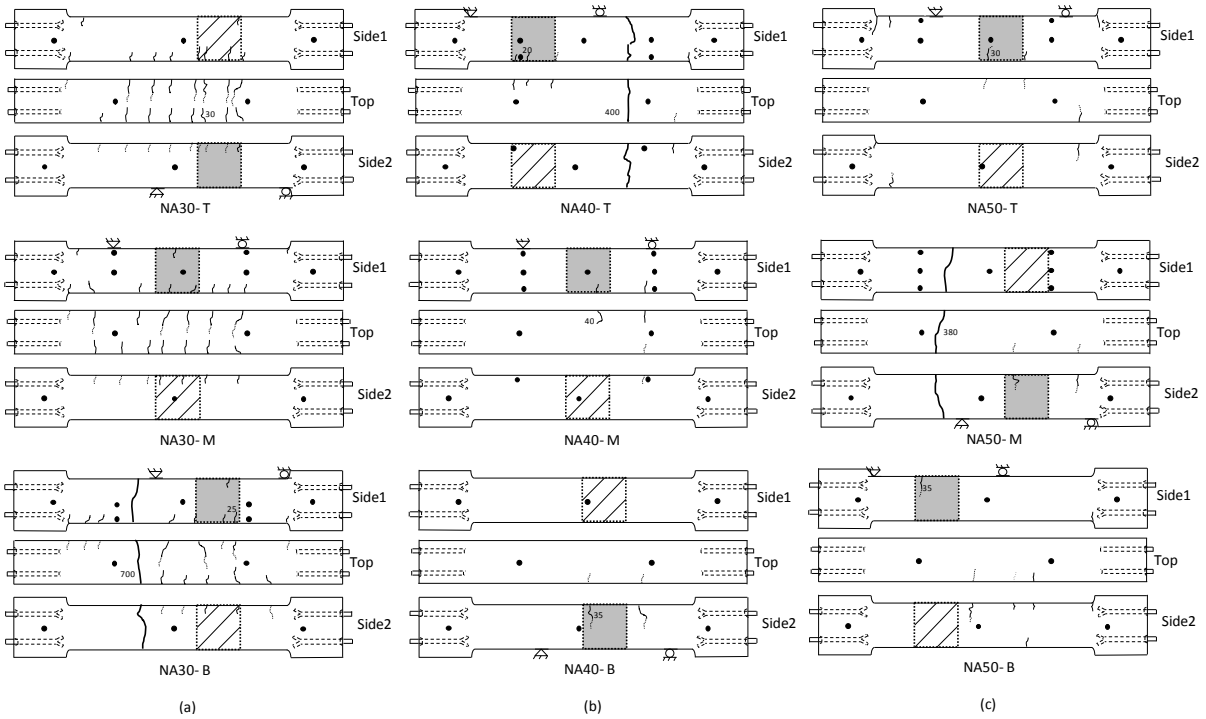

Figure 5. 1 Distribution of the macro and full depth cracks a- NA30, b-NA40, c-NA50. (shaded grey and diagonal lines zones are critical tension and compression zone, respectively, when prisms tested in bending).

Table 5.1 presents details on the through cracks for all mixes including cracking time and width of the crack. It can be seen that the higher the w/c ratio, the later the time of cracking and the lower the final crack width. The reasons behind this behaviour will be discussed in section 5.3.3.

Table 5. 1 Cracking time and width of crack.

Mix and specimen code	Cracking time (day)[a]	Crack width (μm)	
		Initial [a]	Final [b]
NA30-B	0 [c]	50	700
NA40-T	5	50	400
NA50-M	18	200	380

[a] Drying time or crack width when the crack is visible along the entire top surface. [b] Crack width after 28 days of drying. [c] Specimen cracked 24h after casting.

5.3.2 Restrained Shrinkage

This section presents and discuses the development of shrinkage strains over time (on the specimen sides and top surfaces) in the restrained specimens located at the top (T), middle (M) and bottom (B) of the restraining frame. For the sides (Side), values presented are the average of four measurements taken at the centre line. For the top surface (top), one measurement was taken at its centre over 300mm. The results of the specimens which did not crack during the restraining period are presented and discussed first followed by a discussion on the cracked specimens.

5.3.2.1 Un-cracked specimens

Figures 5.2 (a-f) show the development of shrinkage strains on the un-cracked specimens for all mixes. Just as for the free shrinkage specimens (see Part I), the shrinkage developed on the top surface is higher than that on the sides. For all mixes the strains developed on the top surface are higher than those developed on the sides during the drying exposure time. For example, on the first day of drying, for w/c 0.3, 0.4 and 0.5 the strains developed on the top surface (average of two specimens) were higher than those developed on the sides by 54%, 118% and 63%, respectively. Similar behaviour was also observed on the free shrinkage specimens and this was attributed to the higher porosity of the top surface and to the better compaction of the bottom surface.

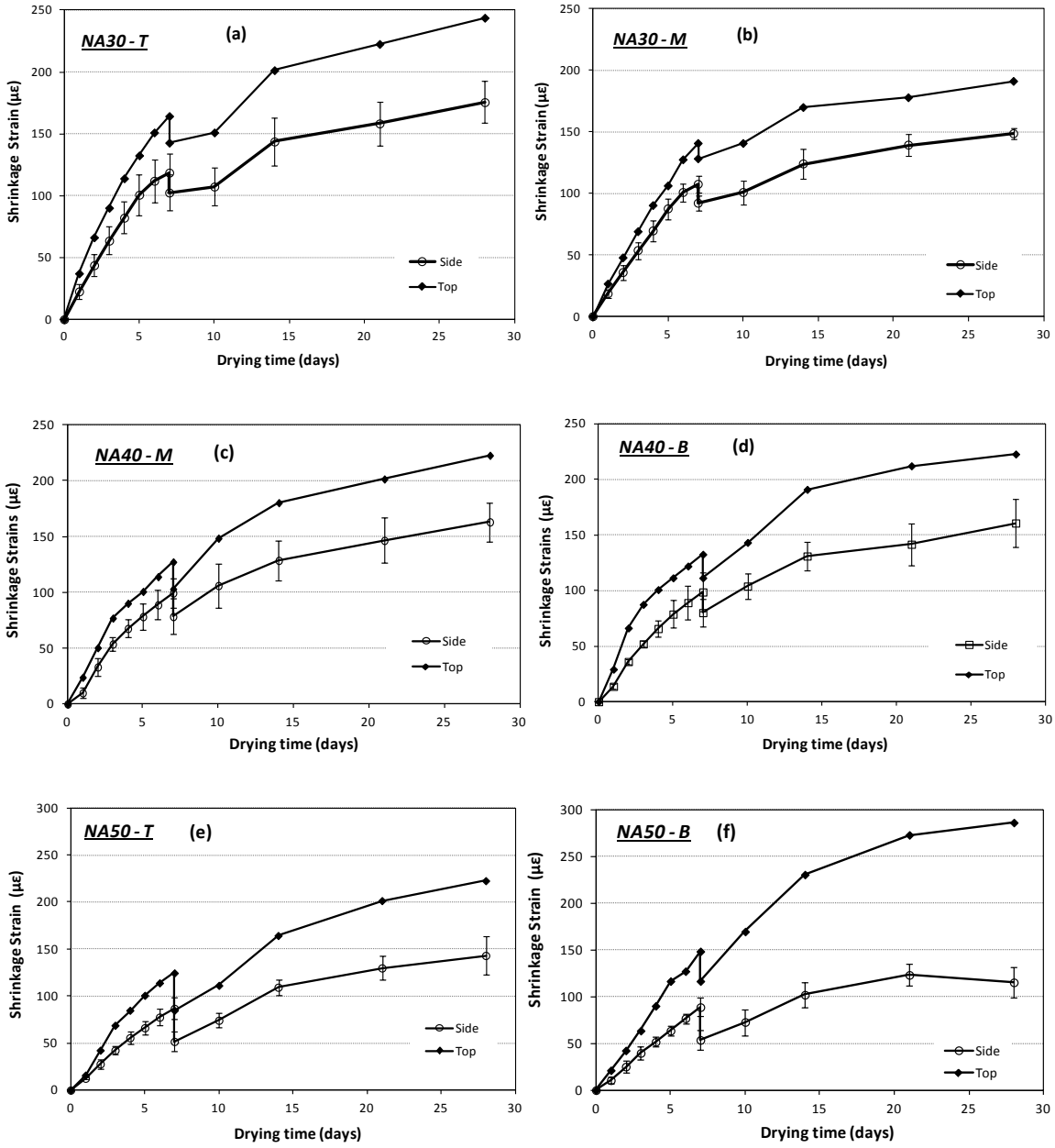

Figure 5. 2 Shrinkage strains developed on the top and sides (average) of the uncracked specimens, (a-b) mix NA30, (c-d) mix NA40, (e-f) mix NA50.

The average shrinkage strain on the sides at 7 days is compared for all w/c ratios in Figure 5.3. It can be seen that the lower the w/c the higher the shrinkage rate is, as was the case with the free shrinkage specimens. This can be attributed to the higher autogenous shrinkage of low w/c ratio mixes.

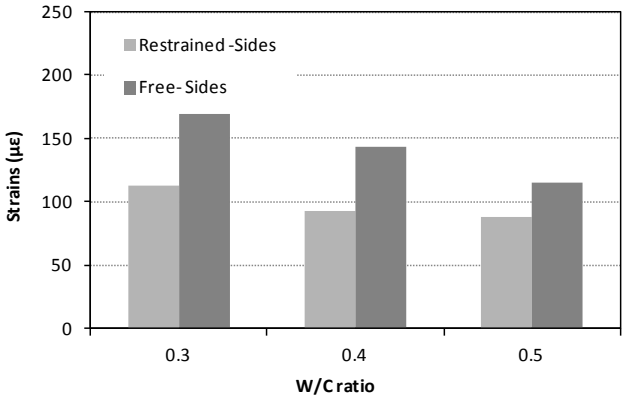

Figure 5. 3 Average shrinkage strain on the sides at 7 days for free and restrained specimens.

The sharp reduction in shrinkage strains, seen in Figure 5.2 on day 7 for all specimens, is due to the release of the strain on the main threaded bars that link the two columns of the restraining frame. Releasing the strain was done to compensate for some strain loss and to increase the RF that decreases with time (as will be discussed in subsection 5.3.4). The two readings at 7days represent the readings prior to and just after strain releasing. This time was chosen since the results of the trial mixes revealed that all three mixes at 7 days achieved more than 80% of their 28 day strength. The release of the frame led to strain recovery (on the sides) of 16 με (average of T and M specimens) for mix NA30, 20 με (average of M and B specimens) for mix NA40 and 35 με (average of T and B specimens) for mix NA50. Strain recovery measured on the top surface was similar to that on the sides. Due to the fact that all mixes had the same level of prestress applied on the frames, it is normal to expect that mixes with higher w/c ratio (0.5) exhibit more strain recovery than the mixes with lower w/c ratio due to their elastic modulus. Hence, the amount of prestress applied in all mixes appears to be consistent.

5.3.2.2 Cracked specimens

NA30 (B specimen)

The development of shrinkage strains on specimen B is shown in Figure 5.4. A crack of 50 μm was observed on the specimen after demoulding (24h after casting and before the start of drying). After 3 days of drying, the width of the crack increased to 70 μm, which explains the apparent expansion in the early ages in the regions where the crack developed, whereas concrete in the other regions continues to shrink (see Figure 5.5). Early cracking for this mix is likely to be caused by high autogenous shrinkage which is estimated at 20 με after 1day [19]. Another possible reason is thermal shrinkage caused by the transient temperature

rise due to cement hydration during hardening as shown in Figure 5.6, which represents the evolution of temperature inside the concrete (T, M and B specimens) monitored by using thermo-couples.

The effect of releasing strain in the frame after 7 days can be seen as a sharp increase in the strain in the regions where the crack developed. For example, the strain on the top, Side1, A (upper edge of side1) and Side1,1 increased from -82 με, -100 με, -30 με to -1659 με, -1712 με, -1484με, respectively. The average strain increase in these regions corresponds to 0.47mm increase in the crack width. After 7days and up to the end of drying time, the crack width kept increasing with a similar rate in all cracked regions. The crack width at the end of the exposure time was 0.7 mm.

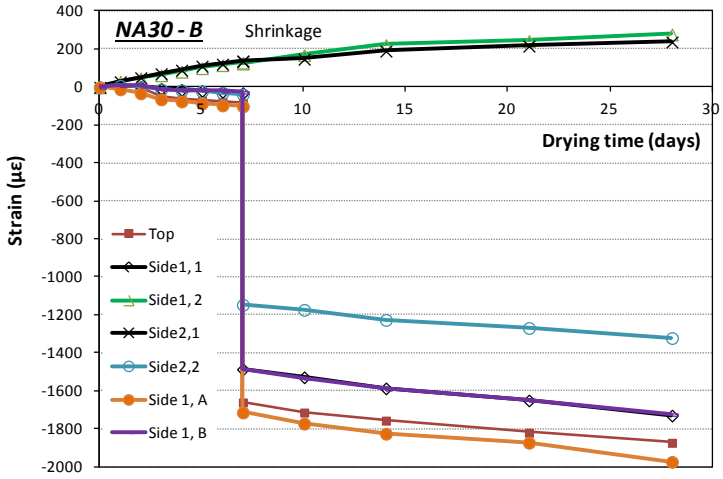

Figure 5. 4 Development of shrinkage strains on specimen B (mix NA30).

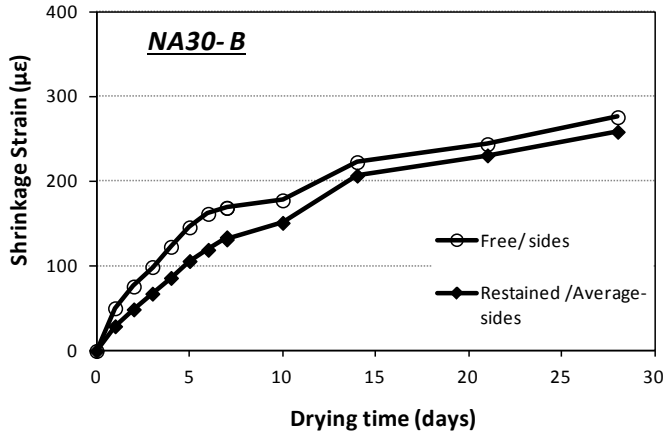

Figure 5. 5 Shrinkage strains of the sides of free specimens and those of restrained specimens in the uncracked regions for mix NA30.

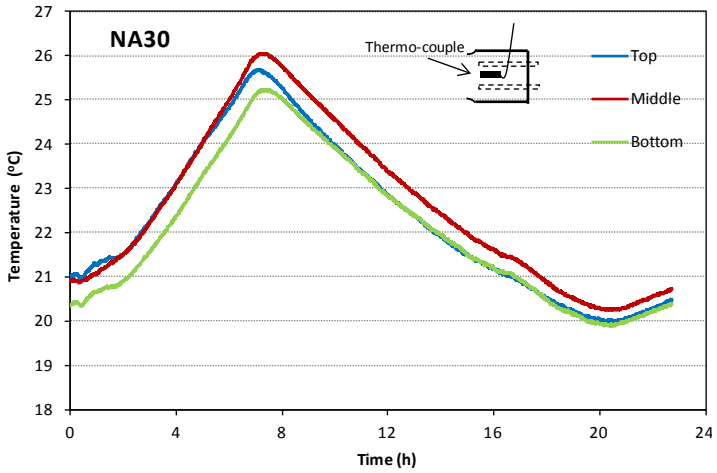

Figure 5. 6 Temperature evolution inside the concrete due to cement hydration for restrained specimens (mix NA30).

NA40 (T specimen)

Figure 5.7 shows the development of shrinkage strains on specimen T measured on the sides (Side1,1, Side1,2, Side2,1, Side2,2), on the top (top), upper edge of side1 (Side1,A), upper edge of side2 (Side2,A) and centre of side1 (Side1,B). The first through crack of width 50μm developed on day 5. This can be seen as a sharp reduction in shrinkage strain on Side1,2, Side2,1, top, Side1,A and Side2,A (where the crack developed). Side1,1 and Side2,2 remained uncracked and carried on shrinking (same as the free specimens see Figure 5.8). Between day 5 and 7, a very slow rate of strain development (crack width increase) was observed in the cracked regions.

A sharp increase in the strain (apparent expansion) occurred after strain release on day 7. Strains on the top, Side1,A and Side2,A increased from -80 με, -103 με, -106 με to -578 με, -596 με, -636 με, respectively; the average strain increase in these regions corresponds to 0.15 mm increase in the crack width. The estimated crack width on the top and the edges was higher than that on the centre of the sides. After 7 days, the crack width increased with similar rate in all cracked regions. At the end of the test, the crack width reached around 0.4 mm.

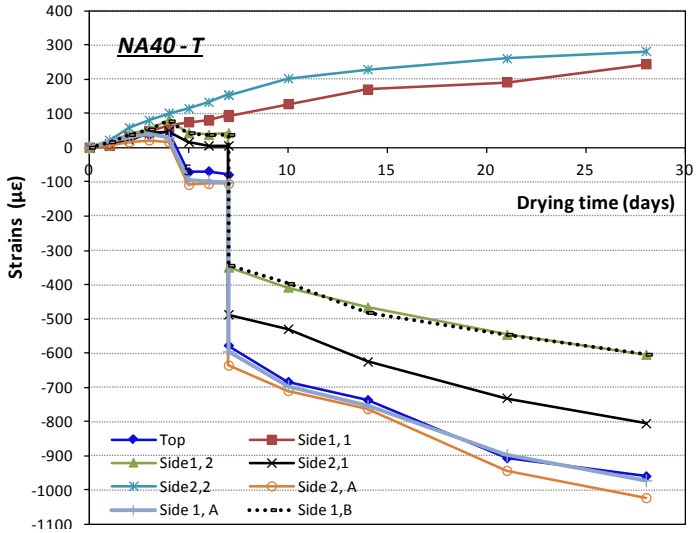

Figure 5. 7 Development of shrinkage strains on specimen T (mix NA40).

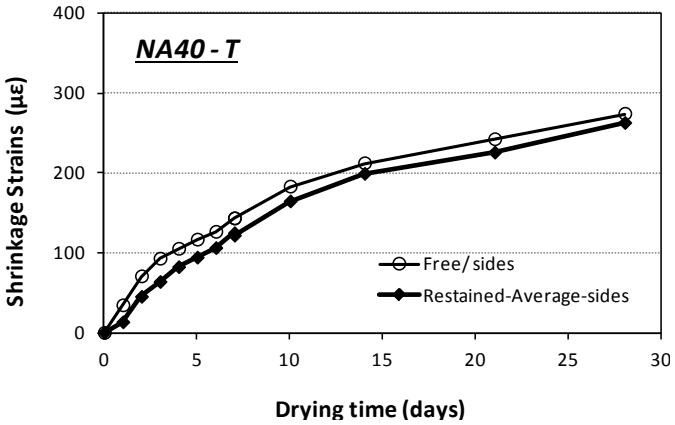

Figure 5. 8 Shrinkage strains of the sides of free specimens and those of restrained specimens in the uncracked regions for mix NA40.

NA50 (M specimen)

The development of shrinkage for specimen M is shown in Figure 5.9. None of the specimens of mix NA50 cracked before or right after releasing the strain in the frame. Up to 7 days, all regions experienced shrinkage with higher values on the top and edges than the other regions. Releasing the strain recovered 40 με of strain (on the top) and an average of 36 με of strain (on the sides). However, no full depth crack was observed. Up to 14 days, in some regions the concrete kept on shrinking, while in other regions the shrinkage strains either decreased or remained constant. A crack of 0.25 mm width was observed on day 18. The effect of the crack on the strain values can be seen as a sharp change in strain from

positive values (shrinkage) to negative values (expansion). For example, the strain on the top, Side1,A and Side1,1 changed from 77 με, 58 με, 90 με (on day 14) to -935 με, -1049 με, -652 με, (on day 21), respectively. However, in other regions, where no through cracks developed, strains were similar to free shrinkage strains (see Figure 5.10). The average strain increase on the top and the edge (Side1,A) corresponds to a crack width of 0.32 mm. The crack width was found to be 0.38 mm at the end of the drying exposure time (28 days).

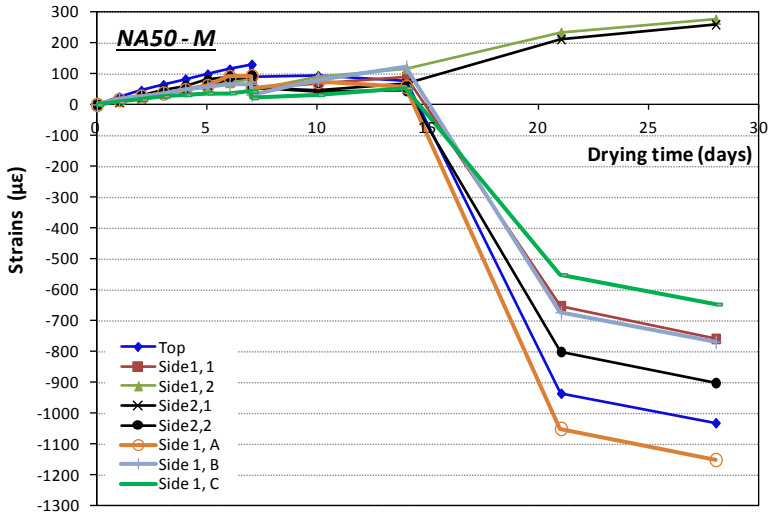

Figure 5. 9 Development of shrinkage strains on specimen M (mix NA50).

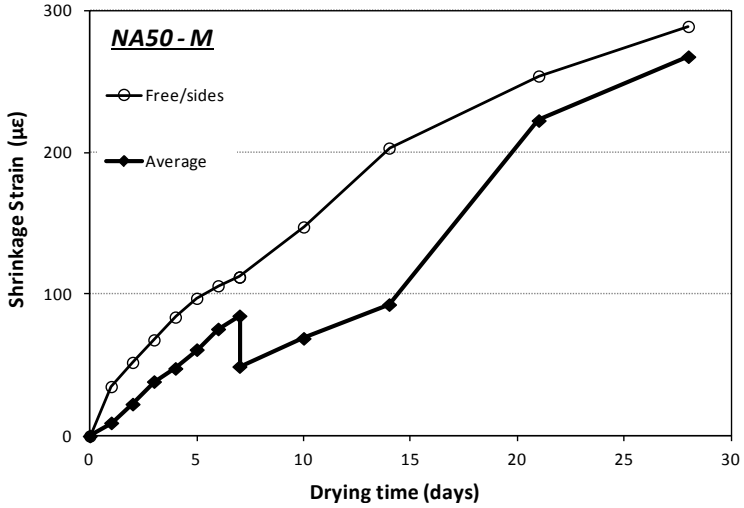

Figure 5. 10 Shrinkage strains of the sides of free specimens and those of restrained specimens in the uncracked regions for mix NA50.

5.3.3 Failure of Concrete under Restrained Conditions

The results of the restrained shrinkage of the specimens that cracked show that the failure (time of cracking and final crack width) of restrained concrete varies according to the w/c ratio. This can only be attributed to the effect of the strength (magnitude and rate of development) since all mixes were subjected to the same restraint and drying conditions.

Figure 5.11a shows the compressive strength (f_{cu}) development of all mixes, whilst Figure 5.11 b shows the predicted stiffness (E_c) development according to Eurocode-2 [19]. If ultimate strength is used as a failure criterion, the weaker mix (w/c= 0.5) is expected to fail first. However, the lower w/c ratio (high strength) mix (w/c= 0.3) failed earlier (at 24 h) than the mixes with higher w/c ratios (lower strength), w/c= 0.4 at 4 days and w/c=0.5 at 18days. Similar result were reported by Altoubat and Lange [3]. It is therefore, important to understand factors responsible for the failure of restrained concrete. One factor can be the stress history (magnitude and rate of development) which depends on the stiffness (magnitude and rate of development) and shrinkage strains. For w/c =0.3 the stiffness develops faster (Figure 5.11b) which can lead to higher tensile stress developing at very early ages. Furthermore, autogenous and thermal shrinkage strains are higher in low w/c ratios mixes and less moderated by creep.

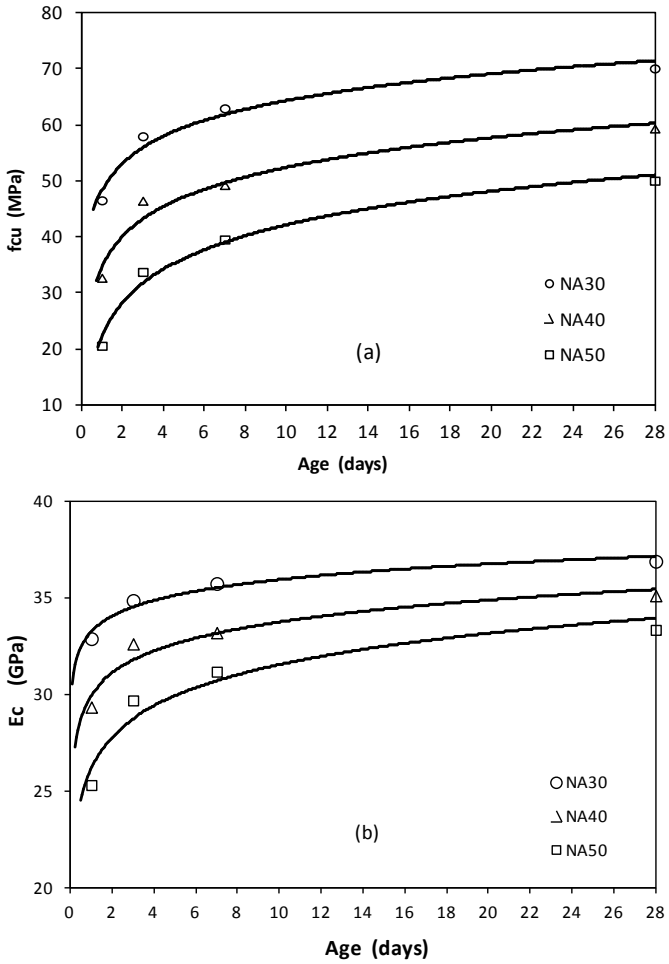

Figure 5. 11 (a) Evolution of compressive strength, (b) and predicted evolution of elastic modulus for all mixes.

5.3.4 Restraint Factor RF

5.3.4.1 Theoretical RF

Linear elastic Finite Element Analysis (FEA) was undertaken (see Figure 5.12) to assess strain losses due to deformations of the restraining frame and local deformations of the specimens ends. Similar analysis was also undertaken by the authors previously [18] for the single rig. The analysis was carried out by applying a tensile force on each of the threaded bars to simulate the tensile force that develops inside restrained concrete upon drying. The analysis shows that there are global deformations (bending and contraction) in the restraining frame and local deformations at the ends (where the threaded bars are attached to the frame). For example, when a 100 με of concrete shrinkage (E_c= 26 GPa) is restrained, the expected tensile force will result in a total strain loss (shortening and bending of the

beams and deformations of the ends) of 205 με, 112 με and 132 με for T, M and B specimens, respectively. It should be noted that the top concrete specimen is likely to resist the rotation of the frame and hence its RF may be better than determined by this analysis. For the single rig, the same tensile force causes a total strain loss of 263 με. This means that the use of the frame reduced the strain loss by an average of 43% (22% for T, 57% for M and 50 % for B).

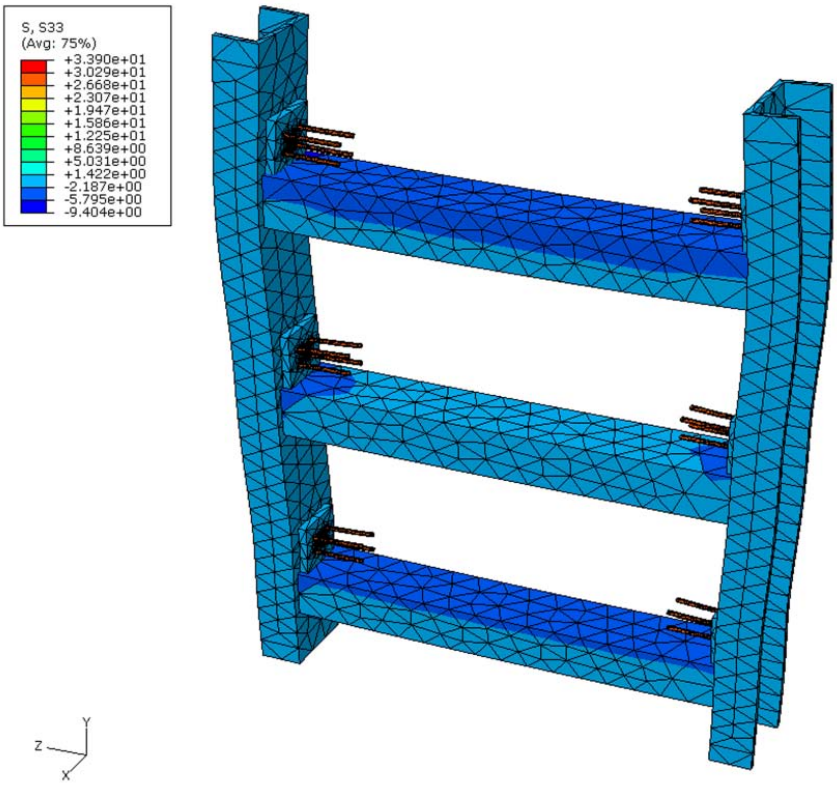

Figure 5. 12 Deformed shape and axial stresses of the restraining frame.

To determine the variation of the estimated (theoretical) RF over time and compare it with the apparent (measured) RF for the restraining frame, a procedure developed in previous work by the authors [18] is used to estimate the theoretical RF of the rig. Figures 5.13 (a-c) show the estimated RF of the T, M and B specimens for all mixes. As expected the lower the w/c ratio of the mix the lower the RF as stiffer concrete can pull in the ends more, thus leading to more deformation and strain loss.

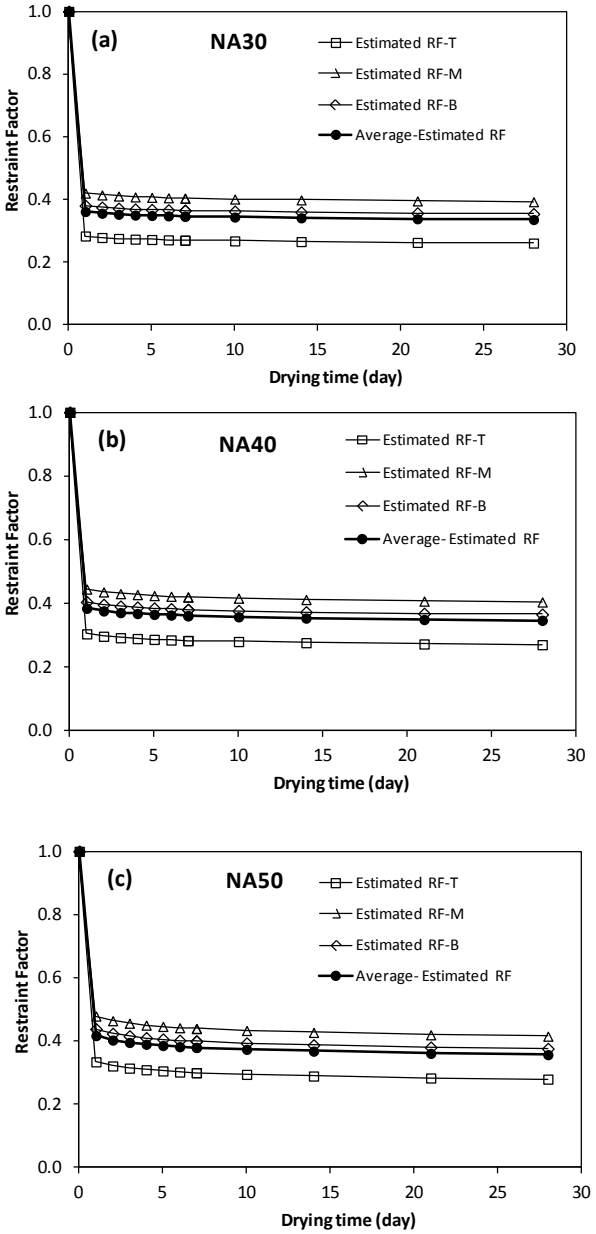

Figure 5. 13 Estimated RF of the T, M and B specimens a- NA30, b- NA40, c- NA50.

5.3.4.2 Results of Un-cracked specimens

NA30

Figures 5.14 a and b show the RF versus time of non-failed specimens for NA30. As expected the RF for the sides is higher than the top surface. For example, the RF after one day of drying for specimens T and M are 55% and 63% (on the sides) and 42% and 58% (on the top), respectively. However, by day 7, the RF for specimens T and M decreases to 30% and 36% (on the sides) and to 18% and 30% (on the top), respectively. After releasing the

strain on day 7, the RF of specimens T and M increased on average 9% on the sides and 8.5% on the top. This was caused by an expansion of around 15 με. After this time, RF more or less stabilizes.

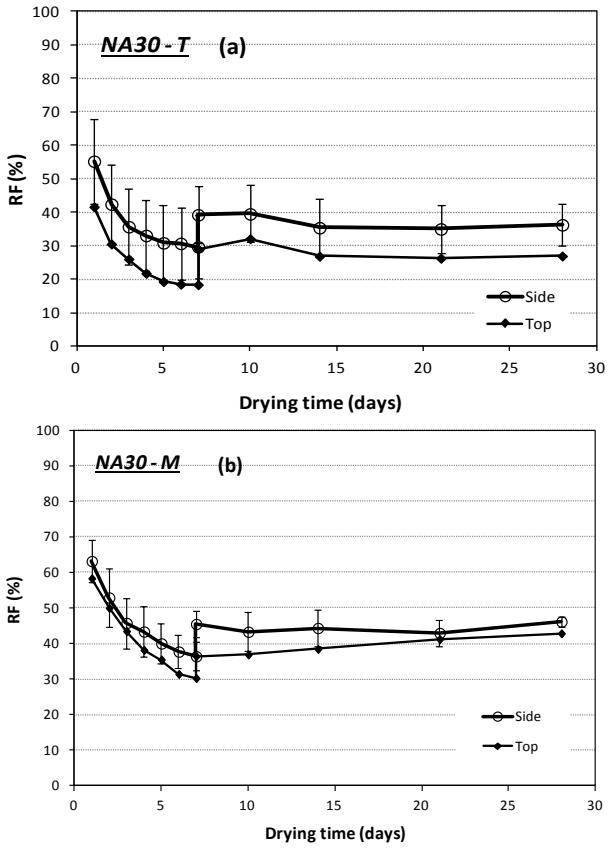

Figure 5. 14 Restraint factor versus drying time on the sides and the top surface for mix NA30 a- Specimen T, b- Specimen M.

NA40

Figures 5.15 a and b show the development of the RF for mix NA40. For the first few days, the RF for the sides is higher than that of the top, but after that the opposite applies. After 24h of drying exposure, the RF values of the M and B specimens were 71% and 60% (for sides) and 59% and 50% (for top), respectively. These values decreased to 31% and 31% (for sides) and 43% and 40% (for top) after 7 days. For both specimens the development of RF slows down after the first few days. After releasing the strain, specimen T failed (as discussed in section 3.2.2). The RF on average increased by 14%, corresponding to an apparent expansion of around 20 με.

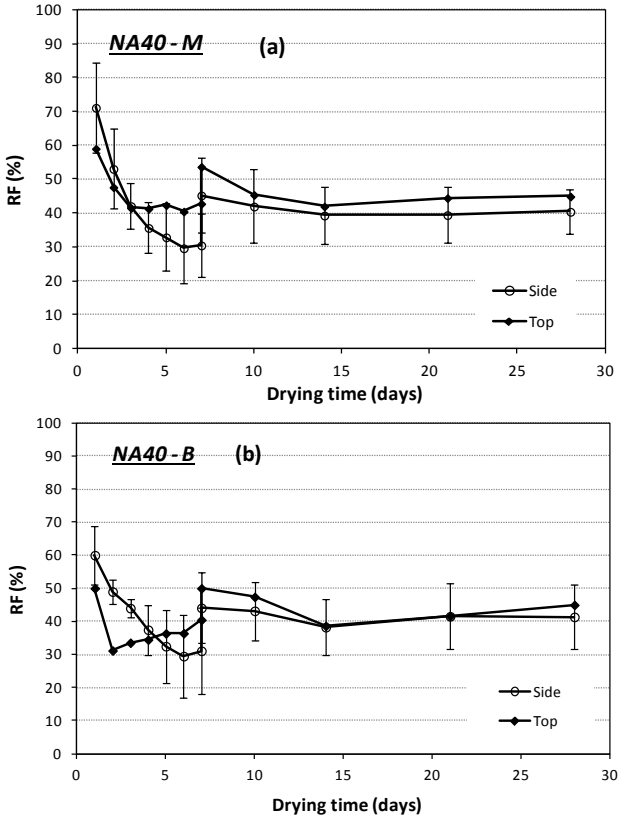

Figure 5. 15 Restraint factor versus drying time on the sides and the top surface for mix NA40 a- Specimen M, b- Specimen B.

NA50

The RF development of un-cracked specimens T and B for mix NA50 are shown in Figures 5.16 a and b. Unlike mix NA30, RF for the top is higher than that of the sides, especially during the first week of drying. After 24h of drying, the RF values of the T and B specimens were 64% and 70% (for sides) and 76% and 69% (for top), respectively, These values decreased sharply by an average of 45% on the sides and 33% on top just before releasing the strain in the frame. After strain release, none of the specimens failed and the RF of the sides increased to around 53 % due to an apparent expansion of around 35 με.

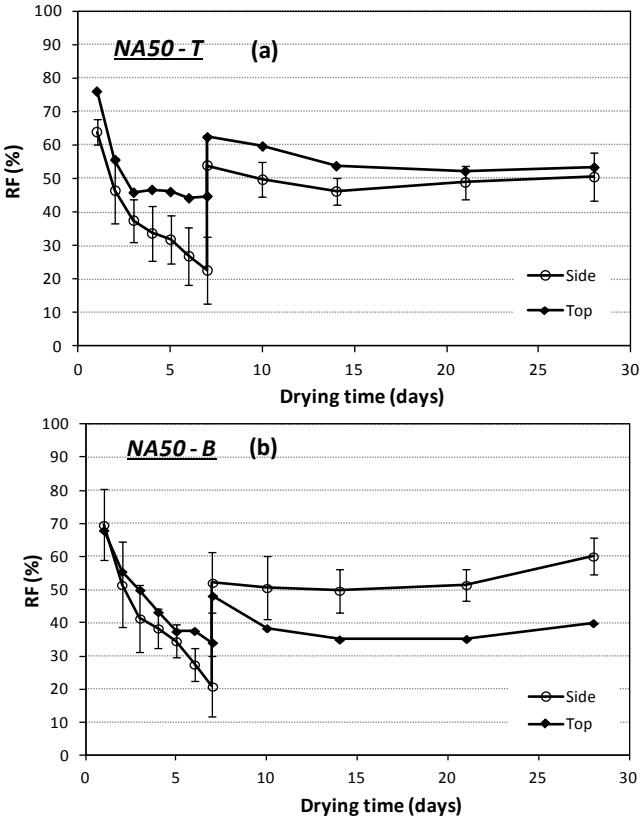

Figure 5. 16 Restraint factor versus drying time on the sides and the top surface for mix NA50 a- Specimen T, b- Specimen B.

5.3.4.3 Discussion on RF of un-cracked specimens

Overall RF loss

Figures 5.17 (a-f) show theoretical (estimated) and the apparent (measured) RF of the uncracked specimens for each mix. It can be seen that the majority of strain and RF loss for all specimens can be attributed to the relative stiffness between the frame and the concrete specimens. Nonetheless, the theoretical prediction still underestimates the long-term RF loss, possibly due to some loss of stiffness or creep (relaxation) of concrete due to the enforced expansion.

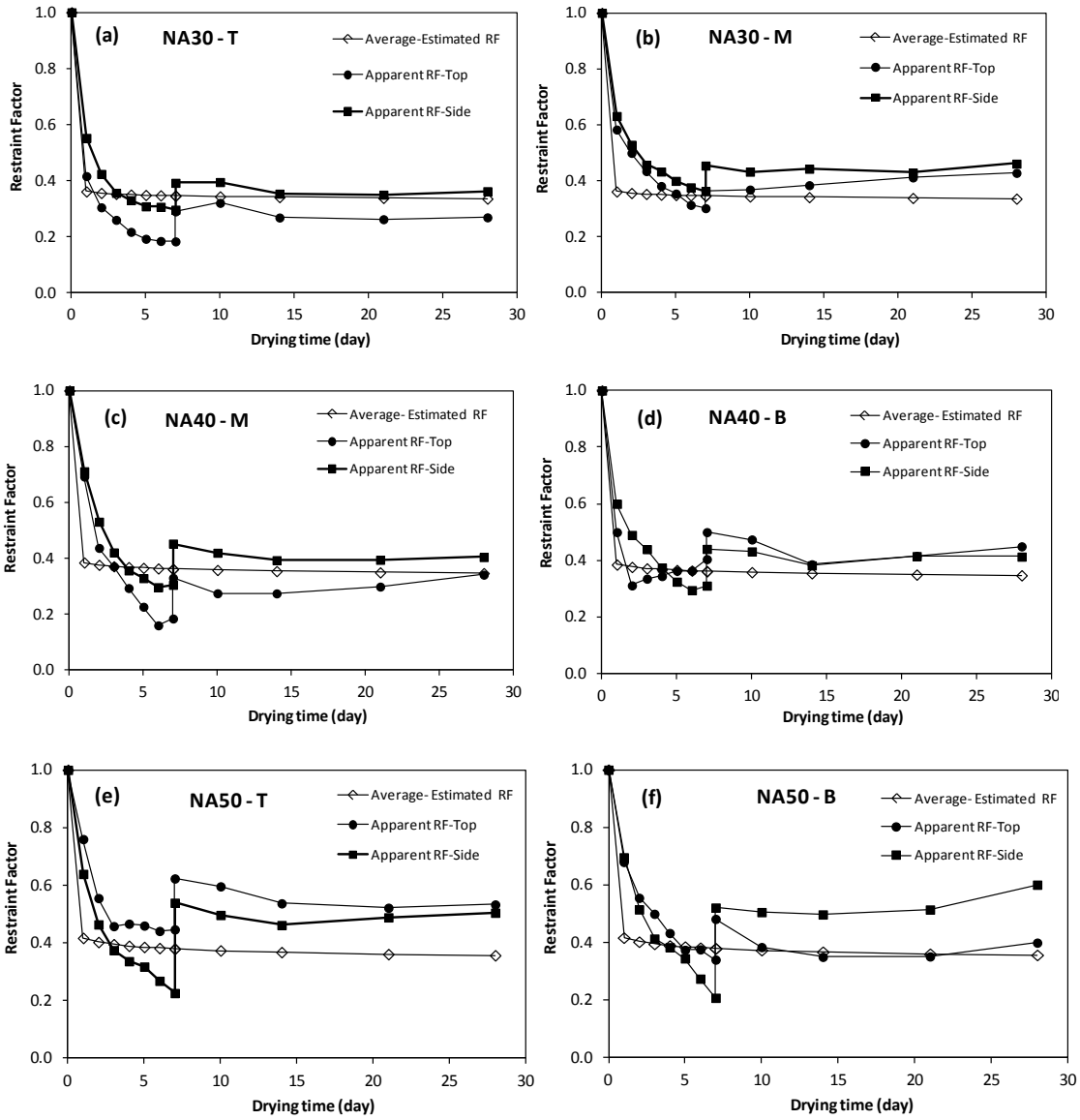

Figure 5. 17 Average theoretical RF and measured RF on the top and the sides of un-cracked restrained specimens for all mixes.

Initial RF loss

Apparent RF is initially very high for all mixes and on all surfaces (see Figures 5.17 a-f), but decreases at a high rate during the first few days. This may be attributed to that fact that the early age microcracking may have reduced the stiffness gain of the concrete, resulting in less strain loss than expected. After that initial stage and up to 7 days, the rate of reduction in RF either slows down (stabilises) or even increases. This can be due the effect of unwanted cracks developing at the end of the specimen beyond the shrinkage measuring region, impairing the restraint efficiency of these anchored ends and resulting in low apparent RF.

Difference between RF on the top and sides surfaces for different mixes

The RF at the top is lower than that of the average of the sides for mix NA30, whereas the opposite applies for NA50. For mix NA40, the RF at the top is lower only for the first few days. It was observed, from both free (Part I) and restrained shrinkage strains, that for all mixes the shrinkage strains on the top are always higher than those developed on the sides. Hence, the RF (measured) is expected to be lower at the top than the sides. This can explain the trend of RF of mixes NA30 and NA40, but not that of mix NA50. Therefore, there should be another factor that affects the RF results. This could be the effect of shrinkage curvature (due to difference in shrinkage strains between top, sides and bottom surfaces of the concrete specimens), shown in Part I for free shrinkage. To assess the effect of the shrinkage curvature on the RF, the efficiency of the frame in restraining curvature should be evaluated. This can be done by comparing the amount of the curvature on the restrained and free specimens. The restrained specimens curvature can be obtained by calculating the difference in restrained shrinkage strains, between the top and the sides of the specimens. Though the configuration of the frame does not allow measuring shrinkage strains at the bottom of the restrained specimen, curvature of the upper half of the specimens (k_{T-S}) can be obtained.

Figures 5.18 (a-c) show the evolution of the average curvature for the free specimen and the relative restrained curvature for uncracked specimens for all mixes. It can be seen that there is significant difference in the degree of restraint that the frame provides against shrinkage curvature for different mixes. The stronger the mix, the lower the degree of restraint and this can explain why the RF at the top is not always lower than that of the sides. There is almost no restraint against curvature for mix NA30, since the top surface shrinks more than the sides leading to lower RF values at the top than the side (see Figure 5.14). For the weaker mix NA50 which wants to curve more, there is more resistance to the curvature by the frame and as a result, the apparent RF at the top is higher than that for the sides (see Figure 5.16).

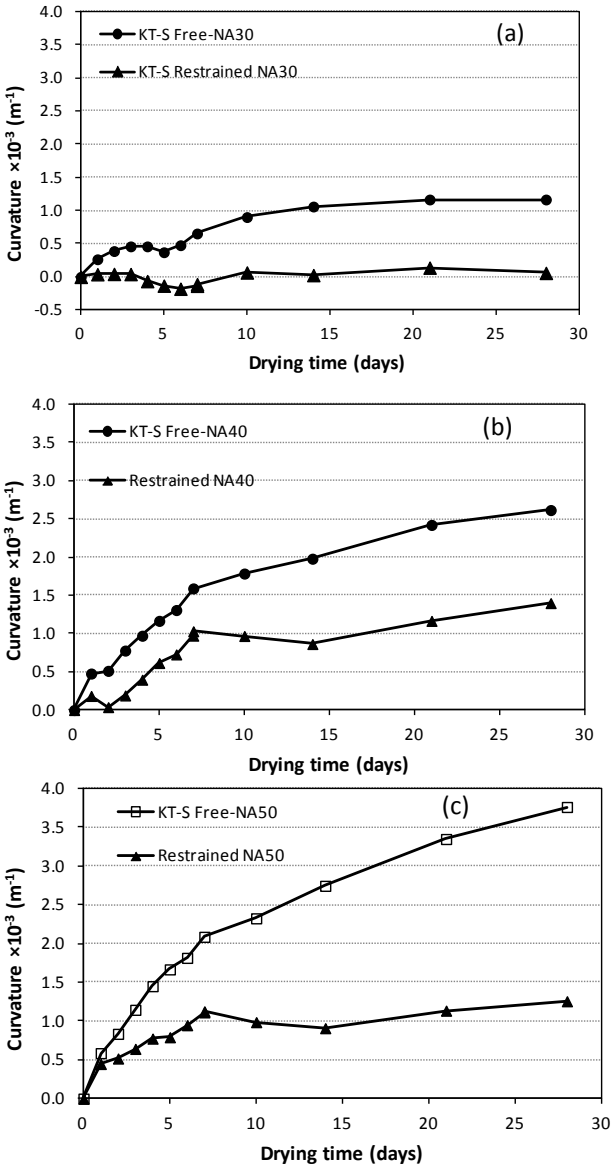

Figure 5. 18 Average shrinkage curvature developed on free specimens and average shrinkage curvature restrained by the frame, (a) mix NA30, (b) mix NA40, (c) mix NA50.

5.4 Mechanical Properties

Almost all previous studies utilize uniaxial compression tests to quantify the effect of drying on concrete mechanical properties (strength and stiffness). Such mechanical properties may be affected by the drying shrinkage (without external restraint) in two ways:

1) The strength increases as a result of an increase in capillary pressure (which acts as isotropic pressure) on the C-S-H particles when saturation decreases. This can lead to a stiffening effect by increasing the bonding between the C-S-H particles [20-22]. This is

amplified by the confining effect of the core of the specimen due to moisture gradients increasing the concrete rigidity [7] .

2) The strength and the stiffness decrease due to the formation of microcracks (which develop due to non-uniform shrinkage, enhanced by local restraint by the aggregates) [20].

The evolution of the mechanical properties is dominated by the opposing effects of these two phenomena: strengthening (stiffening) of materials and drying shrinkage induced microcracking [20, 23].

5.4.1 Compressive Strength (Cubes)

Compressive strength after 1, 3, 7 and 28 days of curing is presented in Table 5.2 and Figure 5.11. Table 5.2 also includes the standard of deviation (SD) of the results and the normalized strength to that of NA40. As expected, the high strength concrete (w/c =0.3) exhibited higher compressive strength and also showed higher rate of strength development in comparison to mixes 0.4 and 0.5 w/c.

Table 5. 2 Compressive strength, normalized strength and standard deviation (SD) of all mixes.

Mix Type	Compressive Strength (MPa) at different ages				Normalized Strength at different ages				SD			
	1	3	7	28	1	3	7	28	1	3	7	28
NA30	46.6	58.0	63.0	70.1	1.42	1.25	1.28	1.18	0.6	0.4	0.6	1.4
NA40	23.7	46.5	49.3	59.4	1	1	1	1	0.6	0.7	1.2	0.3
NA50	20.6	33.8	39.6	50.1	0.63	0.73	0.8	0.84	0.5	0.3	0.3	0.5

5.4.2 Compressive Strength (Prisms)

The compressive strength was also determined from specimens exposed to free (F) and restrained shrinkage (R) and for the control prisms (water cured prisms, WC) as shown in Figure 5.19 a-c. The tests were conducted on portions of prisms already tested and broken in bending. All results presented in this section are the average of three tests per mix and

normalized to the values of the compressive strength of the water cured cube specimens (Cube) at 28 days.

A comparison between the normalized compressive strength obtained from portions of water cured prisms (WC) with those obtained from water cured cube specimens (Cube), for all mixes, reveals that the difference between the two samples is negligible. Hence, using the BS 1881-119 [15] approach to obtain compressive strength can be considered fairly accurate.

As expected, drying (in both conditions free and restrained) reduces the compressive strength by about 10-14%. Regardless of the w/c ratio, the normalized strength of the dried specimens is in the range of 0.86-0.87 for F specimens and in the range of 0.86-0.90 for R specimens. Though surface microcracking due to shrinkage could reduce compressive strength, its effect appears to be relatively small compared to the long term effect of maturity. This may partly explain discrepancies in the results in the previous studies [20].

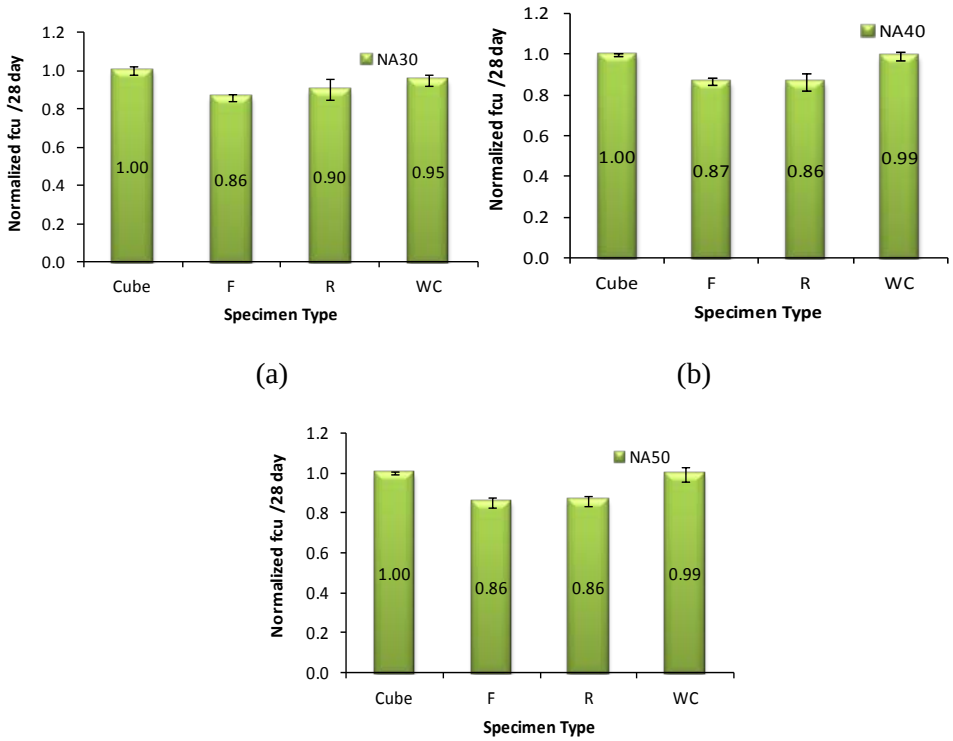

Figure 5. 19 Normalized compressive strength a- NA30, b- NA40, c- NA50.

There is insignificant difference between the compressive strength of F and R specimens. This means that the cracks developed on the unrestrained specimens and on the restrained specimens had almost the same effect on the compressive strength of the concrete. One

possible reason behind this is the way the specimens are tested in the compression machine. Most shrinkage induced macrocracks (developed on the edges) lay in the regions close to the upper and lower plates of the machine (see Figure 5.20), which are well confined. Hence, this test may overestimate the actual strength by up to 10-15%.

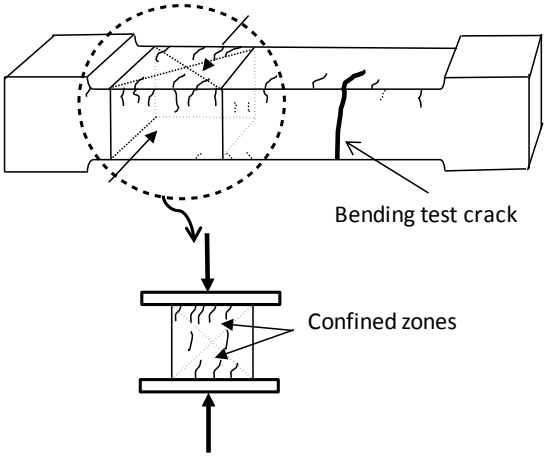

Figure 5. 20 Sample for compressive strength test from a restrained specimen.

5.4.3 Flexural Strength

After 28 days of drying, the free shrinkage specimens were prepared for the bending test. The position of the supports and load points varied according to the type of the specimens (free or restrained). This is explained below:

Free Shrinkage specimens

When possible, the bending test was conducted twice on two parts of the same specimen. The position of the supports and the point loads in the two cases are illustrated in Figure 5.21.

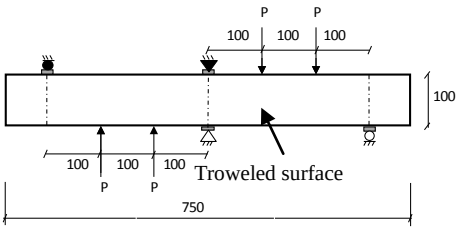

Figure 5. 21 Positions of supports and loads in bending test for free shrinkage specimens (dimensions in mm).

Restrained Shrinkage specimens

The load points and supports used are shown in Figure 5.22. The location of these were selected so as to capture within the critical region the widest crack and as many cracks caused by the restrained shrinkage. In Figure 5.1, the critical region is shaded in grey when in tension and with diagonal lines when in compression. The macrocracks and their maximum width at the edge are also shown in the Figure 5.1.

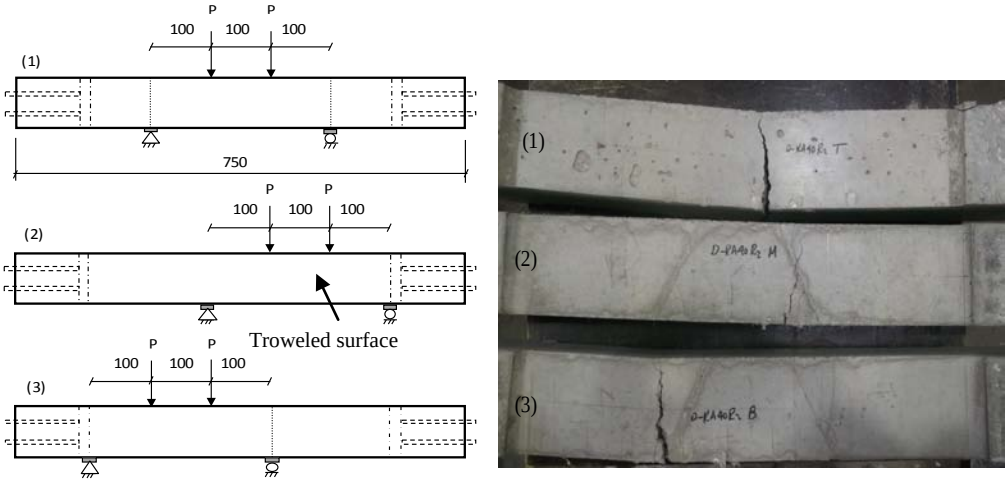

Figure 5. 22 Positions of supports and loads in bending test for restrained shrinkage specimens (dimensions in mm).

Figures 5.23 a-c show the average (from 3 specimens) load-deflection curves for water cured (WC) and free shrinkage specimens (F), as well as the curves of all restrained shrinkage specimens (R_T, R_M and R_B) for all mixes. Table 5.3 shows the results of the flexural strength (magnitude and normalized to that of WC) for all mixes. It is clear that shrinkage induced cracks affect the flexural strength of mixes with different w/c ratios in a different manner.

For mix NA30, in comparison to WC, F specimens showed lower flexural strength (decrease of 23%). The strength reduction for the restrained specimens was in a similar range of 11-24%. The free and restrained specimens of mix NA40 showed comparable or even higher flexural strength to that of the WC specimens. For mix NA50, the flexural strength was slightly increased (by 5%) for F specimens or slightly reduced (by 2-5%) for restrained specimens.

It is clear that shrinkage of concrete under free and restrained conditions affects the flexural strength of low w/c (0.3) mixes more than that of high w/c mixes (0.4 and 0.5). This may be due to higher autogenous and thermal shrinkage (due to hydration). The higher rate of

shrinkage (autogenous and drying, see Part I) and elastic modulus evolution (see Figures 5.11) of mix NA30 (w/c= 0.3), in comparison to mixes NA40 and NA50, also leads to faster rate of tensile stress development. A higher rate of shrinkage and elastic evolution also reduces relaxation by creep. These lead to earlier and more intensive microcracking (see Figure 5.1) which can affect adversely the flexural strength.

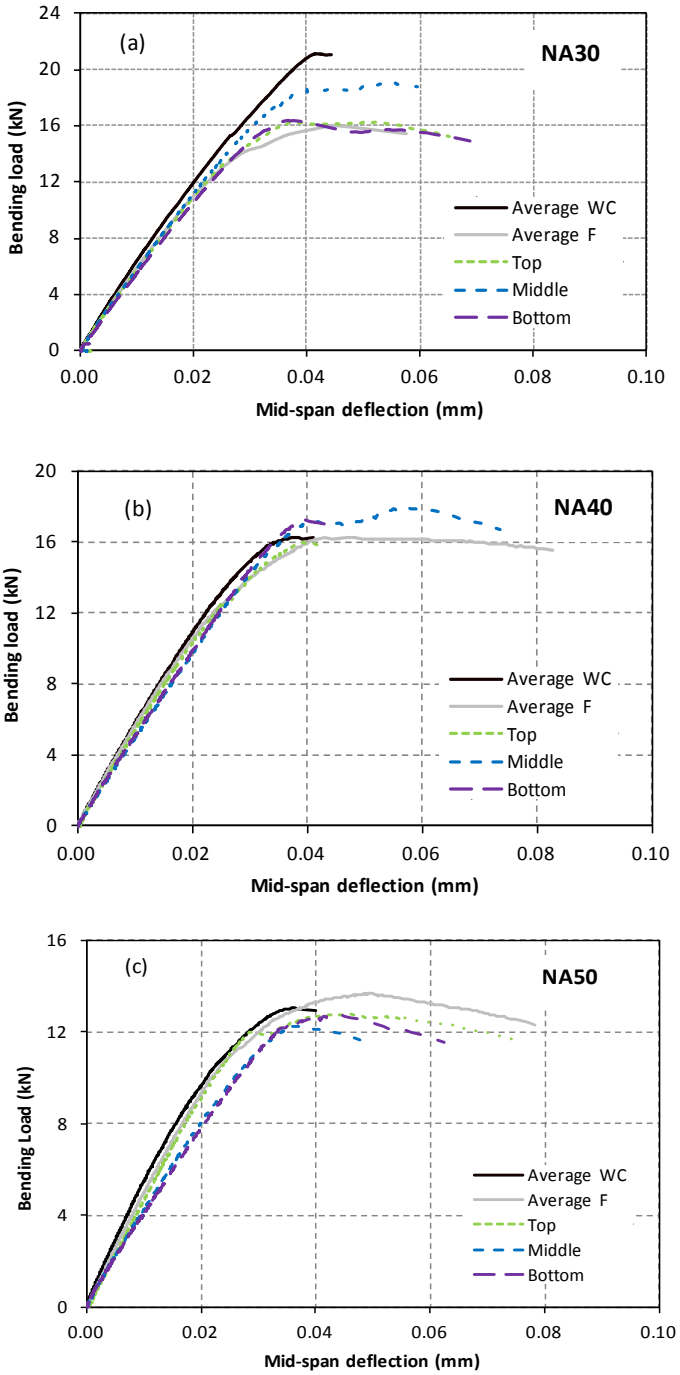

Figure 5. 23 Load-deflection curves for WC (average), F (average) and restrained specimens, a-NA30, b- NA40, c-NA50.

Table 5. 3 Flexural strength and E_{fmax} for all mixes.

Mix	No. of specimens	Type of specimen	Flexural strength in MPa (*)	Normalized Flexural strength	E_{fmax} in GPa (*)	Normalized E_{fmax}
NA30	3	WC	6.4 (0.1)	1	42.3 (0.2)	1
	4	F	4.9 (0.3)	0.77	38.6 (2.3)	0.91
	1	R_T	4.8	0.76	37.6	0.85
	1	R_M	5.7	0.89	38.0	0.89
	1	*R_B*	*4.9*	*0.77*	*35.6*	*0.84*
NA40	3	WC	4.9 (0.2)	1.0	39.7 (0.3)	1
	4	F	4.9 (0.3)	1.0	38.7 (0.2)	0.97
	1	*R_T*	*4.6*	*0.94*	*36.3*	*0.91*
	1	R_M	5.1	1.04	33.5	0.84
	1	R_B	5.0	1.02	33.4	0.84
NA50	3	WC	3.9 (0.4)	1.0	36.2 (4.2)	1
	5	F	4.1 (0.3)	1.05	34.3 (1.2)	0.95
	1	R_T	3.8	0.98	32.2	0.89
	1	*R_M*	*3.7*	*0.95*	*27.3*	*0.75*
	1	R_B	3.8	0.98	25.8	0.71

*Standard deviation. Values in *italic* represents results of cracked restrained specimens.

5.4.4 Flexural Elastic Modulus E_{fmax}

Figures 5.24 a-c show the averaged E_{flex}- bending load curves for WC and F specimens and the curves of restrained specimens (Top, Middle and Bottom) for all mixes. The results of E_{fmax} (magnitude and normalized to that of WC) for all mixes are also shown in Table 5.3. In general, it can be seen that shrinkage induced cracks affected negatively the E_{fmax} of both free and restrained specimens with more pronounced effects on the restrained specimens.

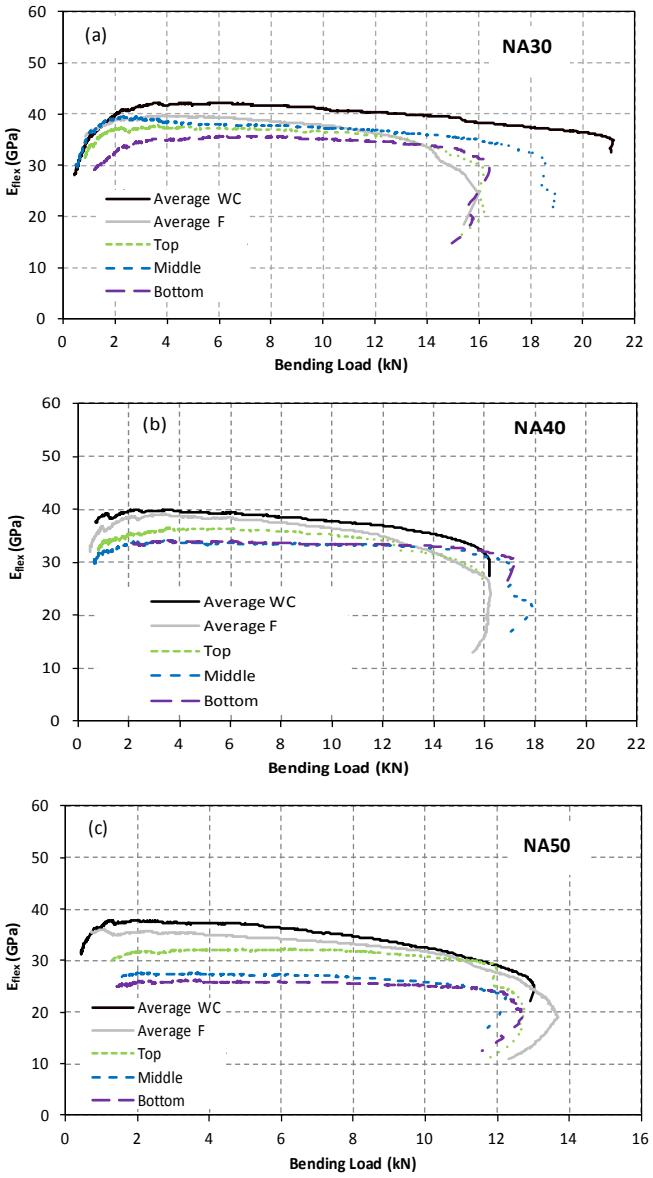

Figure 5. 24 Flexural elastic modulus versus bending load for WC, F and restrained specimens, a- NA30, b- NA40, c- NA50

In comparison to that of the WC specimens, the average E_{fmax} of the unrestrained specimens decreased by 9%, 3% and 5% for mixes NA30, NA40, and NA50, respectively. Just as the flexural strength, the damage of E_{fmax} in the mix with low w/c ratio (0.3) was higher than mixes with high w/c ratios (0.4 and 0.5). This reduction is also attributable to the same previously mentioned effect of surface microcracking.

Macro and micro cracks affected the E_{fmax} more adversely in restrained specimens. In particular, E_{fmax} for R_M and R_B of mix NA50 was lower than that of the WC specimens by 25% and 29% , respectively, whereas E_{fmax} of specimen R_T reduced by only 11%. The lower reduction of R_T specimen may be due to the fact that during drying exposure, two

macrocracks developed at the ends of the specimen which may have reduced the restraint efficiency resulting in less cracking development see Figure 5.1. The reduction in E_{fmax} of the restrained specimens for mixes NA40 and NA30 was in the range of 9-16 % and 11-16 %, respectively as can be seen in Table 5.3. These results point towards creep as a mechanism of relaxation that stretches the material, creating many microcracks and reducing the elastic modulus. In fact there is a correlation between the width of the cracks in the critical region and E_{fmax} loss as shown in Figure 5.25.

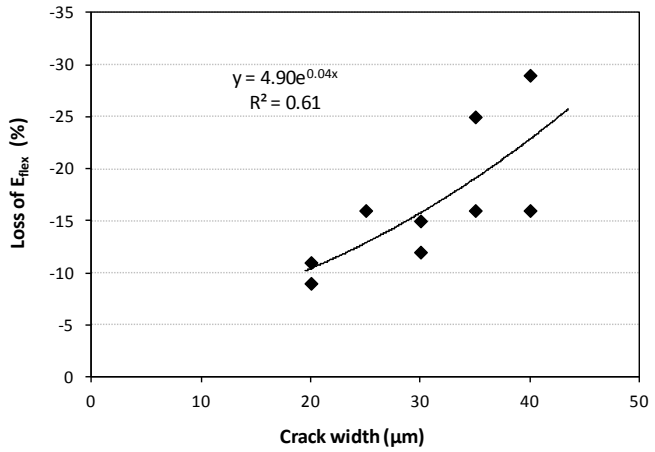

Figure 5. 25 Effect of crack width on the loss of E_{fmax}.

5.5 Conclusions

For restrained concrete, cracking and failure due to shrinkage strains is a function of the concrete properties, since they govern the stiffness and the stress history.

For the proposed "passive" restraining frame, the majority of strain and RF loss can be attributed to the relative stiffness between the frame and the concrete specimens. Long-term RF loss may also be recorded due to loss of stiffness in the anchored zone and creep of concrete due to the enforced expansion.

Apparent RF decreases at a relatively high rate over the first few days due to early age microcracking which slows down elastic modulus development. Nonetheless, microcracking reduces the overall stiffness gain of the concrete, resulting in less overall strain loss than expected.

Drying (in both conditions free and restrained) reduces the compressive strength of concrete by about 10-14%. Though surface microcracking due to shrinkage is expected to reduce

compressive strength, its effect appears to be relatively small compared to the long term effect of maturity on strength. This may partly explain discrepancies in compressive strength trends in previous studies.

There is insignificant difference between the residual compressive strength of free and restrained specimens, possibly due to the fact that most restrained shrinkage induced macrocracks are found in the regions close to the upper and lower plates of the compression test machine, which are well confined. Hence, the standard compression test may overestimate the actual strength of concrete. Frictionless surfaces may help reduce this problem.

Shrinkage induced cracks affect the flexural strength of concrete mixes with different w/c ratios in a different manner. The effects are more pronounced for mixes with low w/c (0.3) (reduction 11-24%) than for mixes with high w/c (0.4 and 0.5) (reduction in the range of 2-5%). This may be due to high autogenous and early thermal shrinkage (due to hydration). A higher rate of shrinkage and elastic modulus evolution can lead to a faster rate of tensile stress development and may reduce relaxation /creep if stiffness develops too fast. This can lead to earlier and more intensive microcracking which can affect adversely the flexural strength.

For "Free" shrinkage specimens, just as the flexural strength, the damage of E_{fmax} in the mix with low w/c ratio (0.3) was higher (reduction of 9%) than high w/c ratios mixes (0.4 and 0.5) (reduction of 3-5%) due to the effect of surface microcracking.

For restrained specimens, the reduction in E_{fmax} for w/c ratios 0.3 and 0.4 was up to 16% whilst mix 0.5 suffered the highest reduction up to 29%. This is despite the fact that this mix had little or no flexural strength loss.

Overall, macro and micro cracks affected the E_{fmax} more adversely in restrained specimens. These results point towards creep as a mechanism of relaxation that stretches the material, creating many microcracks reducing the elastic modulus. The higher this relaxation the larger it takes for the through crack to develop as was the case with w/c 0.5.

There is a correlation between increasing width of cracks in the critical region and flexural elastic modulus loss.

References

1. Bažant, Z.P. and L.J. Najjar, *Drying of concrete as a nonlinear diffusion problem.* Cement and Concrete Research, 1971. **1**(5): p. 461-473.
2. Wittmann F.H., *Creep and Shrinkage Mechanisms*, in *Creep and Shrinkage in Concrete Structures*, Z.P. Bažant and Wittmann F.H., Editors. 1982, John Wiley &Sons: Chichester. p. 129-161.
3. Altoubat, S.A. and D.A. Lange, *Creep, shrinkage, and cracking of restrained concrete at early age.* ACI Materials Journal/ SP, 2001. **98**(4): p. 323-331.
4. ACI 231R-10, *Report on Early-Age Cracking: Causes, Measurement, and Mitigation*, in *ACI Committee 231*. 2010, American Concrete Institute: Farmington Hills, U.S.A.
5. Neville, A.M., *Properties of concrete*. 1995, Harlow: Longman Group.
6. Nielsen, K.E.C., *Effect of various factors on the flexural strength of concrete test beams* Magazine of Concrete Research, 1954. **March 1954**: p. 105-114.
7. Yurtdas, I., et al., *Evolution of the mechanical behaviour of a high performance self-compacting concrete under drying.* Cement and Concrete Composites, 2011. **33**(3): p. 380-388.
8. Bisschop, J. and J.G.M. Van Mier, *Drying shrinkage microcracking in cement-based materials.* Heron, 2002. **47**(3): p. 163-184.
9. Idiart, A.E., *Coupled analysis of degradation processes in concrete specimens at the meso-level*, in *Geotechnical Engineering and Geoscience* 2009, Polytechnic University of Catalunya: Barcelona.
10. Shiotani, T., J. Bisschop, and J.G.M. Van Mier, *Temporal and spatial development of drying shrinkage cracking in cement-based materials.* Engineering Fracture Mechanics, 2003. **70**(12): p. 1509-1525.
11. Bentur, A., *Early-Age Shrinkage and Cracking in Cementitious Systems.* Concrete Science and Engineering, 2001. **3**: p. 3-12.
12. ACI 207.2R, *Report on Thermal and Volume Change Effects on Cracking of Mass Concrete*, A.C. 207, Editor. 2002, American Concrete Institute: Farmington Hills, U.S.A.
13. Abbasnia, R., P. Godossi, and J. Ahmadi, *Prediction of restrained shrinkage based on restraint factors in patching repair mortar.* Cement and Concrete Research, 2005. **35**(10): p. 1909-1913.
14. BS EN 12390-3:2009, *Testing hardened concrete Part 3: Compressive strength of test specimens*. 2009, British Standards Institution: London.
15. BS 1881-119:2011, *Testing concrete. Method for determination of compressive strength using portions of beams broken in flexure (equivalent cube method)*. 2011, BSI: London-UK. p. 12.
16. ASTM-C1018-97, *Standard Test Method for Flexural Toughness and First-Crack Strength of Fiber-Reinforced Concrete (Using Beam With Third-Point Loading)*. 1997, ASTM International.
17. Japan Society of Civil Engineers(JSC)-SF4, *Methods of tests for flexural strength and flexural toughness of steel fibre reinforced concrete*. 1994, Concrete Library of JSCE. p. 58-61.

18. Younis, K.H. and K. Pilakoutas, *Assessment of Post-Restrained Shrinkage Mechanical Properties of Concrete* ACI Materials, 2014. **Submitted for publication**.

19. BS EN 1992-1-1:2004, *Eurocode 2: Design of concrete structures — Part 1-1: General rules and rules for buildings* 2004, British Standard Institution: London, UK.

20. Yurtdas, I., et al., *Influences of water by cement ratio on mechanical properties of mortars submitted to drying.* Cement and Concrete Research, 2006. **36**(7): p. 1286-1293.

21. Kanna, V., R.A. Olson, and H.M. Jennings, *Effect of shrinkage and moisture content on the physical characteristics of blended cement mortars.* Cement and Concrete Research, 1998. **28**(10): p. 1467-1477.

22. Pihlajavaara, S.E., *A review of some of the main results of a research on the ageing phenomena of concrete: Effect of moisture conditions on strength, shrinkage and creep of mature concrete.* Cement and Concrete Research, 1974. **4**(5): p. 761-771.

23. Burlion, N., F. Skoczylas, and T. Dubois, *Induced anisotropic permeability due to drying of concrete.* Cement and Concrete Research, 2003. **33**(5): p. 679-687.

Chapter 6

Post-Restrained Shrinkage Behaviour of Concrete Made with Recycled Materials

Younis, K.H. , K. Pilakoutas and K. Neocleous, *Post-restrained shrinkage behaviour of concrete: Effect of Recycled Materials.* Cement and Concrete Composites, 2014.***to be Submitted***.

Shrinkage induced cracks can have an adverse effect on strength and durability of concrete in particular when using recycled aggregate (RA). Randomly distributed steel fibres are normally used to control crack development due to shrinkage. This study examines the effect of recycled tyre steel fibres (RTSF) -extracted from post consumer tyres- and RA -from construction and demolition waste- on the restrained shrinkage behaviour of concrete. Experiments were performed on six mixes in different drying and restraining conditions to determine free and restrained shrinkage, loss of mass, compressive strength, flexural strength and flexural elastic modulus. The results show that whilst conventional fibres do not affect much shrinkage strain development, RTSF increase initial shrinkage strains due to higher air content in the mix. Despite that, it was found that RTSF lead to an overall better flexural performance, even when using RA concrete due to the role of RTSF in controlling shrinkage induced microcracking, enhancing tensile relaxation and promoting auto-healing of microcracks. The results confirm that it is possible to use RA to produce concrete for structural applications.

This chapter consists of a "stand alone" journal paper and includes relevant bibliography at the end of the chapter. Appendix G provides further test results.

6.1 Introduction

To enhance the sustainability of concrete, recycled aggregate (RA) and recycled aggregate concrete (RAC) is beginning to be used in practice. However, there are concerns relating to RA and RAC variability, low density, high water absorption and porosity which can result in low quality concrete (low compressive, tensile and flexural strength and low elastic modulus). Another critical issue is high shrinkage [1-4] due to the heterogeneous composition, high porosity and water absorption and low restraint from RA particles. High shrinkage can increase the cracking tendency, in particular when RAC is restrained. On the other hand, the higher creep of RAC [2, 4], and its lower elastic modulus, can play a role in reducing the effects of shrinkage induced tensile stresses. Very limited work has been conducted on the behaviour of RAC under restrained conditions.

Concrete loses volume in response to the chemical reactions of hydration, as well as to initial temperature and moisture loss. This volume loss, or shrinkage, can lead to unacceptable strain development and limit state perfromance [5, 6]. Due to internal (e.g. aggregate and reinforcement) and external (e.g. ground or adjacent members) restraints, shrinkage strains also cause tensile stresses. When tensile stresses exceed the strength of the concrete, cracks develop. Such cracks can start before the application of external loads and even at very early ages [7]. Shrinkage induced cracks can adversely affect structural appearance, structural strength and durability of concrete. Delaying the development of cracks and minimizing their width are vital in mitigating performance deterioration.

Randomly distributed steel fibres are often used to control crack development due to shrinkage strains. It is reported by some [8-11] that the addition of fibres can decrease free shrinkage in concrete. This is attributed to the physical restraining effect (similar to aggregate restraining effect) which develops due to the interfacial bond between fibres and matrix [12]. Other studies [11, 13-15] show that the addition of low contents of steel fibres (less than 1% by volume) does not alter the shrinkage behaviour of concrete. Finally, some studies [16, 17] show that fibres may be responsible of an increase in the porosity of concrete resulting in higher free shrinkage strains. Therefore, it appears that there is no general agreement on the effect of fibres even on the free shrinkage behaviour of concrete.

Undoubtedly, the most significant effect of fibres in concrete is their ability to control crack width and propagation after matrix failure. In this respect, fibres can play three significant roles: 1) encourage the development of fine smeared cracks rather than a few wide cracks, 2)

transfer tensile stress across cracks, 3) enable the long-term healing/(sealing) of cracks [18, 19].

The effect of fibres on the shrinkage behaviour of concrete under restrained conditions is commonly studied using the ring test [10, 14, 20-23] or linear ('passive' or 'active') test configurations [7, 24-26]. These tests have been used to show that fibres delay the occurrence of cracks and reduce the width of shrinkage induced cracks. Altoubat and Lange [7] studied the effect of fibres (0.5% volume) on the early age shrinkage-creep interaction behaviour of concrete under restrained conditions. Although both type of mixes (plain and FRC) used in the study failed more or less at the same level of shrinkage induced stress, it was found that steel fibres delay failure time, in comparison to plain mixes, by 44% and 21% for w/c ratios of 0.32 and 0.4, respectively. This was attributed to the role of fibres in enhancing the tensile relaxation mechanism of concrete due to creep (basic and drying creep), by engaging a larger volume of the matrix in stress transfer and reducing micro level damage (microcracking). Altoubat and Lange [27] classified the "real" and "apparent" mechanisms of creep into beneficial and detrimental. The real mechanism associated with moisture movement was considered beneficial and the apparent mechanism associated with microcracking detrimental. They concluded that steel fibres enhance the desirable creep mechanisms and suppress the undesirable mechanism of microcracking.

Due to the random distribution of steel fibres in concrete, large quantities are needed to yield the same structural performance of a conventionally reinforced concrete. This can make the use of industrial steel fibres (IF) non-economical. Recycled Tyre Steel Fibre (RTSF) extracted from post-consumer tyres can be utilized as a cheaper alternative to IF. The first investigations on the mechanical properties of recycled tyre steel fibre reinforced concrete (RTSFRC) mixes to examine their structural performance were started at the University of Sheffield [28-30]. Utilizing RTSF in concrete has considerable environmental benefits since only a small fraction of the energy needed to make steel wire is used in their production. Two unpublished experimental studies on the free shrinkage behaviour of these fibres were conducted under the EU project "Ecolanes" [30]. The shrinkage behaviour of RTSF concrete under restrained conditions has not been explored yet.

In previous work [31], the authors developed techniques to upgrade the performance of RA and RAC by treating the surface (coating) of RA using reactive microfillers (e.g silica fume) and by adding RTSF to the RAC. The promising results (enhancement of the ITZ and an increase of 30% in compressive strength) have led the authors to investigate the effect of

these techniques on other properties of RAC such as flexural strength, modulus of elasticity and shrinkage behaviour (both free and restrained).

This chapter aims to examine the effect of RTSF on the shrinkage behaviour of RAC under restrained conditions. For comparison purposes, the work includes mixes with industrial steel fibres (ISF) and natural aggregate (NA). A restraining frame (see Figure 6.1) and procedure to assess the post-shrinkage behaviour of concrete, previously developed (in chapter 4 and 5) are utilized. In the next sections, experimental details and testing procedures will first be explained followed by results and discussion on shrinkage behaviour (free and restrained) and post-shrinkage mechanical properties for the investigated mixes.

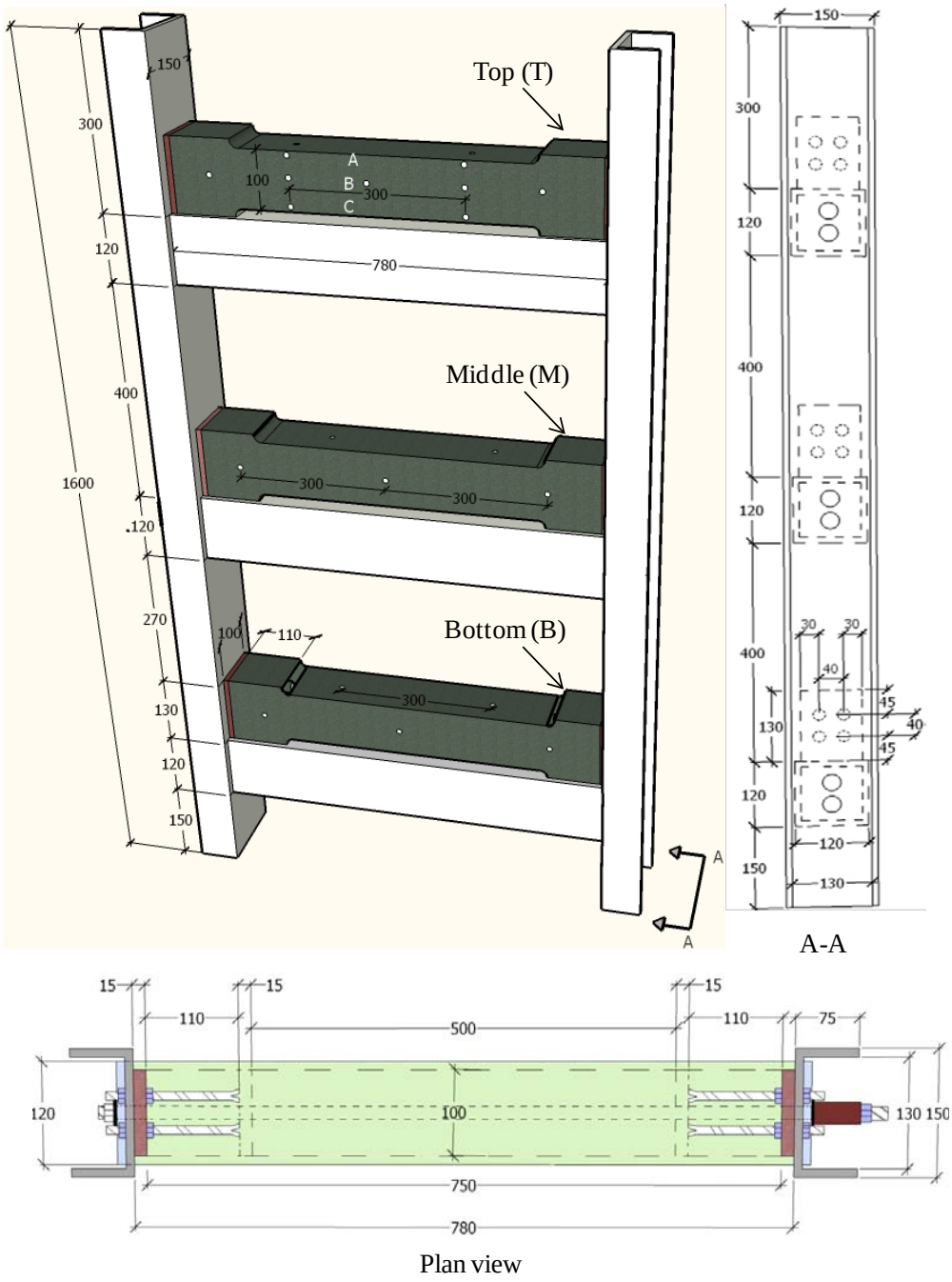

Figure 6. 1 Frame for restrained shrinkage test (dimensions in mm).

6.2 Experimental Details and Testing Procedures

6.2.1 Materials

In this study, Ordinary Portland Cement (OPC) CEM I 52.5 N, complying with BS EN 197-1 [32] was used. Natural sand was used as fine aggregates (maximum size of 5mm). Two types of coarse aggregate (CA) (maximum size of 20 mm) were used; a natural (gravel) river

aggregate and recycled aggregate (RA) (denoted as RAm in this chapter) obtained from crushing a mix of construction and demolition waste CDW containing crushed concrete, masonry (brick) and asphalt. Table 6.1 presents the main properties of the NA and RAm coarse aggregate. Silica fume SF (2% by cement mass) in liquid form was used to coat the RAm to improve its properties. More details on the composition and other properties of the RAm can be found elsewhere [31].

Table 6. 1 Properties of coarse aggregate.

Property	NA	RAm
[a] Particle density (Mg/m^3)	2.63	2.37
Bulk density (kg/m^3)	1668	1234
Water absorption (%)	1	5.5
Los Angeles, LA (%)	23	35

[a] Saturated surface dry.

Industrial fibres from a cold-drawn process (type I according to BS EN 14889-1) were used and they had a deformed shape as shown in Figure 6.2. The fibre length was 50 mm and the diameter was 1.0 mm. The fibres had nominal tensile strength of 1100 MPa.

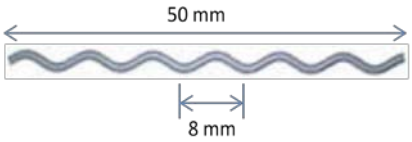

Figure 6. 2 Industrial steel fibres (ISF).

The RTSF used in this research were obtained by post-processing tyre wire derived from the mechanical processing of post-consumer tyres [33]. The RTSF used had a diameter in the range of 0.1-0.2 mm and a tensile strength of around 2000 MPa [34] The RTSF comes in variable lengths ranging from 3-30 mm (5% of the fibres had length shorter than 3mm and 5% longer than 30 mm). The length distribution as determined using a specially developed image analysis technique is shown in Figure 6.3.

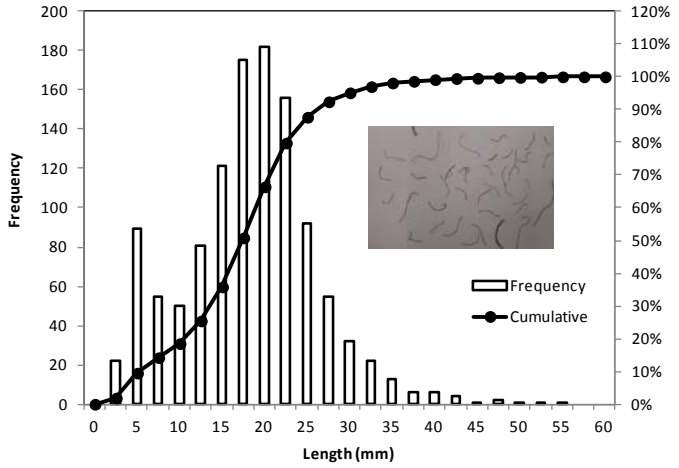

Figure 6. 3 Length distribution of RTSF.

6.2.2 Variables and Mix Proportions

Six different mixes were prepared with the same w/c ratio (0.4) as shown in Table 6.2. The mixes can be divided into two groups according to the type of coarse aggregate used. All mixes had the same quantity of cement (375 kg/m^3), water (150 kg/m^3) and fine aggregate (715 kg/m^3), whilst the quantity of coarse aggregate used was 1147 kg/m^3 for group 1 (NA) and 1037 kg/m^3 for group 2 (RAm). The volume of aggregate was kept constant for all mixes (0.7 m^3). Only one content (2% mass of concrete = 48 kg/m^3) of fibre was used with all FRC mixes. Different amounts of superplasticizers were used (see Table 6.2) to achieve concrete with workability (slump test) between 70-110 mm.

Table 6. 2 Variables of research and code of mixes.

Mix	Type of coarse aggregate	Fibre type and content %[a]	Mix code	SP[b](l/m^3)
1	NA	0 (plain)	NA40	1.12
2	NA	R, 2	NA40R2	2.25
3	NA	I, 2	NA40I2	2.25
4	NA	R, (1) + I, (1)	NA40R+I	2.25
5	RAm	0 (plain)	RAm40	1.40
6	RAm[c]	R, 2	RAm40R2	2.50

[a] By concrete mass (R= Recycled, I=Industrial). [b] Superplastiziser. [c] The surface of the RAm is treated by coating them with silica fume.

6.2.3 Geometry and Preparation of Specimens

For each mix: twelve (100mm) cubes, three control prisms 100*100*500 mm, three prisms 100*100*750 mm for free shrinkage tests, and three prisms (in one frame) for the restrained shrinkage tests (see Figure 6.1) were cast. The concrete was compacted following the recommendations of BS EN 12390-2 [35]. The compaction of the concrete specimens in the restraining frame was achieved by rigidly attaching the frame to the vibrating table through a steel bar.

6.2.4 Strain Measurements

After compaction and levelling, a rectangular perspex piece was placed on the top surface of each specimen in the restraining frame. The specimens were then covered by plastic sheets to prevent moisture loss before demoulding at 24h. After demoulding, the control prisms were stored in water while the specimens in the restraining frame and the prisms for free shrinkage were maintained in laboratory environment (22 ±2 ^{o}C and RH of 45 ±5 %).

A Demec gauge was used to measure shrinkage strains with length of 300 mm and precision of 5.2 με. The Demec gauge points spaced at 300 mm were bonded to the concrete surface using a rapid-hardening adhesive.

The location of the Demec points for the free shrinkage specimens is shown in Figure 6.4a and for the restrained specimens in Figure 6.1. At the centre of each surface of the concrete prisms, three demec points were attached to obtain two readings over a length of 300 mm at specified times.

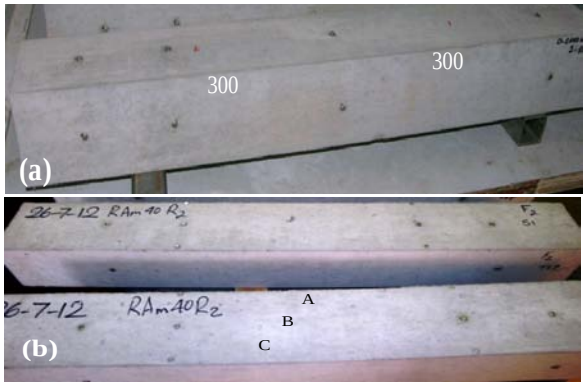

Figure 6. 4 Location of Demec points for free shrinkage specimens (values presented are in mm).

Demec points were bonded at 24h just prior to the transfer of the prisms (free and restrained) to the drying environment. For the restrained specimens, Demec points were fixed to the sides and top of each specimen as can be seen in Figure 6.1. In some cases, and to examine the distribution of the shrinkage across the depth of the concrete specimen, Demec points were attached on the sides surfaces at three depths from the trowelled surface (5 mm (top A), 50 mm (middle B), and 95 mm (bottom C)), see Figures 6.4b and 6.1. The first shrinkage strains were measured at 24h (immediately after the adhesive hardened) and at 24 hours intervals for the first week, followed by measurements at 10, 14, 21 and 28 days. Two or three readings were taken for each gauge length, and the average values calculated.

6.2.5 Restraint Factor (RF)

According to ACI 207.2R [36] the degree of restraint or restraint factor RF is the ratio of actual stress induced by the restrained volume change to the stress which would develop if the specimen was fully restrained. This can also be seen as the ratio of restrained shrinkage to free shrinkage strain [37]. Assuming a modulus of elasticity that is constant, equation 1 can be used to calculate the RF:

$$\mathrm{RF} = \frac{\varepsilon_R}{\varepsilon_{free}} \qquad (6\text{-}1)$$

where:

ε_R Restrained shrinkage strain = shrinkage strain measured on the free specimen - shrinkage strain measured on the restrained specimen.

ε_{free} Free shrinkage strain (strain measured on the free specimen).

6.2.6 Crack Detection

Cracks were measured using an optical microscope (40x, precision 20 μm) and a digital microscope (200x, precision 10 μm). The reported crack width is the crack opening at its widest, normally at the edges of the specimens. A width of 20 microns or less was used to define the microcracks, since wider cracks were visible to the naked eye when properly illuminated.

6.2.7 Loss of Mass (loss of moisture)

The loss of mass for the free shrinkage specimens were determined at regular intervals using a balance with the precision of 0.1 g. The first reading, which is considered as the initial mass, was taken at 24h (after the Demec points were bonded).

6.2.8 Compressive Strength

The compressive strength was obtained at 1, 3, 7, 28 days using the 100 mm cubes and BS EN 12390-3:2009 [38]. Compressive strength was also obtained from the prisms (free, restrained and water cured prisms) tested in bending, by following the recommendations of BS 1881-119:2011[39]. The compressive strength test for prisms was conducted one or two days after the bending test.

6.2.9 Bending Tests (Flexural Strength and Modulus of Elasticity)

Specimens were tested in four-point flexural loading over a length of 300 mm following the recommendations of the ASTM C1018 [40]. To eliminate errors from support displacement and torsion, a yoke [41] was used to mount the deflection transducers. Two linear variable displacement transducers (LVDTs), placed on opposite sides of the specimen, were used to determine the average central deflections. From the load versus-deflection curve, the flexural strength and stiffness were calculated. Flexural modulus of elasticity E_{flex} (GPa) was determined based on the theory of classical elasticity [42]. The flexural elastic modulus for the concrete (E_{fmax}) was determined as the maximum value in the range of 30% to 60% of the ultimate bending load.

6.3 Results and Discussion - Free Shrinkage Tests

6.3.1 Steel Fibre Reinforced (SFR) NAC

Shrinkage strains (average of three specimens) measured on plain and SFR-NAC mixes are presented in Figure 6. 5. The addition of 2% (by mass) of IF and 2% of blend fibres appears to have an insignificant influence on shrinkage strain. However, the addition of same amount of RTSF, increased the shrinkage strains of the concrete by 35-85 % at early ages (first week) but only 15% at 28 days.

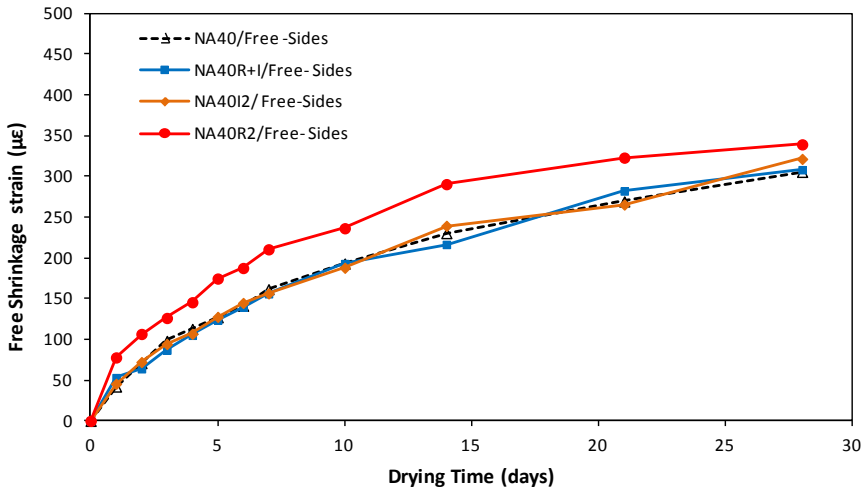

Figure 6. 5 Development of free shrinkage strains of plain and SFR-NAC.

As explained earlier there is no general agreement on the effect of steel fibres on free drying shrinkage of concrete. Fibres can reduce the shrinkage of concrete through their stiffness by restraining the shrinkage of cement paste. On the other hand, steel fibres may increase the shrinkage as a result of increased porosity, as air voids can be trapped on their surface. In these tests there was insignificant difference between the shrinkage values of the plain concrete (NA40) and the mixes reinforced with ISF (NA40I2 and NA40R+I). However, the mix reinforced with RTSF (NA40R2) exhibited high shrinkage at the early ages. This may be attributed to: 1- the curved shape of the RTSF providing less restrain than ISF (which are more linear and rigid). 2- the smaller diameter of RTSF (4-10 times than ISF) leading to much larger number per volume and larger surface area, which can lead to more trapped air and high porosity. Alternatively, at the micro-level, due to the much better distribution of RTSF fibres, less micro damage (drying microcracks) will develop in the concrete. Consequently, more intact material per unit volume is expected and higher shrinkage will be developed on the macro-level. Similar explanation was given by Altoubat and Lange [7] to account for the higher shrinkage of concrete with (0.5 by volume) polypropylene fibers. These mechanisms will be discussed again later when other results are examined.

6.3.2 Plain and SFR-RAC

Figure 6.6 shows free shrinkage strains (average of three specimens) developed at the centre of the specimen sides for mixes NA40, RAm40 and RAm40R2. As expected, both 28 day shrinkage strain and their rate of development at the early ages for RAC are higher than those of NAC. The shrinkage strains are 306 με and 405 με at 28 days for NA40 and

RAm40, respectively. The shrinkage strains of the RAC is higher than that of NAC by about 31% at 1 day and by 35% at 28 days.

The process of drying of RAC is different than that of NAC. Upon drying, for NAC the moisture migrates mainly from the cement paste to the surrounding environment, whereas, in RAC, due to the heterogeneity in composition and the high porosity of the RA, moisture diffuses out of the concrete through both cement paste and the aggregate itself. Therefore, the shrinkage of RAC is usually higher than that of NAC. Another reason for the higher shrinkage of RAC can be the low elastic modulus of RA that provides lower restraining effect to the shrinkage tendency of the cement paste.

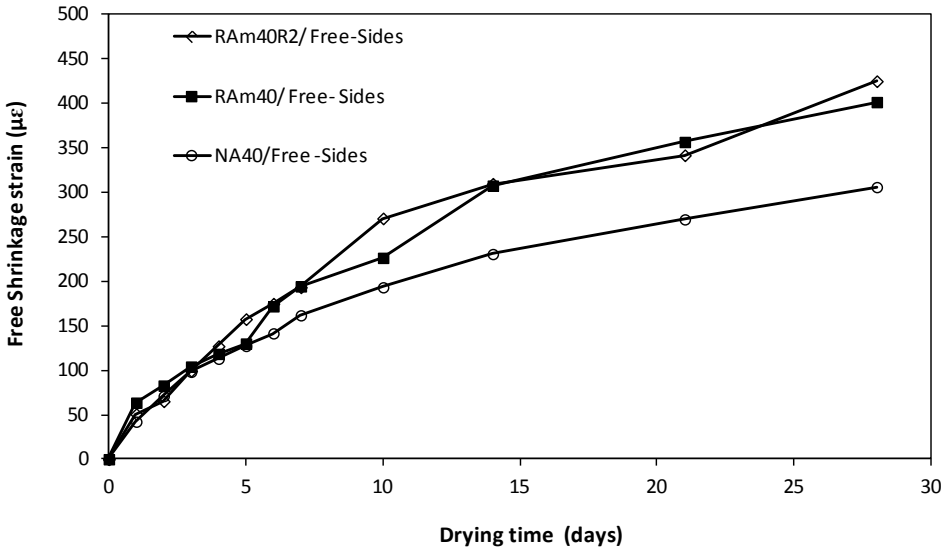

Figure 6. 6 Development of free shrinkage strains of plain NAC, plain RAC and RAC reinforced with RTSF.

Figure 6.6 also shows that the addition of 2% (by mass) of RTSF and the treatment of RA with SF had an insignificant effect on the shrinkage values of RAC. This may be the result of two competing effects: increase of shrinkage caused by the effect of RTSF (additional micro voids) and reduction in shrinkage due to the coating of the RA. Though the amount of SF used in this study (2%) is quite small in comparison to other studies, the coating may have densified the ITZ of the RAC and hindered moisture migration to the RA. It should be noted that SF is known to increase shrinkage of concrete [6, 43].

6.3.3 Effect of Surface and Depth

SFR-NAC

For all mixes, the shrinkage strains at the top, side and bottom surfaces were different. The highest shrinkage strains were observed at the top surface and the lowest at the bottom surface, strains on the sides were about the average of the two other faces (see Figures 6.7, 6.8 and 6.9). This may be due to concrete bleeding which usually happens at the top (troweled) surface altering the microstructure of this surface and possibly resulting in slightly higher porosity which in turn causes faster drying and more shrinkage. Furthermore, concrete is better compacted at greater depths resulting in more dense concrete which tends to shrink less. This difference in shrinkage strains between surfaces at different depths indicates that upon drying the concrete will also bend due to curvature (see section 3.4).

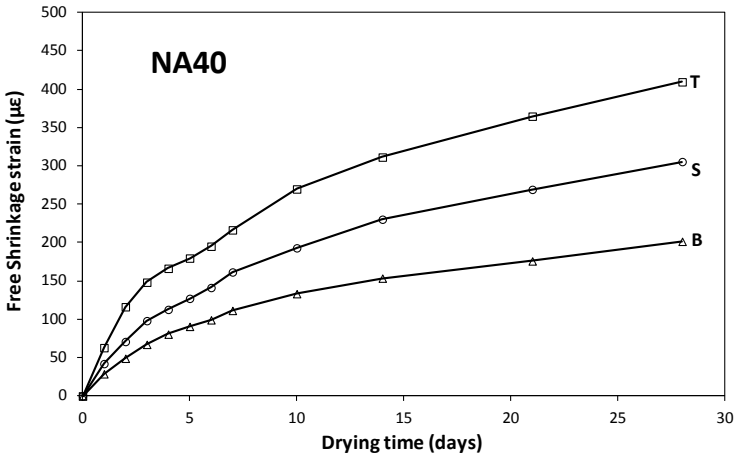

Figure 6. 7 Development of free shrinkage strains of NA40 at top (T), sides (S) and bottom (B) surfaces.

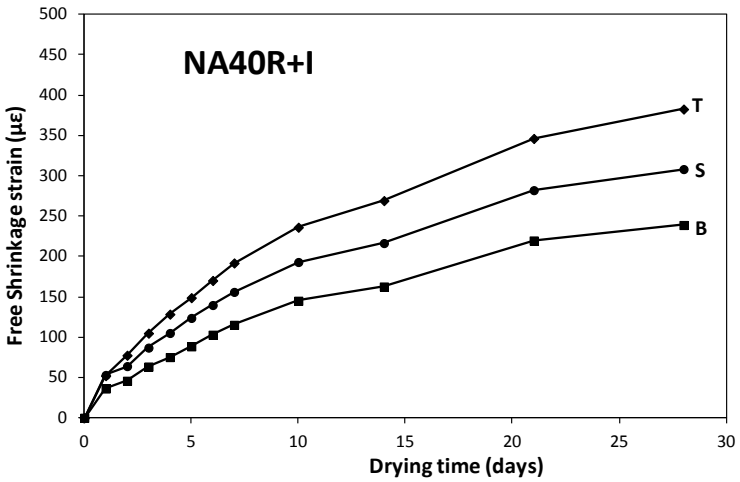

Figure 6. 8 Development of free shrinkage strains of NA40R+I at top (T), sides (S) and bottom (B) surfaces.

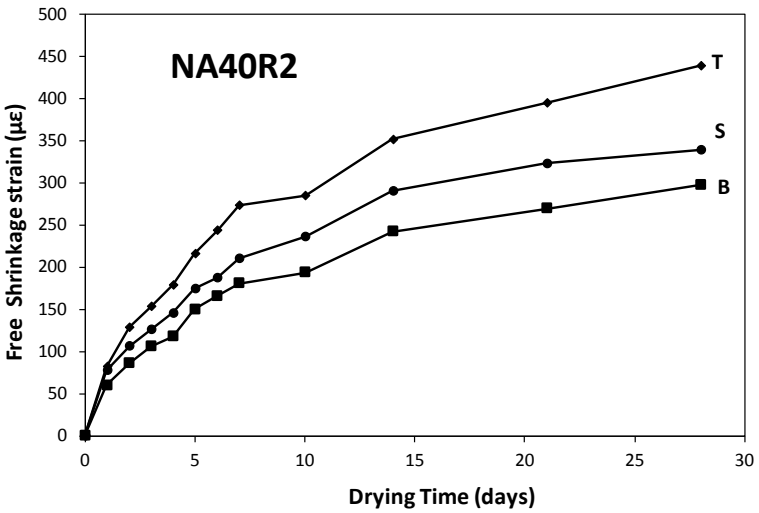

Figure 6. 9 Development of free shrinkage strains of NA40R2 at top (T), sides (S) and bottom (B) surfaces.

The difference in shrinkage strains measured on the different surfaces of SFR-NAC mixes is substantially lower than that of plain concrete (particularly at the early ages) as can also be seen in Figure 6.10a. Figure 6.10a shows the ratio between the strains developed at the top relative to those at the bottom (Δ_{T-B}) and Figure 6.10b the ratio between the top and the sides (Δ_{T-S}). The mix reinforced with 2% of RTSF exhibits a lower difference than the mix reinforced with blended industrial and recycled steel fibre. The differences in shrinkage strain (Δ_{T-B}) for mixes NA40R2 and NA40R+I were less than those for NA40 by around 80% and 75% at the very early age (first few days) and by around 55% and 45% thereafter (up to 28 days).

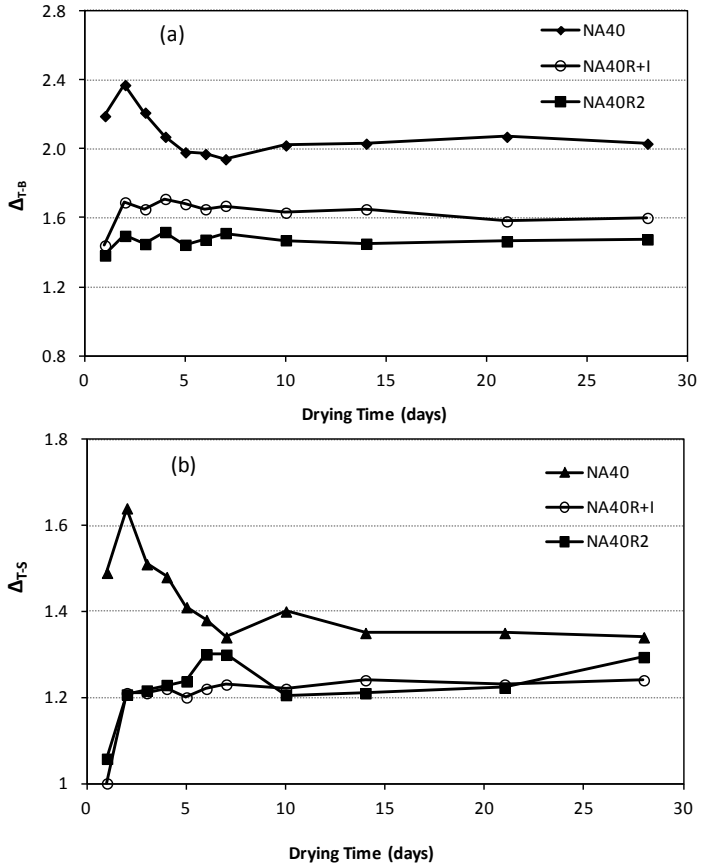

Figure 6. 10 Strain ratio (for mixes NA40, NA40R+I and NA40R2) between a- top and bottom surfaces, b- top and side surfaces.

SFR-RAC

For the mixes containing RA (both plain and SFR), the shrinkage strains on the top surface were higher than the sides and the bottoms surfaces (see Figures 6.11 and 6.12). This behaviour is similar to that of NAC mixes. However, the differences (Δ_{T-B} and Δ_{T-S}) are much lower in comparison to the mixes with NA as seen in Figures 6.13 and 6.14. The difference in shrinkage strain (Δ_{T-B}) of the plain RAC was less than that of plain NAC by around 100% at the very early age (first few days) and by around 70% thereafter (up to 28 days).

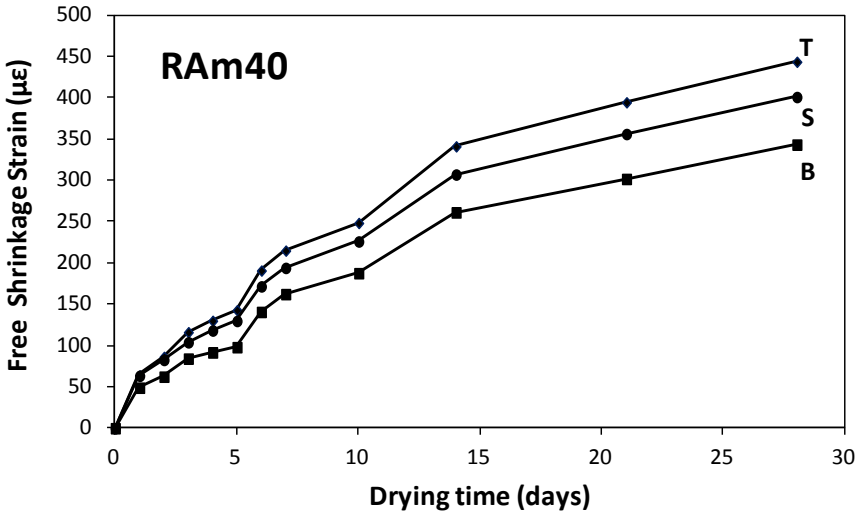

Figure 6. 11 Development of free shrinkage strains of RAm40 at top (T), sides (S) and bottom (B) surfaces.

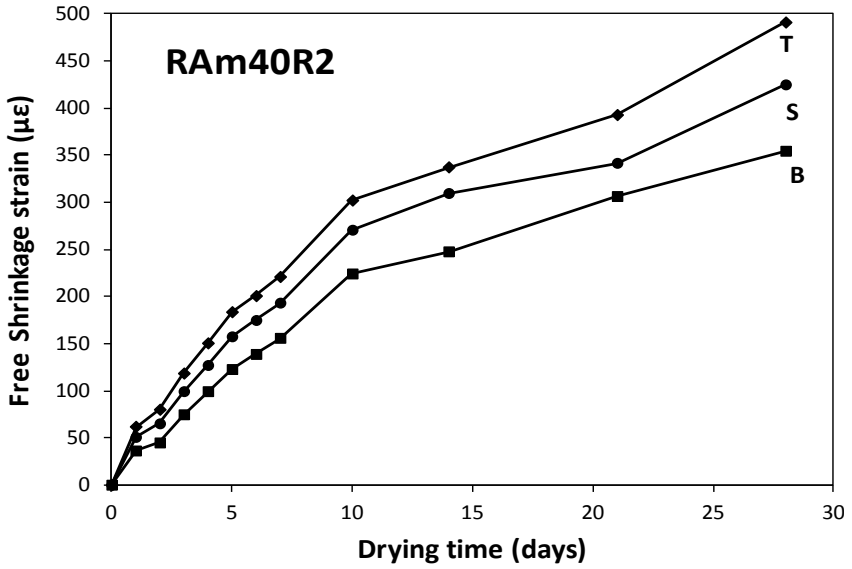

Figure 6. 12 Development of free shrinkage strains of RAm40R2 at top (T), sides (S) and bottom (B) surfaces.

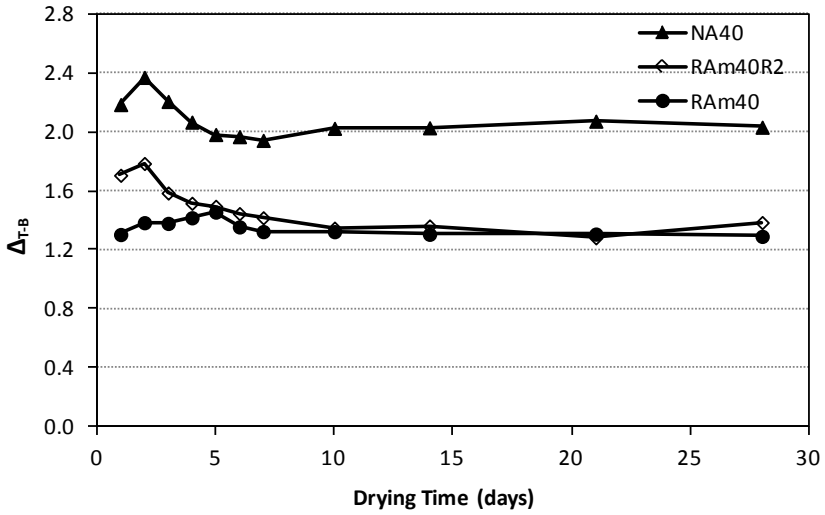

Figure 6. 13 Strain ratio (for mixes NA40, RAm40 and RAm40R2) between top and bottom surfaces.

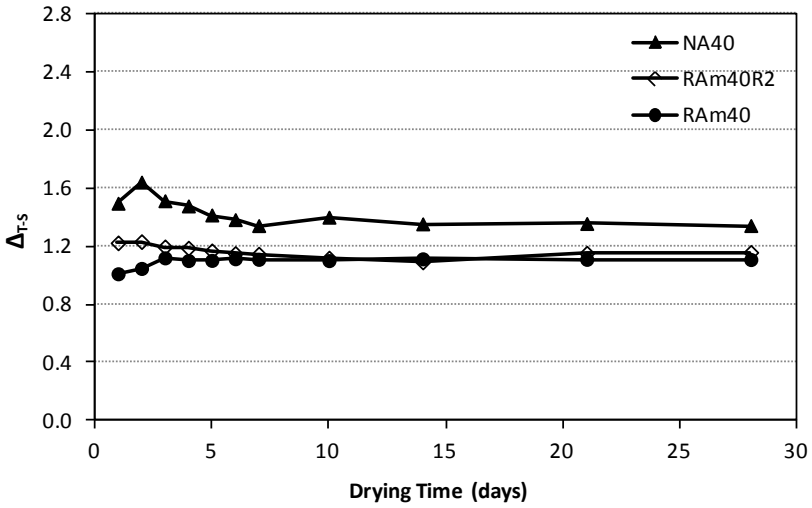

Figure 6. 14 Strain ratio (for mixes NA40, RAm40 and RAm40R2) between top and side surfaces.

6.3.4 Shrinkage Curvature of SFR-NAC

SFR-NAC

Figure 6.15 (a and b) show the development of shrinkage curvature (average of three specimens) over time for mixes NA40R2 and NA40R+I. Curvature is shown as calculated between top and sides (k_{T-S}), sides and bottom surfaces (k_{S-B}) and average (k_A). For NA40R2, it can be seen that the curvature of the upper half of the concrete specimens is higher than the lower half, whereas, for NA40R+I, curvatures are more uniform. The curvature of the plain concrete is higher than that of FRC (see Figure 6.16).

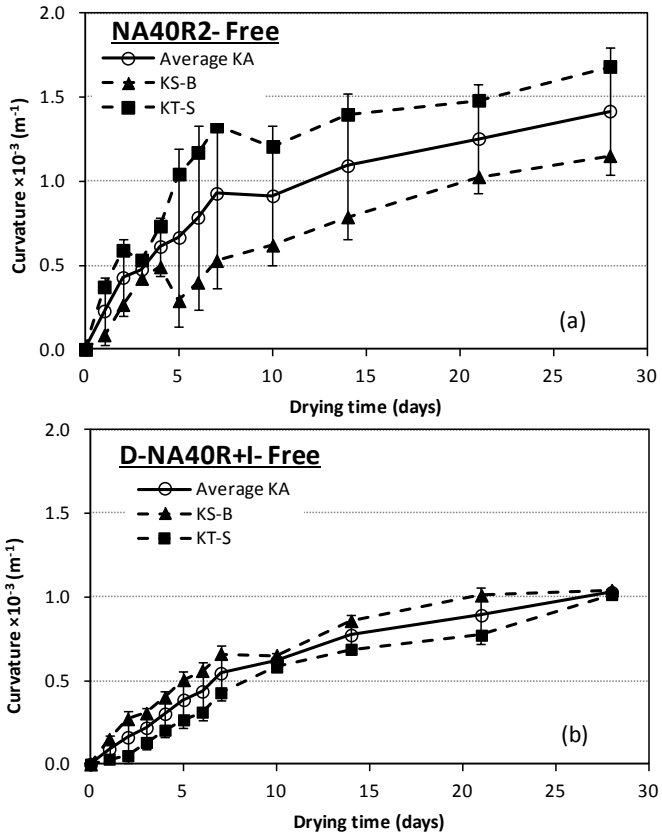

Figure 6. 15 Shrinkage curvature developed on the free specimens, (a) mix NA40R2, (b) mix NA40R+I.

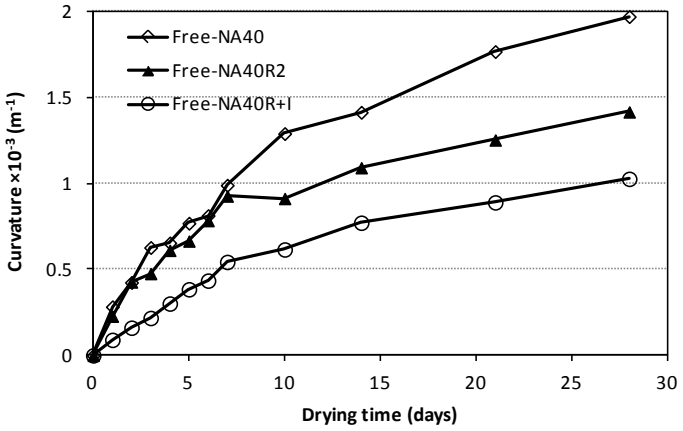

Figure 6. 16 Average shrinkage curvature of fibre reinforced concretes compared to plain concrete.

SFR-RAC

The development of curvature (k_{T-S}, k_{S-B} and k_A) over time for mixes RAm40 and RAm40R2 is shown in Figure 6.17 (a and b). There is no significant difference in the average curvature (kA) for plain and SFR-RAC as can be seen in Figure 6.18. Figure 6.18 also shows that the shrinkage curvature of RAC mixes (both plain and SFR) is lower than that of plain NAC.

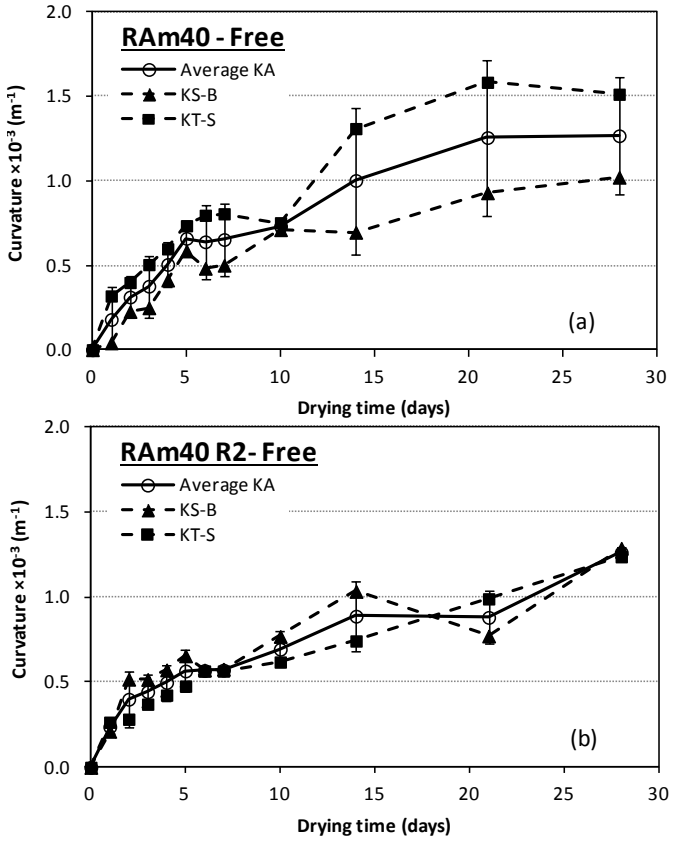

Figure 6. 17 Shrinkage curvature developed on the free specimens, (a) mix RAm40, (b) mix RAm40R2.

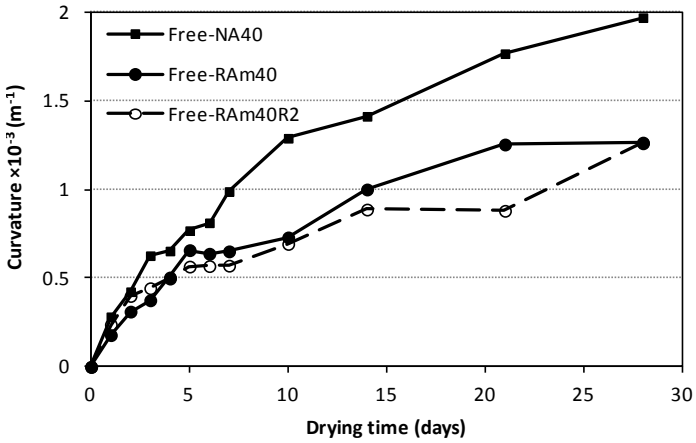

Figure 6. 18 Comparison of average shrinkage curvature for plain and fibre reinforced RAC and plain NAC.

There is clearly a mechanism that results in relatively large curvatures in free NAC specimens and RA and fibres appear to mitigate the effect.

6.3.5 Mass Loss

NAC

The curves of mass loss versus drying time for plain and SFR-NAC are presented in Figure 6.19. In general, it can be seen that the addition of 2% (by mass) of ISF or RTSF or a blend of (1% IF + 1% RTSF) did not alter the trend of mass loss.

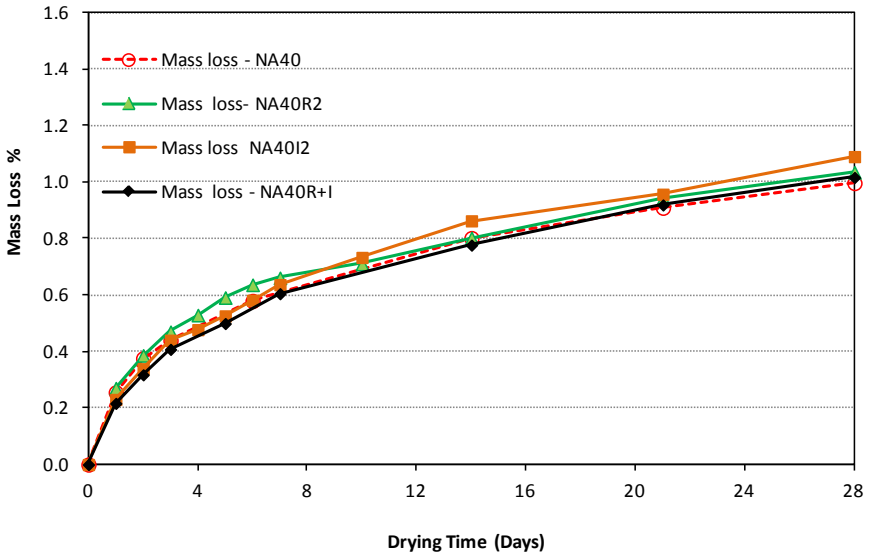

Figure 6. 19 Mass loss versus time for plain and fibre reinforced NAC.

Since the mass loss in Figure 6.19 is almost identical for all mixes, it is expected that the shrinkage strains will be similar. However, the shrinkage strains for NA40R2 are higher than these of NA40 (see Figure 6.5). This confirms that though the overall cement shrinkage might be the same, better distributed fibres (such as RTSF) can reduce damage at the micro level, leading to higher shrinkage strains at the macro level. If this is true, then a better structural performance is expected.

RAC

The results of mass loss for the plain and SFR-RAC (RAm40 and RAm40R2) mixes are shown in Figure 6.20. The figure also shows the results of mix NA40. As expected, both moisture loss and its rate of RAC are higher than NAC. The mass loss behaviour of the RAC mixes is consistent with their shrinkage strain development, as there was no difference between the shrinkage strains of these two mixes (RAm40 and RAm40R2) (see section 6.3.2).

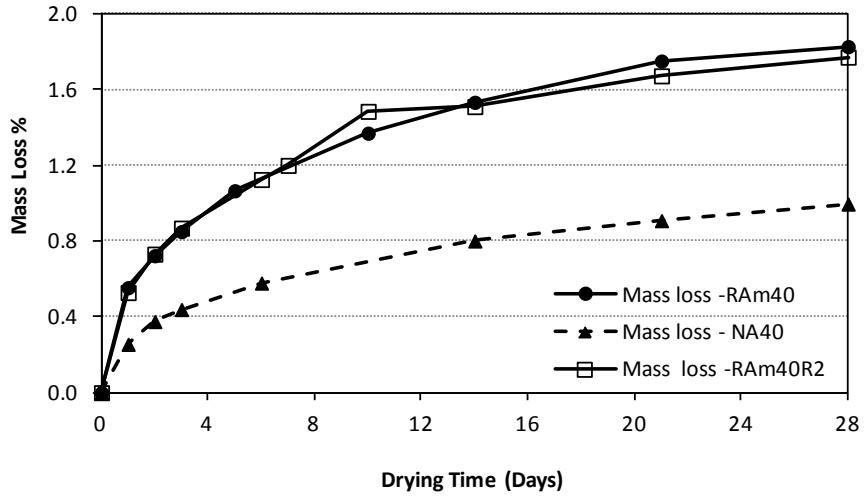

Figure 6. 20 Mass loss versus time for plain and fibre reinforced RAC and plain NAC.

6.3.6 Mass Loss vs Free Shrinkage Strain

The shrinkage strain versus mass loss curves for NAC with steel fibres are shown in Figure 6.21. It appears that the addition of fibres (regardless of type) has an insignificant effect on the relationship behaviour of shrinkage strain versus mass loss for these mixes.

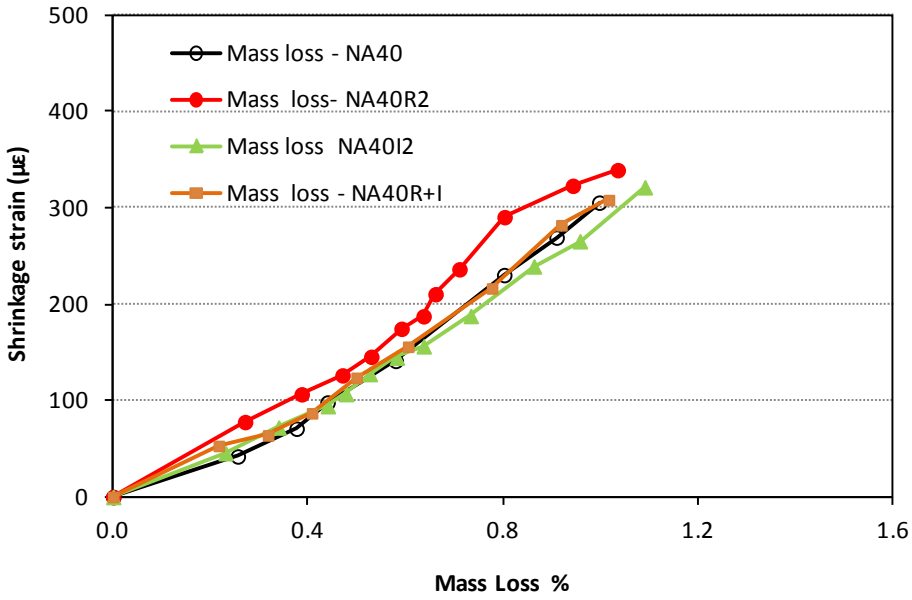

Figure 6. 21 Mass loss-shrinkage strains curves for plain and fibre reinforced NAC.

The effect of the aggregate type on the shrinkage strain-mass loss curves is shown in Figure 6.22. As expected, there is a significant difference between the two mixes NAC and RAC

which confirms that the development of shrinkage strains is a function of mass loss for a given type of aggregate and w/c ratio.

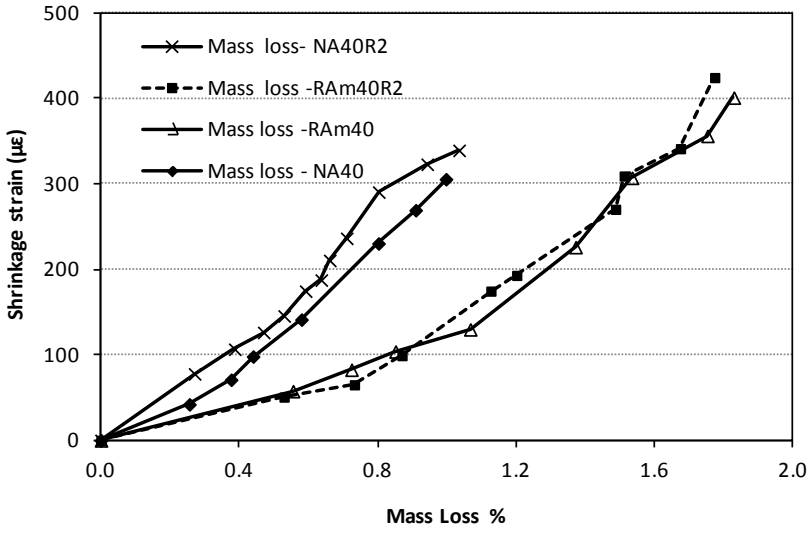

Figure 6. 22 Effect of recycled fibre and type of coarse aggregate on mass loss-shrinkage strains curves.

6.4 Results and Discussion - Restrained Shrinkage

6.4.1 Crack Characterization

In all mixes, microcracks were detected on all surfaces (sides and top) from the first day of drying. The width of these microcracks was in the range of 10-20 μm when first detected. Most of the microcracks were developed on the upper edges of both sides. Shrinkage on these regions is higher than other regions as observed during the free shrinkage tests. For plain concrete mixes, some of these microcracks propagated and coalesced into macrocracks (cracks with width of more than or equal to 20 μm and up to 50 μm, visible if properly illuminated), while others turned first into a through crack (crack along the entire top surface) and then propagated to a full-depth crack.

It is important to mention that no through or full depth cracks developed for the SFR-NAC mixes. Figures 6.23(a-c) show the distribution of the macro and full depth cracks for mixes NA40, RAm40 and RAm40R2 at the end of the exposure time (28 days). Solid lines represent macro cracks or through cracks and dotted lines indicate the non-visible part (microcracks) of these cracks. Microcracks on their own are not shown. Figure 6.24 shows the development of the cracking strain for the four specimens with through cracks.

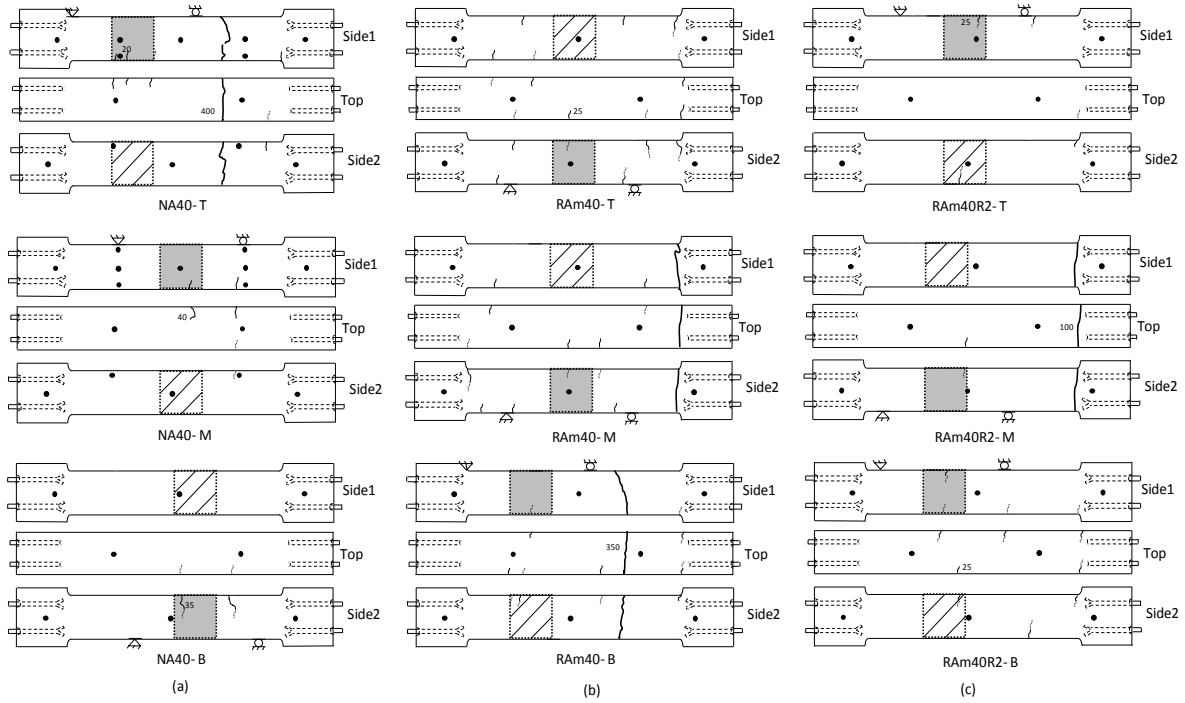

Figure 6. 23 Distribution of the macro and full depth cracks, a- NA40, b-RAm40, c- RAm40R2. (shaded grey and diagonal lines zones are critical tension and compression zone, respectively, when prisms tested in bending).

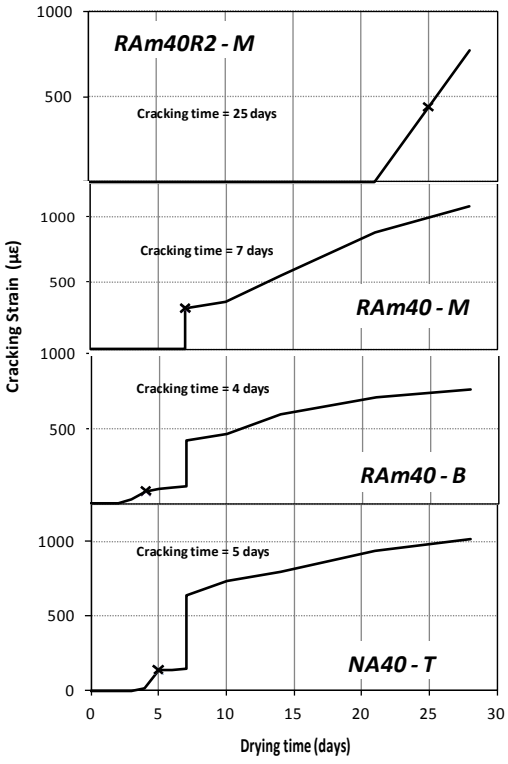

Figure 6. 24 Cracking time and strain for NAC and RAC.

6.4.2 Failure of FRC under Restrained Conditions

NAC

The behaviour of plain concrete (chapter 5) (for different w/c ratios) under restrained conditions revealed that the failure of restrained plain concrete varies according to the w/c ratio and the use of strength alone as a criterion for determining the time of restrained concrete failure (cracking) is misleading. It was found that both stress history (magnitude and rate of development) and cracking, depend on stiffness and shrinkage strain magnitude and rate of development.

It is important to mention that specimen T in mix NA40 failed after 5 days of drying under restrained conditions. In this study, none of the NAC mixes reinforced with RTSF and IF failed during the drying exposure time. This underlying the ability of fibres in enhancing tensile relaxation/creep and redistributing internal stresses, thus reducing damage at the micro level [7, 44].

For plain RAC, specimens B and M failed after 4 and 7 days of drying, respectively. For SFR-RAC, specimen B failed at day 25. This delay in cracking may be attributed to the role of fibres in enhancing the tensile relaxation of restrained concrete.

Through cracks developed during the first week in one specimen of both plain NAC and RAC. Early cracking for RAC was somehow expected, since its initial (day 1) shrinkage strains were higher (by 31%) than for NAC (see section 6.3.2). On the other hand, its lower overall stiffness (see section 6.5.2.1) is expected to lead to higher creep [2, 45] which could delay the initiation of cracks. In this case, it appears that these two opposing mechanisms cancelled one another.

6.4.3 Shrinkage Strains

Shrinkage strains developed on the restrained specimens are presented and discussed in this subsection. For side strains (Side), values presented here are the average of four measurements taken along the centre line of the specimen. For the top surface (top), one measurement was taken at its centre line over 300mm. The results are presented and discussed first for SFR-NAC followed by plain and SFR-RAC mixes.

6.4.3.1 Plain and SFR- NAC

Figure 6.25a shows the results for all specimens of mix NA40I2. It can be seen that there is little variability between the specimens Top (T), Middle (M) and Bottom (B), the same applied for all mixes. This confirms that the test rig (frame) is restraining all three specimens equally, though not completely. Just as in free shrinkage specimens, the shrinkage developed on the top surface of restrained specimens is higher than that on the sides, by about 89% for mix NA40I2 on the first day of drying.

Figures 6.25b shows the development of shrinkage strains on the sides (average of T, M and B specimens) for all mixes (NA40I2, NA40R+I, NA40R2 and NA40).

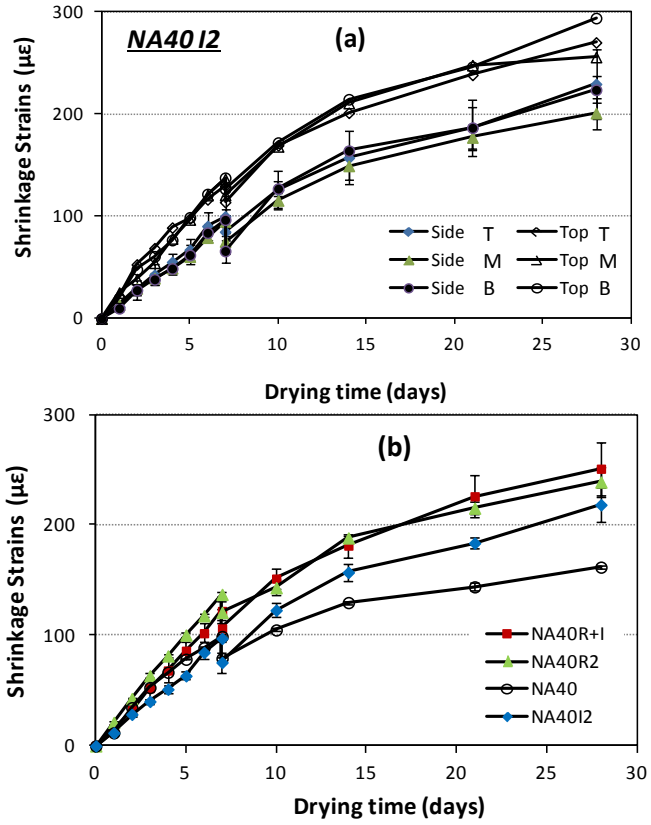

Figure 6. 25 Shrinkage strains (average) of T, M and B specimens, a- mix NA40I2 (on top and sides), b- all mixes (only sides).

The sharp reduction seen on shrinkage strains on day 7 is due to the release of strain from the prestressed bars that link the two columns of the restraining frame. As in chapter 5, releasing the strain was used to increase the RF, which decreases with time (as will be discussed in section 4.4). The release of the frame led to strain recoveries (on the sides) of 22 με (average of three specimens) for mix NA40I2, 15 με for mix NA40R+I and 16 με for

mix NA40R2. Strain recovery measured on the top surface was similar to that measured on the sides.

Figure 6.25b shows that overall there is little difference in shrinkage strains between the different FRC mixes. However, there is clear difference between plain and FRC mixes. Mixes reinforced with RTSF show higher overall shrinkage strains. This can be attributed to the ability of these fibres to reduce the microcrcaking (softening) of restrained concrete (similar to the effect of RTSF on free shrinkage see section 6.3.1). It seems that fibers play a significant role in engaging a larger volume of the matrix in the transfer of tensile stresses in restrained concrete. This results in less microcracking and is reflected on the macro level as higher shrinkage strains [27]. Similar behaviour was also reported by Altoubat and Lange [27]. Bazant and Raftshol [46] and others [47, 48] (cited in [44]) also pointed out the effect of strain softening due to microcracking on modifying the shrinkage behaviour of plain concrete.

6.4.3.2 Plain and SFR-RAC

Results of Un-cracked specimens

Figures 6.26 a and b show the development of shrinkage strains on the side and top surfaces for un-cracked restrained specimens of mixes RAm40 and RAm40R2. The figures also show the results of mixes NA40 and NA40R2. Just as in NAC mixes, RAC mixes exhibit higher strains on the top than the sides. Figure 6.25a shows that for measurements on the sides, overall there is insignificant difference in shrinkage strains between the plain and FRC mixes of both NAC and RAC. However, at early ages the shrinkage of the plain NAC is higher than that of RAC. This can again be attributed to the development of more microscracks in RAC (due to higher shrinkage, see Figure 6.6) leading to less measured shrinkage strain. For plain mixes, higher shrinkage strains are measured on the top surface for RAC, possibly due to the higher surface porosity.

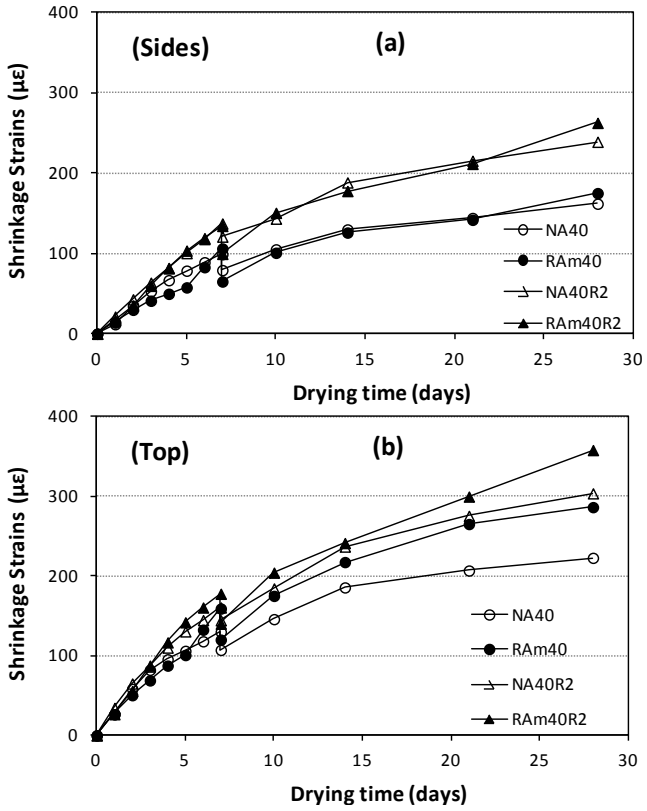

Figure 6. 26 Shrinkage strains developed on the a-Sides and b- Top, average of the un-cracked specimens.

6.4.4 Restraint Factor RF

6.4.4.1 Theoretical RF

The procedure developed in chapters three and five is used to estimate the theoretical RF of the restraining frame using linear elastic FEA and the expected development of concrete properties according to Eurocode-2 [49]. Figures 6.27a shows the estimated RF for a typical mix (NA40I2) for all specimens (T, M and B). Similar results were determined for the other mixes as shown in Figure 6.27b which shows the average RF (average of T, M and B specimens) for all mixes is around 40%. The RF curves are similar due to the fact that for the different mixes there are small differences in the expected elastic modulus and its rate of development. It should be noted that most of the loss in restraint is the result of anchor deformations.

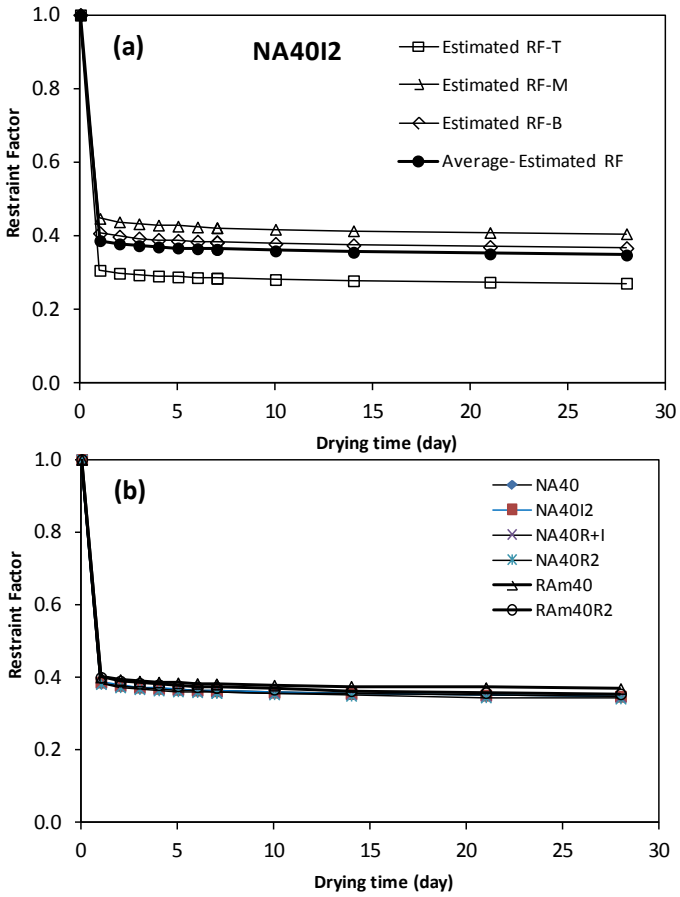

Figure 6. 27 Estimated (theoretical) RF, a- for the T, M and B specimens of mix NA40I2, b- average RF for all mixes

6.4.4.2 Apparent RF

The development of apparent RF for a typical mix (NA40R+I) on the sides and the top of the specimens is shown in Figures 6.28(a-c). It can be seen that the RF developed at the top is lower than that on the sides, especially during the first week of drying, due to the fact that shrinkage develops faster on the top surface than the sides. After 24h of drying, the average RF for mix NA40R+I (T, M and B specimens) was 68%. The RF decreases sharply by an average of 30% up to 7days. At 7 days, after strain release, none of the specimens failed and the RF on the sides increased to around 38 % due to an apparent enforced expansion of around 15 με.

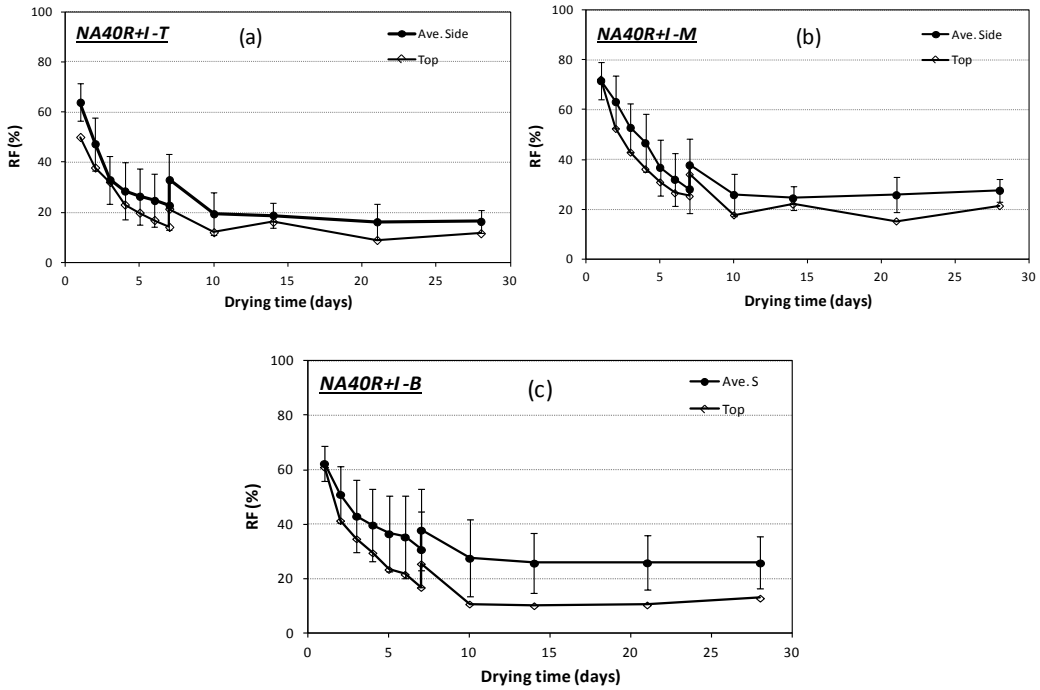

Figure 6. 28 Apparent (measured) RF of mix NA40R+I, a- T specimen, b-M specimen , c- B specimen.

Similar behaviour was observed for the other mixes. Table 6.3 shows the average RF on the sides (average of two specimens for NA40 and RAm40R2, three for all SFR-NAC and one for RAM40) on the first day of drying (RF_1) and just before (RF_{7B}) and right after (RF_{7A}) strain release and the amount of recovered strain for all mixes.

Table 6. 3 Restraint factor and recovered strains for all mixes.

Mix	RF_1 (%)	RF_{7b} (%)	RF_{7a} (%)	Recovered Strain (με)
NA40	65	31	45	20
NA40I2	68	38	50	22
NA40R+I	69	30	38	15
NA40R2	67	34	42	16
RAm40	72	44	65	41
RAm40R2	65	29	47	35
Estimated*	40	37	37	-

* Avearge value of estimated RF of all mixes.

Figure 6.29 shows the estimated and apparent average RF values for mix NA40I2. It can be seen that initially, in comparison to the estimated RF, the apparent RF is very high, but the

RF catches up after a few days. This may be attributed to the effect of the early age microcracks ("apparent" mechanism of drying creep) which may have negatively affected the apparent stiffness gain of the restrained concrete. A lower stiffness gain means less strain loss than expected and, hence, higher RF. After that initial stage, the rate of decrease in RF slows down and the values of apparent RF reach the estimated values and drop even lower (as can be seen in Table 6.3) at the age of 7 days. This may be due the effect of undesired cracks, beyond the shrinkage measuring region, impairing the restraint efficiency of the anchored ends.

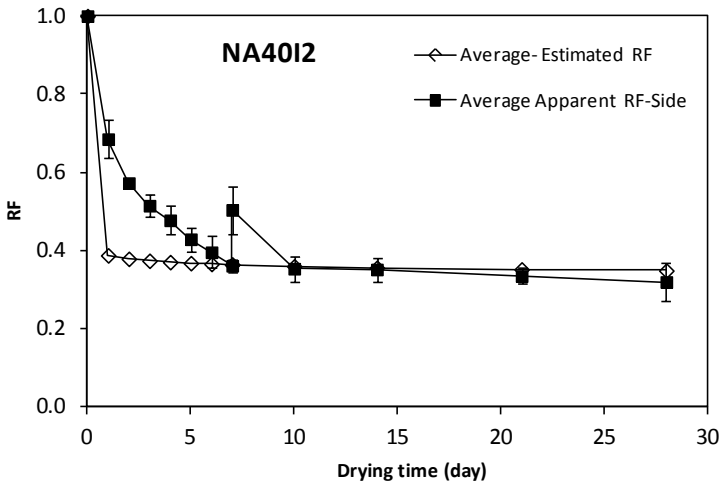

Figure 6. 29 Development of estimated and apparent RF for mix NA40I2.

6.5 Results and Discussion - Mechanical Properties

6.5.1 Compressive Strength

The results of the compressive strength at 28 days and their standard deviation (SD) for all mixes are presented in Table 6.4. The compressive strength was determined for cubes cured in water (Cube) and for portions of prisms (broken in bending) under free (F) and restrained shrinkage (R) and water cured (WC) conditions. All results presented in this section are the average of three specimens per mix and normalized to the values of the compressive strength of the water cured cube specimens (Cube) at 28 days.

Table 6. 4 Compressive strength, normalized strength and standard deviation (SD) of SFR-NAC mixes.

Mix Type	Compressive Strength at 28 days, MPa (SD)				Normalized Strength			
	Cube	F	R	WC	Cube	F	R	WC
NA40	59.4 (0.3)	51.5 (1.0)	51.2 (2.6)	58.8 (01.3)	1.0	0.87	0.86	0.99
NA40R2	66.0 (1.7)	61.9 (2.1)	60.7 (2.6)	70.8 (1.8)	1.0	0.94	0.92	1.07
NA40I2	60.2 (2.0)	57.8 (3.0)	53.9 (0.8)	59.9 (2.9)	1.0	0.96	0.90	0.99
NA40R+I	62.2 (1.9)	56.7 (1.6)	53.9 (3.6)	61.2 (0.6)	1.0	0.91	0.87	0.98
RAm40	43.5 (1.4)	40.1 (0.4)	39.8 (0.6)	45.2 (1.3)	1.0	0.92	0.91	1.04
RAm40R2	54.4 (2.0)	49.7 (0.6)	49.0 (0.7)	55.0 (1.2)	1.0	0.91	0.90	1.01
Average					1.0	0.92	0.90	1.01

Cubes

For "Cube" specimens, the addition of 2 % (by mass of concrete) RTSF increased the compressive strength of NAC by 12%. ISF at 2% had an insignificant effect on the compressive strength. The addition of blended (1% RTSF+1% ISF) fibres resulted in an increase of 5%.

As expected, the use of RA (mix RAm40) resulted in 27% lower compressive strength in comparison to that of NA40. Table 4 also shows that the inclusion of 2% of RTSF and the surface treatment of RA with 2% of SF increased the strength of RAC by 25%. Similar results were obtained by the authors in a previous study [31] (chapter 2).

Prisms

The compressive strength from prisms for WC is similar to those of the Cubes. In fact, on average they are slightly stronger, but that can be attributed to the fact that on one axis the specimen is confined by additional concrete.

On average, air dried specimen 'F' had a 8% less compressive strength than that of the Cube at 28 days partly due to less hydration and partly due to the development of microcracks induced by differential shrinkage. Surprisingly, the restrained specimen 'R' only differed from 'F' specimens by 2% which means that the shrinkage cracks induced by external restraint did not have as significant effect as one might expect.

6.5.2 Flexural Behaviour

After 28 days of drying, the free shrinkage specimens were tested in bending. The position of the supports and load points varied according to the type of the specimens (free or restrained), as described below:

a) For free shrinkage specimens, when possible, the bending test was conducted twice on two parts of the same specimen. The position of supports and point loads in the two tests are illustrated in Figure 6.30.

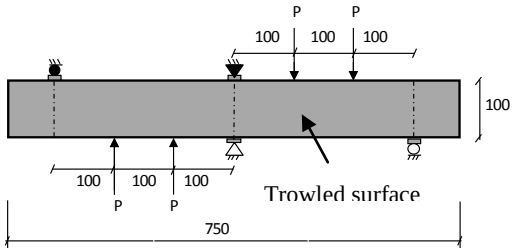

Figure 6. 30 Position of supports and loads in bending test for free shrinkage specimens (dimensions in mm).

b) For restrained shrinkage specimens, the load points and supports used are shown in Figure 6.31. The location of these was selected so as to capture the widest crack (and as many cracks caused by restrained shrinkage) within the critical region. In Figure 6.23 (see section 6.4.1), the critical region is shaded grey when in tension and with diagonal lines when in compression.

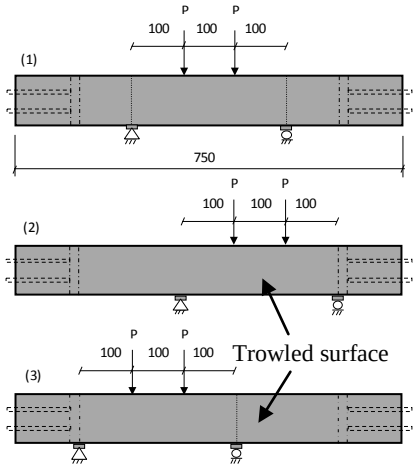

Figure 6. 31 Position of supports and loads in bending test for restrained shrinkage specimens (dimensions in mm).

Tables 6.5 shows the results of the flexural elastic modulus (E_{fmax}), flexural strength (fl_{LOP}) at the limit of proportionality (LOP) and the ultimate flexural strength (fl_{ult}) of WC, F and R specimens for all mixes. The results are the average of three or four specimens, as shown in Table 6.5. Table 6.5 also shows the normalized results to the values of WC specimens. The flexural strength (fl_{LOP}) is determined at the estimated first crack load. This is not easy to assess visually, hence, the load versus calculated flexural elastic modulus (E_{flex}) curve is used. Typical load-deflection and E_{flex}-bending load curves are shown in Figures 6.32 a and b. The first crack is considered to initiate at a load at which E_{flex} drops to $0.85E_{fmax}$ as shown for mix NA40R+I/ restrained-bottom specimen.

Table 6. 5 Flexural strength (fl_{LOP} and fl_{ult}) and E_{fmax} for all mixes.

Mix	No. and Type of specimen		E_{fmax} in GPa (*)		Normalized E_{fmax}	Flexural strength (Ultimate)			Flexural strength (LOP)		
						MPa (*)		Normalized	MPa (*)		Normalized
NA40	3	WC	39.7 (0.3)		1.0	4.9 (0.2)		1.0	4.7 (0.3)		1.0
	4	F	38.7 (0.2)		0.97	4.9 (0.3)		1.0	4.1 (0.1)		0.87
	1	*R_T*	*36.3*	34.4 (0.1)	*0.91*	*4.6*	4.9 (0.3)	*0.95*	*4.3*	4.7 (0.1)	*0.91*
	1	R_M	33.5		0.84	5.1		1.04	4.8		1.02
	1	R_B	33.4		0.84	5.0		1.02	4.9		1.04
NA40I2	3	WC	33.4 (1.0)		1.0	5.7 (1.2)		1.0	4.4 (0.5)		1.0
	3	F	34.2 (0.5)		1.02	5.7 (0.5)		1.0	5.2 (0.3)		1.18
	1	R_T	32.5	31.2 (1.2)	0.98	5.1	5.2 (0.9)	0.90	4.9	4.8 (0.5)	1.11
	1	R_M	30.3		0.91	6.1		1.07	5.2		1.18
	1	R_B	30.8		0.92	4.3		0.75	4.2		0.95
NA40R2	3	WC	36.2 (0.1)		1.0	5.9 (1.0)		1.0	5.2 (0.1)		1.0
	3	F	34.1 (3.6)		0.94	5.6 (0.8)		0.95	5.2 (0.7)		1.0
	1	R_T	36.7	36.6 (1.8)	1.01	5.8	6.1 (0.3)	0.98	5.4	5.5 (0.3)	1.04
	1	R_M	38.3		1.06	6.0		1.0	5.9		1.13
	1	R_B	34.7		0.96	6.4		1.08	5.4		1.04
NA40R+I	3	WC	32.7 (1.6)		1.0	6.4 (0.1)		1.0	4.6 (0.8)		1.0
	3	F	35.5 (3.6)		1.07	5.4 (0.5)		0.84	4.6 (0.4)		1.0
	1	R_T	33.5	34.1 (2.8)	1.01	5.9	5.7 (0.4)	0.92	5.3	5.2 (0.4)	1.15
	1	R_M	31.7		0.97	5.2		0.81	4.8		1.04
	1	R_B	37.1		1.12	6.0		0.94	5.5		1.19
RAm40	3	WC	30.5 (0.7)		1.0	4.7 (0.1)		1.0	4.6 (0.2)		1.0
	4	F	26.6 (0.9)		0.87	5.0 (0.3)		1.05	4.4 (0.3)		0.97
	1	R_T	24	24.6 (1.8)	0.79	4.9	4.7 (0.2)	1.04	4.7	4.4 (0.4)	1.02
	1	*R_M*	*23.2*		*0.76*	*4.4*		*0.94*	*4.0*		*0.87*
	1	*R_B*	*26.6*		*0.87*	*4.7*		*1.00*	*4.5*		*0.98*
RAm40R2	3	WC	30.4 (0.6)		1.0	5.2 (0.5)		1.0	5.1 (0.4)		1.0
	4	F	26.8 (2.1)		0.88	5.5 (0.4)		1.05	5.0 (0.4)		0.98
	1	R_T	25.6	24.6 (0.9)	0.84	5.7	5.5 (0.1)	1.10	5.2	4.9 (0.4)	1.02
	1	R_M	24.2		0.8	5.5		1.05	5.3		1.04
	1	*R_B*	*23.8*		*0.78*	*5.1*		*0.98*	*4.2*		*0.83*

*Standard deviation. Values in *italic* represents results of restrained specimens that cracked under restrained conditions.

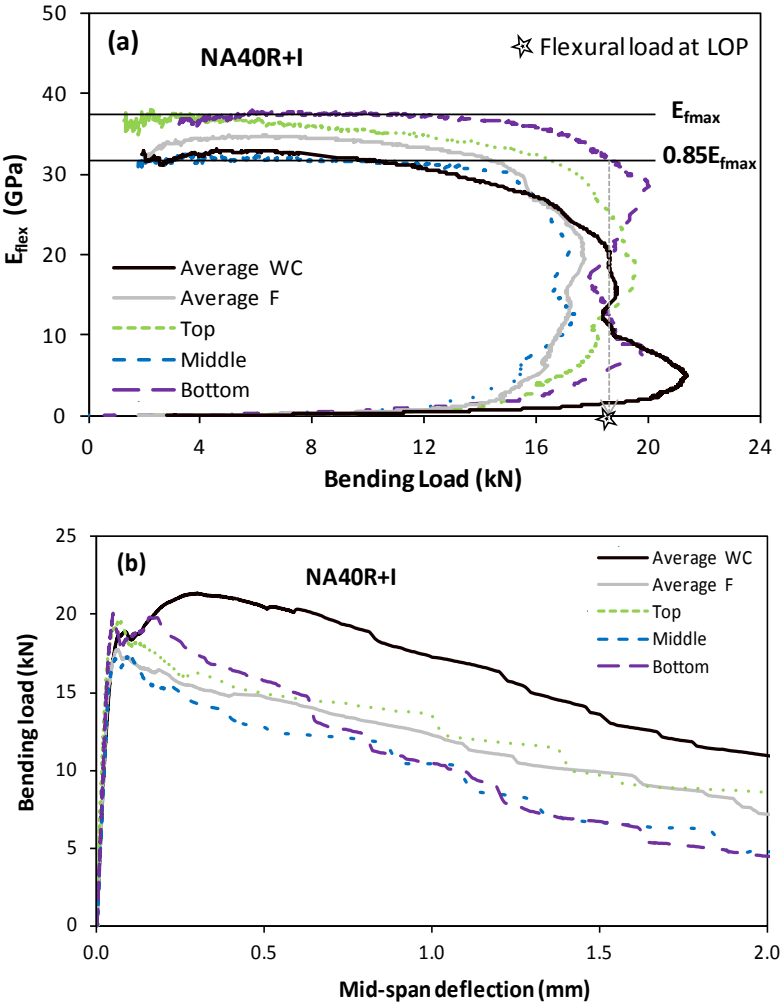

Figure 6. 32 a-Load-deflection, b- E_{flex} -bending-load curves for: WC , F and R specimens (Top, Middle and Bottom) for mix NA40R+I.

6.5.2.1 Flexural Elastic Modulus E_{fmax}

NAC

The E_{fmax} of WC and F specimens for mix NA40 (plain NAC) is higher than that of FRC mixes (NA40I2, NA40R+I and NA40R2). This may be attributed to the higher air voids content (see Table 6.6) of FRC mixes (due to fibre addition). The theoretical air content shown was determined for each mix based on the measured density and rule of mixtures..

Table 6. 6 Theoretical air content and measured density for all mixes.

Property	Mix Type					
	NA40	NA40I2	NA40R+I	NA40R2	RAm40	RAm40R2
Density (kg/m3)	2375	2355	2376	2367	2246	2241
Air content (%)	2.9	5.1	4.2	4.6	5.7	7.2

Short (RTSF) fibres appear to enhance the stiffness of restrained specimens. This will be further examined by comparing the results of WC, F and R specimens for each mix.

For mix NA40 (plain mix), the E_{fmax} of F specimens is slightly lower than E_{fmax} of WC specimens. However, E_{fmax} is lower by up to 16 % for specimens subjected to restrained shrinkage. This is expected as shrinkage induced cracks can cause some loss of stiffness due to the lengthening/softening of restrained specimens.

For the mixes with short fibres (RTSF), the E_{fmax} for F and R specimens were comparable or slightly higher (in the case of R specimens) than those of the WC specimens. Surprisingly, this means that the lengthening of the specimens due to the restraint did not lead to softening.

RAC

The E_{fmax} of plain and FRC- RAC mixes is lower (by 23% for WC specimens) than that of NAC mixes possibly due to the softer nature of the RA themselves and their higher air content (see Table 6.6). For RAm40, the E_{fmax} of the F specimens was lower by 13% and by 24% for R specimens in comparison to WC specimens, partly also due to a lower hydration rate. The addition of RTSF and the surface treatment of RA did not alter the E_{fmax} of the RAC. This can be attributed to the effect of the higher air void content in this mix.

Role of fibres under restrained conditions

Under restrained conditions, FRC mixes performed better in comparison to the plain mix. This can be attributed to the role of fibres in enhancing tensile creep/relaxation mechanisms by better control (reduce) of microcracks as reported by Altoubat and Lange [50]. Altoubat and Lange stated that fibres can: 1- enhance the' beneficial' (real) mechanisms of creep by the ability of fibres in providing more uniform distribution of internal stresses and engaging

a larger volume of the matrix in stress transfer; and 2- reduce the 'detrimental' (apparent) mechanism of creep (microcracking). These mechanisms are also predicted to lead to higher shrinkage of restrained specimens for mixes with fibres as was observed in this study (see Figures 6.25 and 6.26). The better control and delay of the propagation of microcracks to macrocracks can also assist in the self-healing of microcracks.

6.5.2.2 Flexural strength (fl_{LOP} and fl_{ult})

NAC

For the plain mix (NA40), the flexural performance of F specimens was lower by 13% (in terms of fl_{LOP}) and comparable (in terms of fl_{ult}) compared to those of WC specimens. Unexpectedly, the flexural strength of R specimens was similar to WC specimens.

For the FRC mixes (apart from NA40I2), the fl_{LOP} for F and R specimens were comparable or slightly higher (in the case of R specimens) than those of the WC specimens.

All FRC specimens exhibited comparable or higher flexural performance (fl_{LOP} and fl_{ult}) in comparison to the plain concrete. It appears that mixes with short fibres (RTSF) performed better than ISF, in particular for WC and R specimens.

RAC

For mix RAm40, the fl_{LOP} of F and R specimens were only slightly lower than that of WC specimens.

Similar to the NAC, both free and restrained specimens of RAC containing RTSF and treated RA showed unexpectedly comparable fl_{LOP} and slightly higher fl_{ult} compared to those of the WC specimens.

The addition of RTSF and surface treatment of RA resulted in higher (10-14 %) fl_{LOP} and fl_{ult} for WC, F and R specimens of RAC

6.5.2.3 Discussion on Flexural Properties

The unexpected flexural performance with and without fibres can be attributed to the effect of two additional mechanisms (beside the role of fibres mentioned in subsection 6.5.2.1): 1- shrinkage curvature and internal stress state, 2- self-heal of microcracks. These mechanisms are explained below:

Shrinkage curvature and internal stress state

The shrinkage curvature (due to differences in strain between the top and bottom surfaces) observed on the free specimens (section 6.3.4) can increase the self induced tensile stresses leading to microcracks and increase the intensity of the microcracks induced by differential shrinkage. The shrinkage curvature under free condition is higher than for the restrained condition as can be seen in Figures 6.33 a and b which show the shrinkage curvatures for typical plain and FRC mixes. The lower shrinkage curvature of restrained specimens may be due to restraint induced tensile stresses that reduce shrinkage curvature by stretching the concrete specimen. This (restraint induced tensile stress) can also change the state of internal stresses of concrete from tensile (on the surface) and compression (in the core) in the free load condition (F specimens), to a more uniform distribution of tensile stresses over the cross section in the restrained condition (R specimens). This can result in more, but smaller and shorter, microcracks. The change in microcrack characteristics (number, size and distribution) may be the possible reason behind the better or comparable flexural behaviour (fl_{LOP} and fl_{ult}) of R specimens in comparison to F specimens.

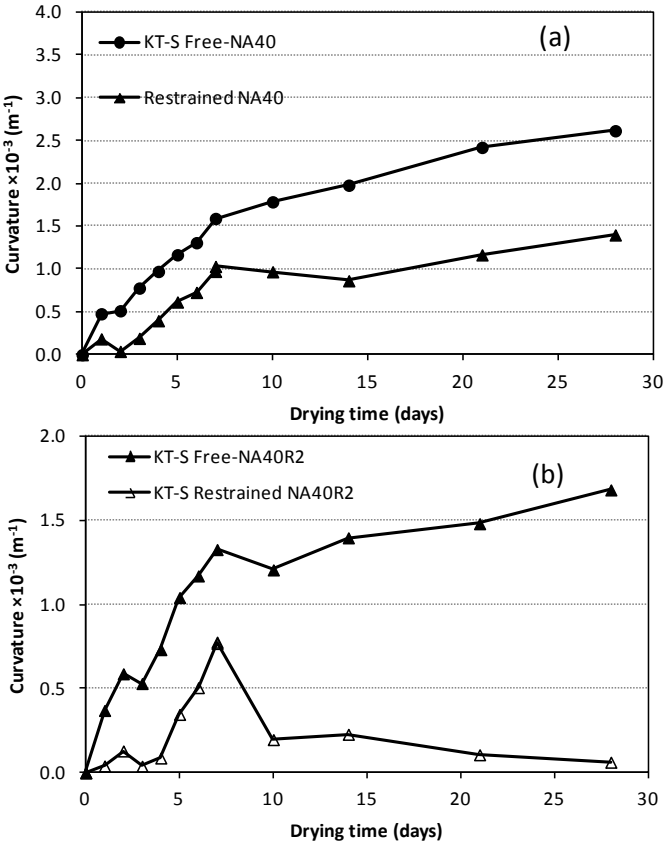

Figure 6. 33 Comparison between shrinkage curvature of free and restrained specimens of mixes, a-NA40, b- NA40R+I and c- NA40R2.

Self-heal of microcracks

Smaller microcracks can also facilitate self-healing. The development of micrcocracks creates moisture gradients inside the concrete due to the creation of local vacuum zones. Such gradients promote permeation of moisture to the microcracks from the capillaries in the vicinity promoting hydration of unhydrated cement particles. Provided the microcracks are small enough, this results in healing [51].

6.5.2.4 Discussion on Effect of Restrained Shrinkage on Mechanical Properties

Restraining of concrete leads to a 10% reduction in compressive strength. For plain NAC, the flexural elastic modulus (E_{fmax}) also reduced by 16% but this did not reduce the flexural strength, in particular for the restrained specimens. It appears that restraining had a

beneficial effect on strength by moderating the internal stresses developed due to differential shrinkage.

The addition of fibres in NAC mixes, especially the short recycled fibres (RTSF), appears to have affected the E_{fmax} but has slightly increased the flexural behaviour.

The addition of RTSF and the treatment of RA significantly improved the compressive strength of RAC, but had no effect on the E_{fmax} due to the nature of the RA. However, the flexural strength obtained was higher than that of NAC without fibres and similar to the performance of NAC with fibres. This confirms that recycled fibres can address the weaknesses of RA and lead to RAC of comparable mechanical performance to that of NAC.

6.6 Conclusions

This chapter examined the effect of RA and RTSF on the shrinkage behaviour of concrete under unrestrained and restrained conditions. The following can be concluded.

- Conventional steel fibre at 2% dose had no effect on free shrinkage. RTSF increased initial shrinkage strains due to higher air content and lower internal restraint.

- Relative to NAC, RA from CDW reduced the compressive strength by 27% , the flexural modulus of elasticity by around 23% and increased shrinkage by 31% (at 1 day) and 35% (at 28 days).

- Despite their differences in mechanical performance, under restrained conditions NAC and RAC cracked at around the same time.

- The compressive strength of restrained specimens only reduced by around 2% relative to unrestrained specimens. In unreinforced NAC, the elastic modulus decreased by up to 16%. However, for RTSF reinforced specimens the elastic modulus did not decrease.

- The flexural strength of all specimens was not affected much by the different exposure conditions. Nonetheless, the restrained specimens of the mixes with RTSF appear to have a slightly higher flexural strength than without fibres and without restrain.

- It is concluded that RTSF, despite increasing the air content of concrete, control shrinkage induced microcracks propagation better than IF. It is believed that this is a result of the role

of short fibres in enhancing the tensile creep behaviour of concrete by : 1) providing more uniform distribution of internal stresses and engaging a larger volume of the matrix in stress transfer; 2) reducing the micro-damage, and 3) promoting self healing of microcracks. Hence, they are ideal for enhancing the flexural properties of RAC to the level achieved by NAC.

References

1. Hansen, T.C. and E. Boegh, *Elasticity and Drying Shrinkage of Recycled-Aggregate Concrete.* Journal of the American Concrete Institute, 1985. **82**(5): p. 648-652.
2. Hansen, T.C., *Recycled of Demolished Concrete and Masonry* 1992, London: E & FN SPON.
3. Katz, A., *Properties of concrete made with recycled aggregate from partially hydrated old concrete.* Cement and Concrete Research, 2003. **33**(5): p. 703-711.
4. Ajdukiewicz, A. and A. Kliszczewicz, *Influence of recycled aggregates on mechanical properties of HS/HPC.* Cement & Concrete Composites, 2002. **24**(2): p. 269-279.
5. Bishop J., *The early age Behaviour of Concrete Industrial Ground Floor Slabs*. 2001, loughborough University: loughborough, UK
6. ACI 231R-10, *Report on Early-Age Cracking: Causes, Measurement, and Mitigation*, in *ACI Committee 231*. 2010, American Concrete Institute: Farmington Hills, U.S.A.
7. Altoubat, S.A. and D.A. Lange, *Creep, shrinkage, and cracking of restrained concrete at early age.* ACI Materials Journal/ SP, 2001. **98**(4): p. 323-331.
8. Chern, J.-C. and C.-H. Young, *Compressive creep and shrinkage of steel fibre reinforced concrete.* International Journal of Cement Composites and Lightweight Concrete, 1989. **11**(4): p. 205-214.
9. Tan, K. and P. Paramasivam, *Creep and Shrinkage Deflections of RC Beams with Steel Fibers.* Journal of Materials in Civil Engineering, 1994. **6**(4): p. 474-494.
10. Swamy, R.N. and H. Stavrides, *Influence of Fiber Reinforcement on Restrained Shrinkage and Cracking.* Journal of the American Concrete Institute, 1979. **76**(3): p. 443-460.
11. Zhang, J. and V.C. Li, *Influence of Fibres on Drying Shrinkage of Fibre-Reinforced Cementitious Composite*. Journal of Engineering Mechanics, ASCE, 2001. **127**(1): p. 37-44.
12. Mangat, P.S. and M.M. Azari, *A Theory for the Free Shrinkage of Steel Fibre Reinforced Cement Matrices.* Journal of Material Science 1984. **19** (7): p. 2183-2194.
13. Li, Z., M.A. Perez Lara, and J.E. Bolander, *Restraining effects of fibers during non-uniform drying of cement composites.* Cement and Concrete Research, 2006. **36**(9): p. 1643-1652.
14. Grzybowski, M. and S.P. Shah, *Model to Predict Cracking in Fiber Reinforced-Concrete Due to Restrained Shrinkage*. Magazine of Concrete Research, 1989. **41**(148): p. 125-135.
15. Altoubat, S.A. and D.A. Lange, *Creep, shrinkage, and cracking of restrained concrete at early age.* Aci Materials Journal, 2001. **98**(4): p. 323-331.
16. Wang, K., S.P. Shah, and P. Phuaksuk, *Plastic Shrinkage Cracking in Concrete Materials- Influence of Fly Ash and Fibres.* ACI Materilas Journal, 2001. **98**(6): p. 458-464.
17. Aly, T., J.G. Sanjayan, and F. Collins, *Effect of polypropylene fibers on shrinkage and cracking of concretes.* Materials and Structures 2008. **41**: p. 1741–1753.

18. Hoff, G.C., *Durability of fiber reinforced concrete in a severe marine environment.* ACI Special Publication, 1987. **100**.

19. ACI 544.1R-96, *State-of-the-Art Report on Fiber Reinforced Concrete* 1996, ACI: Detroit. p. 1-66.

20. Pour-Ghaz, M., et al., *Experimental Methods to Detect and Quantify Damage in Restrained Concrete Ring Specimens.* Journal of Advanced Concrete Technology, 2011. **9**(3): p. 251-260.

21. Shah, H.R. and J. Weiss, *Quantifying shrinkage cracking in fiber reinforced concrete using the ring test.* Materials and Structures, 2006. **39**(9): p. 887-899.

22. Grzybowski, M. and S.P. Shah, *Shrinkage Cracking of Fibre Reinforced Concrete.* ACI Materials Journal, 1990. **87**(2).

23. Kwon, S.H. and S.P. Shah, *Prediction of early-age cracking of fiber-reinforced concrete due to restrained shrinkage.* ACI Materials Journal, 2008. **105**(4): p. 381-389.

24. Kovler, K., *Testing System for Determining the Mechanical-Behavior of Early Age Concrete under Restrained and Free Uniaxial Shrinkage.* Materials and Structures, 1994. **27**(170): p. 324-330.

25. Carlsward J. , *Shrinkage Cracking of Steel Fibre Reinforced self compacting Concrete Overlays*, in *Department of civil and Environmental Engineering*. 2006, Lulea University of Technology: Lulea,Sweden.

26. Weiss, W., W. Yang, and S. Shah, *Shrinkage Cracking of Restrained Concrete Slabs.* Journal of Engineering Mechanics, 1998. **124**(7): p. 765-774.

27. Altoubat, S.A. and D.A. Lange, *The Pickett effect at early age and experiment separating its mechanisms in tension.* Materials and Structures, 2002. **35**(4): p. 211-218.

28. Pilakoutas, K., K. Neocleous, and H. Tlemat, *Reuse of steel fibres as concrete reinforcement.* Engineering Sustainability,, 2004. **157**(ES3): p. 131-138.

29. Tlemat, H., K. Pilakoutas, and K. Neocleous, *Stress-strain characteristic of SFRC using recycled fibres.* Materials and Structures, 2006. **39**(3): p. 365-377.

30. Neocleous, K., et al. (2011) *Fibre-reinforced roller-compacted concrete transport pavements*. Proceedings of the ICE - Transport **164**, 97-109.

31. Younis, K.H. and K. Pilakoutas, *Strength prediction model and methods for improving recycled aggregate concrete.* Construction and Building Materials, 2013. **49**(0): p. 688-701.

32. BS EN 197-1:2011, *Cement. Composition, specifications and conformity criteria for common cements*. 2011, British Standard Institution: London, UK.

33. Musacchi, E., P. Iacobucci, and M. Pierfelice, *Potential Process for Cleaning and Sorting of the recycled fibres, Deliverable report 13, FB6 STREP Project Ecolanes (031530).* 2008.

34. Tlemat H., *Steel fibres from waste tyres to concrete: testing, modelling and design*, in *Department of Civil and Structural Engineering*. 2004, The University of Sheffield: Sheffield UK.

35. BS EN 12390-2:2009, *Testing hardened concrete Part 2: Making and curing specimens for strength tests.* 2009, British Standards Institution: London.

36. ACI 207.2R-95, *Effect of Restraint, Volume Change, and Reinforcement on Cracking of Mass Concrete*, A.C. 207, Editor. 1995, American Concrete Institute: Farmington hills, MI, USA. p. 47.

37. Abbasnia, R., P. Godossi, and J. Ahmadi, *Prediction of restrained shrinkage based on restraint factors in patching repair mortar.* Cement and Concrete Research, 2005. **35**(10): p. 1909-1913.

38. BS EN 12390-3:2009, *Testing hardened concrete Part 3: Compressive strength of test specimens*. 2009, British Standards Institution: London.

39. BS 1881-119:2011, *Testing concrete. Method for determination of compressive strength using portions of beams broken in flexure (equivalent cube method)*. 2011, BSI: London-UK. p. 12.

40. ASTM-C1018-97, *Standard Test Method for Flexural Toughness and First-Crack Strength of Fiber-Reinforced Concrete (Using Beam With Third-Point Loading).* 1997, ASTM International.

41. Japan Society of Civil Engineers(JSC)-SF4, *Methods of tests for flexural strength and flexural toughness of steel fibre reinforced concrete*. 1994, Concrete Library of JSCE. p. 58-61.

42. Younis, K.H. and K. Pilakoutas, *Assessment of Post-Restrained Shrinkage Mechanical Properties of Concrete* ACI Materials, 2014. **Submitted for publication**.

43. Kovler, K., and Zhutovsky S., , *Over view and future trends of shrinkage research.* Materials and Structures, 2006. **39**: p. 827-847.

44. Altoubat, S.A. and D.A. Lange. *Early age shrinkage and creep of fiber reinforced concrete for airfield pavement*. in *Aircraft/Pavement Technology In the Midst of Change*. 1997.

45. Fan, Y., J. Xiao, and V.W.Y. Tam, *Effect of old adhered mortar on creep of recycled aggregate concrete.* Structural Concrete, 2013: p. n/a-n/a.

46. Bazănt, Z.P. and W.J. Raftshol, *Effect of cracking in drying and shrinkage specimens.* Cement and Concrete Research, 1982. **12**(2): p. 209-226.

47. Wittmann F.H., *Creep and Shrinkage Mechanisms*, in *Creep and Shrinkage in Concrete Structures*, Z.P. Bažant and Wittmann F.H., Editors. 1982, John Wiley &Sons: Chichester. p. 129-161.

48. Alvaredo, A. and F.H. Wittmann. *Shrinkage as influenced by strain softening and creep formation*. in *Creep and Shrinkage of Concrete, Proc. of the 5th International RILEM Symposium*. 1993: E & FN SPON

49. BS EN 1992-1-1:2004, *Eurocode 2: Design of concrete structures — Part 1-1: General rules and rules for buildings* 2004, British Standard Institution: London, UK.

50. Altoubat, S.A. and D.A. Lange, *A New Look at Tensile Creep of Fiber-Reinforced Concrete.* ACI Special Publication, 2003. **216**.

51. Rossi, P., J.-L. Tailhan, and F. Le Maou, *Comparison of concrete creep in tension and in compression: Influence of concrete age at loading and drying conditions.* Cement and Concrete Research, 2013. **51**: p. 78-84.

Chapter 7

Summary and Conclusions, and Recommendations for Future Work

This chapter presents the main conclusions that can be drawn from the work conducted in this thesis. The chapter also proposes some recommendations for future work, aiming to facilitate the use of recycled materials and enhance the understanding of the behaviour of concrete containing such materials under restrained conditions.

7.1 Summary and Conclusions

This study forms part of a wider body of work that aims to facilitate the use of recycled materials such as RA and RTSF in the production of structural concrete through developing a better understanding of shrinkage behaviour of NAC and RAC under restrained conditions. To achieve this:

1- An experimental study was conducted, using RA originating from processing CDW and crushing old laboratory concrete samples, to characterise the properties of RA. The properties of RAC was quantified and compared with NAC. Surface treatment of RA and the addition of short RSTF were used to improve the properties of RAC.

2- A new restrained shrinkage test and a procedure to quantify the mechanical properties of post-restrained shrinkage of concrete was developed. A parametric study was conducted to:

a) check the effectiveness of the developed restraining frame,

b) quantify the effects of restrained shrinkage induced cracks on the behaviour of concrete mixes incorporated RA, surface treated RA and RTSF.

Based on the results, the following conclusions can be drawn:

7.1.1 Characterisation of RA and Properties of RAC

- The results of the WA tests show that, regardless of type of RA, more than 70% of their 24hr WA capacity can be achieved when immersing RA in water for 10min. For this reason, to overcome the issue of high absorption, it is recommended to leave the RA in the mixer with half of the mixing water for 10 minutes.

- A clear relationship can be identified between the particle density of RA and its strength (LA), WA and porosity. When the particle density decreases, its strength decreases whilst its WA and porosity increases.

- The particle density of RA seems to have a strong relationship with very good correlation with the strength of RAC. It was found that an 8% increase in particle density leads to an increase of approximately 10 % in concrete strength, regardless of RA content. Therefore, just as in NA, the particle density of RA seems to be

predominantly responsible for the density of RAC. Also, the density of RA appears to directly affect the strength of RAC. Consequently, to produce high quality of RA from CDW, density separation is vital.

- There is a good correlation between LA of RA and the normalized strength of RAC. It is proposed that the use of LA coefficient alongside the particle density is used to quantify the effect of RA on the strength of RAC.

- The most important parameters (ρ_{rd}, LA, WA and RA content) that affect the strength performance of RAC were used to develop a strength predictive model.

7.1.2 Methods to Improve RAC Strength

- PMT and WMT were examined as techniques to treat the surface of RA-M (coating with reactive and non-reactive microfillers). The results obtained from WMT were slightly better, since all the microfiller used to coat the RA remains in the concrete mix. Reactive microfillers such as GGBS and SF led to an increase in compressive strength of RAC by 6% and 17% respectively (using WMT). FA did not result in any strength improvement possibly due to the large size of FA particles. When non-reactive microfillers (LP) were used, the compressive strength improved by 8%. SF gave the best results and is recommended for surface treatment of RA.

- It appears that the addition of 2% (by mass) RTSF delays/prevents the propagation of microcracks and improves the compressive strength of RAC.

7.1.3 Restrained Shrinkage Test: Pilot Study-Single Rig

- A developed pilot single rig only provided partial restraint and proposals for improvements were made. The RF was found to vary with time due to the concrete strength/stiffness evolution and crack development.

- Bending and compression tests were undertaken on specimens exposed to restrained shrinkage. Results obtained from these tests show that induced cracks can affect the mechanical behaviour (flexural and compressive strength and flexural stiffness) of

concrete by up to 21%. However, this was a very limited proof-of-concept study and a parametric study was recommended to validate this conclusion.

7.1.4 Restrained Shrinkage Test: Parametric Study-Restraining Frame

- A new restrained shrinkage rig (frame) was developed for this parametric study.

- For the free shrinkage tests, the shrinkage strains on the top surface of the concrete specimens are higher than those on the sides and the bottom surface. The variation in strains is higher at an early age and more pronounced in mixes with high w/c ratios. This is attributed to their higher porosity and better compaction of the lower layer of the concrete.

- This study quantifies that free shrinkage specimens develop curvatures due to differences in shrinkage strains along the depth of the specimens. Differential shrinkage can also develop between the surfaces and core of the specimens, which can lead to surface tensile stresses which can amplify the effects of restrained shrinkage.

- In early ages, for the low w/c mix (NA30), the free shrinkage strains and their rate of development are higher than those for higher w/c mixes (NA40 and NA50) due to higher autogenous shrinkage. For later ages, the development of the shrinkage strains of mixes with low w/c ratios slows down faster than for mixes with higher w/c ratios, possibly due to the fact that there is less moisture that can be lost upon drying due to their denser microstructure. Mixes with high w/c ratios initially lose mass faster, due to moisture loss from large capillary pores and this results in relatively low initial shrinkage strain.

- For concrete under restrained conditions, shrinkage strains induced cracking is a function of the concrete properties, since they govern the stiffness and the stress history.

- The majority of strain and RF loss of the proposed "passive" restraining frame, can be attributed to the relative stiffness between the frame and the concrete specimens. Long-term RF loss is also recorded due to loss of stiffness in the anchored zone and creep of concrete due to the enforced expansion.

- Due to early age microcracking, which slows down elastic modulus development, the apparent RF decreases at a relatively high rate over the first few days. Nonetheless, microcracking reduces the overall stiffness gain of the concrete, resulting in less overall strain loss than expected.

- Drying (in both free and restrained conditions) reduces the compressive strength of concrete by about 10-14%. Though surface microcracking due to shrinkage is expected to reduce compressive strength, its effect appears to be relatively small compared to the long term effect of maturity on strength. This may partly explain discrepancies in compressive strength trends in previous studies.

- The residual compressive strength of free specimens does not differ much from that of restrained specimens. This is possibly due to the fact that most restrained shrinkage induced macrocracks are found in the regions close to the upper and lower plates of the compression test machine, which are well confined. Hence, standard compression tests may overestimate the actual strength of restrained concrete. Frictionless surfaces may help address this issue.

- Shrinkage induced cracks affect the flexural strength of concrete mixes with different w/c ratios in a different manner. The effects are more pronounced on mixes with low w/c ratios (0.3) (reduction 11-24%) than on mixes with high w/c ratios (0.4 and 0.5) (reduction in the range of 2-5%). This may be due to high autogenous and early thermal shrinkage (due to hydration). A higher rate of shrinkage and elastic modulus evolution can lead to a faster rate of tensile stress development and may reduce relaxation by creep if stiffness develops too fast. This can lead to earlier and more microcracking, which can affect adversely the flexural strength of concrete.

- For "Free" shrinkage specimens, just as the flexural strength, the damage of E_{fmax} in low w/c ratio (0.3) mix was higher (reduction of 9%) than in high w/c ratios mixes (0.4 and 0.5) (reduction of 3-5%) due to the effect of surface microcracking.

- For restrained specimens, the reduction in E_{fmax} for w/c ratios 0.3 and 0.4 was up to 16% whilst mix 0.5 suffered the highest reduction up to 29%. This is despite the fact that this mix (w/c= 0.5) had little or no flexural strength loss.

- Overall, macro and micro cracks affected the E_{fmax} more adversely in restrained specimens. These results point towards creep as a mechanism of relaxation that

stretches the material, creating many microcracks reducing the elastic modulus. The higher this relaxation the larger it takes for the through crack to develop (as was the case for w/c 0.5).

- There is a clear correlation between increasing width of cracks in the critical region and elastic modulus loss.

7.1.5 Restrained Shrinkage Behaviour of Mixes with ISF, RTSF and RA.

- Industrial steel fibre at 2% dose used for slabs on grade applications did not greatly influence the free shrinkage of concrete. However, RTSF increased initial shrinkage strains due to higher air content and lower internal restraint. Another explanation for the behaviour of RTSF is that, at the micro-level, short fibres (due to their large number per volume) help in reducing micro damage (drying microcracks). As a result, more intact material per unit volume is expected and higher shrinkage is developed on the macro-level.

- In comparison to NAC, RA from CDW lead to: a reduction in the compressive strength by 27% and the flexural modulus of elasticity by around 23% and an increase in shrinkage by 31% (at 1 day) and 35% (at 28 days).

- Despite the fact that the mechanical properties of RAC and NAC were not similar, under restrained conditions, both types of mixes cracked (failed) at around the same time. This can be due to two opposing mechanisms: 1) higher shrinkage strains (of RAC), which can lead to earlier failure. 2) lower stiffness (around 23% in flexural) and expected higher creep which can delay the cracking of RAC by relaxation mechanisms.

- Under restrained conditions, the compressive strength of concrete mixes only reduced by 3% in comparison to unrestrained condition. In unreinforced NAC, the elastic modulus decreased by up to 16%. However, for RTSF reinforced specimens the flexural elastic modulus did not decrease.

- The addition of RTSF and surface treatment of RA resulted in higher (10-14%) flexural performance (fl_{LOP} and fl_{ult}) of RAC in all conditions (WC, F and R).

- The flexural strength of all specimens was not affected much by the different exposure conditions. Nonetheless, the restrained specimens of the mixes with RTSF appear to have a slightly higher flexural strength than without fibres and without restrain.

- In spite of the increase in the air content of concrete, RTSF help control shrinkage induced microcracks propagation better than IF. This can be due to the role of short fibres in enhancing the tensile creep behaviour of concrete by: 1) providing more uniform distribution of internal stresses and engaging a larger volume of the matrix in stress transfer; 2) reducing the micro-damage, and 3) promoting self healing of microcracks. Hence, they are ideal for enhancing the flexural properties of RAC to the level achieved by NAC.

7.2 Recommendations for Future Work

In this section, recommendations for future work are presented. These recommendations are important to improve the understanding of some RAC behavioral issues that due to time restrictions, were not dealt with in this work.

7.2.1 On Improving RAC Properties

1. The effect of surface treatment of RA on the durability of RAC should be further studied to assess the long-term performance of RAC. This can be undertaken through evaluating the transportation mechanisms (such as permeability, diffusivity and sorptivity), pore-structure related properties (porosity) and other properties (freeze and thaw, carbonation and sulphate attack).

2. More contents of SF (4%, 6% and 8%) for RA treatment should be considered to determine the optimum content that provides the best structural and durability performance for RAC.

3. Other types of reactive microfillers (such as Metakaolin) to treat the RA should be examined to find out the other options of high reactivity microfillers that can be used to improve the RAC behaviour.

4. The effect of surface treatment of RA with a small quantity (2% by mass of cement) of SF on the performance of RAC containing 100% recycled concrete aggregate (RCA) should be studied.

5. The microstructure of the ITZs of RAC incorporated treated RA should be quantitatively assessed (using large number of specimens) to obtain a firm conclusion on the improved ITZs of RAC. This can be conducted using techniques such as SEM and image analysis techniques to quantify the porosity of the ITZs of RAC with and without treated RA.

7.2.1 On Restrained Shrinkage

1. The effect of shrinkage induced cracks (due to external restraint) on the durability behaviour of NAC and RAC should be considered to evaluate the effect of these cracks on the long term performance of concrete. This can be achieved by assessing transportation related properties (such as permeability, diffusivity and sorptivity), pore-structure related properties (porosity) and other properties (freeze and thaw, carbonation, corrosion and sulphate attack).

2. The effect of curing (in particular at early ages) on the performance of concrete under restrained (cracking time and post-shrinkage mechanical properties) conditions should be examined.

3. When dealing with restrained shrinkage, studying the effect of autogenous, thermal and drying shrinkage separately on the cracking behaviour of NAC and RAC (with and without fibres) should be considered. This will help to improve understanding the driving mechanisms of concrete cracking, in particular at early ages. For example, sealing the restrained specimens (utilizing self adhesive aluminium foil) can be used to quantify the autogenous shrinkage of concrete under restrained conditions.

4. The technique used to recover strain loss should be improved. A step-wise method to release the applied prestress (on the restraining frame) would help in the better control of the amount of restraint (RF) provided and reduce the effects of sudden release of the applied prestress.

5. The degree of restraint achieved by the developed rigs is still relatively low and stiffer arrangements need to be developed to achieve nearly 100% restraint. This could be achieved by a better control of the overall strain loss.

6. Creep is clearly coupled with shrinkage in the developed set up and it is necessary to assess creep deformations using separate measurements techniques or active control rigs.

7. Taking individual manual measurements of cracks and crack development is extremely time consuming and, hence, optical measurements could be used to reduce effort. This also help to link the effect of cracks and crack development on the strength and stiffness loss.

8. For the restraining frame, the gripping efficiency of the ends (where the concrete is enlarged) should be improved to decrease strain losses at these ends. This can be achieved by using steel plates as the sides of these ends. The sides should have teeth to help the four threaded bars in gripping the ends of the restrained specimen. Easy demoulding with minimal damage to the concrete at the end of the exposure time should be ensured.

9. The utilization of high resolution cameras and image analysis techniques should be considered to measure shrinkage strains, assess surface microcracking and determine cracking time. The use of images will help in initiating shrinkage measurements in a matter of few hours after casting.

10. The effect of the use of short RTSF on the creep behaviour of NAC and RAC should be quantified. Based on the results of this study, RTSF showed good cracking resistance and post-shrinkage mechanical performance, which are attributed to the role of these fibres in enhancing creep/relaxation behaviour of concrete reinforced with such fibres. The study should consider both compression and tensile creep in both condition, sealed (basic creep) and unsealed (drying creep).

Appendices

Appendix A Shrinkage of Concrete

Appendix B Restrained Shrinkage (Effects, Types of Restraints and Assessment)

Appendix C Experimental Results - Chapter 2

Appendix D Experimental Results - Chapter 3

Appendix E Experimental Results - Chapter 4

Appendix F Experimental Results - Chapter 5

Appendix G Experimental Results - Chapter 6

Appendix A:

A. Shrinkage of Concrete

A.1 General

Concrete shrinkage leads to a reduction in the volume of concrete. Concrete shrinks in response to moisture loss, temperature reduction and chemical reactions (hydration). Concrete may experience shrinkage at different times, early ages (hours after casting) and long term (many years) and under a variety of conditions. Generally, there are several types of concrete shrinkage: thermal, plastic, autogenous, drying and carbonation shrinkage. To various degree, they can contribute to cracking in structural concrete elements [1-3]. This appendix reviews types of shrinkage and their main driving mechanisms.

A.1.1 Thermal Shrinkage

Internal and external reductions in temperature result in thermal shrinkage in concrete. Thermal shrinkage of concrete results from temperature decrease at both very early ages (hours after casting) and later ages. The latter includes the impacts of daily base and seasonal base temperature variations, whilst the former is the response of concrete material to the heat produced by the hydration process of cement. This process is accompanied by a heat generation in large quantities, especially in massive concrete structures. In such structures, the dissipation of this heat is relatively slow [4].

Following the placing of the concrete, almost all types of concrete display an expansion induced by the heat generated from cement hydration. After that, the concrete cools and the temperature falls down from a peak value to the ambient temperature. This cooling process force the concrete to shrink [4, 5]. Concrete's temperature reaches a peak value in the first hours after placing and its magnitude depends on the initial temperature and the temperature rise caused by hydration process. The peak value equals to the sum of both initial temperature and temperature rise. The greater the initial temperature and the heat rise, the higher the subsequent decline from peak temperature cooling down to ambient temperature [4, 6]. The amount of thermal shrinkage influenced by many factors such as placement temperature, temperature of fresh concrete and composition of concrete (type of cement and aggregate, mineral admixtures [4]. The parameter that plays a key role in converting the temperature change into strain in concrete is the thermal dilation (expansion) coefficient. It

is generally agreed that this coefficient is a function of the moisture state of the pore system [4, 7] with very low values around 10-12 microstrain/^{o}C for fully saturated pore system and empty (dried) pore system and high values for partly saturated pore system with an ultimate values in the range of 18-25 microstarin/^{o}C. According to Powers and Brownyard [8] (cited in [4]), the high values for the semi saturated pore system is due to redistribution of the pore water and changes in capillary pressure exerted on the solid skeleton of cement paste.

It is reported by Hedlund [9] (cited in [4]) that in the early ages, thermal expansion coefficient changes very rapidly with the strength development of the concrete (see Figure A.1). As can be seen the thermal coefficient reaches almost a constant values of approximately 12 microstrain /^{o}C after 24h.

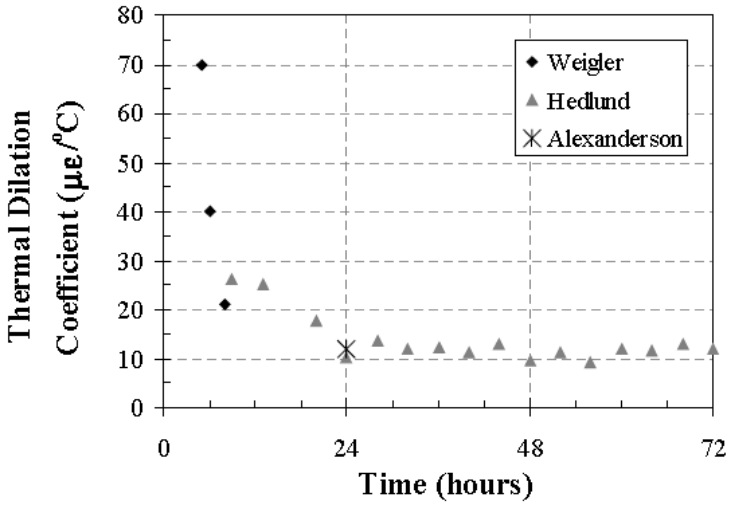

Figure A. 1 Early age thermal dilation coefficient for concrete [9] (cited in Holt [10])

A.1.2 Plastic shrinkage

Plastic shrinkage can be defined as the loss of water from wet concrete to the surrounding environment. The name implies that this type of shrinkage occurs in concrete at very early ages (hours after the concrete is placed) and before it gains any significant strength. It is more common in thin concrete element such as slab and concrete pavements [1]. It happens when the rate of water loss by the evaporation process is greater than the rate at which water from the bleed of concrete is supplied to the surface [1, 11]. The main mechanism of developing plastic shrinkage in fresh concrete is the formation of negative capillary pressure in the concrete. If the water, which surrounds the concrete particles in plastic condition, removed, menisci are formed between these particles. Negative capillary pressure develops as a result of these menisci. A reduction in the volume of the cement paste occurs due to the

capillary pressure which pulls on the cement particles. If the loss of water from the concrete surface continues, the pressure continues to rise and more decrease in the volume of concrete occurs and at a critical value of the capillary pressure the remaining water in the matrix rearranges to form distributed zones with empty pores in between. Plastic shrinkage cracks develops at this point [11, 12].

A.1.3 Autogenous Shrinkage

Autogenous Shrinkage takes place at an early age as a results of the loss of volume (due to consuming water inside the concrete by cement hydration process) under sealed (without moisture loss to the surrounding environment) and isothermal conditions [4, 7]. Chemical shrinkage is considered as the underlying driving mechanism of the development of autogenuos shrinkage [4]. Chemical shrinkage is ‘’ the phenomena in which the absolute volume of hydration products is less than the total volume of unhydrated cement and water before hydration’’ [13] that is volume of the reaction products is smaller than that of reactants due to the densification of the solid phases during the hydration process.

Chemical shrinkage is the dominant factor in autogenous shrinkage during the time prior to setting and self-desiccation becomes dominant after setting [4, 14]. Autogenous and chemical shrinkage are equal as long as the paste is in a liquid state. However, when the time of setting is reached and the hydrated cement has gained certain rigidity, the measured autogenous shrinkage becomes much lesser than the chemical shrinkage. This happens because a solid skeleton begins to form around this time allowing empty pores to form and constraining the extension of the contraction developed by chemical shrinkage. Self-desiccation results from the consumption of the internal water due to the hydration of the cement. The autogenous shrinkage induced by self- desiccation depends on the w/c ratio and it increases with the decrease of w/c. The lack of the external water supply (curing) will lead to self-desiccation and a set of unfilled pores will be generated in the microstructure of cement paste. Consequently, capillary depression will be produced resulting in a measurable physical shrinkage of concrete [4].

As far as the cracking of cement is concerned, it is also believed that the period around this time (setting time) is very crucial and sensitive. Since cement paste or concrete has strength but with low capacity to withstand stresses [15].

The first time when autogenous shrinkage recognized was in 1934 by C.G.Lyman (cited in [16]). At that time however no further research in this field was undertaken [16] as it has not been deemed of major important in normal strength concrete and even, decades after that, a clear distinguish from drying shrinkage (see next section), except possibly for mass concrete, has not established [7]. Nevertheless, the introduction of high strength and high performance concrete which are produced with a very low w/cm ratio, has brought the phenomenon of autogenous shrinkage to the attention of the researchers and become a 'hot topic' [4, 17]

Generally, the typical strain caused by autogenous shrinkage for normal strength concrete is about 20-110 με [2] which is considered small when compared to other type of concrete deformations. On the other hand, a strain of up to 200- 400 με may occur in concrete with low w/c or w/b ratios [18]. Furthermore, it has been reported that the autogenous shrinkage becomes as much as drying shrinkage for low w/c concretes. For example the autogenous shrinkage can reach a value of 40%, 50% and 100% of the total drying shrinkage of concrete with w/c of 0.4, 0.3 and 0.17, respectively [19] (cited in [7]). The development of autogenous shrinkage starts from the very early ages and this potentially increase the risk of cracking [4, 13, 15].

Sometimes external supply of water (curing) is not helpful to mitigate the deformations caused by autogenous shrinkage, in particular when the w/c ratio is very low. This happens due to the fine pore structure of the low w/c concrete, the composition of concrete and the inherent discontinuity of the pore structure of concrete which all reduce the ability of water to penetrate into the concrete in short time [16].

The aforementioned discussion, explains how the phenomena of autogenous shrinkage is complex and it is one of the significant mechanisms for restrained concrete to crack at early age.

A.1.4 Drying Shrinkage

Drying shrinkage of concrete is a time dependent deformation and defined as a change (decrease) in the volume of concrete caused by the migration of the moisture from the concrete's surface to the atmosphere in an environment of low RH and constant temperature. To ensure the workability of concrete at placement time, the quantity of water added to the concrete mix is higher than what exactly the cement needs for the hydration process [20].

Part of this water has no contribution in producing hydration products. Consequently, it will not take part in the chemical reaction between cement and water; hence there is no chemical bond between this water and the solid phase of cement. Therefore, after the completion of curing process, if concrete is exposed to drying conditions, a moisture gradient occurs which cause the moisture to migrate out of the concrete accompanied by a volume reduction [21]. This moisture (water) is exist in the capillary (large) pores and gel (small) pores. The loss of moisture from the former causes insignificant shrinkage deformations, whilst moisture loss from the latter results in considerable shrinkage [18, 22].

The process of moisture movement is a slow process and it depends on the range of RH and the composition of concrete as well as on the degree of hydration at the starting time of drying exposure. Therefore, it takes place over many years to the shrinkage of concrete to reach the ultimate values (long term drying shrinkage). However, significant part of the final value of shrinkage occurs at the first weeks after being exposed to drying and the rate of shrinkage diminishes rapidly with time [17, 18].

The drying shrinkage of concrete has been studied extensively and its main characteristics in terms of mechanisms and affecting factors it has been reported and summarized in several research papers and text books, for example : Bazant and Wittmann [23], Mindess and Younig [24] and Neville [18].

There are several mechanisms behind the shrinkage of concrete, in particular drying shrinkage. The most prominent mechanisms, which have been reported in the literature are explained in next sections.

A.1.4.1 Driving Mechanisms of Drying Shrinkage

The most four known mechanisms of drying shrinkage in concrete that proposed in the literature are: capillary pressure, variations in surface tension, movement of interlayer water and disjoining pressure. These mechanism are all associated with the movement and loss of water from concrete during drying [17, 25]. These mechanisms are complex and interrelated, primarily due to the extended range of the distribution of the microstructure (pore size) of normal concrete mixtures, which determine the various transport mechanisms during drying. The evolution of pore system continues with time as results of hydration and maturity. The transportation of moisture through the pores solids comprises water in a liquid state as well as water vapour. The transportation of moisture may happen in different ways. Permeation

induced by a pressure head, diffusion caused by a concentration gradient, capillary suction resulted from surface tension acting in the capillaries and others are the main mechanisms of moisture transportation and may occur simultaneously within the concrete (particularly in different areas of the cement paste as aggregates usually deemed to be impervious, apart from light weight aggregate and RA) under drying conditions [17, 21].

A detailed explanation of these mechanisms is discussed and summarized by Wittmann [23] and by Kovler and Zhutovsky [17]. A brief of these mechanisms is explained below.

Capillary pressure

Capillary pressure is probably the most well known phenomenon in drying porous media. In brief, under drying, a meniscus is formed in the capillaries of the hardened cement microstructure (capillary pores), resulting in tensile stresses in the capillary water (due to surface tension forces). These tensile stresses are balanced by compressive ones in the surrounding solid, causing shrinkage strains. This mechanism is belived to act in the high RH range (until approximately 50% RH , since it fails to explain shrinkage deformations at low RH [17, 21].

Surface tension

The mechanism of surface tension deals with the attractive forces of atoms or molecules at the surface. This mechanism works at relatively low RH (less than 40%). Above that limit of relative humidity, the whole surface is covered by adsorbed water molecules, thus, the variation in RH can no longer vary the surface tension [17].

Movement of interlayer water

This mechanism is related to the layered-structure of the CSH within the cement gel [23, 26]. In general, it is agreed that interlayer water may diffuse out of the CSH sheets when RH drops to about 10%, resulting in reducing the distance between these layers and causing macroscopic shrinkage strains. Loss of a small amount of interlayer water results in considerable volume reductions [17, 25, 26].

Disjoining pressure

The mechanism of disjoining pressure concerns the interaction between two solid surfaces. As the thickness of the adsorbed water molecule layer increases, disjoining pressure can no longer develop freely. As the relative humidity increases, the adsorption of water tends to

separate the two solid surfaces. Thus, the two surfaces undergo a pressure called “disjoining pressure.” The maximum disjoining pressure occurs at the saturated state. When the system goes from a saturated to unsaturated state, shrinkage occurs because of decreased disjoining pressure [25].

References

1. Concrete Society TR 22 *Non – Structural Cracks in Concrete*. 2010, Concrete Society. : Surrey, UK.
2. Gribniak, V., G. Kaklauskas, and D. Bacinskas, *Shrinkage in Reinforced Concrete Structures: A Computational Aspect.* Journal of Civil Engineering and Management, 2008. **14**(1): p. 49-60.
3. Qiao, P., McLean, D. and Zhuang, J.,, *Mitigation Strategies for Early-Age Shrinkage Cracking in Bridge decks*. 2010, Department of Civil and Environmental Engineering , Washington State University: Pullman, Washington. .
4. ACI 231R-10, *Report on Early-Age Cracking: Causes, Measurement, and Mitigation*, in *ACI Committee 231*. 2010, American Concrete Institute: Farmington Hills, U.S.A.
5. ACI 207.2R, *Report on Thermal and Volume Change Effects on Cracking of Mass Concrete*, A.C. 207, Editor. 2002, American Concrete Institute: Farmington Hills, U.S.A.
6. Hughes, B.P., *A new look at rigid concrete pavement design.* Proceedings of the Institution of Civil Engineers-Transport, 2003. **156**(1): p. 29-36.
7. Altoubat, S.A. and D.A. Lange. *Early age shrinkage and creep of fiber reinforced concrete for airfield pavement*. in *Aircraft/Pavement Technology In the Midst of Change*. 1997.
8. Powers, T. and T. Brownyard, *Studies of the physical properties of hardened Portland cement paste.* Bulletin, 1947. **22**.
9. Hedlund, H., *Stresses in high performance concrete due to temperature and moisture variations at early ages.* 1996.
10. Holt, E.E., *Early age autogenous shrinkage of concrete*. Vol. 446. 2001: Technical Research Centre of Finland.
11. Naaman, A.E., T. Wongtanakitcharoen, and G. Hauser, *Influence of different fibers on plastic shrinkage cracking of concrete.* Aci Materials Journal, 2005. **102**(1).
12. Brown, M.D., Sellers, G., Folliard, K.J., and Fowler, D.W. „ *Restrained Shrinkage Cracking of Concrete Bridge Decks: State-of-the-Art Review*. 2001, Center for Transportation Research, The University of Texas at Austin: Texas.
13. JCI, *Committee Report: Technical Committee on Autogenous Shrinkage of Concrete* in *AUTOSHRINK'98, Worshop on Autogenous Shrinkage of Cocncrete*, E. Tazawa, Editor. 1998, Japan Concrete Institute Japan. p. 5-66.
14. Lamond, J.F. and J.H. Pielert, *Significance of tests and properties of concrete and concrete making materials*. Vol. 169. 2006: Astm International.
15. Altoubat, S.A. and D.A. Lange, *Creep, shrinkage, and cracking of restrained concrete at early age.* ACI Materials Journal/ SP, 2001. **98**(4): p. 323-331.
16. Lam, H., *Effects of internal curing methods on restrained shrinkage and permeability*. 2005, University of Toronto.
17. Kovler, K. and S. Zhutovsky, *Overview and future trends of shrinkage research.* Materials and Structures, 2006. **39**(9): p. 827-847.
18. Neville, A.M., *Properties of concrete*. 1995, Harlow: Longman Group.

19. Tazawa, E. and S. Miyazawa, *Influence of constituents and composition on autogenous shrinkage of cementitious materials.* Magazine of Concrete Research, 1996. **48**(5): p. 15-22.

20. Mehta, P.K. and P.J.M. Monteiro, *Concrete: Microstructure, Properties, and Materials*. 2006, New York: McGraw-Hill.

21. Idiart, A.E., *Coupled analysis of degradation processes in concrete specimens at the meso-level*, in *GEOTECHNICAL ENGINEERING AND GEOSCIENCES*. 2009, Polytechnic University of Catalunya: BARCELONA.

22. Powers, T.C., *Structure and physical properties of hardened Portland cement paste.* Journal of the American Ceramic Society, 1958. **41**(1): p. 1-6.

23. Wittmann F.H., *Creep and Shrinkage Mechanisms*, in *Creep and Shrinkage in Concrete Structures*, Z.P. Bažant and Wittmann F.H., Editors. 1982, John Wiley &Sons: Chichester. p. 129-161.

24. Mindess, S. and J.F. Young, *Concrete, Prentice Hall.* Englewood Cliffs, NJ, 1981: p. 481.

25. Mokarem, D.W., *Development of concrete shrinkage performance specifications*. 2002, Virginia Polytechnic Institute and State University.

26. Bazant, Z.P. and R. L'Hermite, *Mathematical modeling of creep and shrinkage of concrete*. 1988: Wiley New York.

Appendix B:

Restrained Shrinkage (Effects, Types of Restraint and Assessment)

B. General

Deformations caused by shrinkage concrete can only lead to stresses and cracking if they are restrained. Nonetheless, in real life, all concrete elements are practically restrained to some degree, since some restraint always exists and can be provided by supporting elements or from the different parts of the element itself. Degree of restraint is one of the factors that determines the magnitude and distribution of developed tensile stresses and cracking. [1, 2]. Experimental procedures and tests for restrained shrinkage are vital to quantify the restrained shrinkage behaviour of concrete.

In the next sections, the effect of the shrinkage induced cracks on the behaviour of concrete is explained, the types of restraint are described and the available tests and experimental procedures for restrained shrinkage are reviewed and discussed.

B.1 Restrained Shrinkage: Effects and Involved Factors

Shrinkage of concrete causes deformations (strains and curvatures) of all concrete structures. Shrinkage associated deformations can be detrimental to the performance of concrete since concrete is usually restrained. Restrained shrinkage induces tensile stresses which can lead to concrete cracking if theses stresses exceed the tensile strength of concrete. Shrinkage induced cracking is a main concern and challenge in constructing structures with large exposed surface area such as pavements and slabs on grade [2]. Cracks induced by restrained shrinkage of concrete usually compromises its structural integrity. Not only the structural integrity of concrete structures is affected by shrinkage induced cracks, but also its durability, serviceability and maintenance cost. Shrinkage cracks in concrete can considerably affect properties such as permeability, diffusivity, sorptivity and porosity. This significantly enhances the ingress of detrimental substances through these cracks into the concrete. As a result, the effects of freeze-thaw damage, spalling caused by sulphate attack and chloride penetration as well as corrosion of steel reinforcement will potentially increase. Furthermore, reduced stiffness or strength loss and excessive deflection are other impacts of shrinkage cracking [2, 3]. All these deteriorations and structural deficiencies may happen

prior to the application of external loads. Undoubtedly, applying loads on a precracked concrete element can accelerate the cracking process and all associated deficiencies.

The mechanism of the development of shrinkage cracking (due to external restraint) is complicated and depends on several factors. On one side, there are: the extent of shrinkage and its rate of development, the amount of restraint imposed on the concrete, the mechanical properties (tensile strength and elastic modulus) of the concrete at the time when the tensile stresses are developed. On the other side, there is the tensile creep which counteracts the shrinkage effect by acting as a stress relaxation mechanism [2, 4]. Understanding the role of each of these factors in the development of shrinkage induced stresses and the associated cracks is very important in the assessment of cracking tendency and the effects of the cracks on the behaviour of concrete. More importantly, is the need for understanding the effect of the interaction of these factors on the cracking development.

B.2 Restraint Types and Restraint Factor

In general, there are two types of restraints: external and internal. The former can restrain concrete shrinkage on a large " macrscopic" scale and the latter on much smaller scale "meso and micro". External restraints includes: surrounding (supporting) elements (e.g. walls and columns) and (in the case of concrete pavements or slabs on grade) applied loads and base friction [1, 3].

Internal restraint sources comprise of aggregates and reinforcement. Due to their higher modulus of elasticity, reinforcement (steel bars) and aggregates (apart from light weight aggregate) can restrain shrinking concrete. Internal restraint can also be caused by non-uniform drying shrinkage (also called "self-restraint"), which is usually caused by either moisture or temperature gradients [5].

Restraint factor (RF) or restrained degree is usually used as an indication to the extent of restraint applied to the concrete. According to Bentur [6], the RF can be defined as the ratio of the stiffness of the restraining member and the shrinking element and when the two are equal the degree of restraint is 50%, in this case the shrinkage of restrained element is 50% of that of its free shrinkage [6]. According to ACI 207.2R-95 [3] the RF is given as the ratio of actual stress induced by the restrained volume change to the stress which would develop if the specimen was fully restrained. In other words, it is a ratio between the amount of strain that is restrained to the free shrinkage strain [2, 7, 8].

B.3 Assessment of Restrained Shrinkage

Shrinkage of concrete is usually assessed/quantified in two conditions free and restrained. Generally, the free shrinkage is expressed in axial strains (the change in length-longitudinal direction- divided by the original length). There are many of the standard tests that deal with free shrinkage such as BS ISO 1920-8 [9]. The free shrinkage tests consist of casting a concrete beam and measuring the displacement on its ends as a direct relation to the time elapsed after stripping the moulds.

Free shrinkage tests can provide information on the shrinkage behaviour of different concrete mixtures. The effect of different factors such as concrete composition, environment and storing conditions, and size and shape of concrete element can be assessed using these tests. However, such tests cannot provide information on the post-cracking behaviour of concrete under restrained conditions [10-14]. Restrained shrinkage tests help in the assessment of cracking tendencies and the ability of concrete to withstand shrinkage induced tensile stresses [2, 4, 14-16].

Over the last century, numerous test methods have been utilized to assess the behaviour of mortar and concrete when they are restrained from free shrinkage [2, 17]. There is no standardized test to assess the shrinkage behaviour of concrete under restrained conditions [10-12, 14, 18]. However, both the American Association of State Highway and Transportation Officials (AASHTO in 2008) and the American Society for Testing and Materials (ASTM in 2004) adopted the ring test (see Figure B.1) as a standard test for restrained drying shrinkage. The ring test was used as early as 1942 [19] (cited in [2]). The ring test and some other tests used for restrained concrete is described in the following sub-sections.

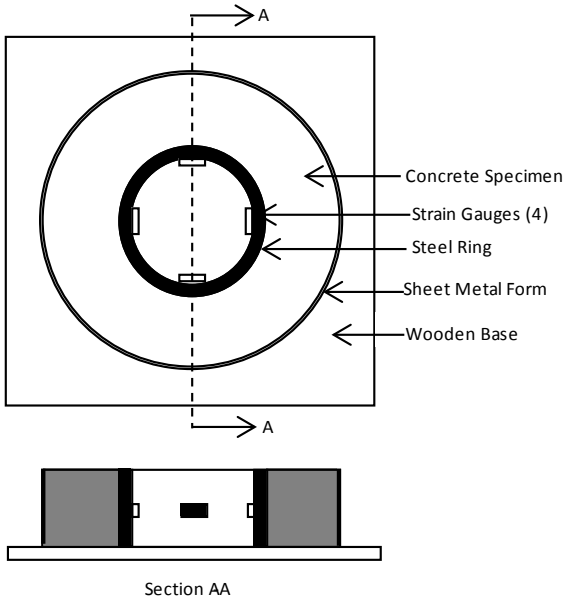

Figure B. 1 Schematic illustration of ring test.

B.3.1 Ring Test

In this test, a concrete annuls (ring) with a specific outer and inner radius is simply cast around the perimeter of an internal steel ring. For a certain period of time the concrete is cured and then exposed to drying conditions (constant temperature around 20 ^{o}C and RH around 50%). The loss of moisture from concrete is allowed either through the circumferential face or through the top and bottom faces. When the concrete ring shrinks circumferential tensile stresses develop, due to restraints provided by the inner steel ring against the free movement of the concrete. The stress distribution depends to some extent on the type (direction) of drying as can be seen in Figure B.2. In the standards mentioned in previous section, it is specified that the top and bottom faces should be sealed, thus allowing drying only through the circumferential face. This results in a maximum tensile stress at the circumference while drying through the top and bottom of the ring leads to a high stress at the internal face as shown in Figure B.2.

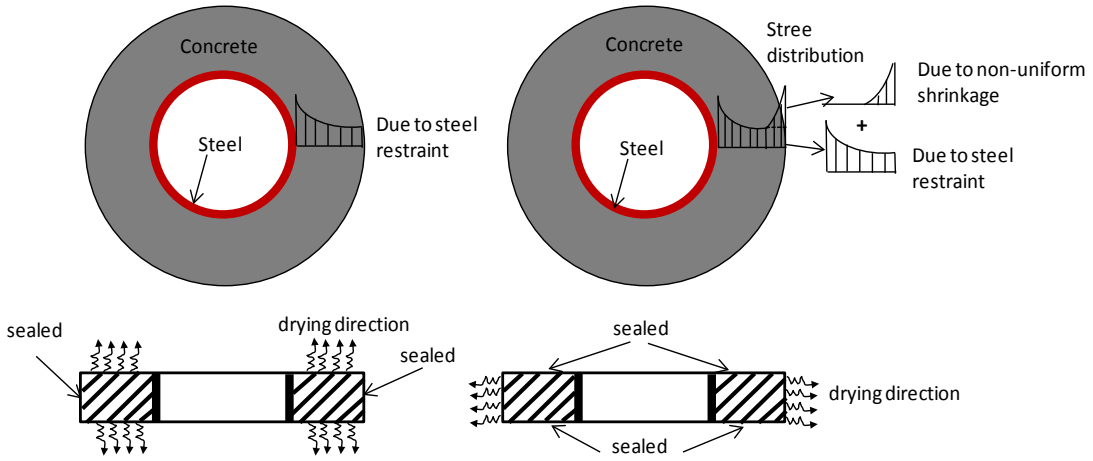

Figure B. 2 Schematic description of the restraint stresses developed in ring test (Weiss *et al* [20]).

Generally, the stress development inside the concrete is usually quantified using strain gauges. Four or two strain gauges are placed on the inner surface of the steel ring and used to determine strain of concrete. The average strain is used to calculate the tensile stress developed inside the concrete. The average developed stress in the concrete ring is calculated by assuming a linear stress distribution throughout the steel ring. The concept of equilibrium is then used, equalizing the compressive force in the steel ring to the tensile force in the concrete ring. This enables the determination of the average tensile stress in the concrete ring [2].

In the ring test, the time that it requires concrete rings made of different mixtures to crack are measured. In addition to the cracking time, the development of the crack width is also monitored and recorded. The free shrinkage strains of the concrete mixtures is also measured using prismatic specimens. Therefore, for a given drying environment, the ring test can provide information on the age at cracking, the width and rate of crack width increase and number of cracks. This information can be used to compare the cracking sensitivity of different concrete mixtures or to assess the efficiency of materials such as fibres in controlling crack width [2, 13, 17, 21]

B.3.1.1 AASHTO Ring Test

In AASHTO ring test [22] , the standard steel ring has a thickness of 12.7 ± 0.4 mm, an outer diameter of 305 mm, and a height of 152 mm. The outer ring form can be made of 6.4 mm thick cardboard with an inside diameter of 457 mm. On the inner surface of the steel

ring, four strain gauges are placed at equidistant points at midheight. The strains from the four gauges are recorded automatically using data acquisition equipment. The wooden base can be made of 0.6 x 0.6 x 0.016 m plywood sheet. Prewetted burlap covered with plastic sheet can be used as concrete curing. After removing the outer form at an age of 24±1 hr, the specimens are transferred to the controlled room (constant air temperature of 23 ± 2^{o}C and 50 ± 5 % RH). Every 30 minutes, the time and strain from the strain gages are recorded. Also, every 2 or 3 days, visual inspection of cracking is conducted. A failure or cracking of a concrete ring is related to sudden reduction of more than 30 με in strain values in one or more strain gauge(s). After cracking, cracking time and crack length and width on the exterior face are recorded [21].

B.3.1.2 ASTM Ring Test

The ASTM ring test [23] is to some extent different from the AASHTO ring. The steel ring in ASTM standard test has thickness of 13 ± 0.12 mm. The outer diameter of the steel ring is 330 ± 3.3 mm and its height is 152 ± 6 mm. Two strain gages are placed on the inner surface (midhieght) of the steel ring and used to measures strains. Data acquisition system is used to automatically record strains at intervals no greater than 30 minutes. The base form can be made of epoxy-coated plywood or other non-reactive surface. PVC or Steel can be sued for the outer form with 406 ± 3 mm inside diameter and 152 ± 6 mm height. The testing drying condition are 23.0 ± 2.0 ^{o}C and 50 ± 4% RH. A 30 με (or more) sudden decrease in strain in one or both strain gauges indicates cracking of the concrete. After that, cracking time and the length and width of crack are recorded. Unless cracking occurs prior to 28 days,the concrete ring is monitored for at least 28 days after the exposure to drying,

B.3.1.3 Comparison between the AASHTO and ASTM Ring Tests

Generally, both standards follow the same concepts and procedures. However, there are some differences between the two methods. The concrete ring dimensions and the maximum size of aggregates allowed are the main differences. The AASHTO standard concrete ring has a thickness of 76.2 mm, with an inner diameter of 305mm and an outer diameter of 457 mm, whilst the ASTM concrete ring has a thickness of 38.1 mm, with an inner diameter of 330 mm and an outer diameter of 406 mm. In ASTM test, the maximum size of aggregate is less than 12.7 mm, whereas there is no requirement for the maximum aggregate size in the

AASHTO test. Due to its higher thickness, the concrete ring in AASHTO allows assessment of larger aggregate sizes. In addition, the time of drying exposure is not specified in AASHTO, whereas, this time is specified as 28 days in ASTM test.

B.3.1.4 Discussion on the ring test

Simplicity and versatility, are the main features of the ring-test. The test is easy to conduct and does not require the use of complicated instruments and heavy machines. Also, the test can be utilized to assess the effect of different materials (such as : fibres and shrinkage reducing admixtures) and to evaluate the effects of influencing factors on the shrinkage cracking behaviour of concrete [12]. These features have led the test to be the more commonly used test to evaluate the potential for shrinkage cracking of different concrete mixtures over the last decade. The same reasons have led ASTM and AASHTO to adapt the ring test as a standard test for restrained shrinkage of concrete [2]. The test can also be used as a quality-control test.

On the other hand, the test does not simulate and cannot predict concrete cracking in actual service life, and rather reflects the relative cracking tendency of concrete mixtures [12, 13, 21, 24]. Also, the strains used to calculate the elastic stresses are not measured directly from the concrete; instead they are measured on the outer face of the steel ring (see Figure B.1), assuming a linear stress distribution throughout the thickness of the steel ring [2]. In addition, the restrained shrinkage strain obtained from the ring test cannot be compared directly with the free shrinkage strain of prismatic specimens [25]. Furthermore, the test cannot quantify the residual strength of cracked concrete. For these reasons, the test can be considered as a qualitative tool to assess the cracking tendency of different concrete mixtures. Researchers have tried to develop other tests in order to find a quantitative tool to assess concrete behaviour under restrained conditions. The next section deals with such tests.

B.3.2 Linear (Longitudinal) and Plate tests

Several other test methods for restrained shrinkage have been proposed. These tests can be classified into two categories: panel (Plate) tests in which the restrain is provided at the circumference of the panel (biaxial restraint) and longitudinal tests which provide unaxial restraint. According to the mode of restrain, the longitudinal tests can be further classified

into: fixed grips, external rigid frame or internal reinforcing bar, or by an active mechanism which facilitates applying a load on one of the grips (the other one is fixed) to prevent shrinkage of the concrete specimen [17, 26]. These methods and the way the data is obtained and results are interpreted are discussed in the following sub-sections.

B.3.2.1 Plate test

The general shape of the plate test is shown in Figure B.3. With the intention of assessing the effect of adding low volume content of polymer fibres on the plastic shrinkage behaviour, the plate test have been used by several studies [27, 28] (cited in [17]). The test includes casting a concrete specimen in a square mould with dimensions of about 1m × 1m, or somewhat smaller. The restrain is provided along the perimeter of the mould using steel bars. The surface of the slab is exposed to drying by blowing air (using a fan) to mimic windy environments. There are different ways used to quantify the extent of concrete cracking such as : maximum crack width, average crack width, total crack length, total crack area (crack width × crack length) and number of cracks per unit area [26].

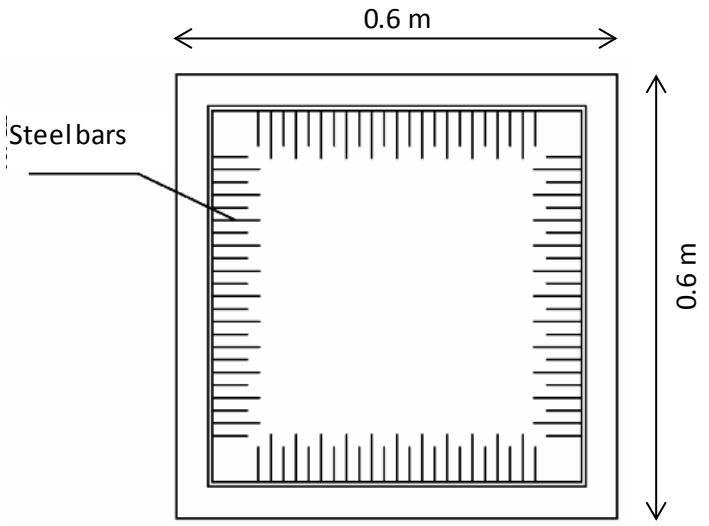

Figure B. 3 Configuration of plate test used by Yokoyama et al [28] (cited in [17]).

B.3.2.2 Linear (Longitudinal) Tests

Shrinkage restrained tests in this category can be divided into three types [17]:

(a) Longitudinal-qualitative test in which linear geometry is used as a restrain to measure cracking only.

(b) Longitudinal-passive test, the test is passive as the restrain is applied by longitudinal bars on which strain gauges are mounted. The rig in this test is partially instrumented to measure the restraining forces and stresses.

(c) Longitudinal-active test, the test is an active test in nature as one of the grips is continuously adjusted to keep the concrete specimen at zero strains or close to it and the other one is fixed.

(d) Fully active longitudinal test, in this type, a close loop computer controlled system is used to adjust the grip position and hold it at zero strain. Meanwhile, the load and strains in restrained and free companion specimen are continuously recorded.

B.3.2.2.1 Longitudinal (Linear)-qualitative

Aiming at assessing the plastic shrinkage cracking in a pre-notched specimens, Berke and Dallaire (1994) [29] used the rig shown in Figure B.4. The width of the rig is 370mm. A metal strip was placed in the rig just before concrete casting. The function of this metal strip is to produce a notch acting as a stress raiser. Also, riser were placed at the ends of the mould to provide end restrain. The restrained specimen was exposed to drying conditions, which achieved by blowing air, for 24h. To determine the cracking (at the end of the drying exposure time), the specimen surface was divide into a mesh (50×50mm). The length and width of cracks in these squares were traced and recorded. The total crack area (average width × length) of the specimen surface was calculated and used as a measure of the cracking tendency for the investigated mixes [17].

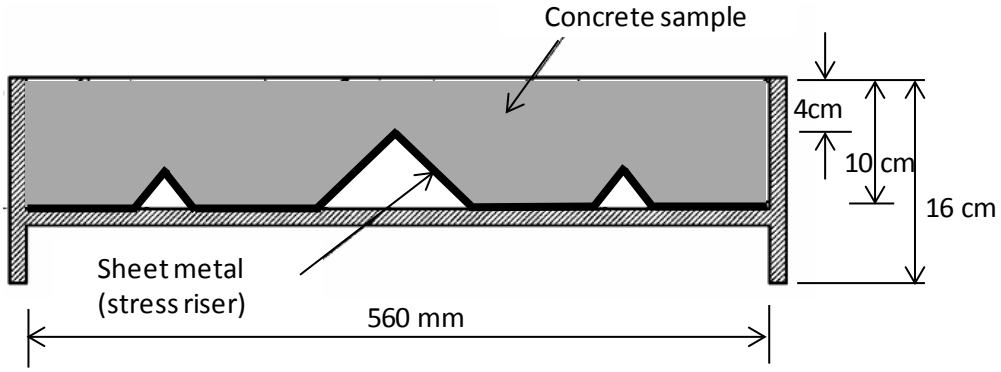

Figure B. 4 Schematic description of the longitudinal restraining rig used by Berke and Dallaire [29].

The restraining rig developed by Banthia *et a.l* [30, 31] is shown in Figure B.5. The restrain is provided using end grips. The rig consists of a 50 mm thick plate base with two vertical posts at the ends. The concrete specimens (40×40×500mm) is cast into a mould with anchors (three bars) at each end. After demoulding, the concrete specimen is mounted on the rig by attaching the anchors rigidly to the vertical posts. The specimen is placed on two frictionless rollers with free movement in the longitudinal direction. The assembly is placed in a chamber with drying conditions of 50^{o}C and 50% RH. A microscope is used to detect cracks. In this test, number, width and length of cracks are recorded. The cracking characteristics of different concrete mixes is measured based on the calculated total crack width and length.

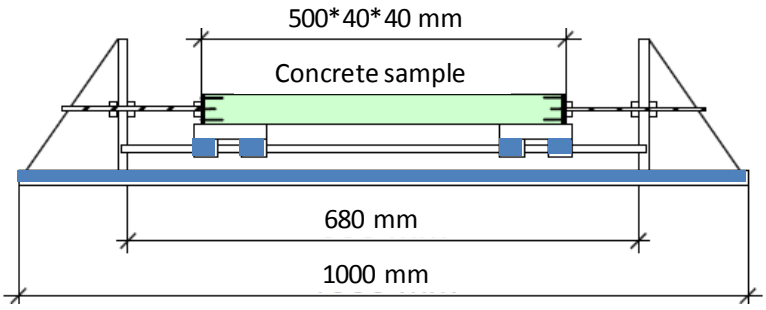

Figure B. 5 Linear rig test with end restraint used by Banthia *et al.* [30].

B.3.2.2.2 Longitudinal (Linear)-Passive

Cracking Frame

To study the effect of thermal stresses on the behaviour of restrained concrete under adiabatic conditions, a linear-passive restraining rig (also called cracking frame) was developed at the University of Munich [17, 32]. It is considered as the first generation of linear stress testing machine [2] and it was adopted by RILEM (Réunion Internationale des Laboratoires d'Essais et de recherche sur les Matériaux et les) as a recommended test method-TC 119 [33] for cracking evaluation, see Figure B.6. The rig consists of two mild-steel crossheads which are connected by two rigid steel linear side bars (100 mm). Fixing the concrete specimen at the ends is important for the rigid linear bars to provide the sufficient restraint. This is achieved by casting the concrete directly into the ends at the crossheads. The ends have "teeth" that hold (grip) the specimens. To provide further gripping and reducing the slippage of the specimen ends, crossbars are bolted on the top and bottom of each crosshead [2, 17, 32].

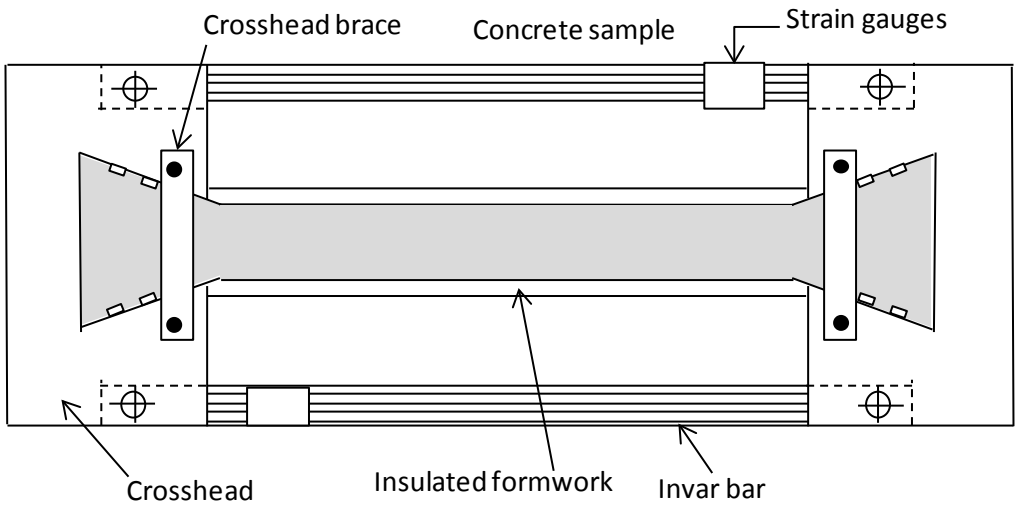

Figure B. 6 Restrained test rig ''Cracking frame'' recommended by RILEM to assess thermal cracking of concrete.

Nickel steel alloy (very low coefficient of thermal expansion $1\times10^{-6}/^{o}C$) is utilized to keep the effect of temperature change on the length change of the linear side bars to minimum level. The linear side bars are instrumented with two strain gauges that can detect very small axial strains caused by the combined effect of the thermal and autoagenous shrinkage [34] (cited in ACI 231.R [2]). The uniaxial stresses developed in the middle part of the concrete specimen is assumed uniform and calculated from the measured strain on the steel bars and the cross section areas of the bars and the concrete specimen. The test can measure restraining stresses in compression and tension. The former develops as the concrete temperature rises (due to hydration) soon after casting and the latter develops on cooling later.

To minimize dissipation of concrete temperature "ensure adiabatic condition", the concrete specimen is insulted by using a formwork made of polystyrene with thickness of 50 mm. Also, there is a 0.2 mm copper plate in between the insulted material and the specimen to ensure uniform thermal change. In addition, the formwork is equipped with a pipe network that enable circulation of water (with different temperature) for more control (adjustment) of thermal conditions. The high insulation system used in the test allows initiation of measurements immediately after concrete casting.

In this thermal test, the concrete specimen can be cooled to the ambient temperature. The concrete specimen is monitored for cracking for four days first. If no cracks develop in the first 4 days, then the system is cooled artificially at a constant rate by decreasing the

temperature (using the circulated water) until cracking occurs. The temperature at which cracking occurs is recorded and called cracking temperature. The cracking temperature is used as an indication to measure the cracking tendency of different concrete mixtures. Higher cracking temperature indicates higher cracking tendency of concrete. Other parameters that can be obtained from the tests are stress development curve, zero stress temperature (temperature at which the developed compressive strength- due to rise in concrete temperature-decreases to zero) corresponding to stress-free condition [26].

Weiss et al (1998) testing rig

A linear passive rig test was introduced by Weiss et al (1998) [14]. The aim of the study was to develop a test method for assessing the shrinkage cracking potential of normal and high strength concrete (with and without fibres) for pavement applications (see Figure B.7). The developed rig consist of a restraining reaction beam (with hollow box section) The longitudinal concrete specimen has a cross-section of 100×25 mm (width × depth) and length of 1m. The mechanism used to grip the concrete ends is achieved using lateral clamping utilizing steel plates and threaded bars at the ends of the specimen to clamp the ends against the reaction beam. In this study, a second rig to simulate base restraint was also developed by same authors . In the second rig, steel strips (6.5×3×100 mm) spacing at 14 mm (centre to centre) were welded on the top surface of the reaction beam. The mechanism used to grip the specimen ends was also used in the second rig. The parameters used to assess the cracking behaviour of different type of concrete (normal and high strength, plain and fibre reinforced concrete) are age of cracking, average crack width, development of crack width and number of cracks (at 50 days).

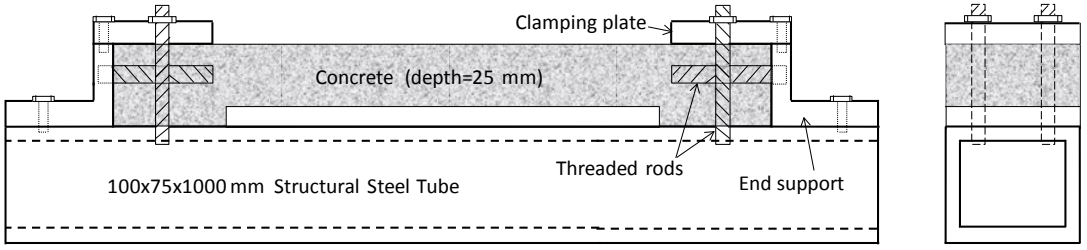

Figure B. 7 Schematic illustration of rig test used by Weiss *et al* [14].

Similar rig configuration to that developed by Weiss et al. [14] was also used by Carlsward, [13] to assess the cracking behaviour of thin overlays exposed to drying shrinkage. under restrained conditions.

Restraining steel bars

Another technique that can be classified as passive method to restrain concrete shrinkage is the use of internal restraining bar(s). The restraint is provided by embedding restraining steel reinforcement bars in the specimen ends (the bar being debonded in the middle part only, see Figure B.8) [4, 35] or with the use of anchor nuts at the end of the specimen. [36]. The cracking behaviour assessed according to the time of cracking, crack width and the increase of crack width with time.

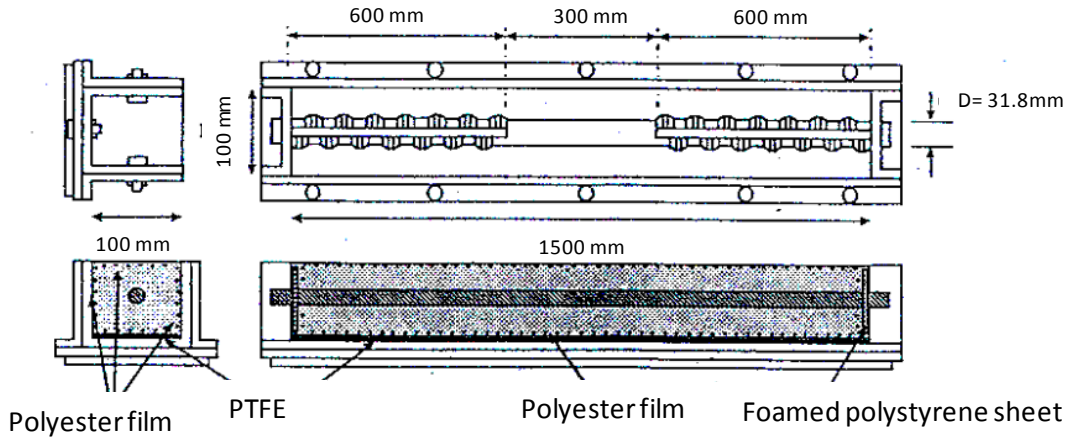

Figure B. 8 Schematic illustration of ring test used by recommended by JCI [35].

B.3.2.2.3 Longitudinal (Linear)-Active

In the passive tests, the extent of stress development in the shrinking element relies on the ratio between the stiffness of the concrete and to that of the restraining element and can provide partial (unknown) restraint. Linear active rigs with no relay on the rigidity of the restraining element were developed aiming at providing high degree of restraint "full restraint". Same configuration of the enlarged ends used in the passive tests was exploited by researchers to develop the active tests [26].

In such rigs, the concrete specimen is gripped at its both ends with one end free to move and the other is fixed. The axial displacement of the movable end is observed using a displacement gauge. The original position of the free end is recovered by applying a tensile load whenever shrinkage deformation occurs. Deformation recovering (applying the load) is achieved manually (using screw) or in an automatic manner (using hydraulic motor). The applied load can be measured using a load cell [17].

According the direction of the specimen alignment, the linear active tests can be divided into vertical and horizontal. The latter facilitates the initiation of the test directly after concrete placement whilst, in the former the tests can be started after one day or later [17].

Horizontal Active Rigs

This configuration of the active rigs was reported by Springenschmid *et al* [33] and Bloom and Bentur [37]. The load used to adjust the length of the specimen is applied in cycles in a way that keeps the deformation between the cycles to very small level (1- 5 micron for 1m long specimen) so as to consider the concrete under "100%" restraint. To assess the thermal stresses and cracking of concrete, Springenschmid *et al* [33] developed their horizontal passive rig (mentioned in preivius section) to an active rig and they called it "Temperature Stress Testing Machine (TSTM)". The TSTM (shown in Figure B.9) was also used to assess the behaviour of concrete under isothermal which included studying the effect of autogenous shrinkage [38] (cited in [17]). This confirmed that TSTM can be used to assess both thermal and atougenous shrinkage under restrained condition and this is very important as in real life stresses induced by thermal (due to hydration) and autogenous shrinkage develop simultaneously. The horizontal rigs was also used by Bloom and Bentur [37] aiming at evaluating concrete cracking induced by autogenous shrinkage for plain and fiber reinforced high strength concrete [17].

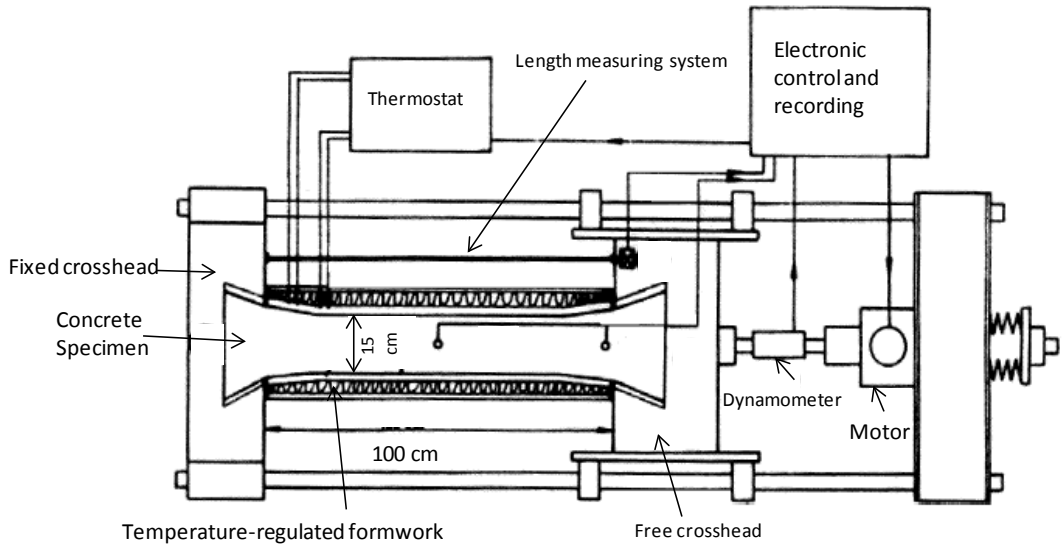

Figure B. 9 Schematic illustration of TSTM test rig (Springenschmid et al. [39] (cited in [2])

Verticall Active Rigs

Similar shape of test rig to that used by the horizontal tests is used by Paillere *et al.* [40] but in this case the concrete specimen tested in vertical position. The lower end of the concrete specimn was fixed and the upper one was movable. The upper end was attached to air pressure equipment. The load required to adjust the change in length of the concrete specimen was recorded with time. The accuracy of measuring change in length was 1 micron.

B.3.2.2.4 Fully automated (closed loop) active test

In 1994, Kovler [16] developed a fully automated test rig. The concept of restraining the concrete specimen in this test is the same as the concept of the horizontal active rigs used by Springenschmid [33] and Bloom and Bentur [37] but instrumented with a closed loop computer controlled system. Such system lead to results with high accuracy. In the test twin specimens were used, one is free to shrink and the other is restrained as shown in Figure B.10.

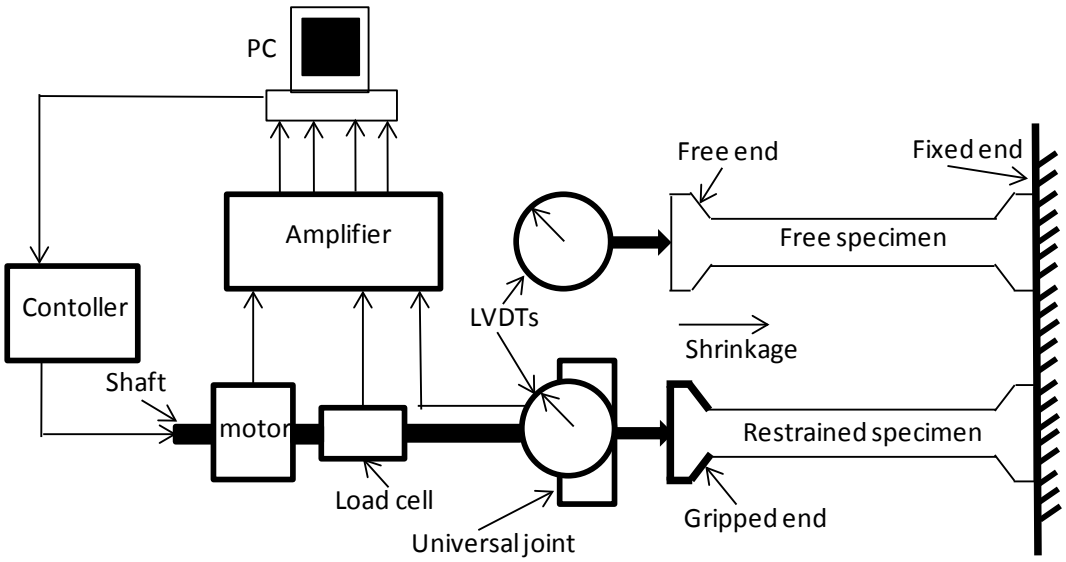

Figure B. 10 Schematic illustration of closed loop of restrained test developed by Kovler [16].

One of the most important feature of this test is the compensation cycle. The compensation cycle is the amount of the load that needed to adjust the movable end every time when a 5 microstrain of shrinkage strain develops in the concrete specimen. Each cycle consists of an

elastic strain (5 microstrain) due the increase in load. The strain between two subsequent applications of load consist of :1- the additional shrinkage strain which is simply the increment of free shrinkage during the cycle (obtained from the free specimen). 2- the creep strain due to the load application as can be seen in Figure B.11. In this type of restrained shrinkage test, a variety of properties can be determined such as:. shrinkage strains and stresses, age of cracking, crack width, rate of stress/strength and development of tensile stress. Additionally, the comparison between two specimens (free and restrained) enable the quantification of creep as relaxation mechanism. Hence, this method has the merit of quantifying creep strain beside determining shrinkage strains and stresses.

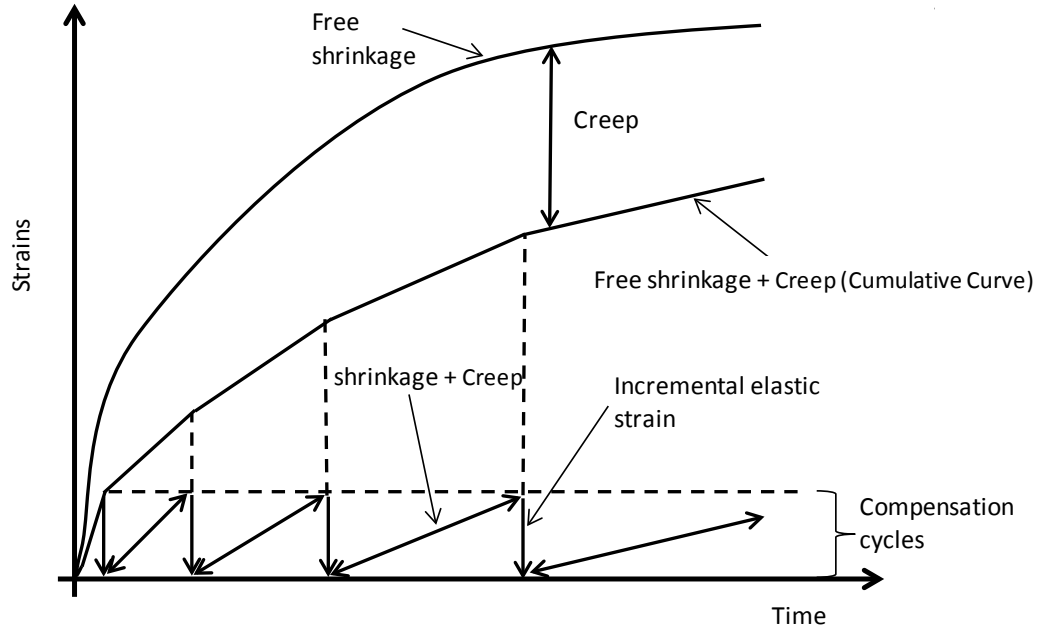

Figure B. 11 Schematic description of the compensation cycles, free shrinkage and creep of concrete in restrained test developed by Kovler [16].

This system motivated other researchers [15, 41, 42] to investigate the behaviour of different type of concretes such as fibre reinforced concrete and high strength concretes and also examine the behaviour of concrete at early ages under restrained conditions.

B.3.2.2.3 Summary and Discussion on Linear Tests

In most of the studies that dealt with these tests, researchers have tried to develop uniaxial restrained shrinkage tests. Therefore, the shape of the specimen is a beam with a square or

rectangular cross section with straight or flared ends. In some of these methods a concrete specimen is cast in a restraining steel frame and connected to the frame by increasing the cross section at both ends in steel crossheads or by utilizing anchors with or without clamping. In some of these tests, the shrinkage stress developed inside the concrete is calculated by using the strain gauge fixed to the surrounding steel frame. Other methods have been introduced by modifying the same previous test rig but with adjustable crossheads. In these methods, a concrete specimen is put in a horizontal position and gripped at its ends. One of these ends is movable and the other is fixed. The drying shrinkage induces horizontal displacements (movement of free end) that is periodically observed by a displacement gauge. The displacment is recovered by applying a tensile load on the specimen after the occurrence of a pre-defined amount of displacement. The tensile load is applied using a load cell and a hydraulic servo actuator. Some of these tests have been developed so they are controlled by using a closed- loop computer control. Some of these tests provide unknown (partial) restrained degree and others provide 100% "full" restrained. By using the above methods, a variety of concrete properties can be obtained. For example shrinkage (drying and autogenous) strain, shrinkage stress, age of cracking, crack width, rate of stress/strength, creep of concrete, development of tensile stress with time and degree of restrained. Some of these properties can only be used as qualitative tools to compare different concrete mixtures, while others can quantify the behaviour of concrete under restrained conditions. However, they do not provide vital information regarding the residual strength of the concrete under restrained conditions and do not quantify the effect of the micro and macro shrinkage induced cracks on the behaviour of concrete.

The drawbacks of these methods can generally be summarized as the following:

- Just as in uniaxial tensile test of concrete, conducting uniaxial restrained shrinkage tests by providing full restraint for the ends is questionable. This is because, practically it is almost impossible to grip the ends of the linear specimen providing full restraint and avoiding slippage and premature failure due to stress concentration [43, 44].

- The way of applying the restraining load needs high accuracy and also the load must be applied in a smooth way without irregularities, so that load shocks can be avoided to prevent premature failure, especially of the concrete at early age. Additionally, avoiding misalignment of the restraining applied load is also difficult [44].

- From a practical prospective when many parameters are needed to be examined, the setting up of such tests and their instrumentation can be too complicated and expensive. For

example, devises with very high accuracy is required to measure displacements and loads [12, 44]. Automatic strain measurements are also difficult since cracking positions are not known a-priori.

- The limited dimensions of the specimens used, in particular the depth, in some of these tests is also another issue. This can limit the use of normal size coarse aggregates. In fact, in some of these tests no coarse aggregate is used at all [12] [21]

- None of these tests allow dismounting the concrete specimen after the exposure to restrained shrinkage without destroying the specimen. Developing a rig that enables dismounting the concrete specimen would facilitate conducting tests such bending and compression test to quantify the effect of the shrinkage induced cracks on the residual mechanical properties such as flexural and compressive strength and elastic modulus.

As a result of the aforementioned difficulties, such tests are avoided in common quality control testing and large-scale parametric study investigations [2, 45-47].

References

1. Bisschop Jan, *Drying Shrinkage Microcracking in Cement-based Materials*, in *Civil engineering and Geoscience*. 2002, Delft University of Technoloy: Delft, Netherlands.
2. ACI 231R-10, *Report on Early-Age Cracking: Causes, Measurement, and Mitigation*, in *ACI Committee 231*. 2010, American Concrete Institute: Farmington Hills, U.S.A.
3. ACI 207.2R-95, *Effect of Restraint, Volume Change, and Reinforcement on Cracking of Mass Concrete*, A.C. 207, Editor. 1995, American Concrete Institute: Farmington hills, MI, USA. p. 47.
4. Carlson, R.W., *Attempts to Measure the Cracking Tendency of Concrete* ACI, 1940. **36**: p. 533-537.
5. Bisschop, J. and J.G.M. Van Mier, *Effect of aggregates on drying shrinkage microcracking in cement-based composites.* Materials and Structures/Materiaux et Constructions, 2002. **35**(252 SPEC.): p. 453-461.
6. Bentur, A., *Early-Age Shrinkage and Cracking in Cementitious Systems.* Concrete Science and Engineering, 2001. **3**: p. 3-12.
7. Leung, C., A. Lee, and R. Lai, *New Testing Procedure for Shrinkage Cracking of Fiber-Reinforced Shotcrete.* Journal of Materials in Civil Engineering, 2007. **19**(3): p. 214-218.
8. Abbasnia, R., P. Godossi, and J. Ahmadi, *Prediction of restrained shrinkage based on restraint factors in patching repair mortar.* Cement and Concrete Research, 2005. **35**(10): p. 1909-1913.
9. BS ISO 1920-8:2009, *Testing of concrete. Determination of the drying shrinkage of concrete for samples prepared in the field or in the laboratory*. 2009, British Standard Institution: London, UK.
10. Grzybowski, M. and S.P. Shah, *Model to Predict Cracking in Fiber Reinforced-Concrete Due to Restrained Shrinkage*. Magazine of Concrete Research, 1989. **41**(148): p. 125-135.
11. Swamy, R.N. and H. Stavrides, *Influence of Fiber Reinforcement on Restrained Shrinkage and Cracking.* Journal of the American Concrete Institute, 1979. **76**(3): p. 443-460.
12. Tritsch, N., Darwin, D. and Browning, J.A. , *Evaluating shrinkage and cracking behaviour of concrete using restrained ring and free shrinkage tests*. 2005, Structural Engineering and Engineering Materials,The University of Kansas Center for Research Inc.: Lawrence, Kansas.
13. Carlsward J. , *Shrinkage Cracking of Steel Fibre Reinforced self compacting Concrete Overlays*, in *Department of civil and Environmental Engineering*. 2006, Lulea University of Technology: Lulea,Sweden.
14. Weiss, W.J., W. Yang, and S.P. Shah, *Shrinkage cracking of restrained concrete slabs.* Journal of Engineering Mechanics-Asce, 1998. **124**(7): p. 765-774.
15. Altoubat, S.A. and D.A. Lange, *Creep, shrinkage, and cracking of restrained concrete at early age.* ACI Materials Journal/ SP, 2001. **98**(4): p. 323-331.

16. Kovler, K., *Testing System for Determining the Mechanical-Behavior of Early Age Concrete under Restrained and Free Uniaxial Shrinkage.* Materials and Structures, 1994. **27**(170): p. 324-330.

17. Bentur, A. and K. Kovler, *Evaluation of early age cracking characteristics in cementitious systems.* Materials and Structures, 2003. **36**(3): p. 183-190.

18. Altoubat, S.A. and D.A. Lange. *Early age shrinkage and creep of fiber reinforced concrete for airfield pavement*. in *Aircraft/Pavement Technology In the Midst of Change*. 1997.

19. Carlson, R.W., *Cracking of Concrete*. The Boston Society of Civil Engineers, 1942. **29**(2): p. 98-109.

20. Weiss, W.J., W. Yang, and S.P. Shah, *Influence of specimen size/geometry on shrinkage cracking of rings.* Journal of Engineering Mechanics-Asce, 2000. **126**(1): p. 93-101.

21. Qiao, P., McLean, D. and Zhuang, J.,, *Mitigation Strategies for Early-Age Shrinkage Cracking in Bridge decks*. 2010, Department of Civil and Environmental Engineering , Washington State University: Pullman, Washington. .

22. AASHTO T 334-08, *Standard Practice for Estimating the Crack Tendency of Concrete*. 2008, AASHTO Washington D.C.

23. ASTM C1581-04, *Standard Test Method for Determining Age at Cracking and Induced Tensile Stress Characteristics of Mortar and Concrete under Restrained Shrinkage*. 2004, ASTM International. p. 791-796.

24. Banthia, N., C. Yan, and S. Mindess, *Restrained shrinkage cracking in fiber reinforced concrete: A novel test technique.* Cement and Concrete Research, 1996. **26**(1): p. 9-14.

25. Tongaroonsri, S. and S. Tangtermsirikul, *Effect of mineral admixtures and curing periods on shrinkage and cracking age under restrained condition.* Construction and Building Materials, 2009. **23**(2): p. 1050-1056.

26. Bentur, A., *Early Age Cracking Tests*, in *Early Age Cracking in Cementitious Systems - Report of RILEM Technical Committee 181-EAS - Early age shrinkage induced stresses and cracking in cementitious systems*, A. Bentur, Editor. 2003, RELIM. p. 241-255.

27. Kraai, P.P., *A proposed test to determine the cracking potential due to drying shrinkage of concrete.* Concrete Construction, 1985. **30**(9): p. 775-778.

28. Yokoyama, K., et al., *Shrinkage and Cracking of High-Strength Concrete and Flowing Concrete at Early Ages.* ACI Special Publication, 1994. **148**.

29. Berke, N. and M. Dallaire, *Effect of low addition rates of polypropylene fibers on plastic shrinkage cracking and mechanical properties of concrete.* ACI Special Publication, 1994. **142**.

30. Banthia, N., M. Azzabi, and M. Pigeon, *Restrained shrinkage tests on fiber reinforced cementitious composites.* Testing of Fiber Reinforced Concrete, 1995. **155**: p. 137-151.

31. Banthia, N., M. Azzabi, and M. Pigeon, *Restrained Shrinkage Cracking in Fiber-Reinforced Cementitious Composites.* Materials and Structures, 1993. **26**(161): p. 405-413.

32. Mangold, M., *Methods for Experimental Determination of Thermal Stresses and Crack Sensitivity in the Laboratory.* RILEM REPORT, 1998: p. 26-39.

33. Springenschmid, R., Breitenbucher, R., Mangold, R.,. *Development of the cracking frame temperature-stress testing machine,* . in *Thermal Cracking in Concrete at Early Ages* 1994. Proceedings RILEM Symposium E&FN SPON.

34. Breitenbücher, R., *Investigation of thermal cracking with the cracking-frame.* Materials and Structures, 1990. **23**(3): p. 172-177.

35. JCI, *Committee Report: Technical Committee on Autogenous Shrinkage of Concrete* in *AUTOSHRINK'98, Worshop on Autogenous Shrinkage of Cocncrete*, E. Tazawa, Editor. 1998, Japan Concrete Institute Japan. p. 5-66.

36. Collins, F. and J.G. Sanjayan, *Cracking tendency of alkali-activated slag concrete subjected to restrained shrinkage.* Cement and Concrete Research, 2000. **30**(5): p. 791-798.

37. Bloom, R. and A. Bentur, *Free and Restrained Shrinkage of Normal and High-Strength Concretes.* Aci Materials Journal, 1995. **92**(2): p. 211-217.

38. Van Breugel, J. K. De Vries, and K. Takada, *Mixture optimization of low water/cement ratio high strength concretes in view of reduction of autogenous shrinkage* in *High Performance Concretes,* . August,1998: Sherbrooke, Canada.

39. Springenschmid, R., E. Gierlinger, and W. Kiernozycki. *Thermal stress in mass concrete: a new testing method and the influence of different cements*. in *Proceedings of the 15th International Congress for Large Dams*. 1985.

40. Paillere A. M., B.M., Serrano J. J. „ *Effect of Fiber Addition on the Autogenous Shrinkage of Silica Fume.* ACI Materials Journal, 1989. **86**(2): p. 6.

41. Igarashi, S., A. Bentur, and K. Kovler, *Stresses and creep relaxation induced in restrained autogenous shrinkage of high-strength pastes and concretes.* Advances in Cement Research, 1999. **11**(4): p. 169-177.

42. Pigeon, M., et al., *Equipment for the analysis of the behaviour of concrete under restrained shrinkage at early ages.* Magazine of Concrete Research, 2000. **52**(4): p. 297-302.

43. Grzybowski, M. and S.P. Shah, *Shrinkage Cracking of Fibre Reinforced Concrete.* ACI Materials Journal, 1990. **87**(2).

44. Altoubat, S.A., *Early age stresses and creep-shrinkage interaction of restrained concrete*. 2000.

45. Altoubat, S.A. and D.A. Lange, *Creep, shrinkage, and cracking of restrained concrete at early age.* Aci Materials Journal, 2001. **98**(4): p. 323-331.

46. Tongaroonsri, S. and S. Tangtermsirikul, *Influence of mixture condition and moisture on tensile strain capacity of concrete.* ScienceAsia, 2008. **34**(1): p. 59-68.

47. Hossain, A.B., and Weiss, W. J., , *Assessing Residual Stress Development and Stress Relaxation in Restrained Concrete Ring Specimens.* Cement and Concrete Composites, 2004. **26**: p. 531-540.

Appendix C:

Experimental Results -Chapter 2

C.1 Constituents of Coarse RA According to BS EN 933-11:2009[1]

Table C-1 Description of constituents of coarse recycled aggregates [1]

Constituent	Description
Rc	Concrete, Concrete products, Mortar, Concrete masonry units
Ru	Unbound aggregate , Natural stone , Hydraulically bound aggregate
Rb	Clay masonry units (i.e bricks and tiles), Calcium silicate masonry units, Aerated non-floating concrete
Ra	Bituminous materials
FL	Floating materials (in volume)
X	Others: Cohesive (i.e clay and soil) Miscellaneous : metal (ferrous and non-ferrous Non-floating wood, plastic and rubber Gypsum plaster
Rg	Glass

C.2 Composition Test Results of Coarse RA

Table C-2 The constituents materials of coarse RA of different sizes*.

Constituents	RA-C			RA-M			RA-B			RA-C1		
	20-14	14-10	10-5	20-14	14-10	10-5	20-14	14-10	10-5	20-14	14-10	10-5
Rc	71.1	80.5	77.3	67.2	70.9	67.3	0.0	0.0	1.0	77.7	76.1	83.1
Ru	28.0	17.3	17.6	17.0	13.3	11.0	0.0	0.0	0.0	22.3	23.9	16.2
Rb	0.5	0.8	1.0	9.8	10.1	12.9	95.0	95.6	89.1	0	0	0
Ra	0.3	1.0	0.9	4.3	4.8	5.7	1.0	1.6	3.0	0	0	0
X	0.0	0.2	1.4	0.7	0.1	2.5	1.2	1.1	3.3	0	0	0
Fine materials	0.1	0.1	1.0	0.1	0.1	0.1	1.1	1.3	2.2	0	0	0.7
Rg	0.0	0.0	0.6	0.9	0.7	0.5	1.7	1.0	1.4	0	0	0
FL	0.2	0.25	0.2	0.7	1.1	0.9	0.4	0.5	0.8	0	0	0

* Sizes are in mm.

C.3 Analysis of Length of Recycled Steel Tyre Fibres

Table C-3 Results of length distribution .

Length (mm)	Frequency	Cumulative %
0	0	0.00%
2.5	22	1.89%
5	89	9.51%
7.5	55	14.22%
10	50	18.51%
12.5	81	25.45%
15	121	35.82%
17.5	175	50.81%
20	182	66.41%
22.5	156	79.78%
25	92	87.66%
27.5	55	92.37%
30	32	95.12%
32.5	22	97.00%
35	13	98.11%
37.5	6	98.63%
40	6	99.14%
42.5	4	99.49%
45	1	99.57%
47.5	2	99.74%
50	1	99.83%
52.5	1	99.91%
55	1	100.00%
57.5	0	100.00%
60	0	100.00%

Table C-4 Results of statistical analysis of length of RTSF fibres.

Statistical Analysis Results	
Mean	16.99
Standard Error	0.23
Median	17.26
Standard Deviation	7.90
Sample Variance	62.4
Kurtosis	0.94
Skewness	0.34
Range	51.75
Minimum	2.06
Maximum	53.80
Count	1167
Confidence Level(95.0%)	0.45

C.4 Bulk Density of Coarse Aggregates

Table C-5 Results of bulk density test of NA and RA.

Type of aggregate	Size mm	Density kg/m^3
Natural	14-20	1646
	10-14	1585
	5-10	1603
	5-20	**1668**
Mixed	14-20	1212
	10-14	1171
	5-10	1184
	5-20	**1234**
Concrete	14-20	1310
	10-14	1283
	5-10	1257
	5-20	**1338**
Brick	14-20	1027
	10-14	1038
	5-10	1026
	5-20	**1042**

C.5 Compressive strength and density of concrete at 28 days

Table C-6 Results of compressive strength at 28 days.

Type	% RA	Compressive strength MPa	Average Strength	Normalized strength
Natural	100%	53.01 53.88 52.49	53.1	1.00
RA-C	20%	48.5 51.9 49.6	50.0	0.94
	50%	46.84 44.09 44.88	45.3	0.85
	75%	45.24 43.85 42.91	44.0	0.83
	100%	41.53 39.55 43.75	41.6	0.78
RA-M	20%	49.73 46.81 47.4	48.0	0.90
	50%	39.8 42.7 42.6	41.7	0.79
	75%	41.7 38.8 37.94	39.5	0.74
	100%	37.2 39.0 38.1	38.1	0.72
RA-B	20%	40.3 40.4 39.42	40.0	0.75
	50%	38.61 39.12 33.3	37.0	0.70
	75%	35.2 31.15 32.85	33.1	0.62
	100%	32.56 29.70 32.23	31.5	0.59

Type	% RA	Compressive strength MPa	Average Strength	Normalized strength
RA-C1	20%	53.60 54.00 52.10	53.2	1.00
	50%	55.50 53.70 53.20	54.1	1.02
	75%	56.80 56.20 54.30	55.8	1.05
	100%	59.18 58.43 57.35	58.3	1.1

Table C-6 Results of concrete density at 28 days.

Type	% RA	Sample No.	Mass in air (kg)	Mass in water (kg)	Density kg/m^3	Average Density	Normalized Density
Natural	100%	1	2386	1385	2384	2378	100%
		2	2370	1374	2380		
		3	2380	1376	2371		
RA-C	20%	1	2350.4	1343	2333	2336	98%
		2	2348.3	1348	2348		
		3	2332.3	1330	2327		
	50%	1	2346	1333	2316	2315	97%
		2	2341	1330	2316		
		3	2338	1328	2315		
	75%	1	2337	1323	2305	2295	96%
		2	2317.5	1307	2293		
		3	2318	1304	2286		
	100%	1	2312	1295	2273	2273	96%
		2	2299	1285	2267		
		3	2314	1298	2278		
RA-M	20%	1	2392	1378	2359	2348	99%
		2	2378	1363	2343		
		3	2368	1357	2342		
	50%	1	2308	1295	2278	2275	96%
		2	2317	1302	2283		
		3	2302	1285	2264		
	75%	1	2285	1269	2249	2242	94%
		2	2279	1260	2237		
		3	2279	1262	2241		
	100%	1	2256	1237	2214	2205	93%
		2	2224	1211	2195		
		3	2241	1225	2206		
RA-B	20%	1	2320	1294	2261	2256	95%
		2	2305	1283	2255		
		3	2318	1289	2253		
	50%	1	2284	1262	2235	2229	94%
		2	2281	1255	2223		
		3	2282	1258	2229		
	75%	1	2214	1186	2154	2150	90%
		2	2211	1182	2149		
		3	2208	1180	2148		
	100%	1	2150	1127	2102	2102	88%
		2	2149	1125	2099		
		3	2151	1129	2105		

Type	% RA	Sample No.	Mass in air (kg)	Mass in water (kg)	Density kg/m^3	Average Density	Normalized Density
RA-C1	20	1	2139	1112	2082	2065	0.87
		2	2124	1095	2065		
		3	2108	1079	2048		
	50	1	2092	1063	2032	2015	0.85
		2	2077	1046	2015		
		3	2061	1030	1998		
	75	1	2045	1013	1982	2156	0.91
		2	2030	997	1965		
		3	2014	981	1949		
	100	1	1998	964	1932	1916	0.81
		2	1983	948	1916		
		3	1967	931	1899		

1. BS EN 933-11:2009, *Tests for geometrical properties of aggregates -Part 11: Classification test for the constituents of coarse recycled aggregate*. 2010, British Standard Institution: London.

Appendix D:

Experimental Results -Chapter 3

D.1 Free Shrinkage

Table D-1 Shrinkage strains (in microstrains) measured on top surface over 50 mm gauge length.

Drying Time (days)	50 mm / Top								
	1	2	3	4	5	6	7	8	Average
1	53	38	31	58	61	73	50	41	51
2	84	57	44	79	72	79	60	65	68
3	102	90	59	86	94	106	86	90	89
4	143	123	101	130	126	139	115	124	125
5	166	141	125	144	142	152	137	138	143
6	176	150	140	151	149	158	147	145	152
7	192	159	148	158	159	172	151	152	161
10	222	180	172	180	186	183	180	179	185
14	168	230	216	216	251	218	245	246	224
21	372	311	288	317	318	302	310	311	316
28	420	352	346	360	337	340	353	352	357
34	462	380	396	432	384	401	396	386	405
41	492	408	414	450	410	406	406	422	426
47	480	468	456	456	462	475	456	468	465
55	510	498	504	480	492	503	480	492	495
75	528	522	516	504	516	541	510	520	520

Table D-2 Shrinkage strains (in microstrains) measured on side surface over 50 mm gauge length.

Drying Time (days)	50 mm / Side								
	1	2	3	4	5	6	7	8	Average
1	40	30	24	48	53	66	42	36	42
2	54	46	34	66	62	72	50	56	55
3	76	72	46	72	82	96	72	78	74
4	106	98	78	108	109	126	96	108	104
5	120	113	96	120	124	138	114	120	118
6	126	120	108	126	130	144	122	126	125
7	132	127	114	132	138	156	126	132	132
10	154	144	132	150	169	174	150	156	154
14	210	192	180	180	228	208	204	214	202
21	270	259	240	264	289	288	258	270	267
28	300	293	288	300	306	324	294	306	301
34	336	327	330	360	366	382	330	336	346
41	362	348	354	366	384	386	348	372	365
47	408	395	384	414	432	432	400	420	411
55	438	418	422	444	456	468	420	444	439
75	468	456	456	474	480	492	462	468	470

Table D-3 Shrinkage strains (in microstrains) measured on top surface over 100 mm gauge length.

Drying Time (days)	100 mm / Top				
	1	2	3	4	Average
1	65	60	65	60	63
2	85	75	85	85	83
3	110	100	110	110	108
4	130	120	135	120	126
5	150	140	145	145	145
6	160	155	155	155	156
7	180	165	170	165	170
10	205	190	195	190	195
14	270	255	250	250	256
21	340	325	330	335	333
28	365	350	355	355	356
34	400	380	395	395	393
41	430	405	430	430	424
47	475	450	470	460	464
55	490	470	480	480	480
75	510	500	510	500	505

Table D-4 Shrinkage strains (in microstrains) measured on side surface over 100 mm gauge length.

Drying Time (days)	100 mm / Side				
	1	2	3	4	Average
1	55	50	52	45	51
2	70	65	68	60	66
3	90	85	90	80	86
4	105	105	110	100	105
5	125	122	125	115	122
6	135	135	135	130	134
7	150	145	148	140	146
10	170	170	170	160	168
14	225	225	225	220	224
21	295	290	295	290	293
28	320	315	315	310	315
34	355	345	350	345	349
41	385	380	385	380	383
47	405	405	405	410	406
55	445	440	450	445	445
75	480	475	485	480	480

Table D-5 Shrinkage strains (in microstrains) measured on top surface over 300 mm gauge length.

Drying Time (days)	300 mm / Top		
	1	2	Average
1	70	70	70
2	90	85	88
3	110	120	115
4	135	125	130
5	150	145	148
6	165	155	160
7	185	180	183
10	215	210	213
14	265	275	270
21	355	345	350
28	385	375	380
34	410	400	405
41	435	450	443
47	485	475	480
55	490	500	495
75	530	520	525

Table D-6 Shrinkage strains (in microstrains) measured on side surface over 300 mm gauge length.

Drying Time (days)	300 mm / Side		
	1	2	Average
1	55	55	55
2	70	80	75
3	95	95	95
4	115	109	112
5	135	140	138
6	150	160	155
7	160	165	163
10	190	185	188
14	235	240	238
21	308	309	309
28	330	340	335
34	365	360	363
41	400	405	403
47	420	435	428
55	460	465	463
75	490	500	495

D.2 Restrained Shrinkage

Table D-7 Shrinkage strains (in microstrains) measured on side surface over 50 mm gauge length.

Drying Time	50 mm /Side														
	1	2	3	4	5	6	7	8	9	10	11	12	13	14	Ave.
1	0	0	12	12	0	0	0	0	36	24	12	24	0	0	9
2	12	24	18	24	12	12	24	0	42	30	24	36	0	0	18
3	24	36	24	36	24	24	36	12	42	42	24	36	12	12	27
4	30	48	36	48	42	42	54	36	48	54	36	48	24	24	41
5	42	54	48	72	60	66	60	60	60	66	48	60	48	42	56
6	54	72	66	90	78	78	72	72	72	84	60	78	60	60	71
7	54	72	66	78	78	66	66	60	60	72	54	60	60	60	65
10	78	102	96	120	102	114	96	96	108	108	90	102	84	96	99
14	102	120	114	144	126	132	120	120	132	132	108	120	108	120	121
21	174	192	186	222	204	192	180	192	204	204	180	180	168	192	191
28	228	228	228	264	240	240	246	264	264	240	234	240	240	240	243
34	288	264	270	306	288	288	294	318	312	276	288	300	300	288	291
41	312	282	288	312	312	312	318	348	336	288	312	312	312	312	311
47	360	330	336	360	372	372	378	396	384	336	372	372	372	360	364
55	396	360	366	384	408	408	396	420	420	372	396	396	408	396	395
75	432	384	414	444	438	432	420	444	450	408	438	432	432	426	428

Table D-8 Shrinkage strains (in microstrains) measured on side surface over 100 mm gauge length.

Drying Time	100 mm / Side				
	1	2	3	4	Average
1	23	0	0	0	6
2	28	22	11	11	18
3	39	34	22	22	29
4	50	45	39	39	43
5	62	50	56	62	57
6	78	67	73	73	73
7	62	62	73	73	67
10	101	95	95	106	99
14	123	112	118	123	119
21	190	179	190	179	185
28	224	213	224	224	221
34	258	246	269	269	260
41	269	263	291	291	279
47	314	308	347	347	329
55	358	347	392	392	372
75	426	414	426	426	423

Table D-9 Shrinkage strains (in microstrains) measured on side surface over 300 mm gauge length.

Drying Time	300 mm / Side		
	1	2	Average
1	20	20	20
2	34	36	35
3	46	46	46
4	56	57	57
5	73	76	75
6	88	92	90
7	84	87	86
10	113	118	116
14	150	160	155
21	220	230	225
28	260	270	265
34	280	290	285
41	315	320	318
47	345	355	350
55	385	395	390
75	430	425	428

D.3 Determination of E_{fmax}

The flexural modulus of elasticity E_{flex} was obtained from the results of bending test. It is calculated from the load-deflection curve (obtained from the bending test) using equation 3-1 (chapter 3). This equation is derived from the elastic theory. In the equation, the second term (of the right side) accounts for shear effects during flexural test. The flexural modulus of elasticity of the concrete prism E_{fmax} is determined from a graph representing the relation between the bending load (P) and the flexural modulus of elasticity E_{flex}, see Figure D.1. E_{fmax} is the maximum flexural elastic modulus determined from the curve in the range of 30% to 60% of the ultimate bending load (P_{ult}) as can be seen in Figure D.1.

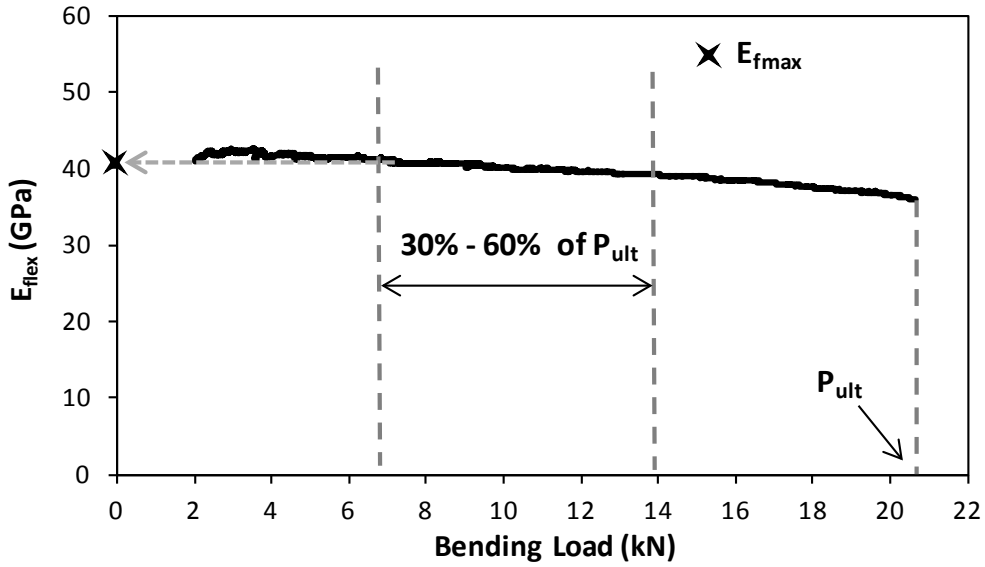

Figure D.1 Determination of E_{fmax} (water cured specimen).

D. 4 Determination of Compressive Strength for Prisms

The compressive strength was obtained for the prisms exposed to water cured, free and restrained shrinkage. The test was performed following the recommendations of BS 1881-119 (2011). This standards adopts a method called equivalent cube method to determine the compressive strength of the hardened concrete portions of prisms broken in flexural (bending test). According to this standard the samples shall be broken portions of prisms which have been tested in flexural. These portions must have a minimum length of not less than the nominal width of the beam plus 50mm. A special steel jig must be used to perform the test. The details of this jig is shown in Figure D.2. Figure D.3 shows portion of broken prisms prepared for compression test.

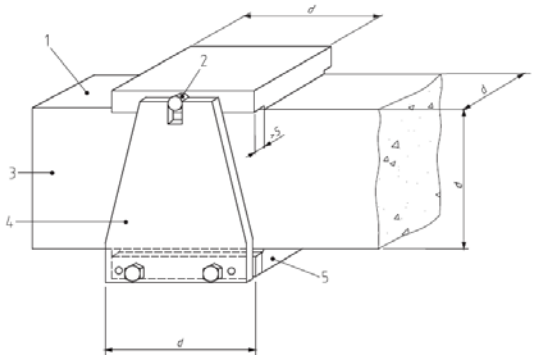

Figure D.2 Details of the jig used for compression test of prisms tested in bending. (BS 1881-119,2011).

Figure D.3 Portion of broken prisms prepared for compression test.

Appendix E:

Experimental Results-Chapter 4

E.1 Free Shrinkage

E.1.1 Shrinkage strains measured on Top (T), Sides (S) and Bottom (B) surfaces over 500 mm length

Mix NA30

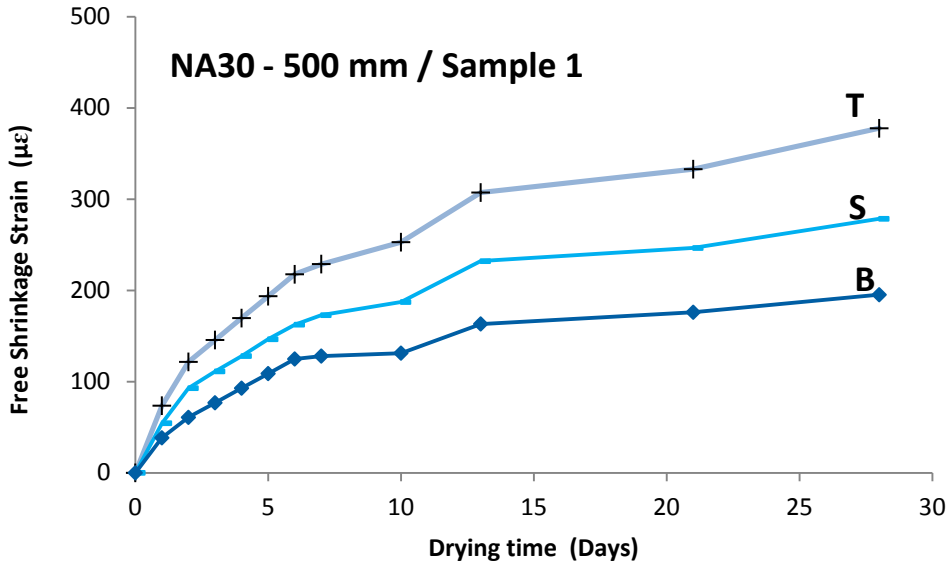

Figure E. 1 Shrinkage strains of mix NA30 /sample 1

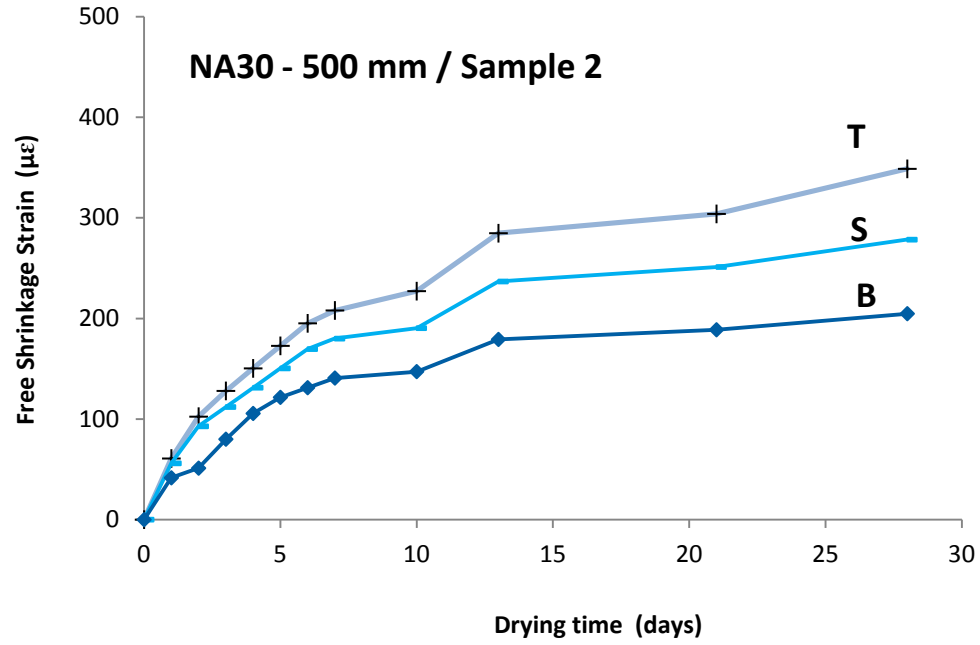

Figure E. 2 Shrinkage strains of mix NA30 /sample 2

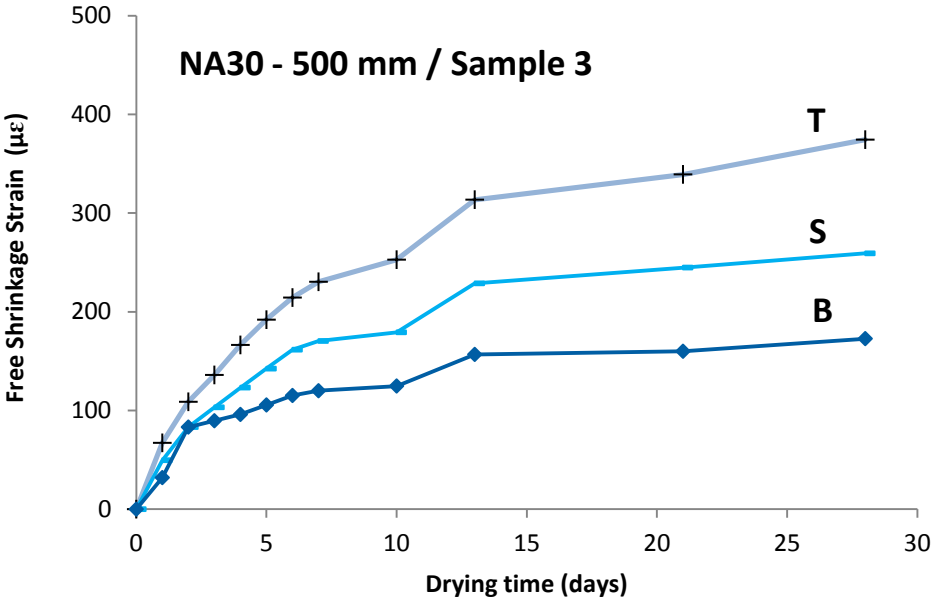

Figure E. 3 Shrinkage strains of mix NA30 /sample 3

Mix NA40

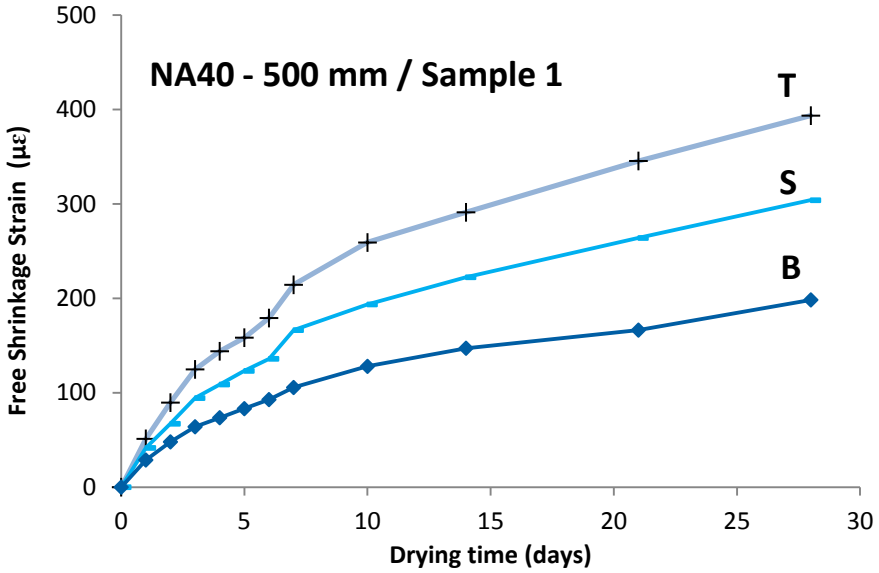

Figure E. 4 Shrinkage strains of mix NA40 /sample 1

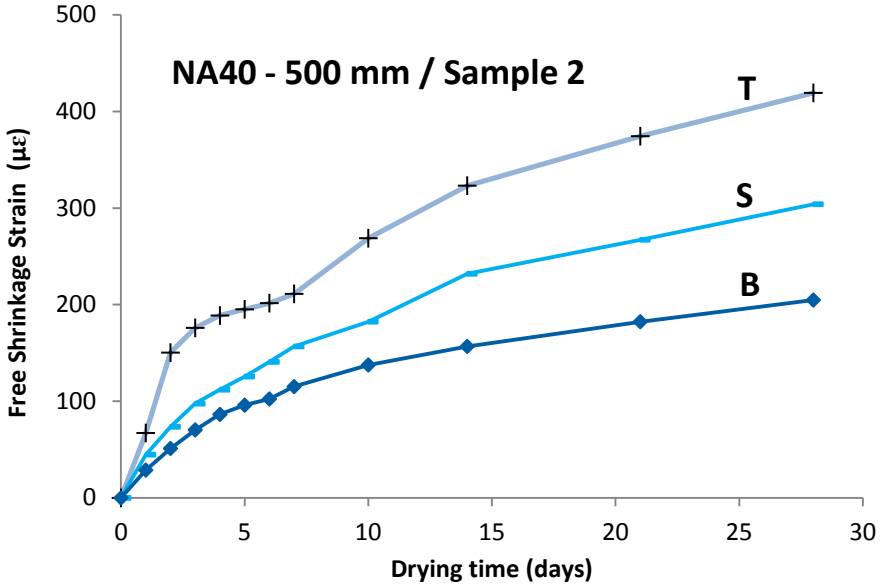

Figure E. 5 Shrinkage strains of mix NA40 /sample 2

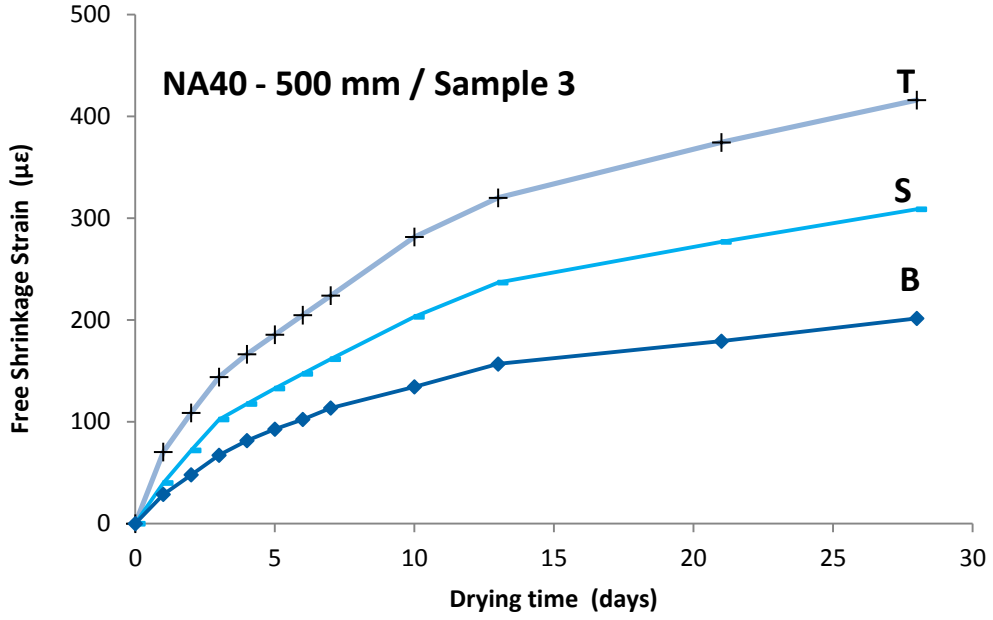

Figure E. 6 Shrinkage strains of mix NA40 /sample 1

Mix NA50

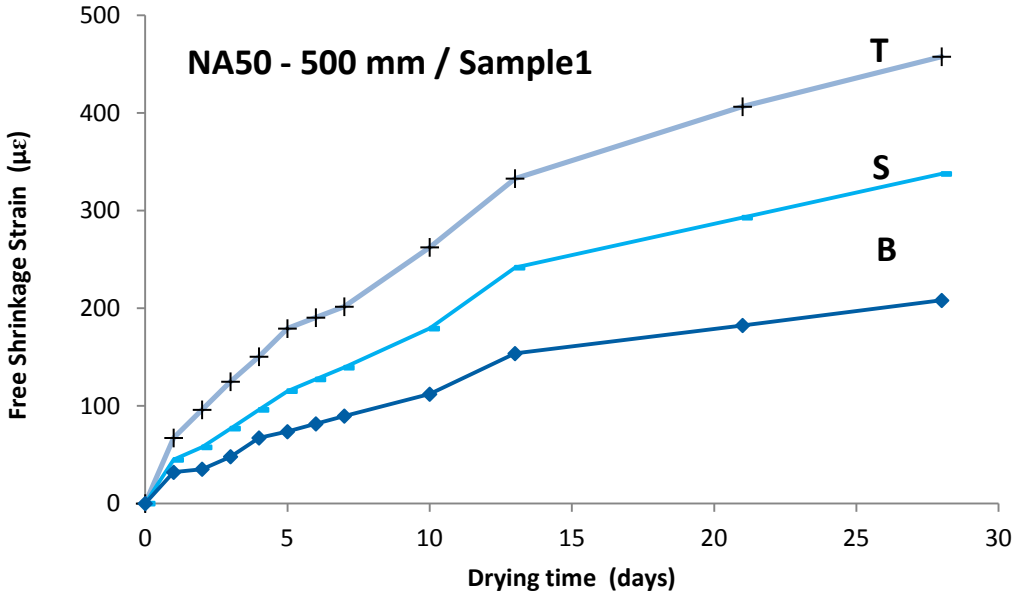

Figure E. 7 Shrinkage strains of mix NA50 /sample 1

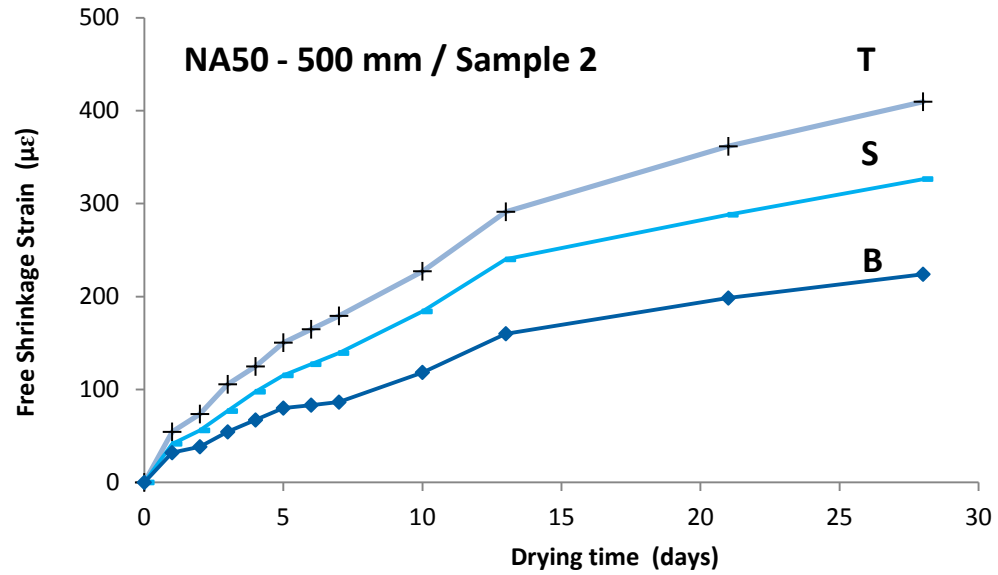

Figure E. 8 Shrinkage strains of mix NA50 /sample 2

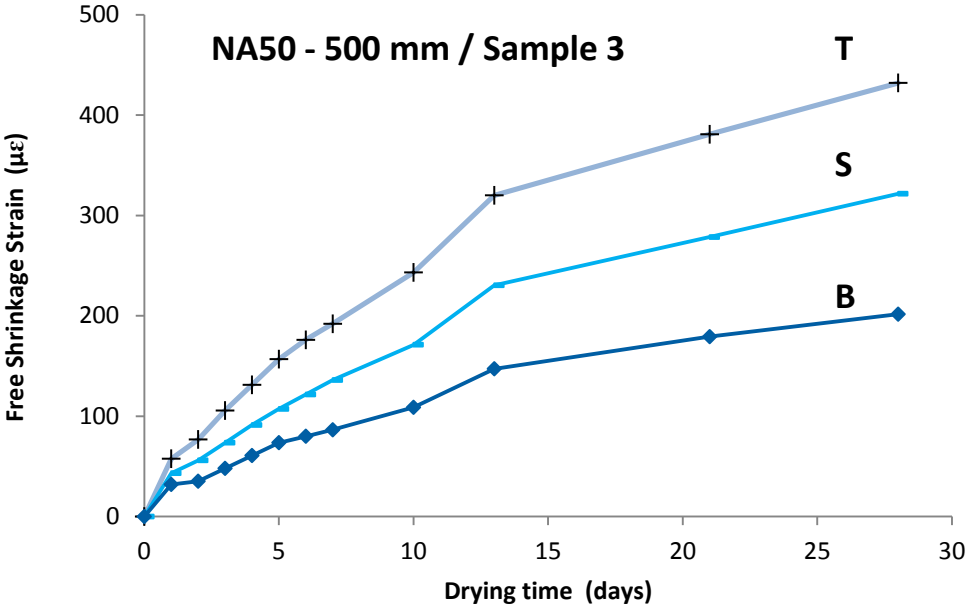

Figure E. 9 Shrinkage strains of mix NA50 /sample 3

E.1.2 Shrinkage strains measured on Top (T), Sides (S) and Bottom (B) surfaces over 300 mm length

Mix NA30

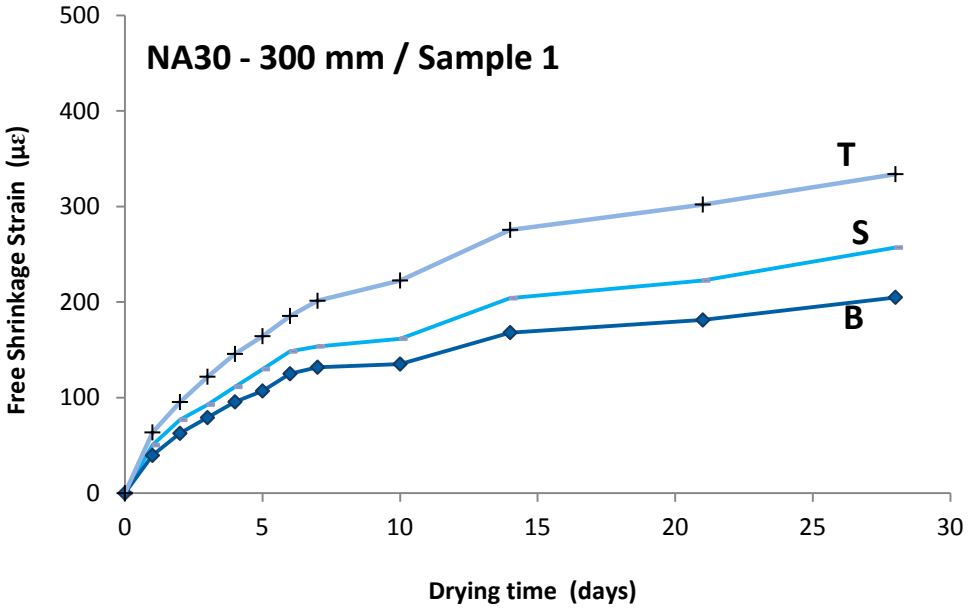

Figure E. 10 Shrinkage strains of mix NA30 /sample 1

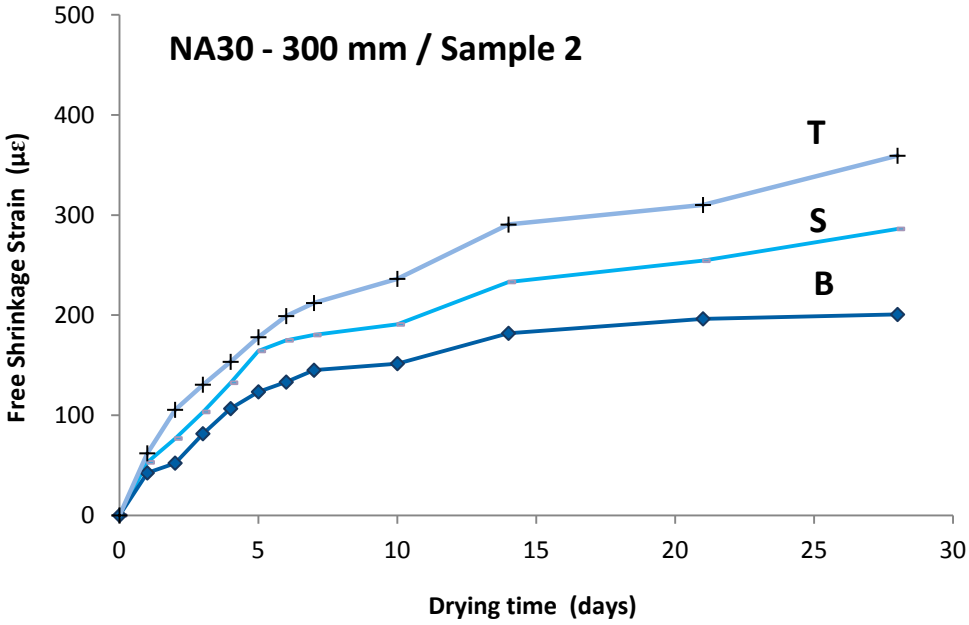

Figure E. 11 Shrinkage strains of mix NA30 /sample 2

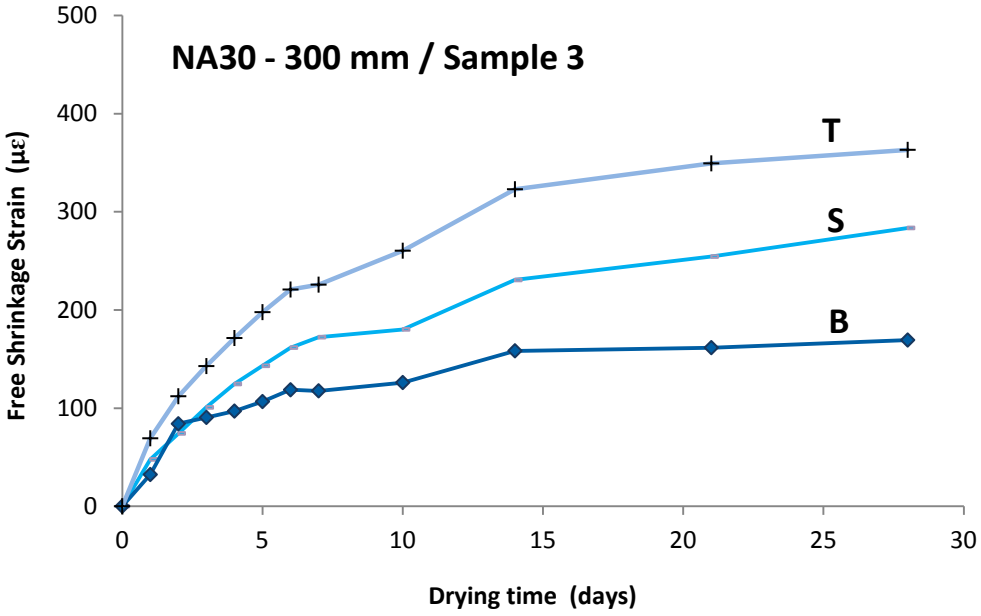

Figure E. 12 Shrinkage strains of mix NA30 /sample 3

Mix NA40

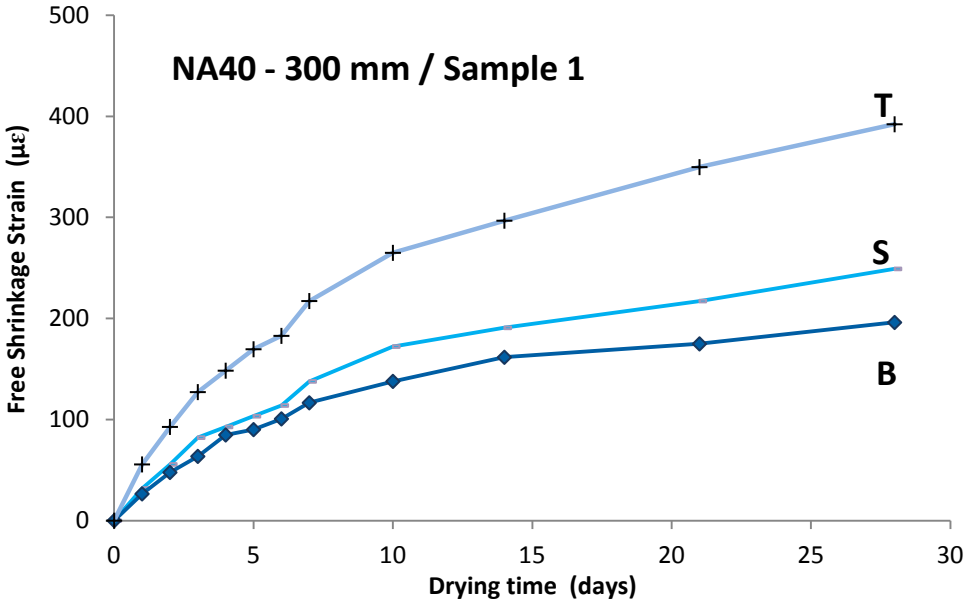

Figure E. 13 Shrinkage strains of mix NA40 /sample 1

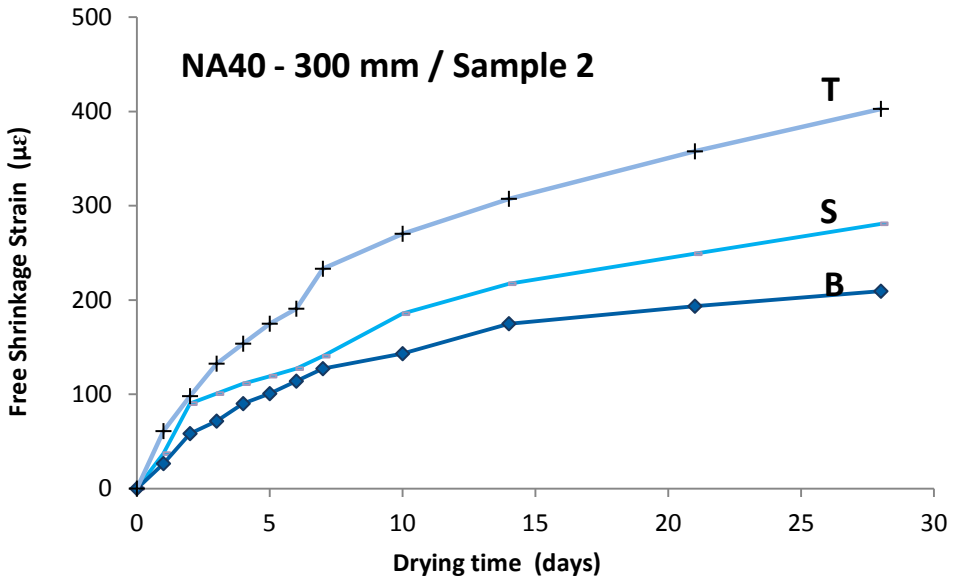

Figure E. 14 Shrinkage strains of mix NA40 /sample 2

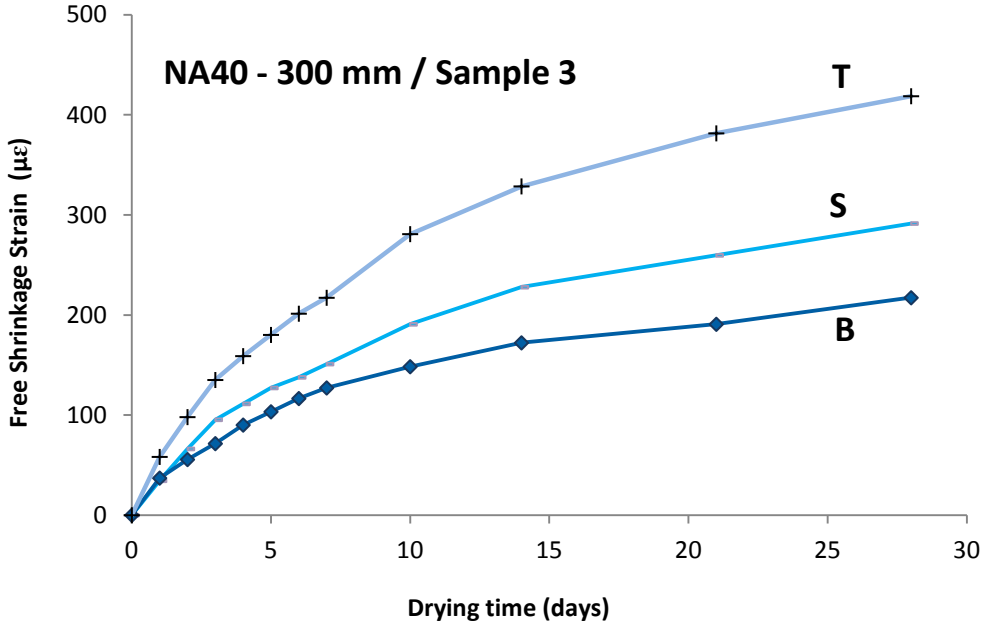

Figure E. 15 Shrinkage strains of mix NA40 /sample 3

Mix NA50

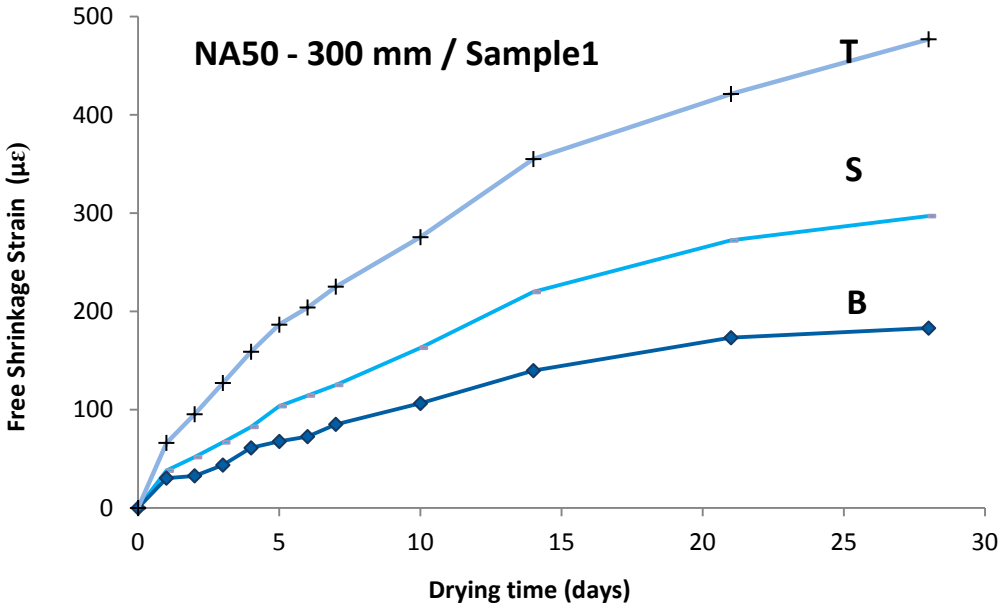

Figure E. 16 Shrinkage strains of mix NA50 /sample 1

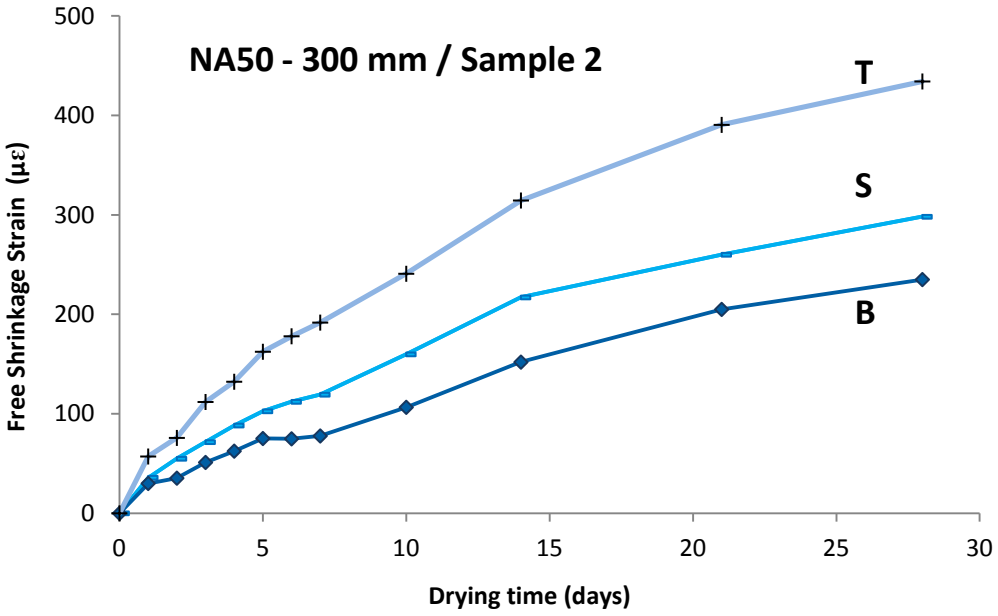

Figure E. 17 Shrinkage strains of mix NA50 /sample 2

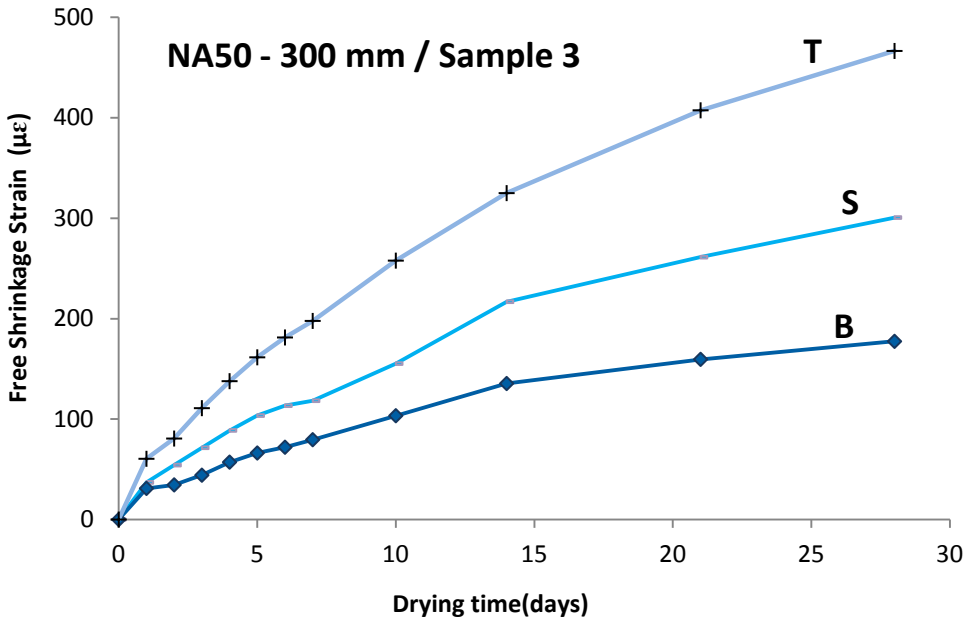

Figure E. 18 Shrinkage strains of mix NA50 /sample 3

Appendix F:

Experimental Results-Chapter 5

F.1 Load -deflection curves

F.1.1 Mix NA30

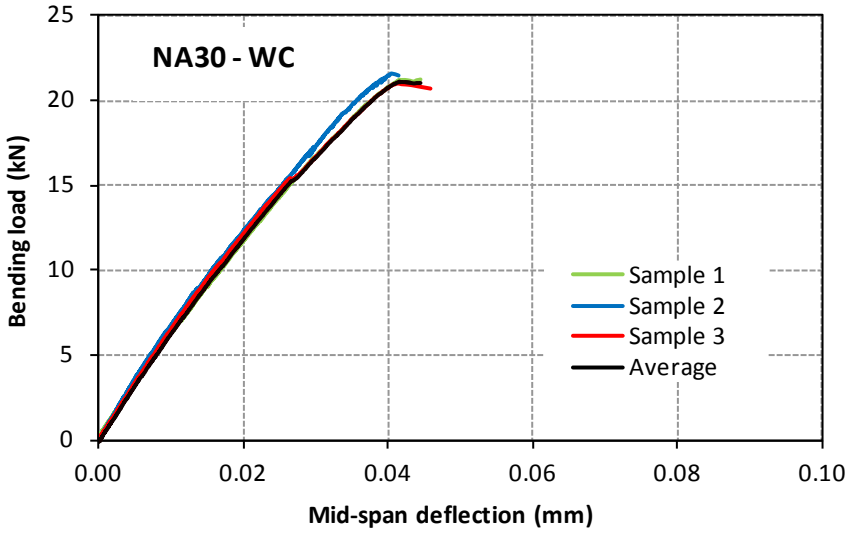

Figure F.1 Load-deflection curve of water cured specimens (mix NA30).

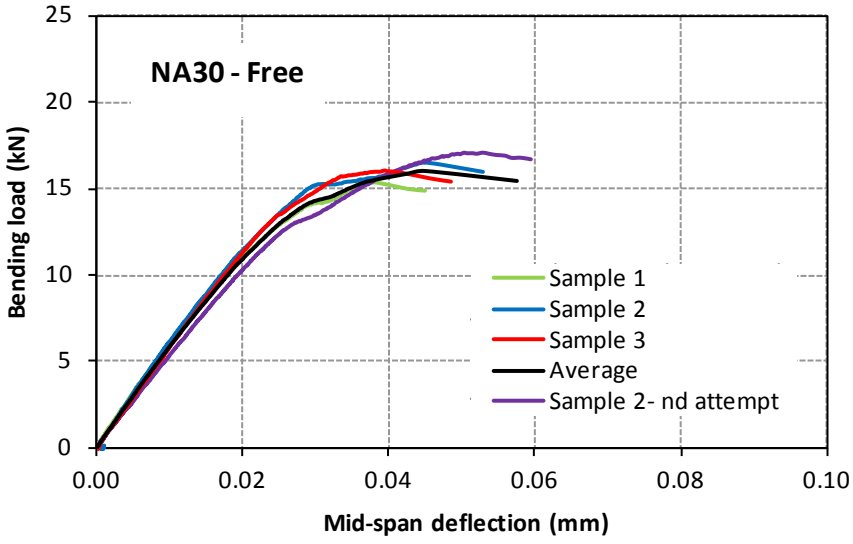

Figure F.2 Load-deflection curve of free specimens (mix NA30).

F.1.2 Mix NA40

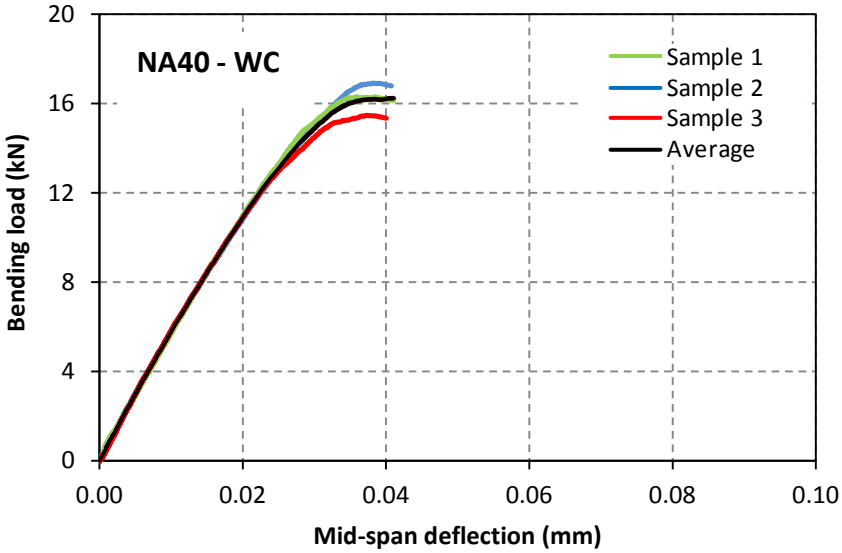

Figure F.3 Load-deflection curve of water cured specimens (mix NA40).

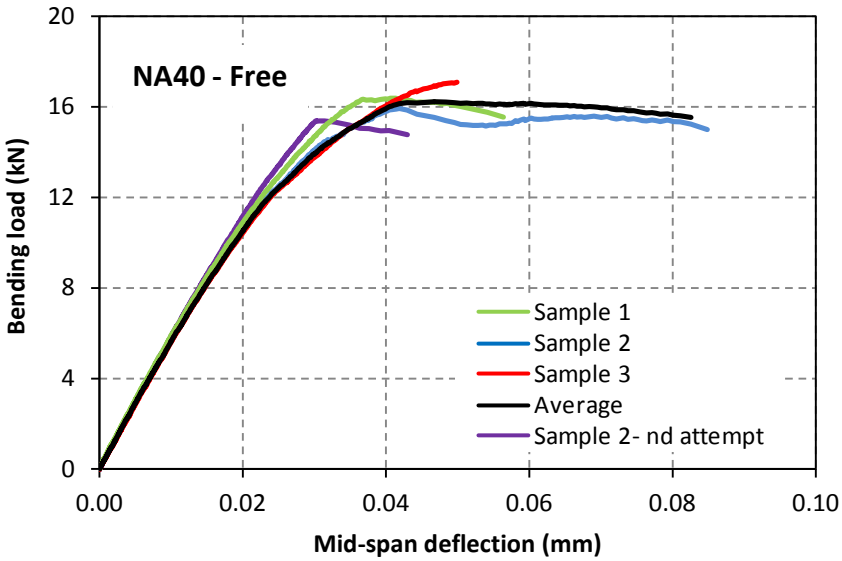

Figure F.4 Load-deflection curve of free specimens (mix NA40).

F.1.3 Mix NA50

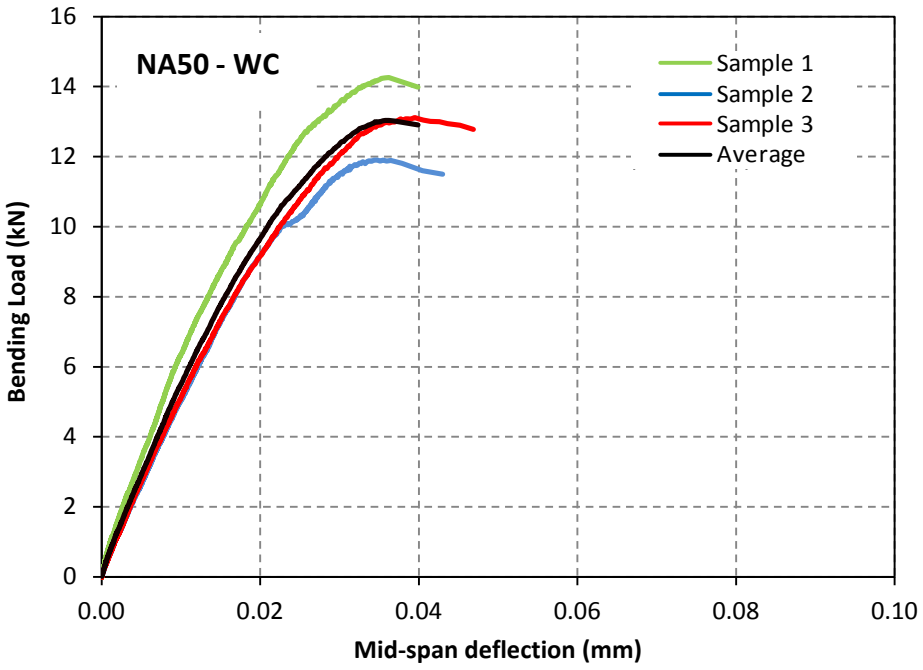

Figure F.5 Load-deflection curve of water cured specimens (mix NA50).

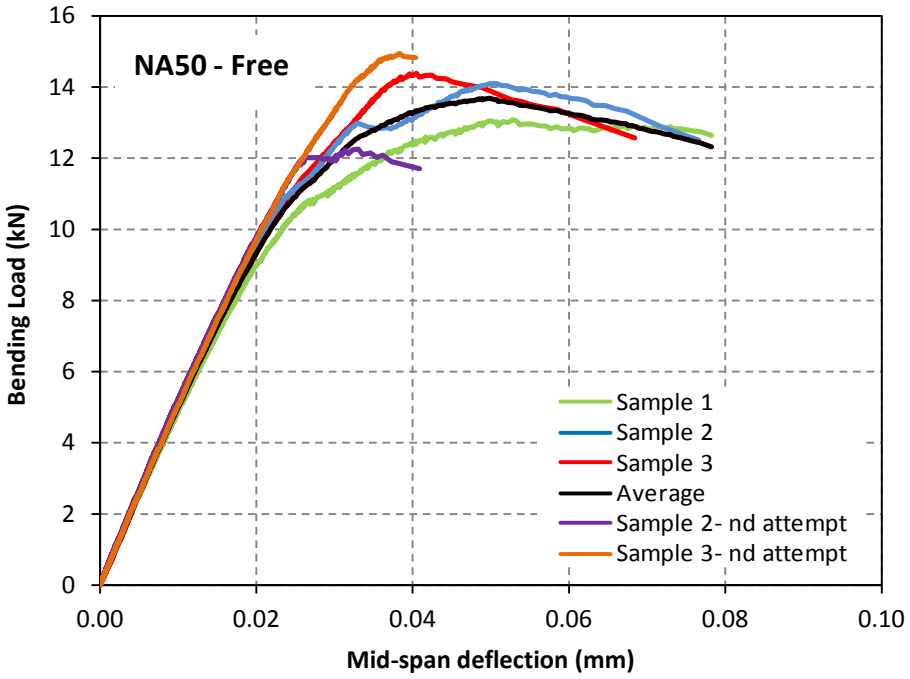

Figure F.6 Load-deflection curve of free specimens (mix NA50).

F.2 Flexural elastic modulus - bending load curves

F.2.1 Mix NA30

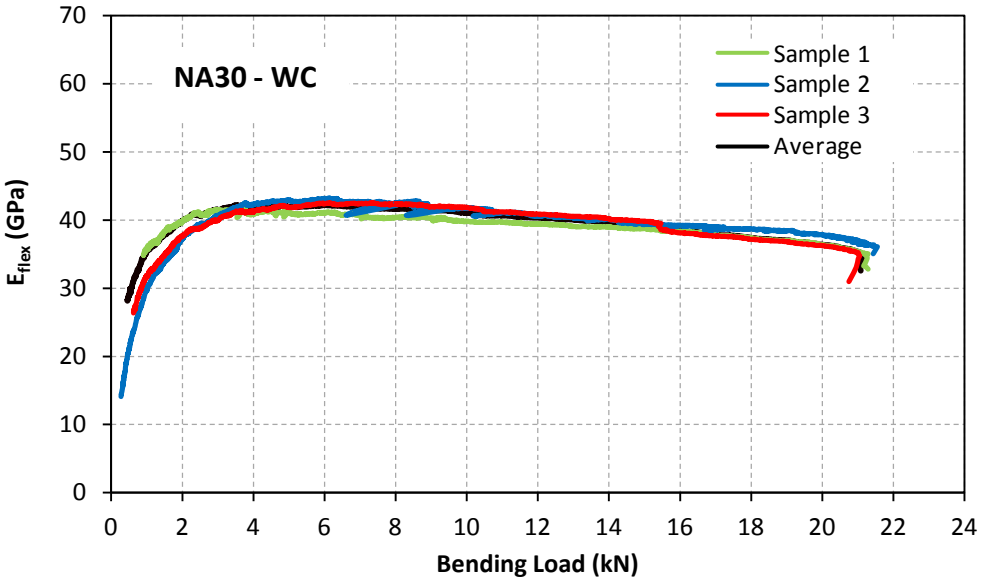

Figure F.7 Flexural elastic modulus - bending load curve of water cured specimens (mix NA30).

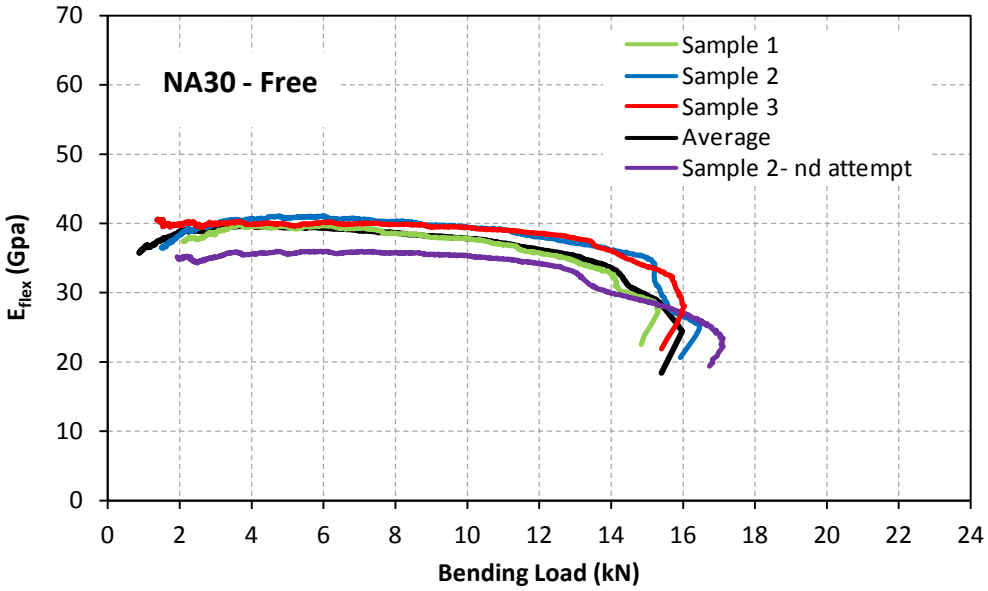

Figure F.8 Flexural elastic modulus - bending load curve of free specimens (mix NA30).

F.2.2 Mix NA40

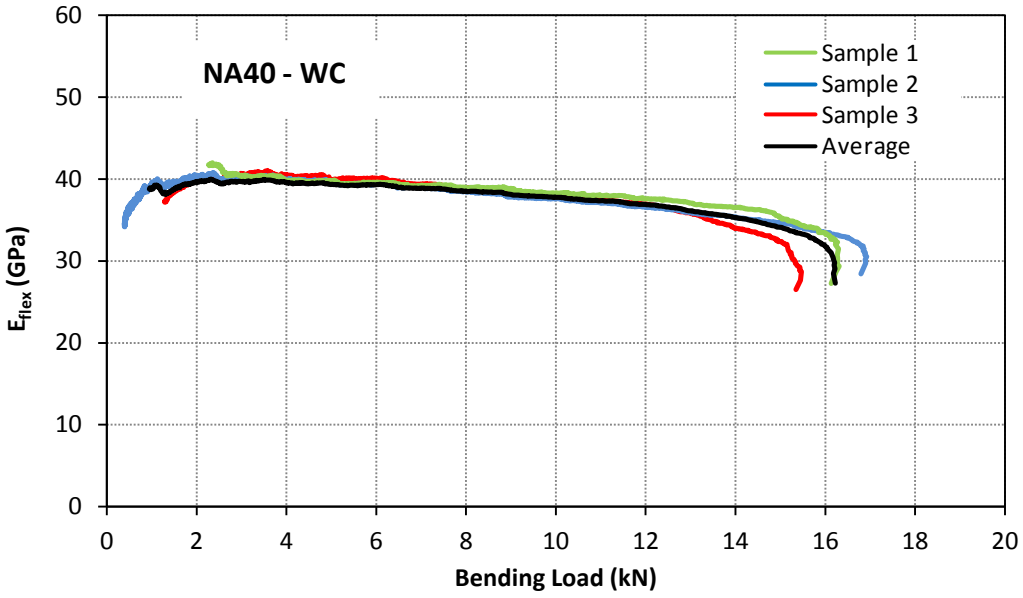

Figure F.9 Flexural elastic modulus - bending load curve of water cured specimens (mix NA40).

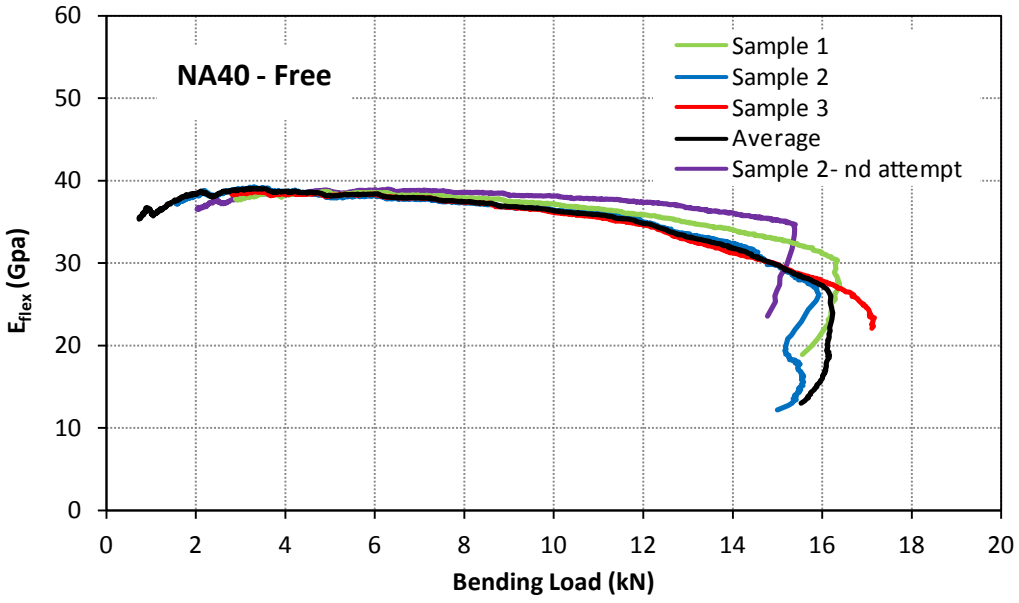

Figure F.10 Flexural elastic modulus - bending load curve of free specimens (mix NA40).

F.2.3 Mix NA50

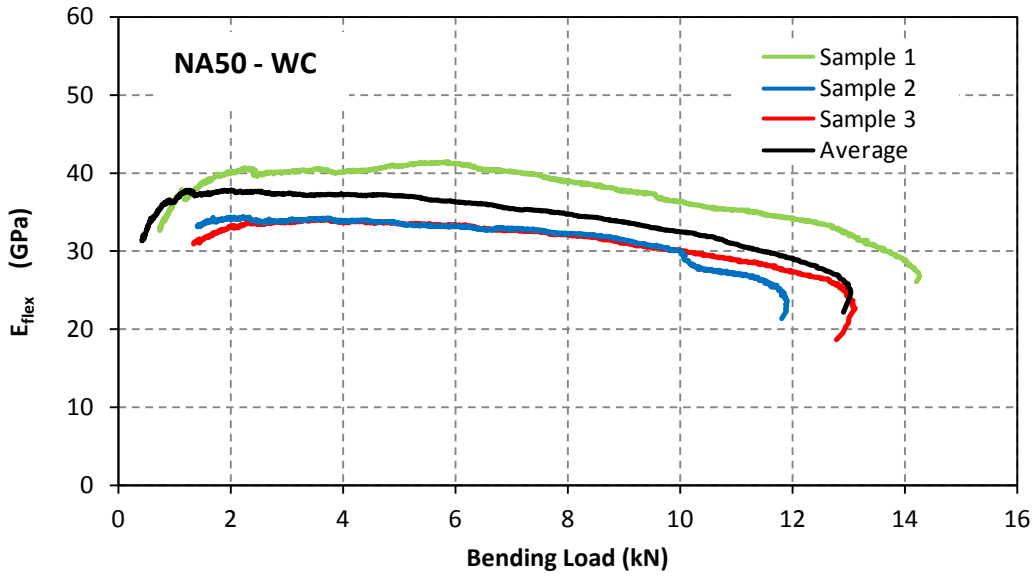

Figure F.11 Flexural elastic modulus - bending load curve of water cured specimens (mix NA50).

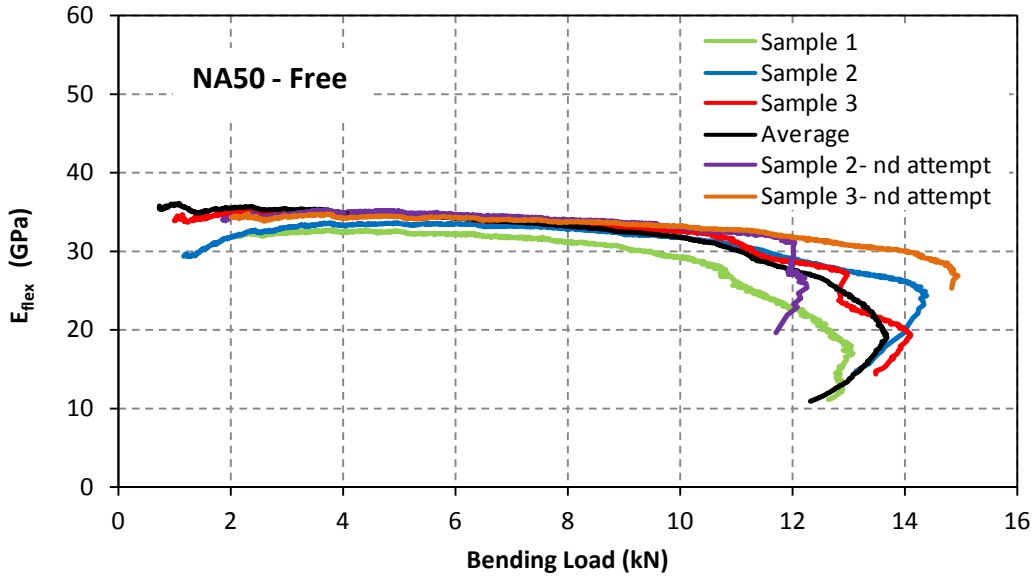

Figure F.12 Flexural elastic modulus - bending load curve of free specimens (mix NA50).

F.3 Results of compressive strength

F.3.1 Mix NA30

Table F.1 Compressive strength of cubes and portions of prisms under WC, F and R conditions- mix NA30

Type and time	Compressive strength Mpa	Average	Normalized strength	SD
Cubes at 1 day	46.41	46.6	66	0.59
	46.05			
	47.2			
Cubes at 3 days	58.45	58.0	83	0.4
	57.88			
	57.69			
Cubes at 7 days	63.65	63.0	90	0.6
	62.46			
	62.88			
Cubes at 28days	68.72	70.1	100	1.4
	71.45			
	70.22			
Free at 28 days	59.51	60.3	86	1.3
	61.81			
	59.62			
Restrained	58.95	63.2	90	3.7
	64.98			
	65.68			
WC specimens	68.43	66.5	95	2.0
	64.45			
	66.55			

SD: standard deviation.

F.3.2 Mix NA40

Table F.2 Compressive strength of cubes and portions of prisms under WC, F and R conditions- mix NA40.

Type and time	Compressive strength MPa	Average	Normalized strength	SD
Cubes at 1 day	32.04	32.7	55	0.6
	32.98			
	33.09			
Cubes at 3 days	46.8	46.5	78	0.7
	45.65			
	46.99			
Cubes at 7 days	49.48	49.3	83	1.2
	50.38			
	48.01			
Cubes at 28days	59.43	59.4	100	0.3
	59.05			
	59.71			
Free at 28 days	50.42	51.5	87	1.0
	51.5			
	52.5			
Restrained	48.65	51.2	86	2.6
	51.1			
	53.76			
WC specimens	59.77	58.8	99	1.3
	57.4			
	59.31			

F.3.3 Mix NA50

Table F.3 Compressive strength of cubes and portions of prisms under WC, F and R conditions- mix NA50.

Type and time	Compressive strength Mpa	Average	Normalized strength	SD
Cubes at 1 day	20.12	20.6	41	0.5
	21.06			
	20.48			
Cubes at 3 day	33.49	33.8	67	0.3
	33.67			
	34.1			
Cubes at 7 day	39.62	39.6	79	0.3
	39.77			
	39.27			
Cubes at 28day	49.56	50.1	100	0.5
	50.06			
	50.57			
Free at 28 days	42.15	42.8	86	1.3
	44.27			
	42.02			
Restrained	41.85	43.0	86	1.2
	43.14			
	44.15			
WC specimens	48.28	49.7	99	1.8
	49.04			
	51.73			

F.4 Photographs

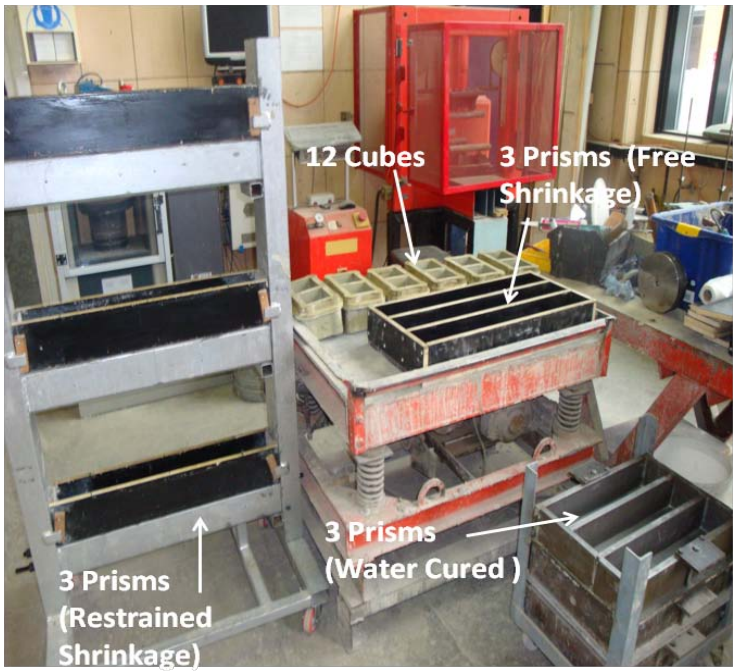

Figure F. 13 Types and number of moulds (used in this study) for each mix

Figure F. 14 Restraining frame just after concrete casting (mix NA50).

Figure F. 15 Monitoring concrete temperature using thermocouples (mix NA30).

Figure F. 16 Restrained specimens at the end of exposure time (Mix NA30).

Figure F. 17 Restrained specimens at the end of exposure time (Mix NA40).

Figure F. 18 Restrained specimens at the end of exposure time (Mix NA50).

Figure F. 19 Measure of free shrinkage using Demec gauages.

Figure F. 20 Demounting of restrained specimens (just before bending test).

Figure F. 21 Concrete prism during bending test using universal hydraulic machine and closed loop system (labview technique) .

Appendix G:

Experimental Results-Chapter 6

G.1 Free Shrinkage

G.1.1 Shrinkage strains measured on top (T), sides (S) and bottom (B) surfaces over 300 mm gauge length

G.1.1.1 Mixes with Natural Aggregate

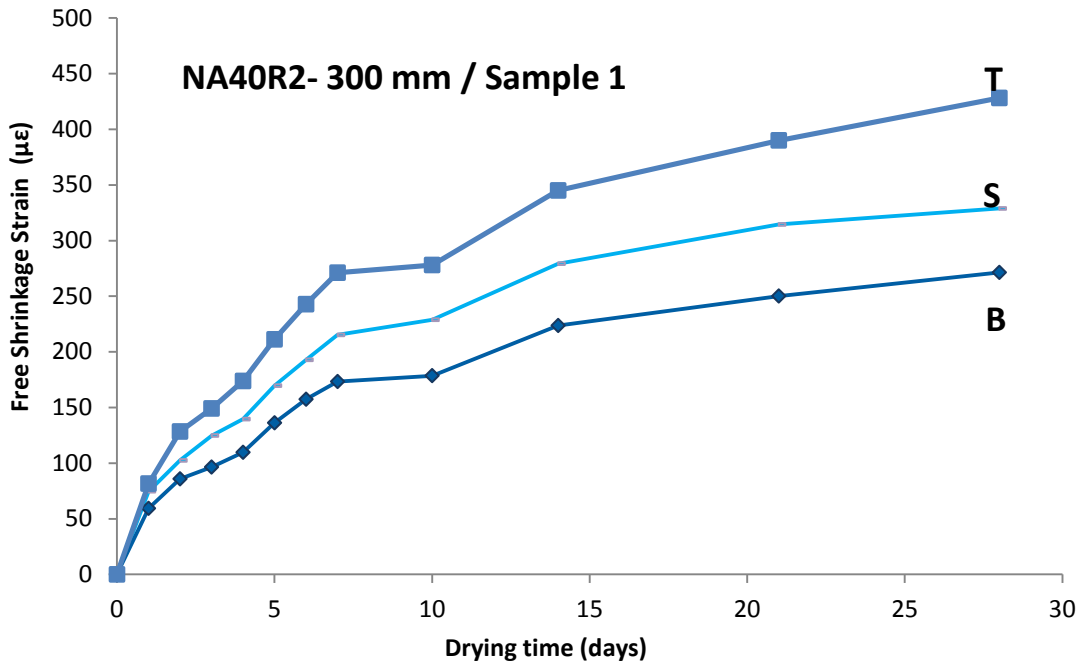

Figure G. 1 Shrinkage strains of mix NA40R2 /sample 1

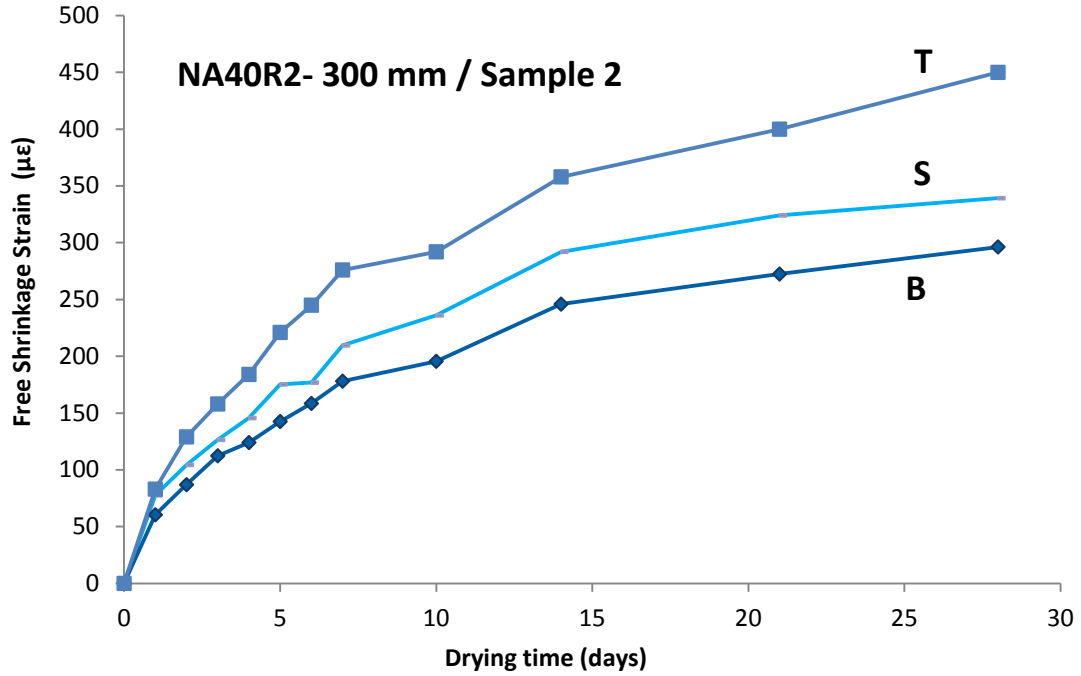

Figure G. 2 Shrinkage strains of mix NA40R2 /sample 2

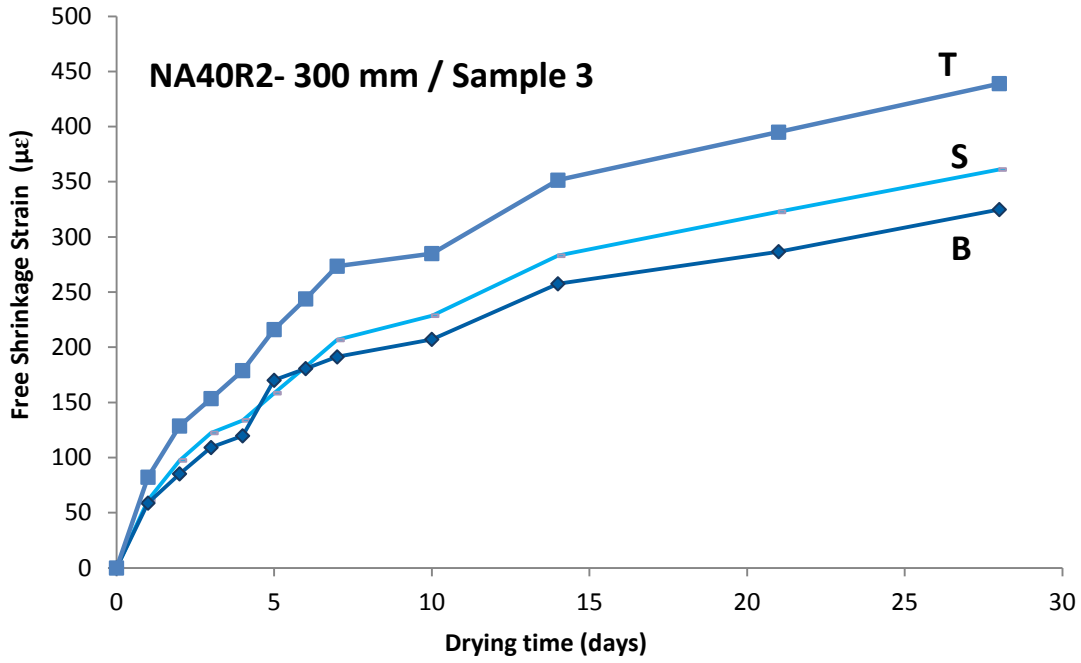

Figure G. 3 Shrinkage strains of mix NA40R2 /sample 3

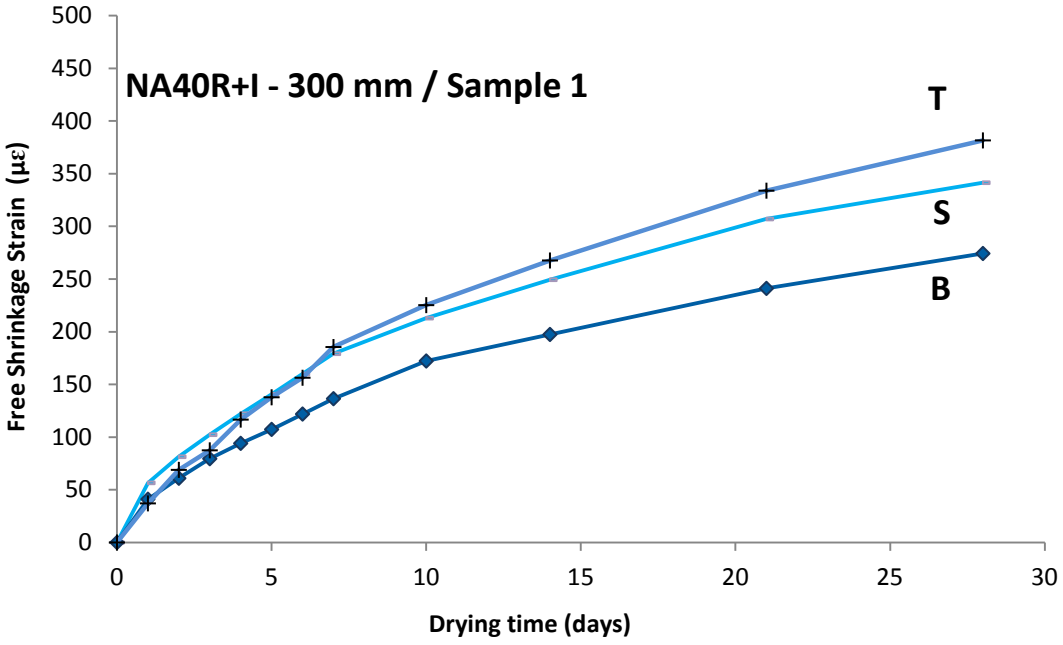

Figure G. 4 Shrinkage strains of mix NA40R+I /sample 1

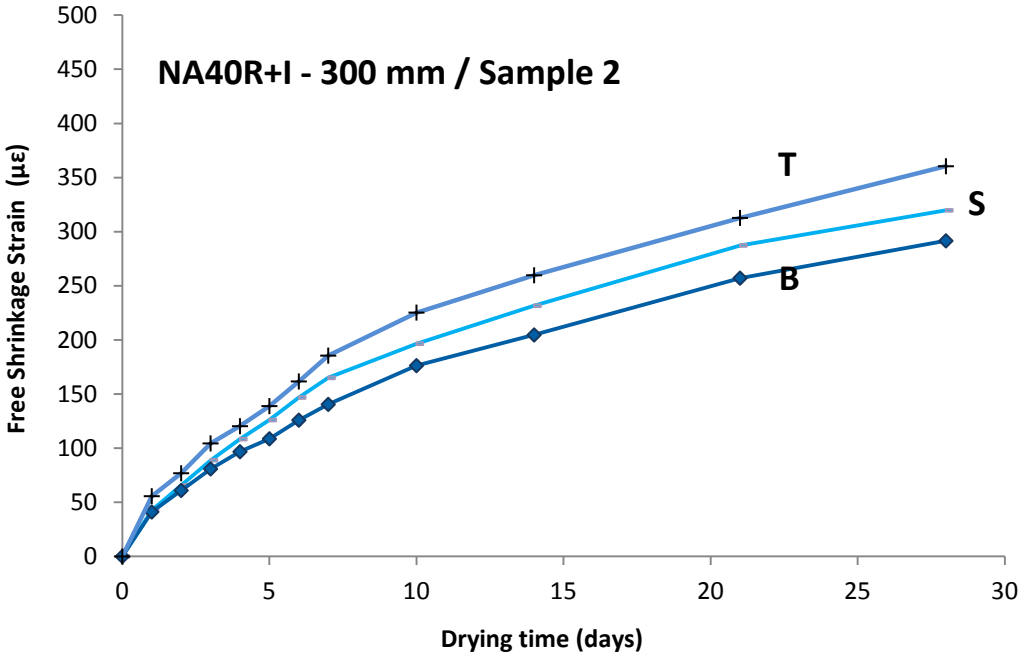

Figure G. 5 Shrinkage strains of mix NA40R+I /sample 2

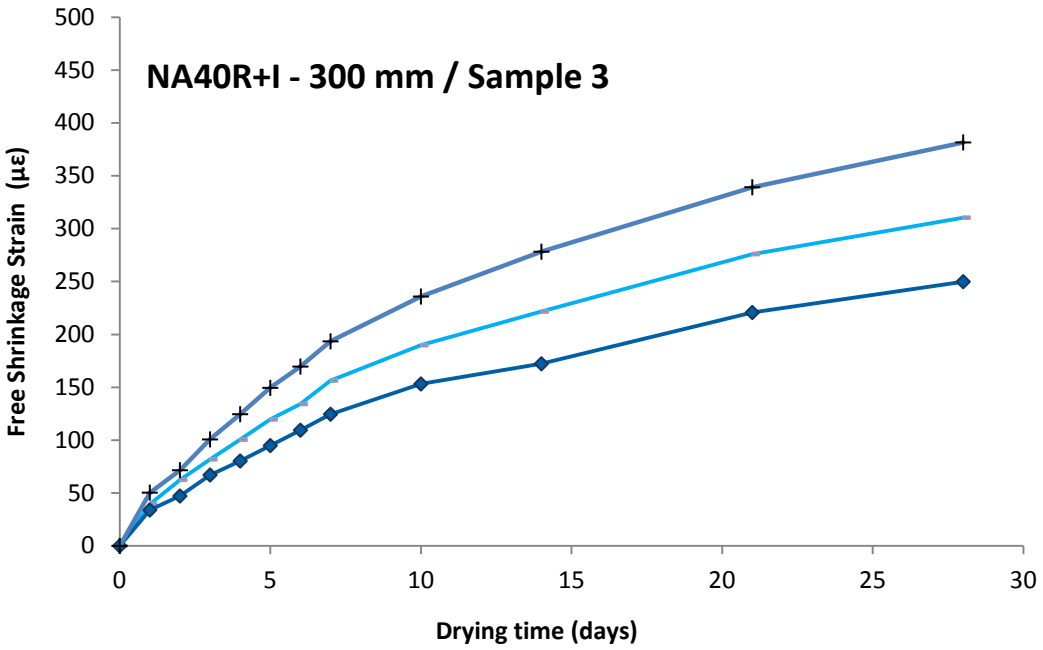

Figure G. 6 Shrinkage strains of mix NA40R+I /sample 3

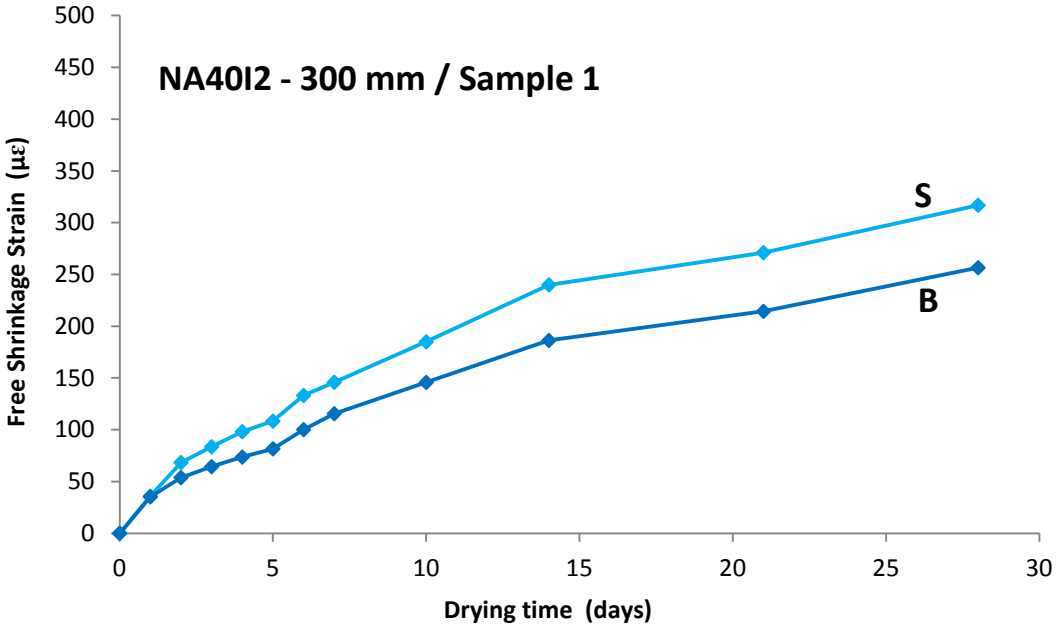

Figure G. 7 Shrinkage strains of mix NA40I2 /sample 1

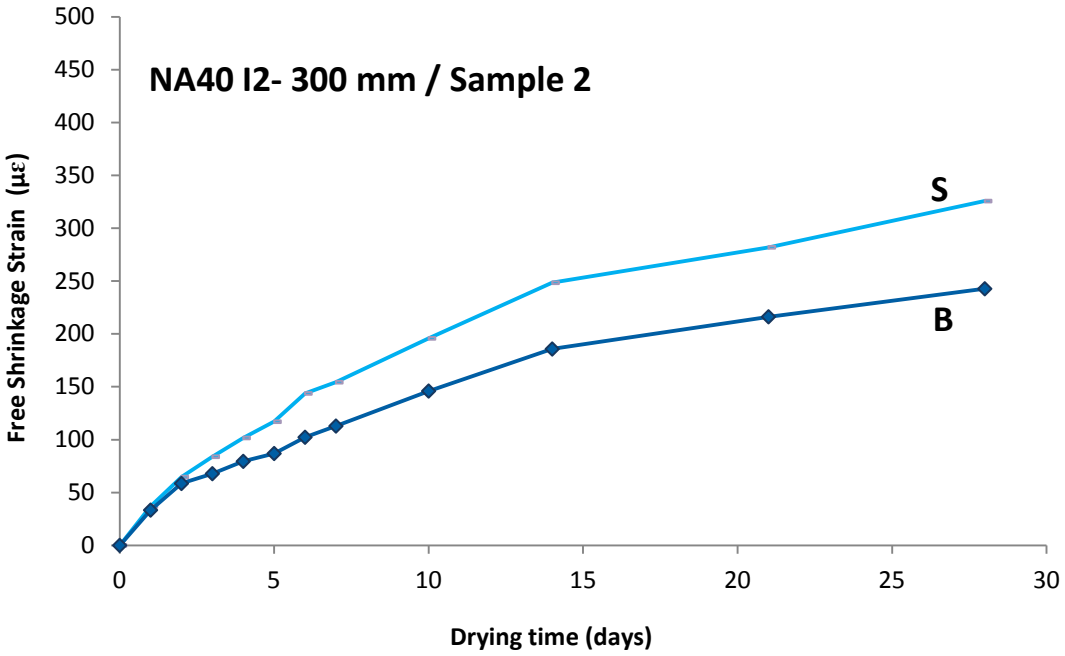

Figure G. 8 Shrinkage strains of mix NA40I2 /sample 2

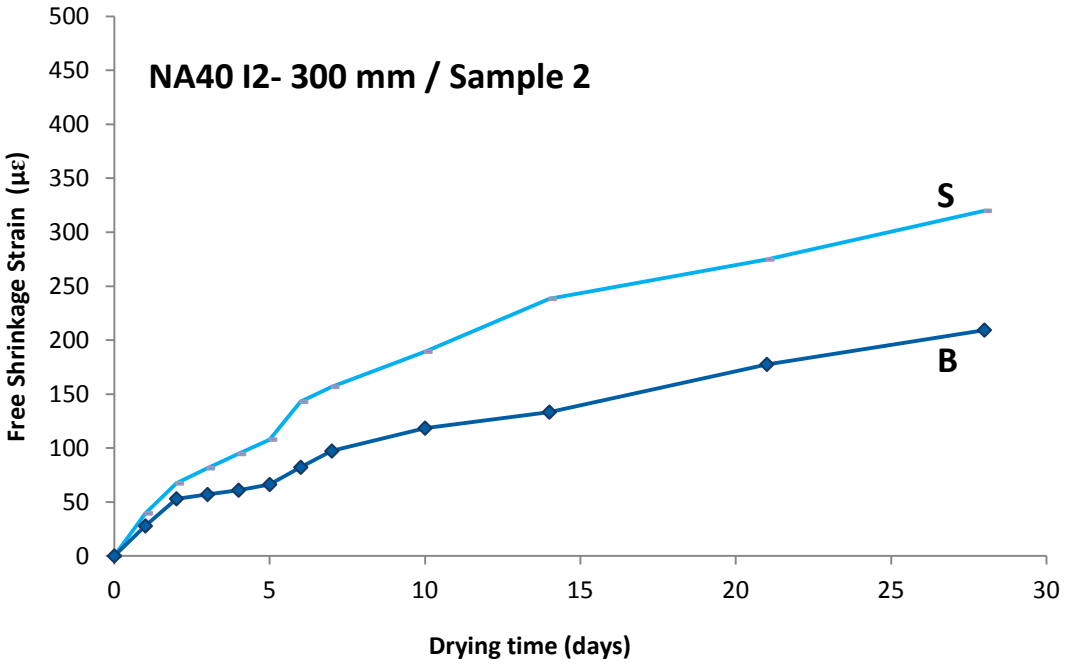

Figure G. 9 Shrinkage strains of mix NA40I2 /sample 3

G.1.1.2 Mixes with Recycled Aggregate

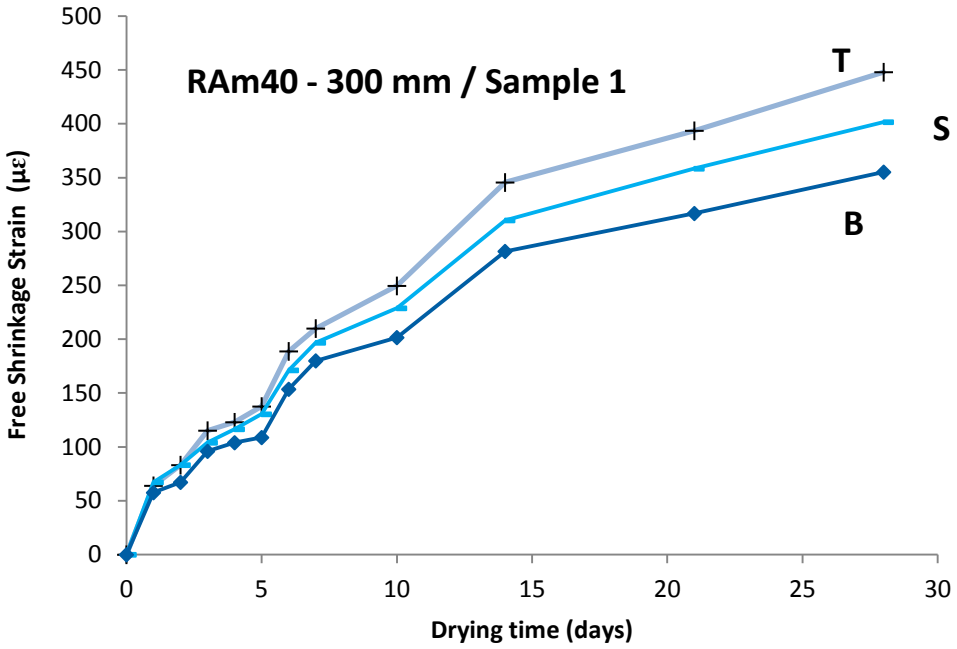

Figure G. 10 Shrinkage strains of mix RAm40 /sample 1

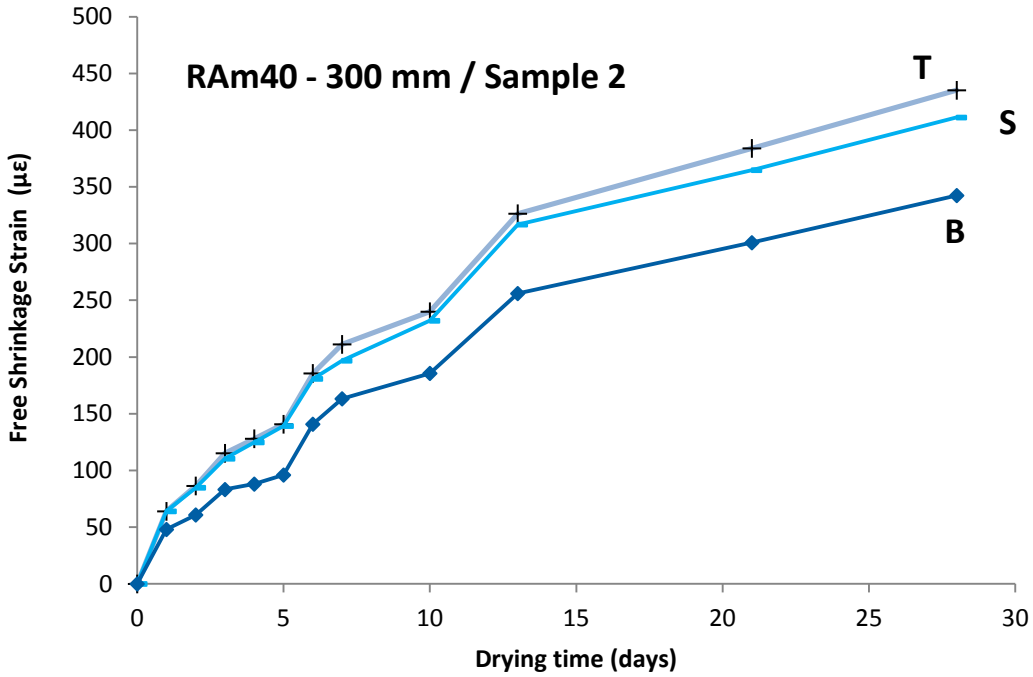

Figure G. 11 Shrinkage strains of mix RAm40 /sample 2

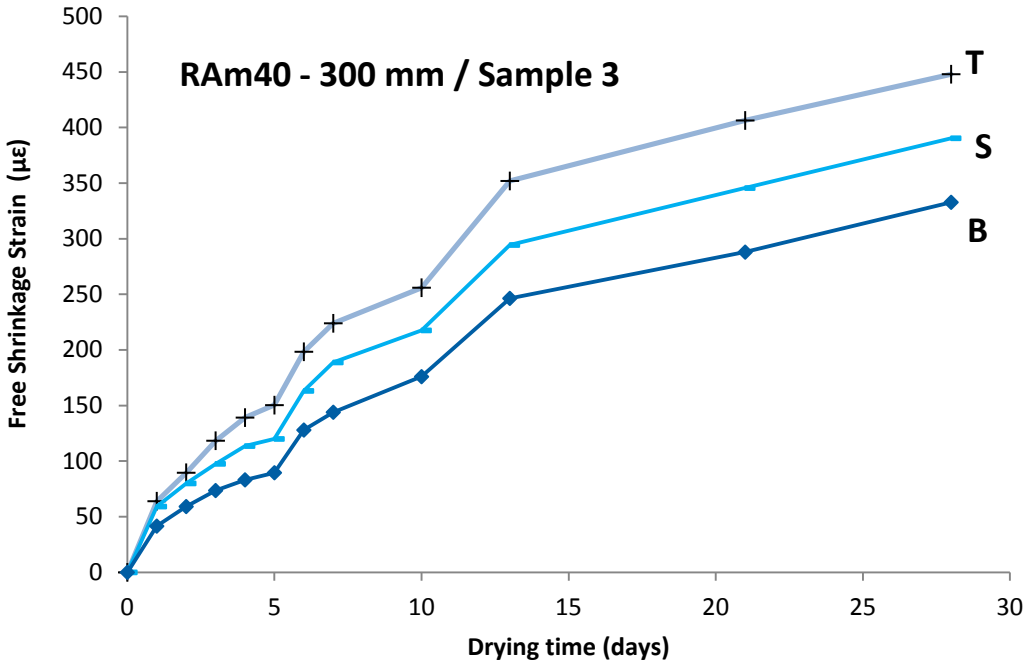

Figure G. 12 Shrinkage strains of mix RAm40 /sample 3

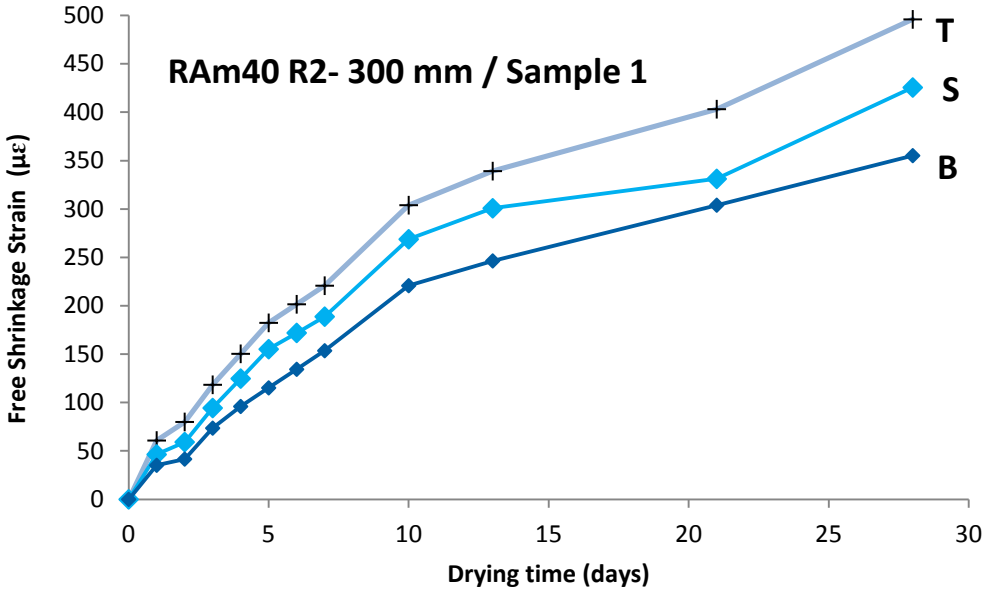

Figure G. 13 Shrinkage strains of mix RAm40R2 /sample 1

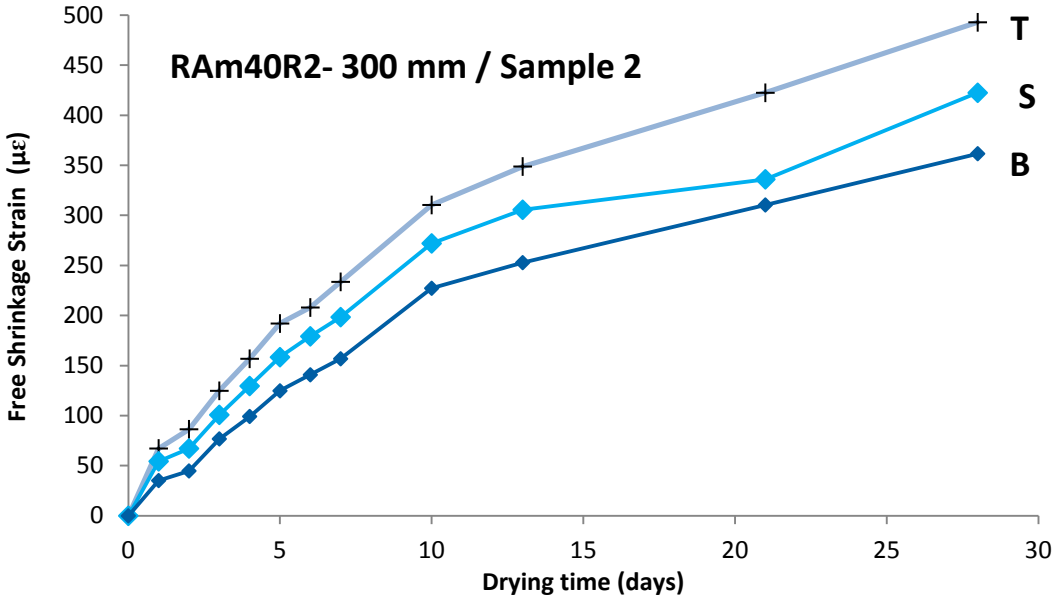

Figure G. 14 Shrinkage strains of mix RAm40R2 /sample 2

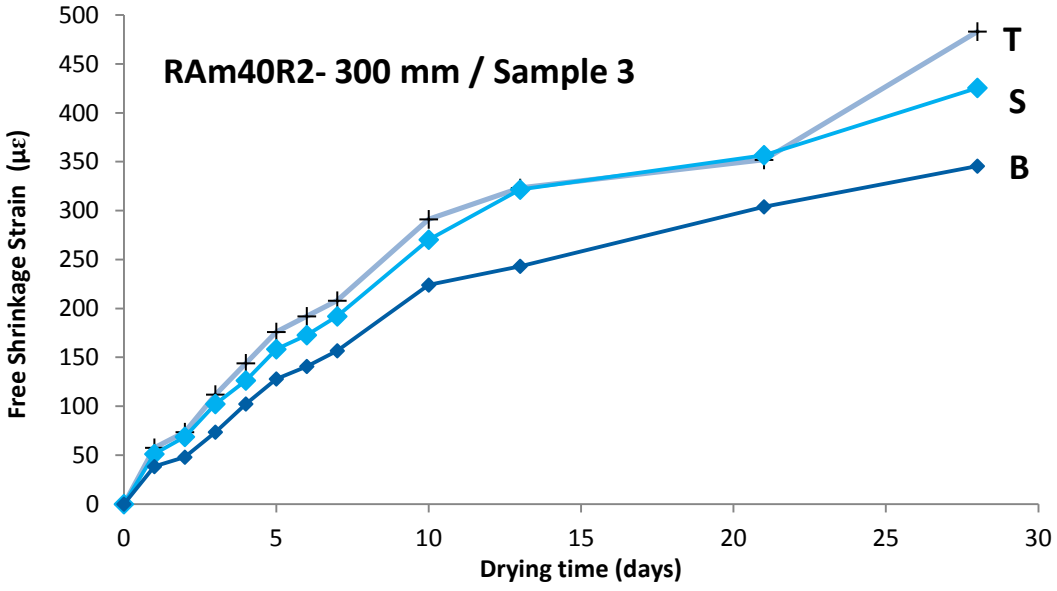

Figure G. 15 Shrinkage strains of mix RAm40R2 /sample 3

G.2 Restrained Shrinkage

In this section the shrinkage strains measured on the top and sides surfaces of the restrained specimens :top (T), middle (M) and bottom (B) are presented.

G.2.1 Strains- Mixes with Natural Aggregate

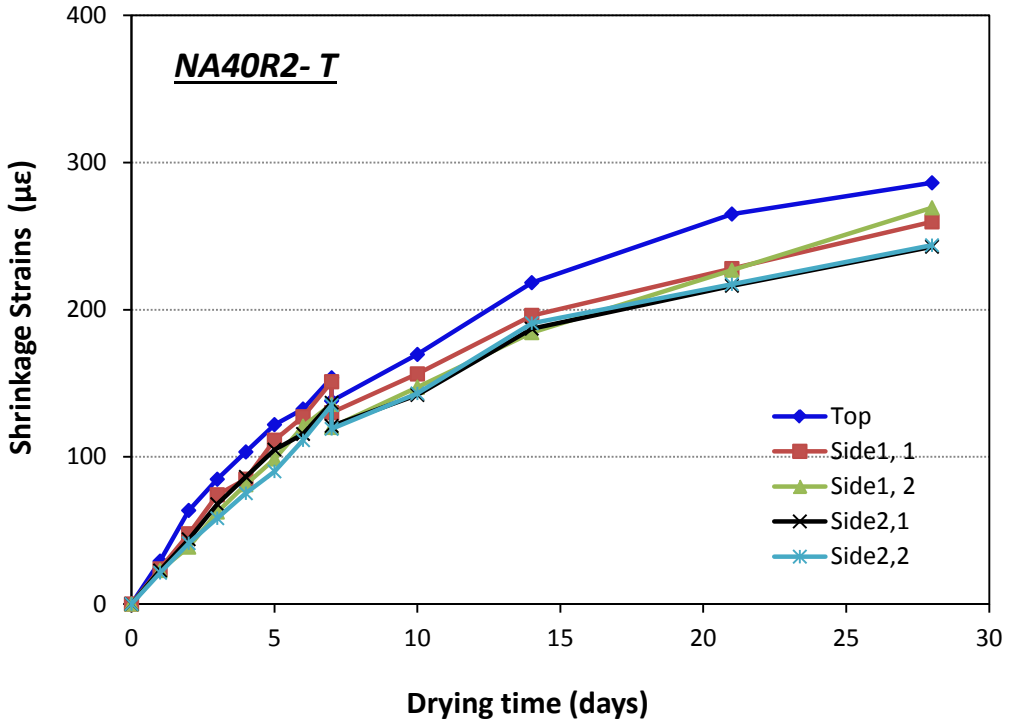

Figure G. 16 Apparent RF of mix NA40R2 /Top specimen

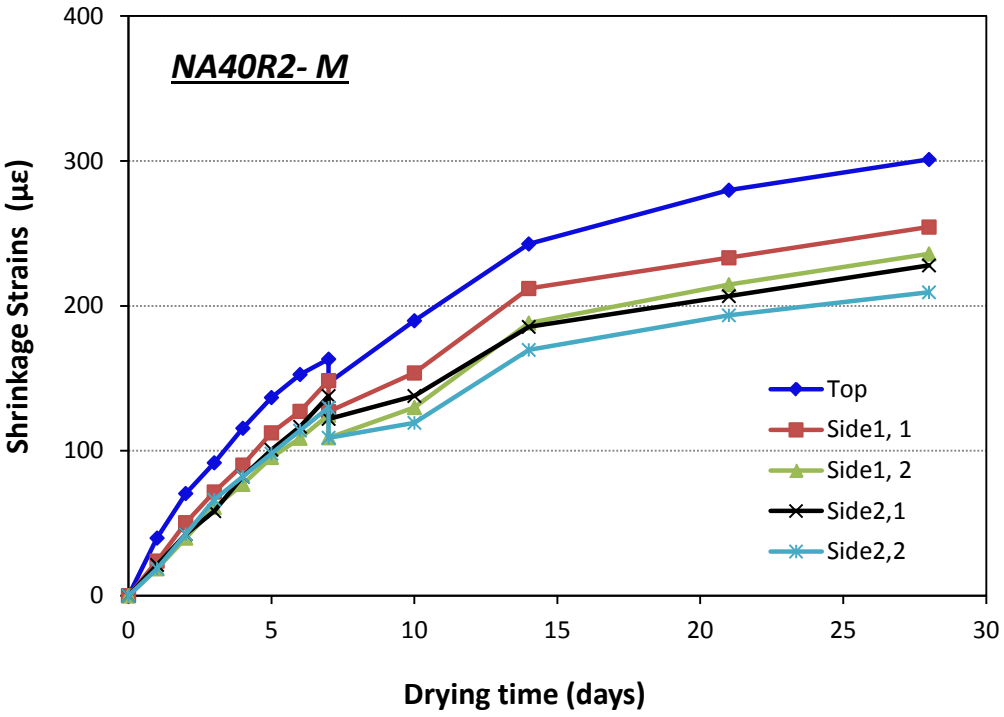

Figure G. 17 Apparent RF of mix NA40R2 /Middle specimen

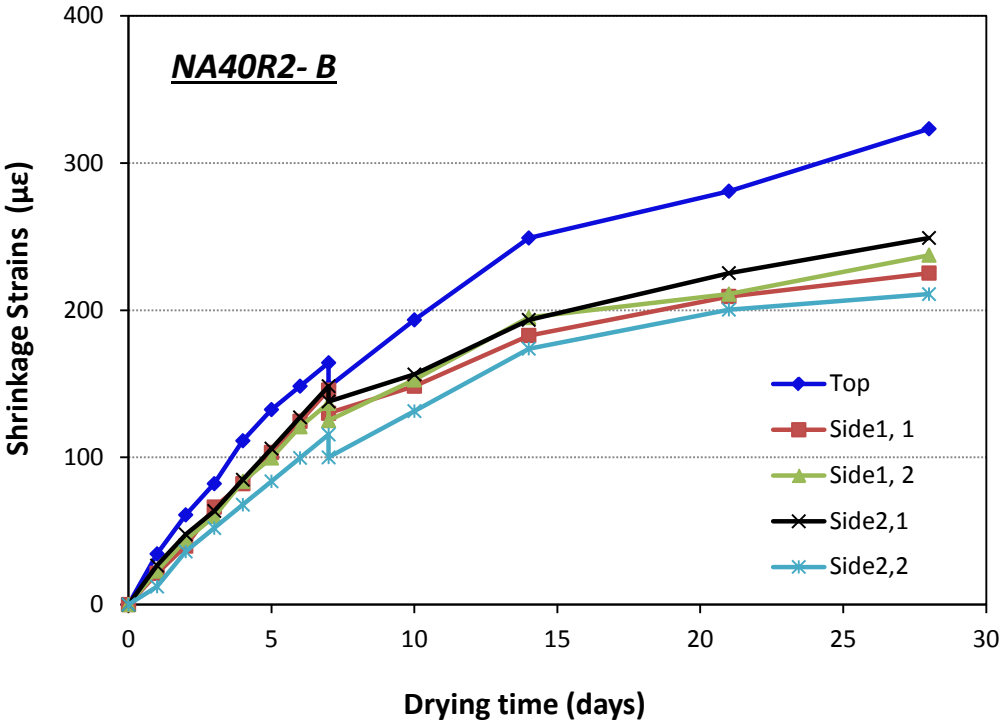

Figure G. 18 Apparent RF of mix NA40R2 /Bottom specimen

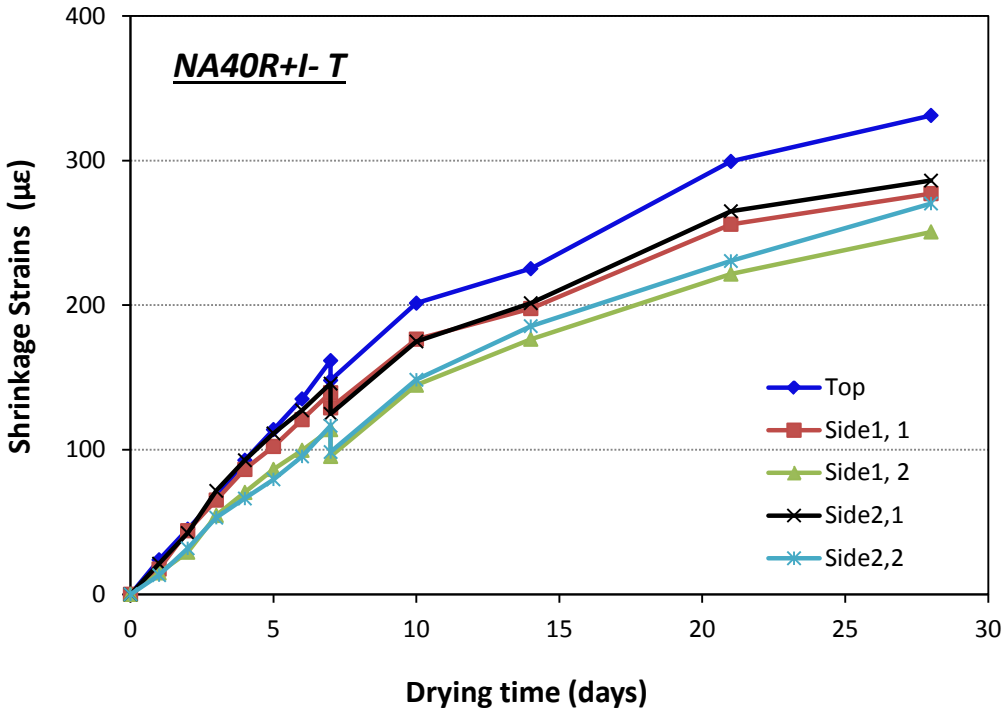

Figure G. 19 Shrinkage strains of mix NA40R+I /Top specimen

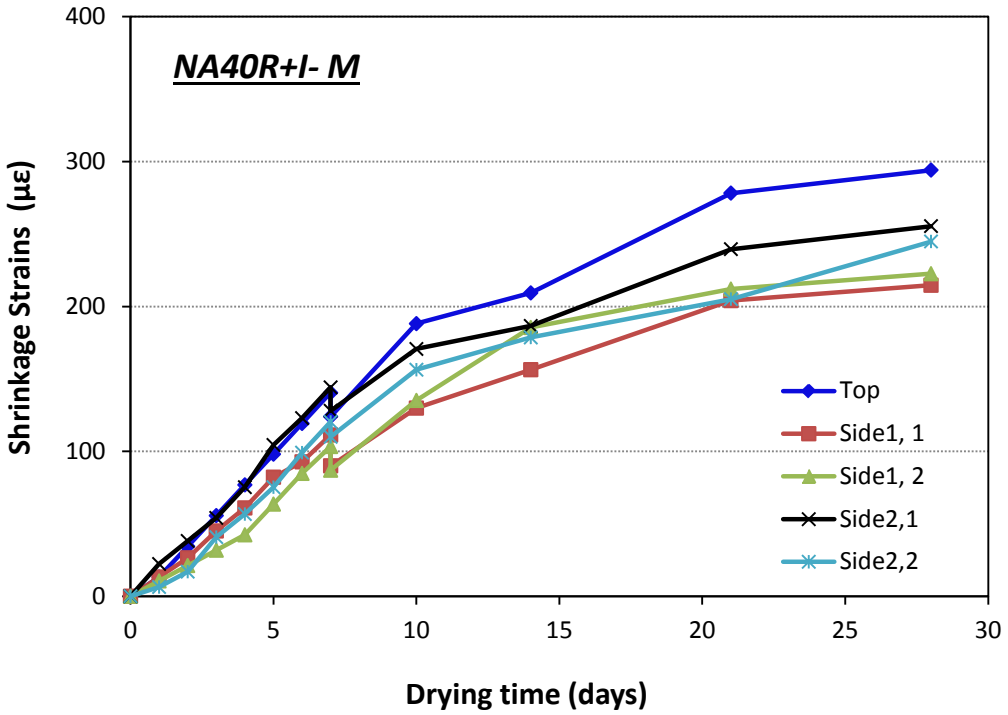

Figure G. 20 Apparent RF of mix NA40R+I /Middle specimen

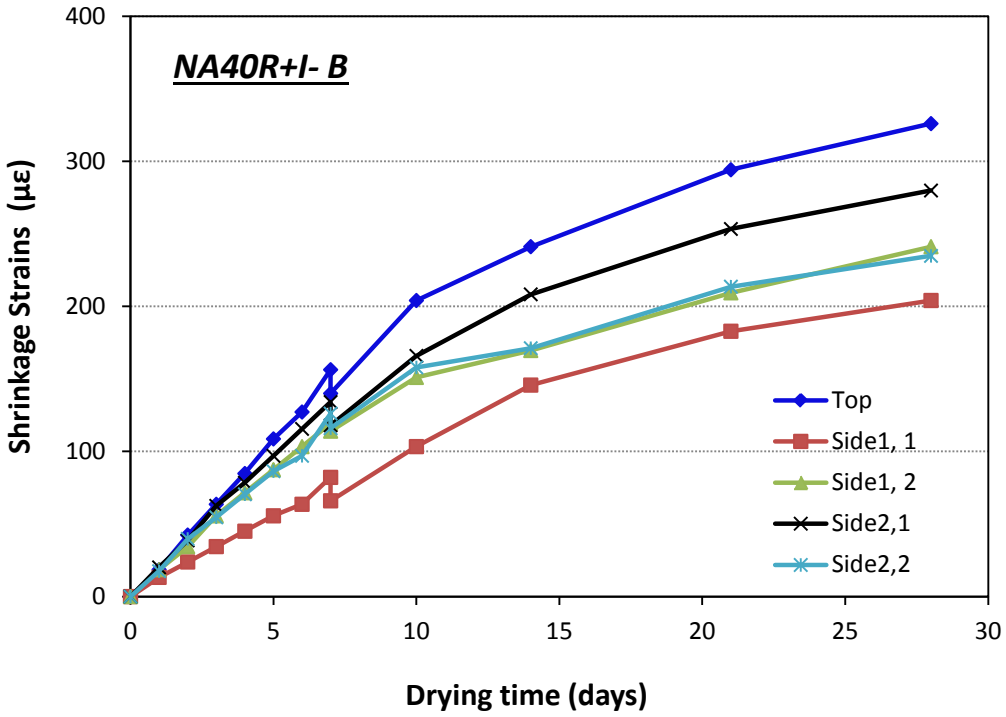

Figure G. 21 Apparent RF of mix NA40R+I /Bottom specimen

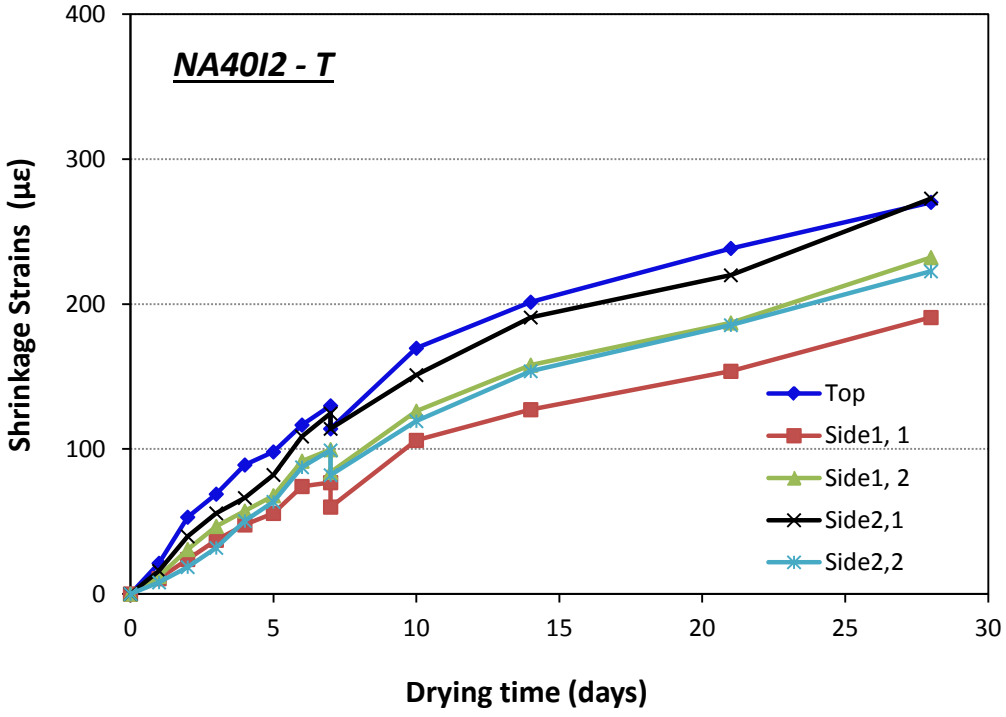

Figure G. 22 Apparent RF of mix NA40I2 /Top specimen

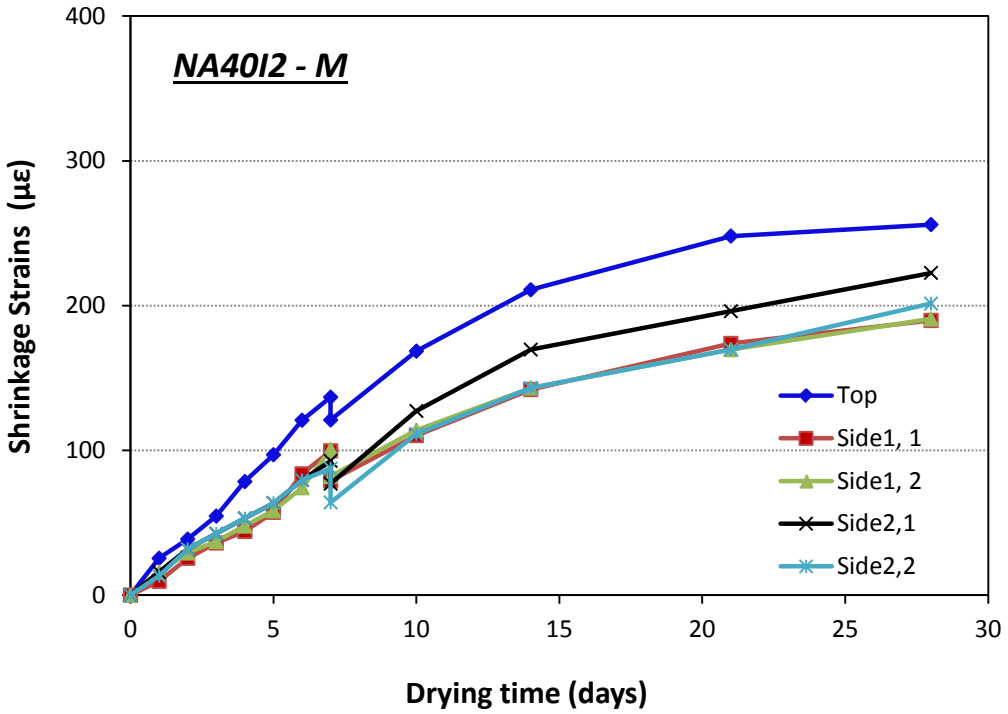

Figure G. 23 Apparent RF of mix NA40I2 /Middle specimen

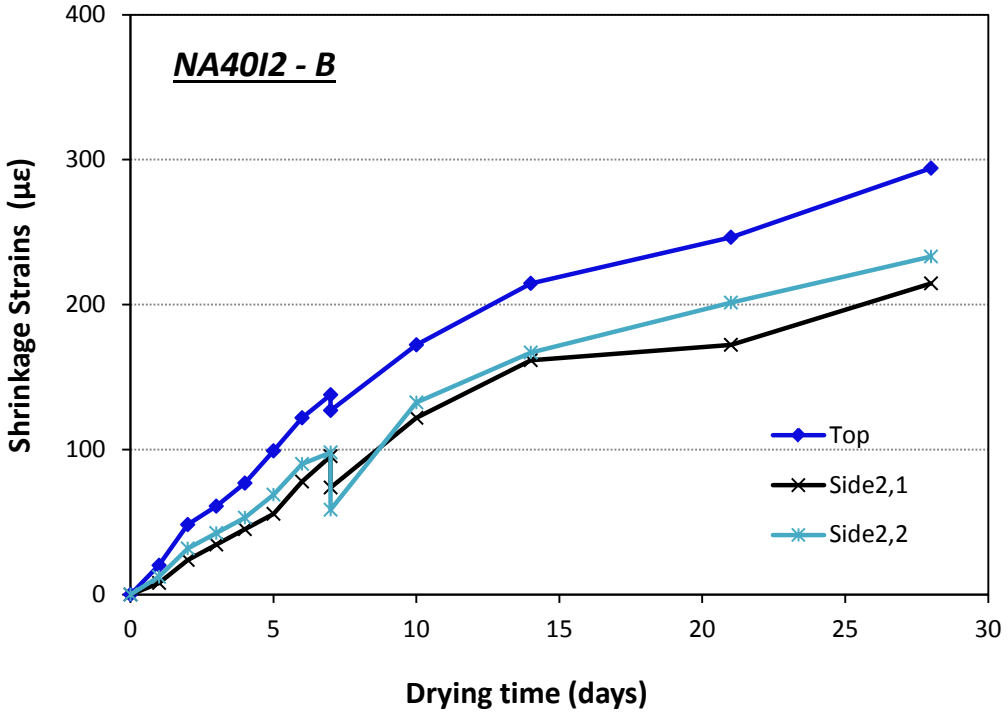

Figure G. 24 Apparent RF of mix NA40I2 /Bottom specimen

G.2.2 Strains- Mixes with Recycled Aggregate

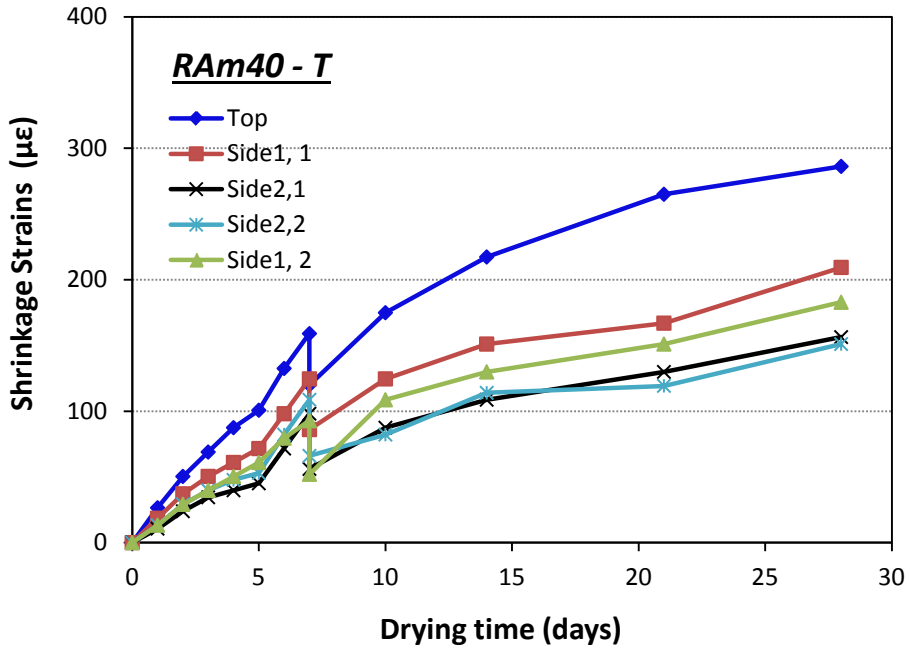

Figure G. 25 Apparent RF of mix RAm40 /Top specimen

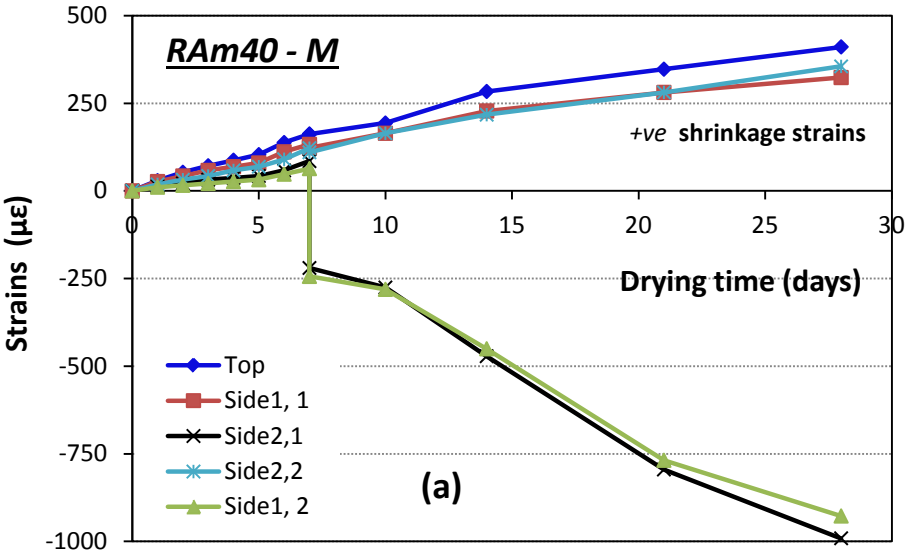

Figure G. 26 Apparent RF of mix RAm40 /Middle specimen

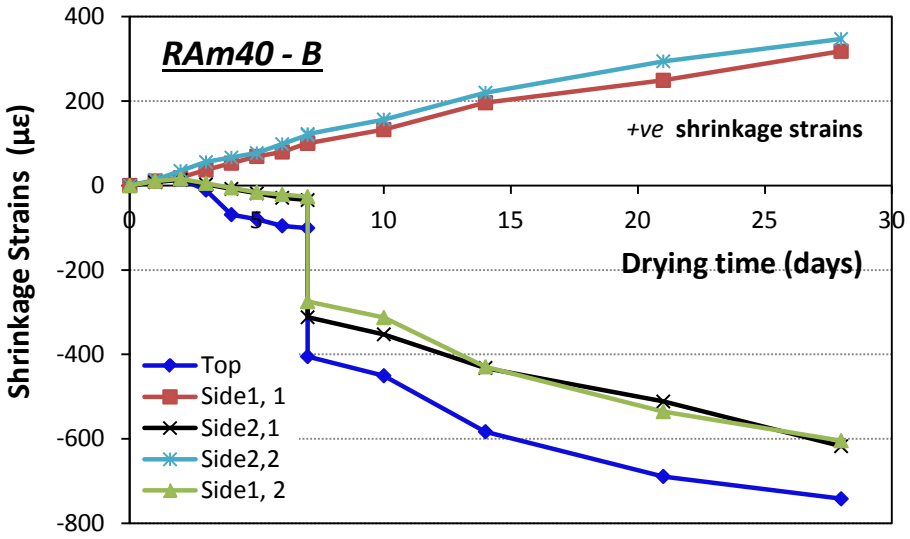

Figure G. 27 Apparent RF of mix RAm40 /Bottom specimen

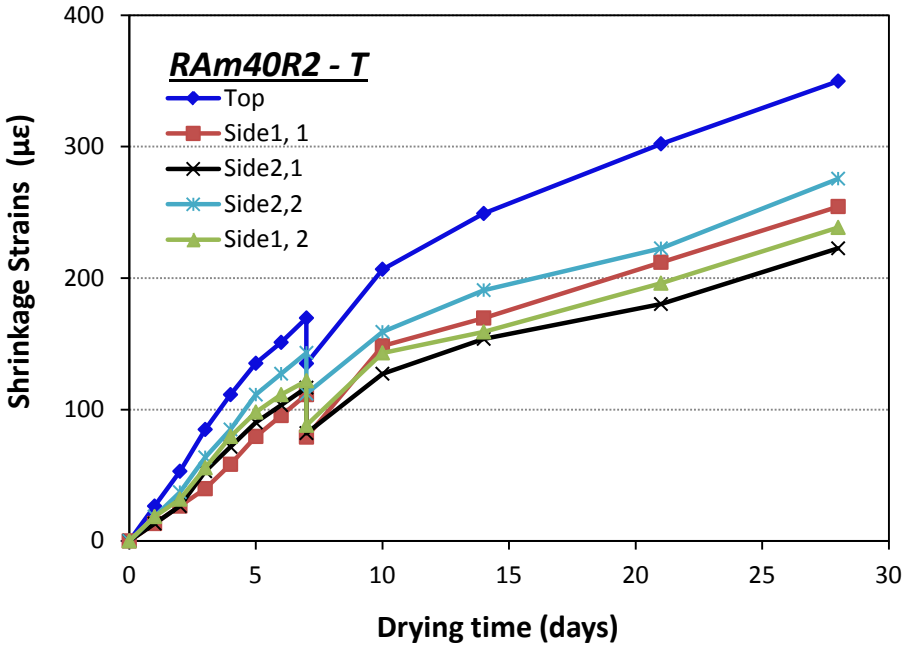

Figure G. 28 Apparent RF of mix RAm40R2 /Top specimen

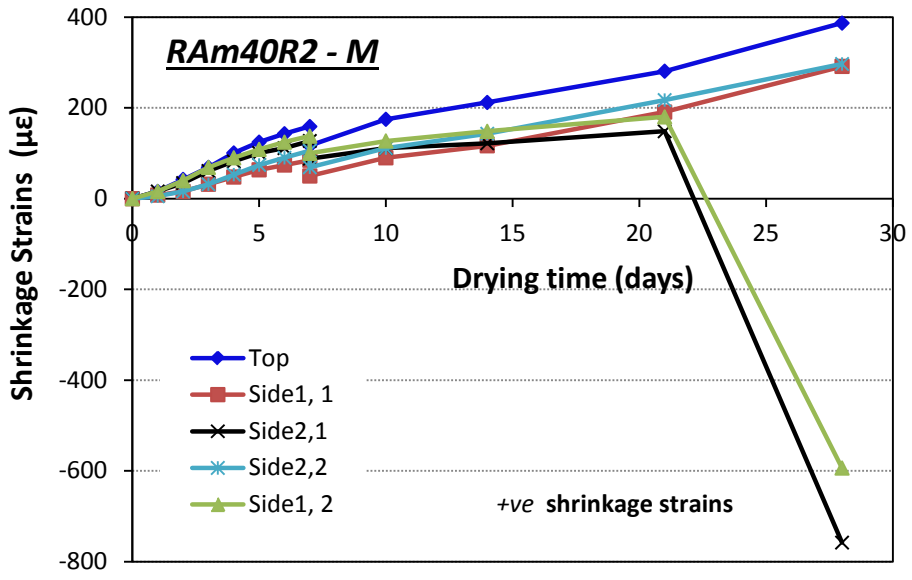

Figure G. 29 Shrinkage strains of mix RAm40R2 /Middle specimen

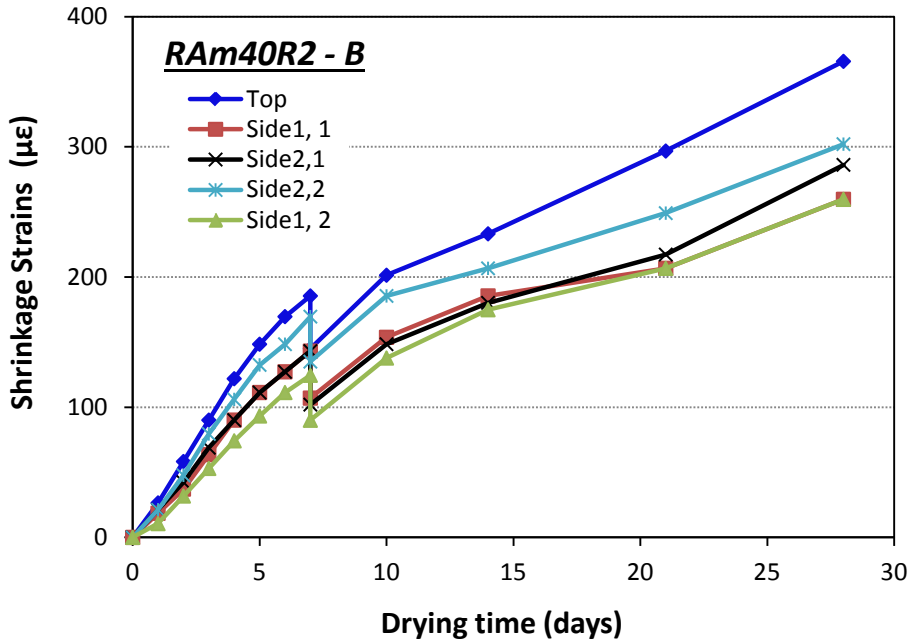

Figure G. 30 Apparent RF of mix RAm40R2 /Bottom specimen

G.3 Apparent Restraint Factor (RF)

G.3.1 Apparent RF for Mixes with Natural Aggregate

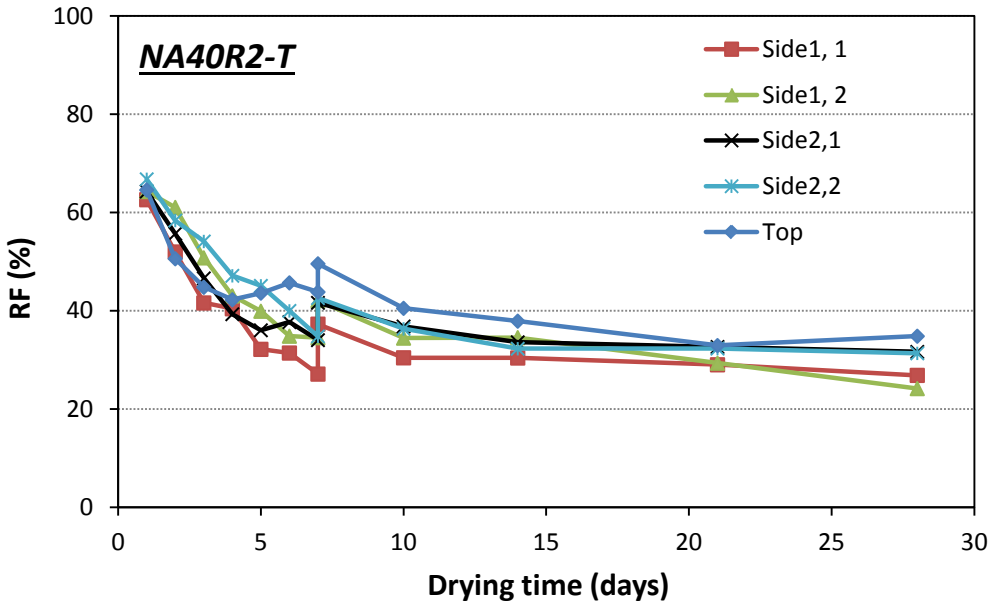

Figure G. 31 Apparent RF of mix NA40R2 /Top specimen

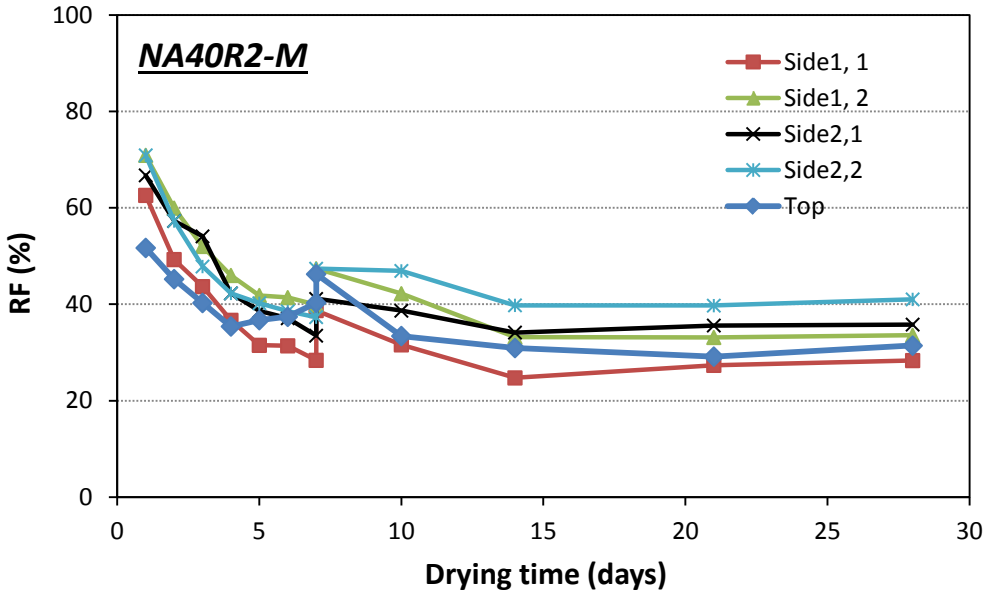

Figure G. 32 Apparent RF of mix NA40R2 /Middle specimen

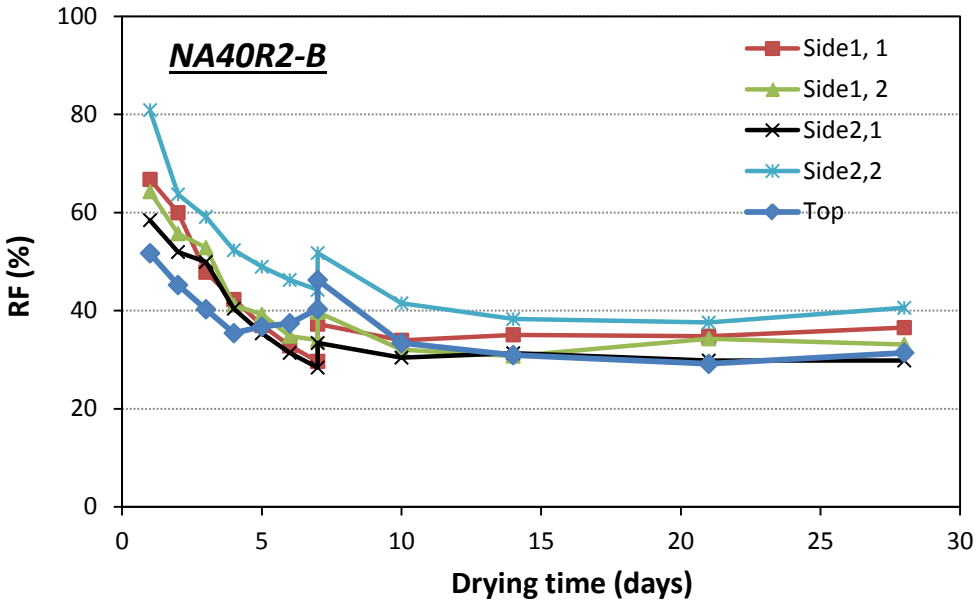

Figure G. 33 Shrinkage strains of mix NA40R2 /Bottom specimen

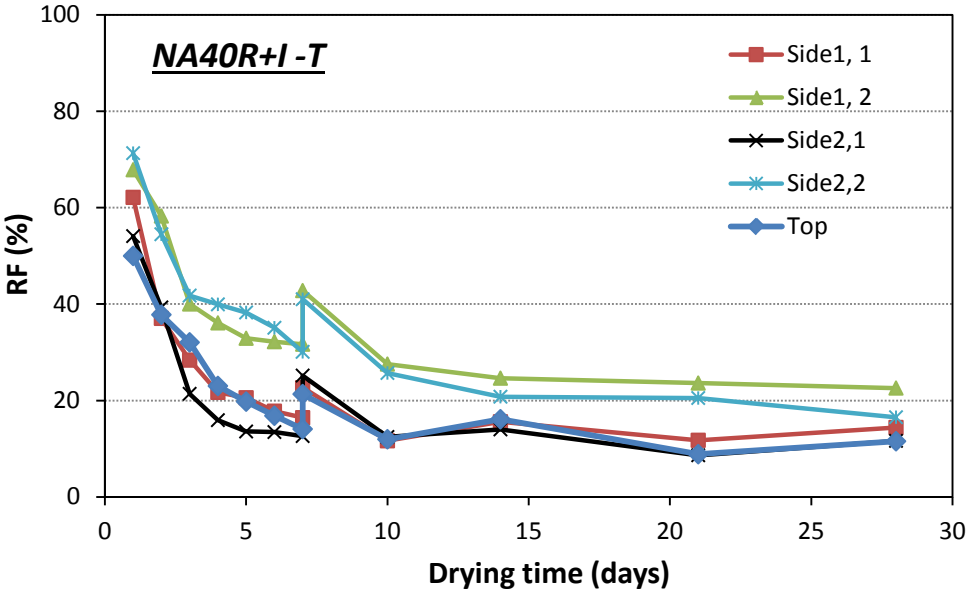

Figure G. 34 Apparent RF of mix NA40R+I /Top specimen

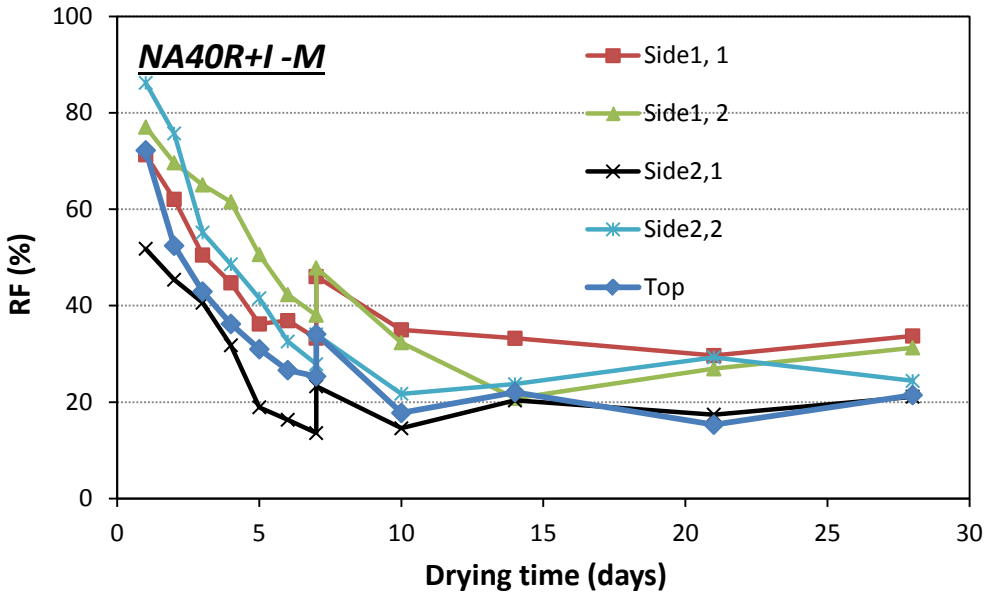

Figure G. 35 Apparent RF of mix NA40R+I /Middle specimen

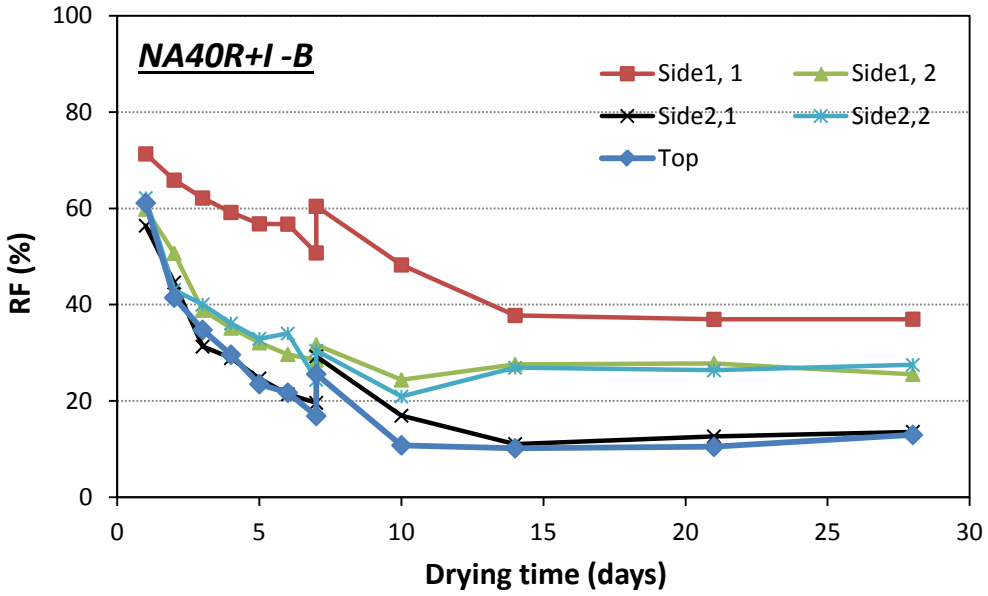

Figure G. 36 Apparent RF of mix NA40R+I /Bottom specimen

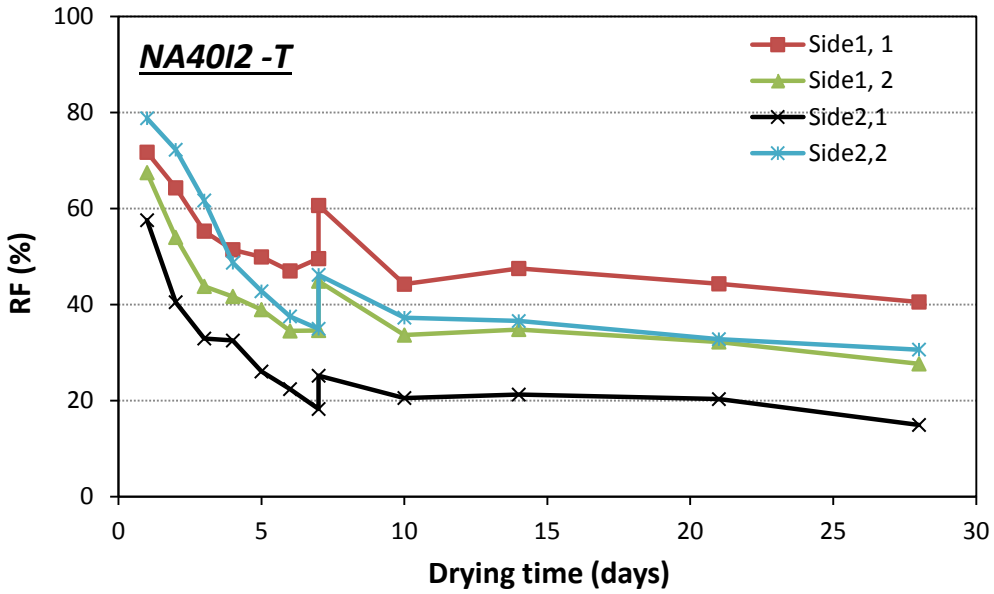

Figure G. 37 Apparent RF of mix NA40I2 /Top specimen

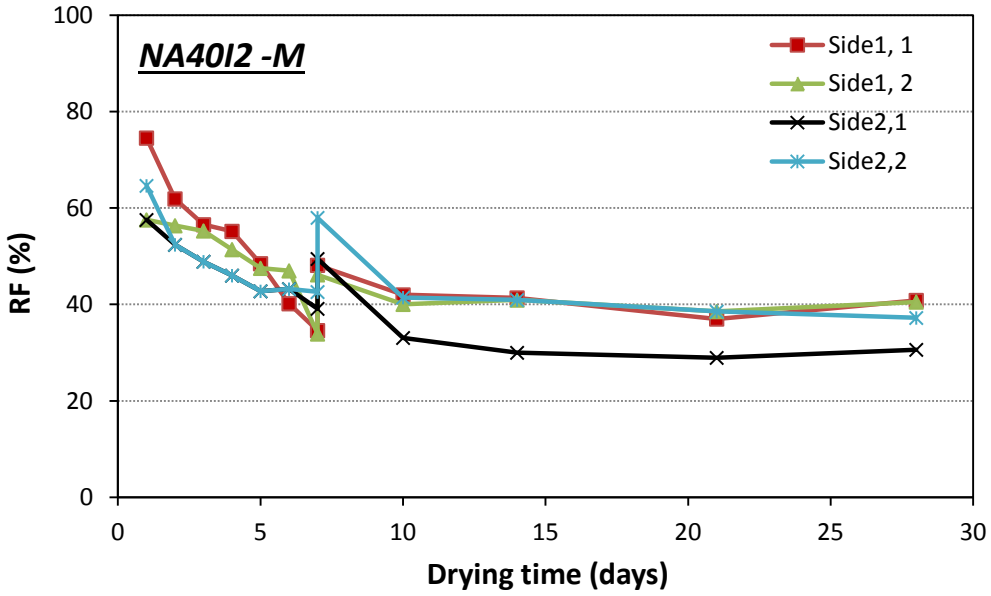

Figure G. 38 Apparent RF of mix NA40I2 /Middle specimen

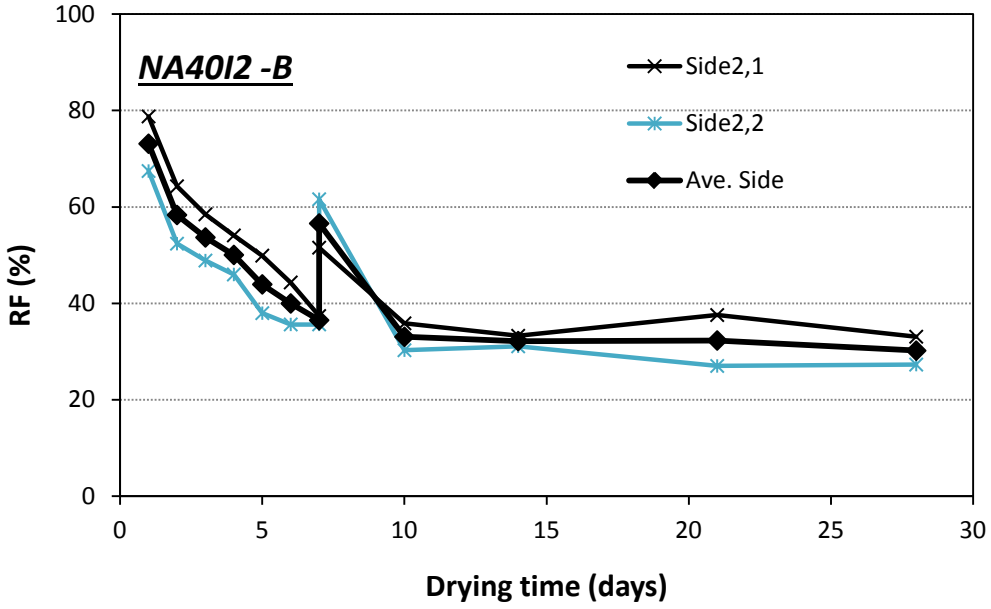

Figure G. 39 Shrinkage strains of mix NA40I2 /Bottom specimen

G.3.2 Apparent RF for Mixes with Recycled Aggregate

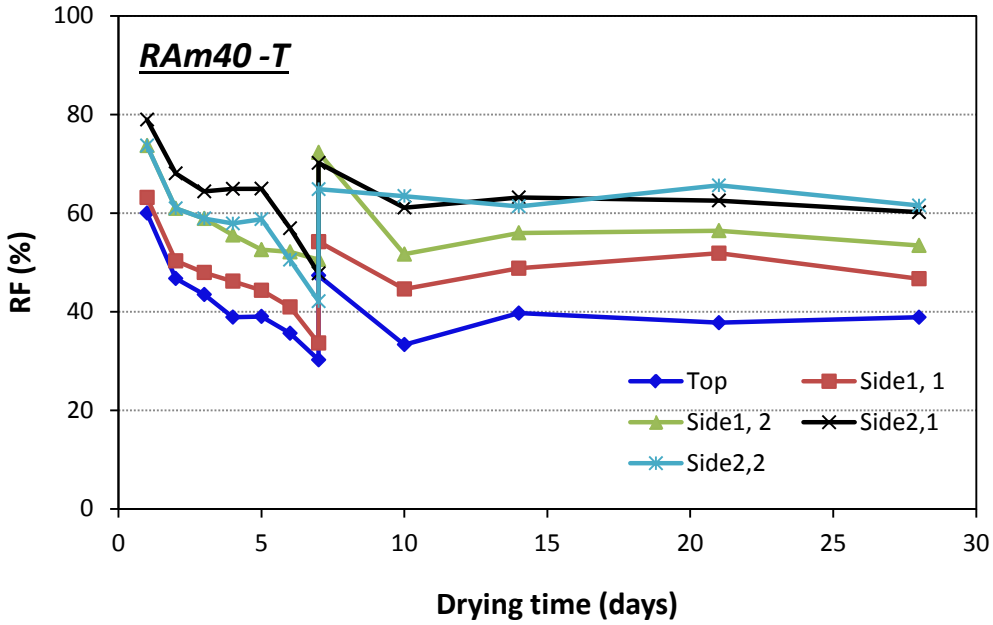

Figure G. 40 Apparent RF of mix RAm40 /Top specimen

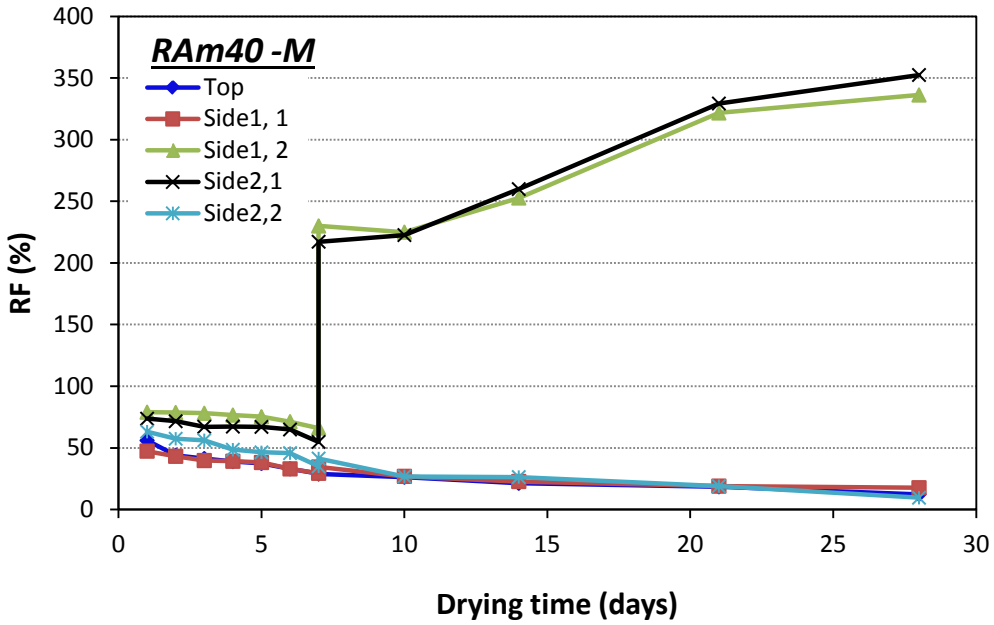

Figure G. 41 Apparent RF of mix RAm40 /Middle specimen

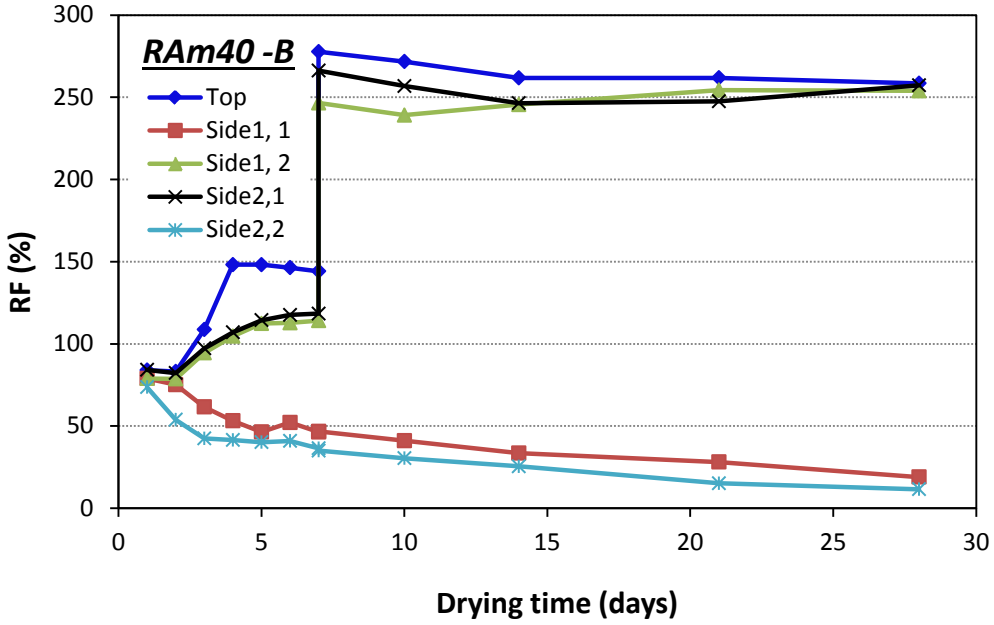

Figure G. 42 Apparent RF of mix RAm40 /Bottom specimen

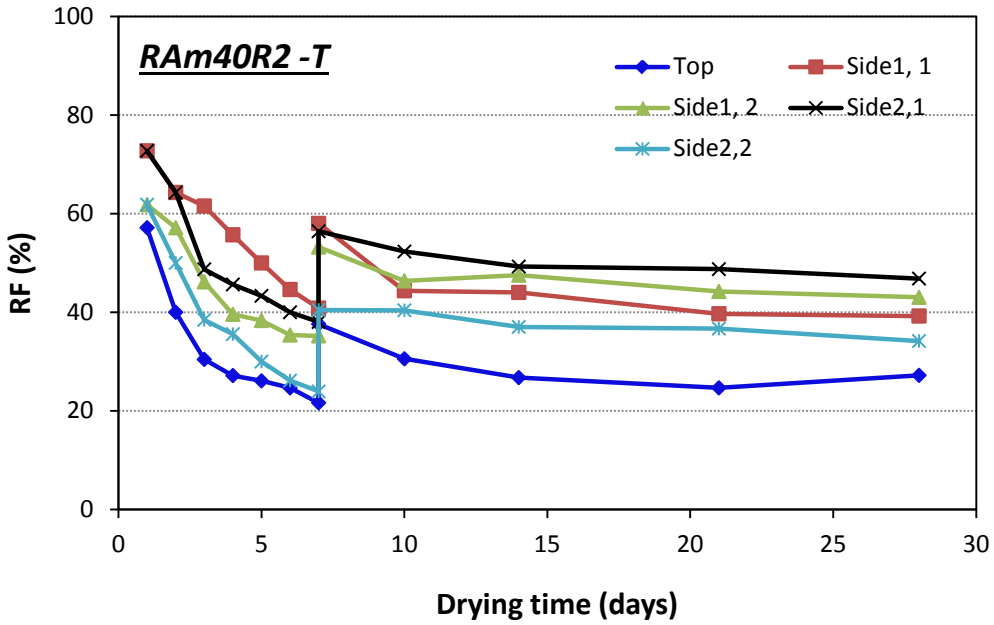

Figure G. 43 Apparent RF of mix RAm40R2 /Top specimen

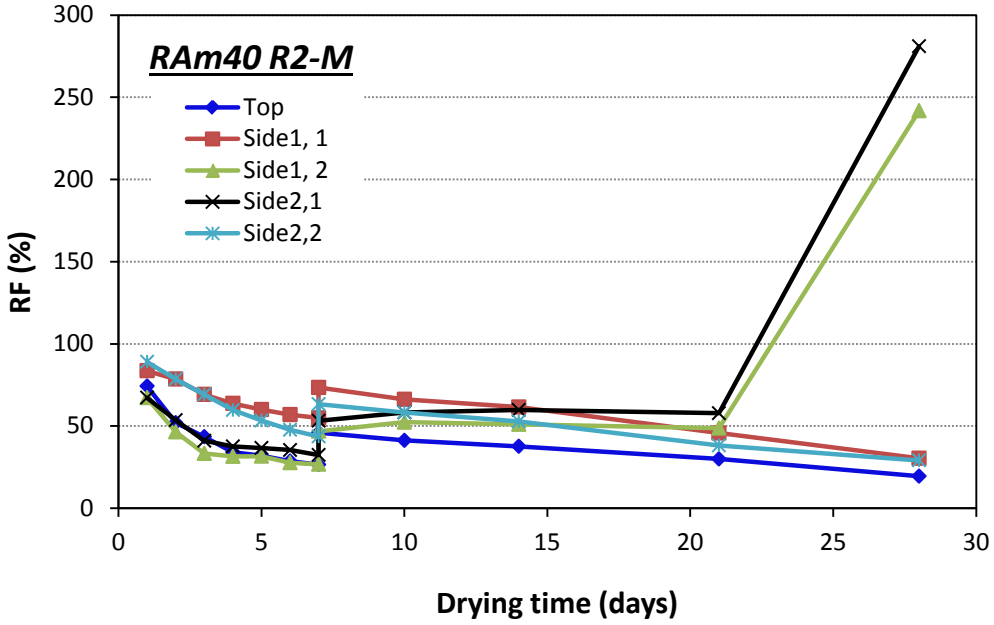

Figure G. 44 Apparent RF of mix RAm40R2 /Middle specimen

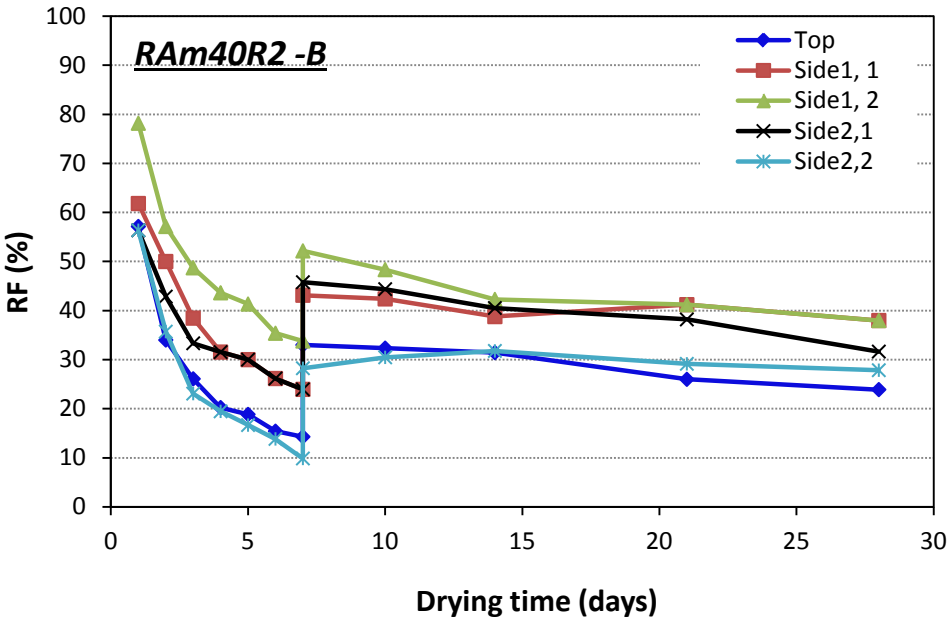

Figure G. 45 Apparent RF of mix RAm40R2 /Bottom specimen

G.4 Estimated Restraint Factor

In this section the Estimated (theoretical) RF of the restrained specimns Top (T), Middle (M) and Bottom (B) are presented .

G.4.1 Estimated RF for Mixes with Natural Aggregate

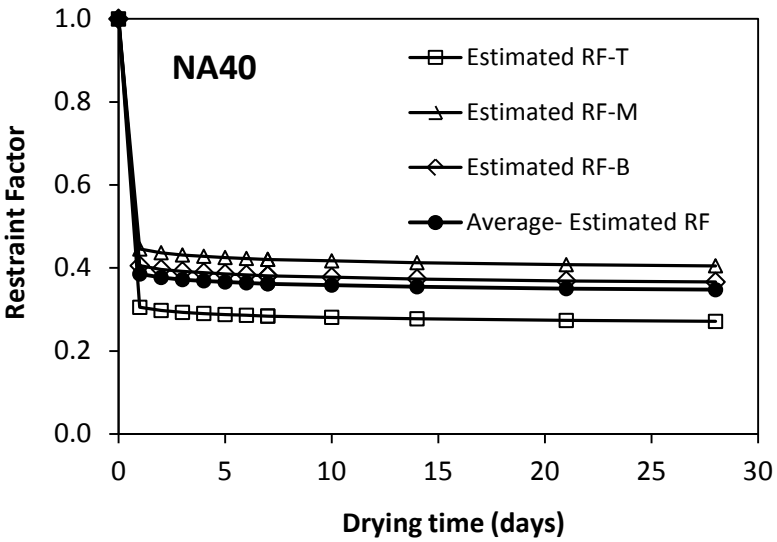

Figure G. 46 Estimated RF of T, M and B specimens - NA40.

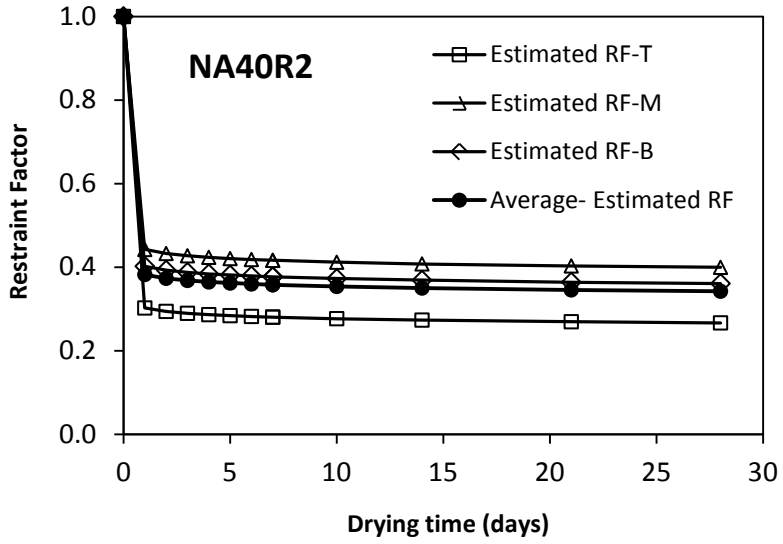

Figure G. 47 Estimated RF of T, M and B specimens - NA40R2.

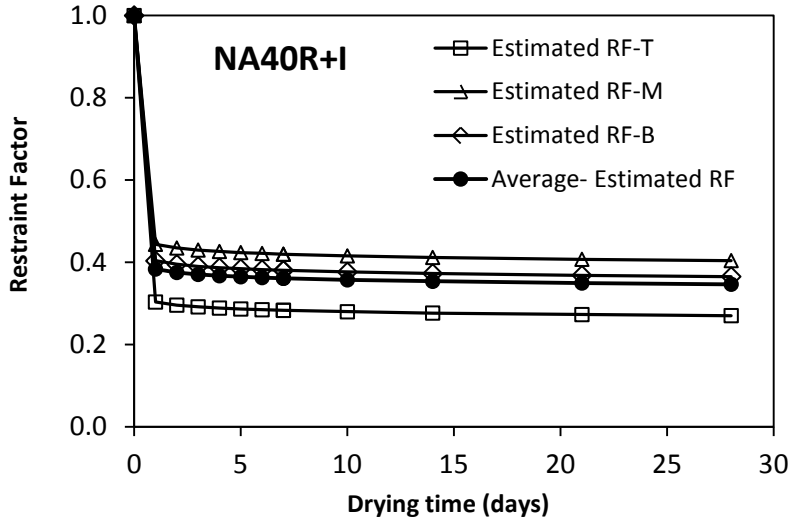

Figure G. 48 Estimated RF of T, M and B specimens - NA40R+I.

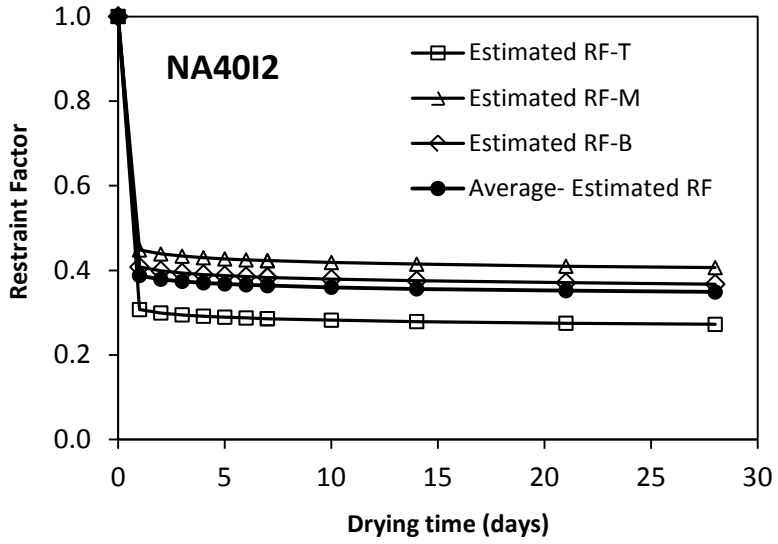

Figure G. 49 Estimated RF of T, M and B specimens - NA40I2.

G.4.2 Estimated RF for Mixes with Recycled Aggregate

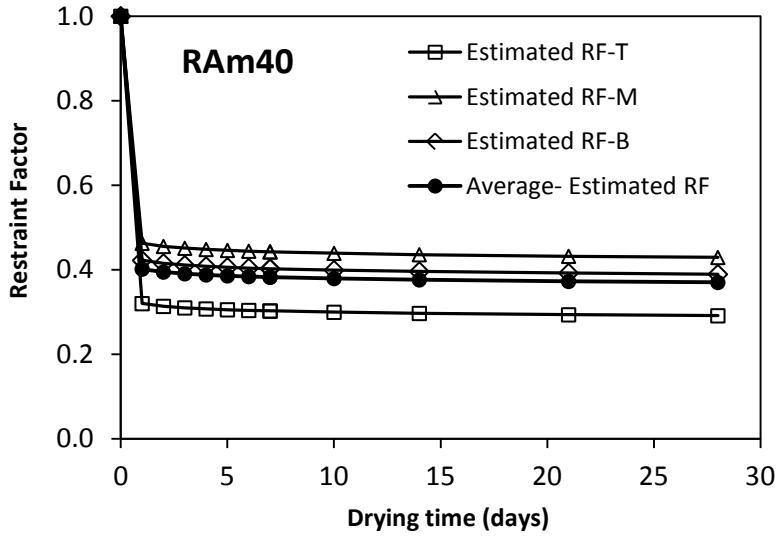

Figure G. 50 Estimated RF of T, M and B specimens - RAm40.

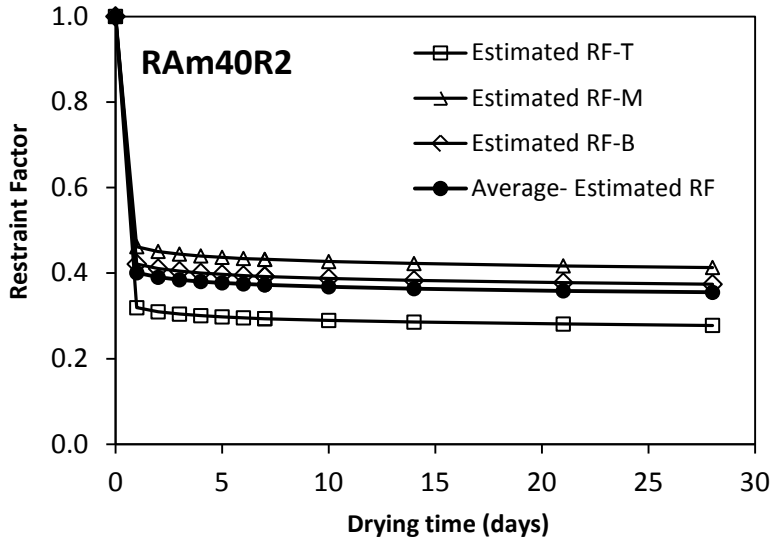

Figure G. 51 Estimated RF of T, M and B specimens - RAm40R2.

G.5 Load -deflection curves

G.5.1 Mixes with Natural Aggregate

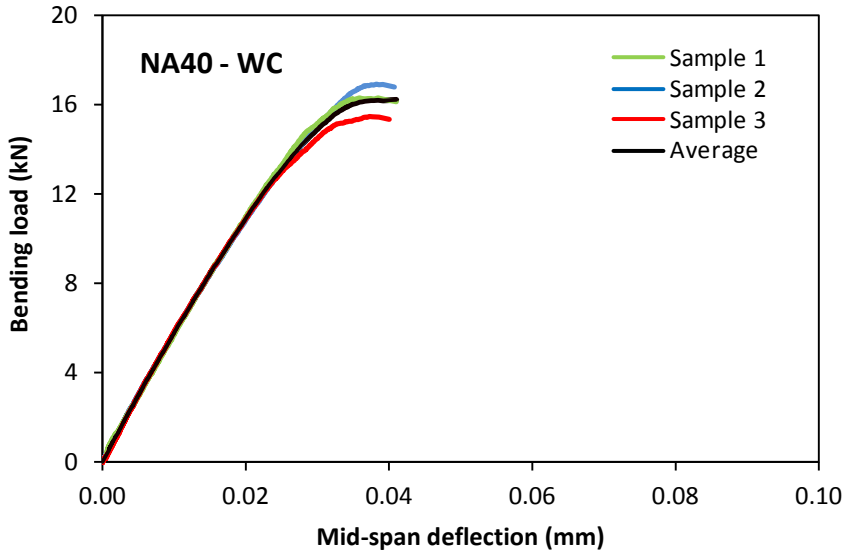

Figure G. 52 Load-deflection curve of water cured specimens (mix NA40).

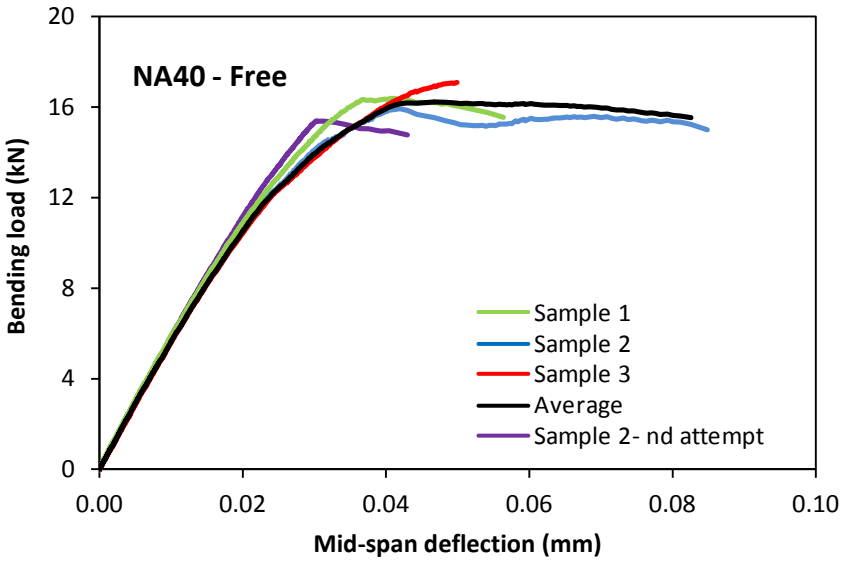

Figure G. 53 Load-deflection curve of free specimens (mix NA40).

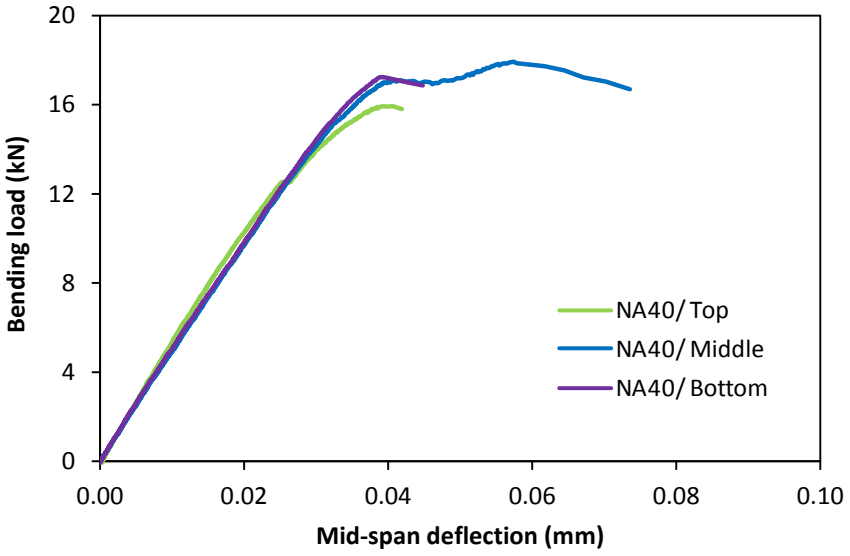

Figure G. 54 Load-deflection curve of restrained specimens (mix NA40).

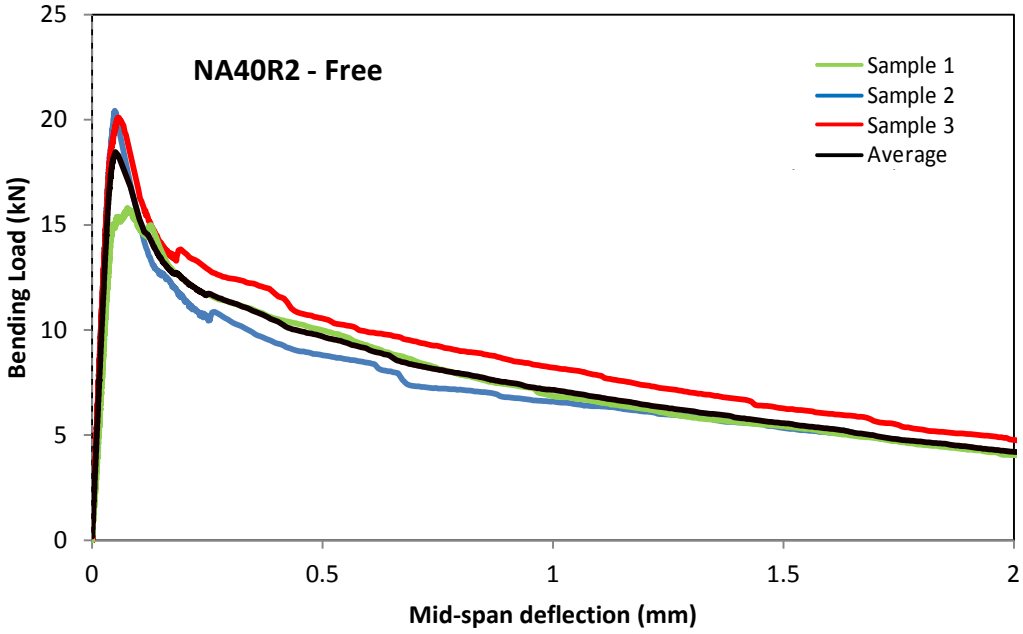

Figure G. 55 Load-deflection curve of free specimens (mix NA40R2).

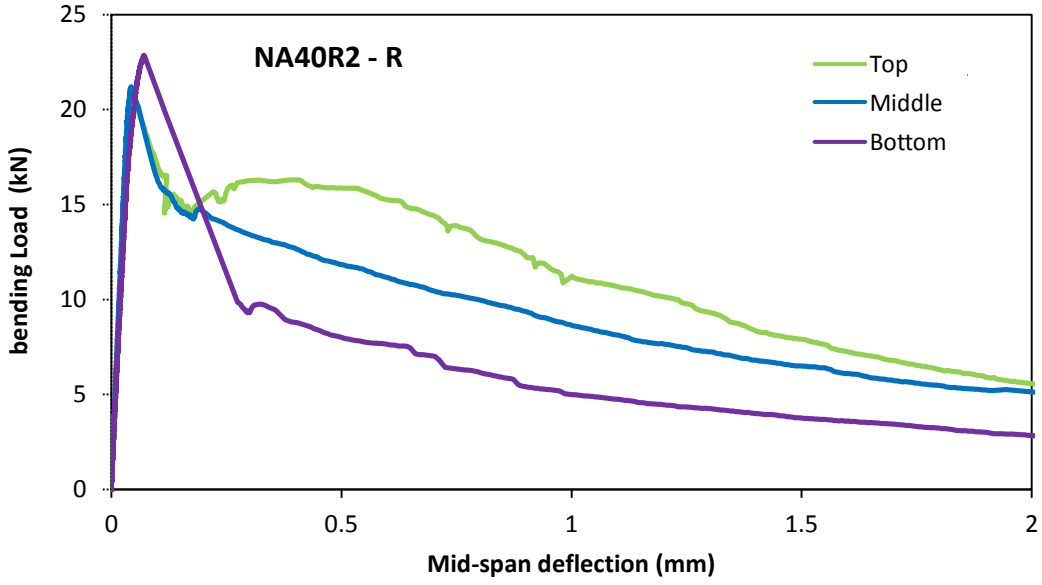

Figure G. 56 Load-deflection curve of restrained specimens (mix NA40R2).

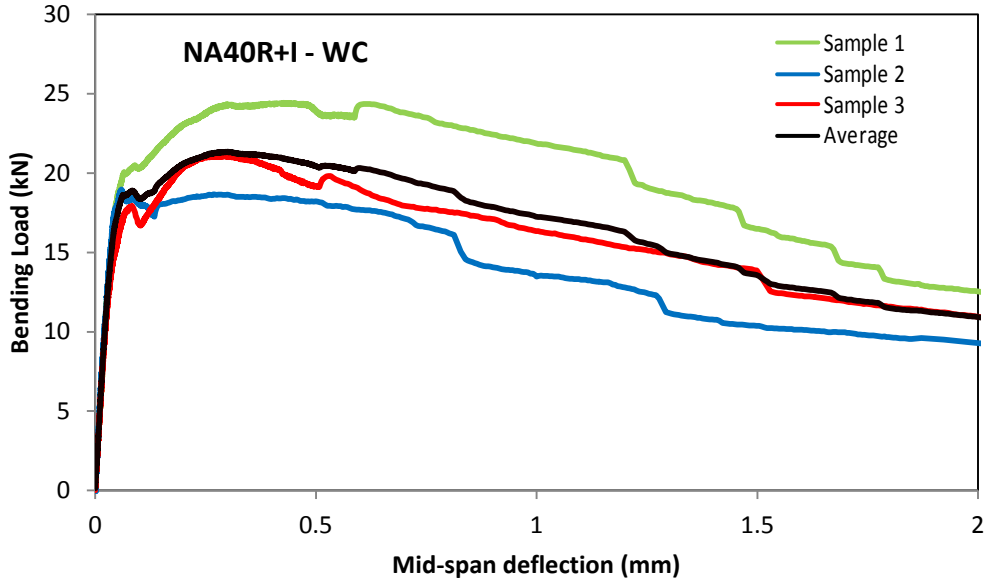

Figure G. 57 Load-deflection curve of water cured (mix NA40R+I).

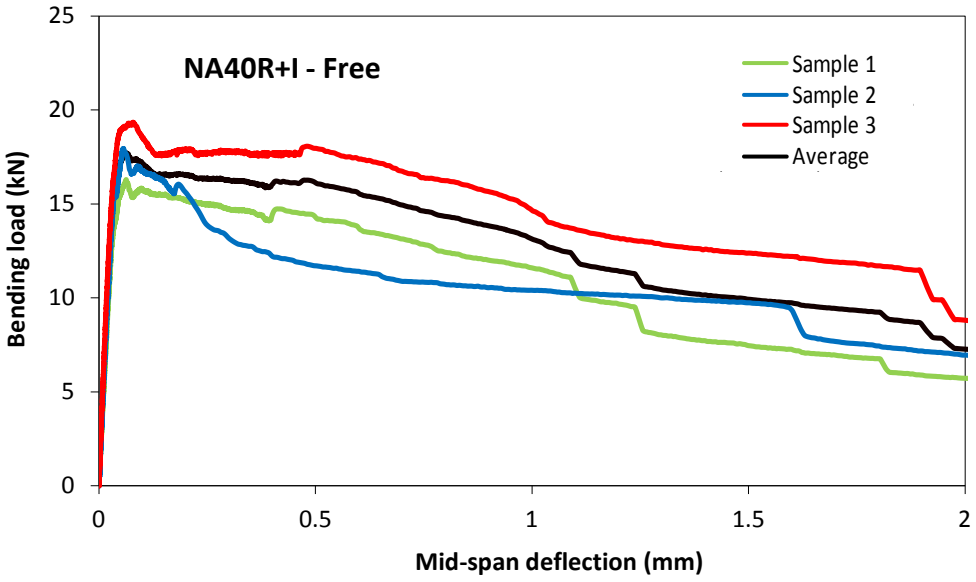

Figure G. 58 Load-deflection curve of free specimens (mix NA40R+I).

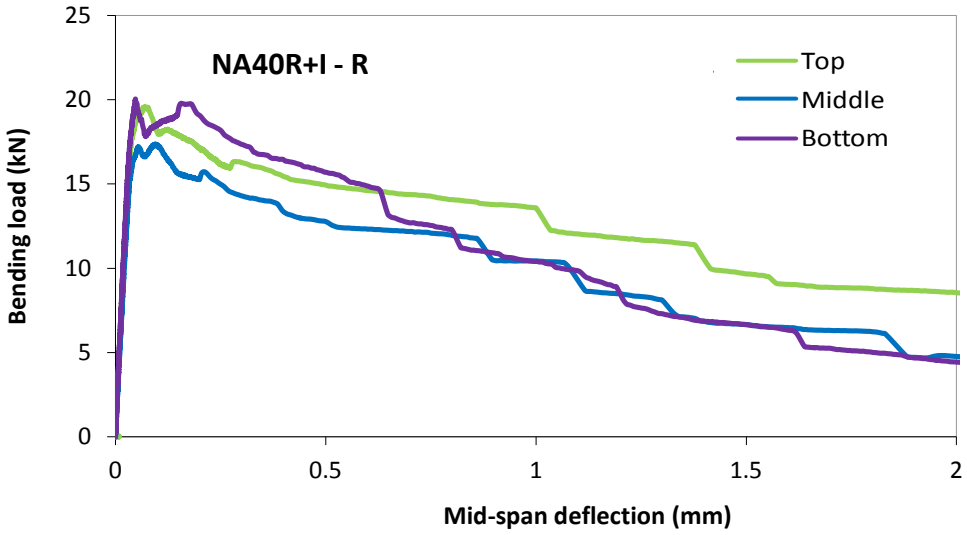

Figure G. 59 Load-deflection curve of restrained specimens (mix NA40R+I).

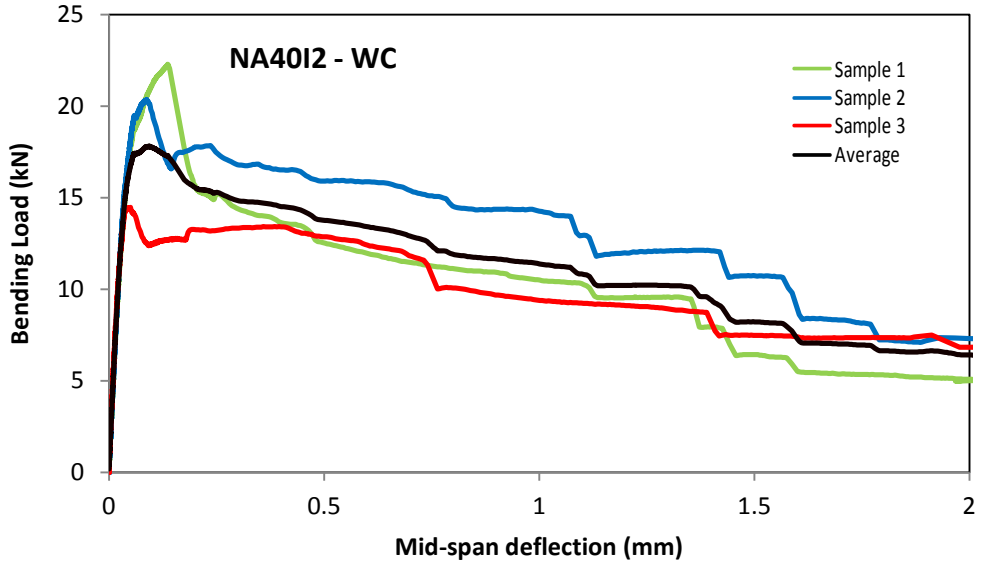

Figure G. 60 Load-deflection curve of water cured (mix NA40I2).

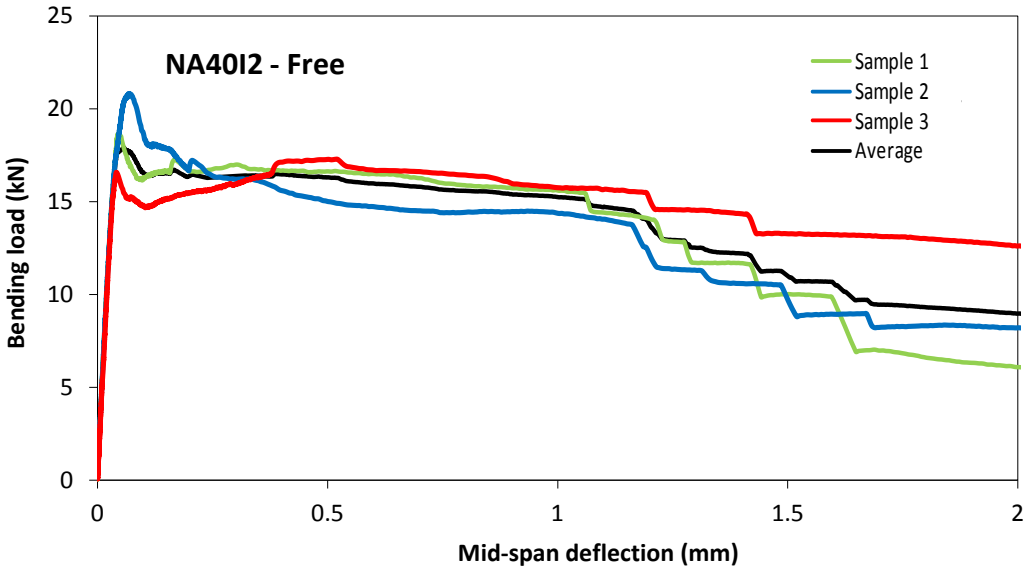

Figure G. 61 Load-deflection curve of free specimens (mix NA40I2).

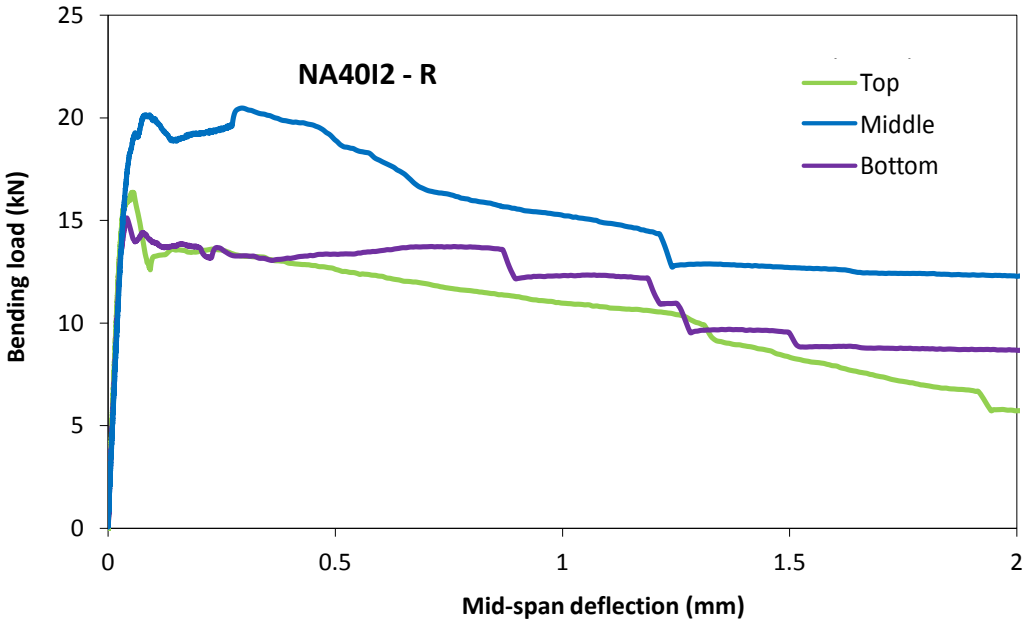

Figure G. 62 Load-deflection curve of restrained specimens (mix NA40I2).

G.5.2 Mixes with Recycled Aggregate

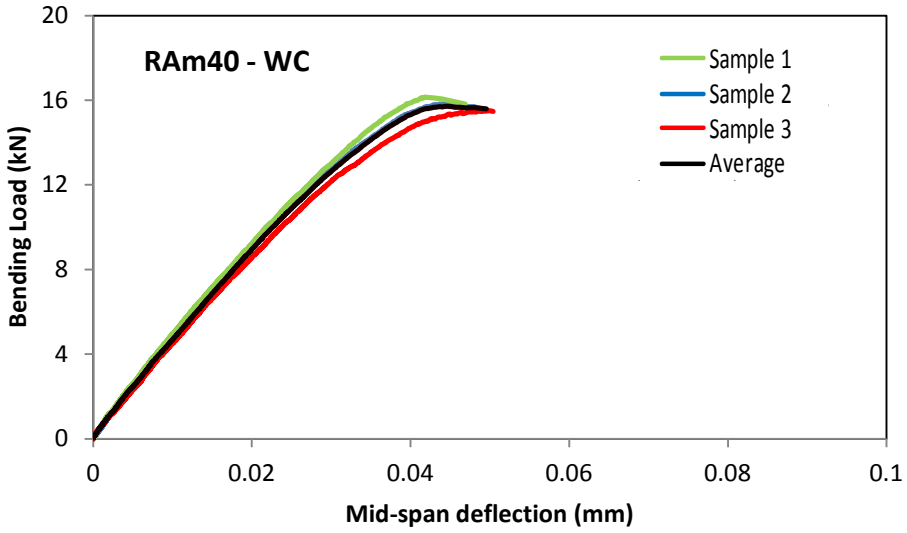

Figure G. 63 Load-deflection curve of water cured specimens (mix RAm40).

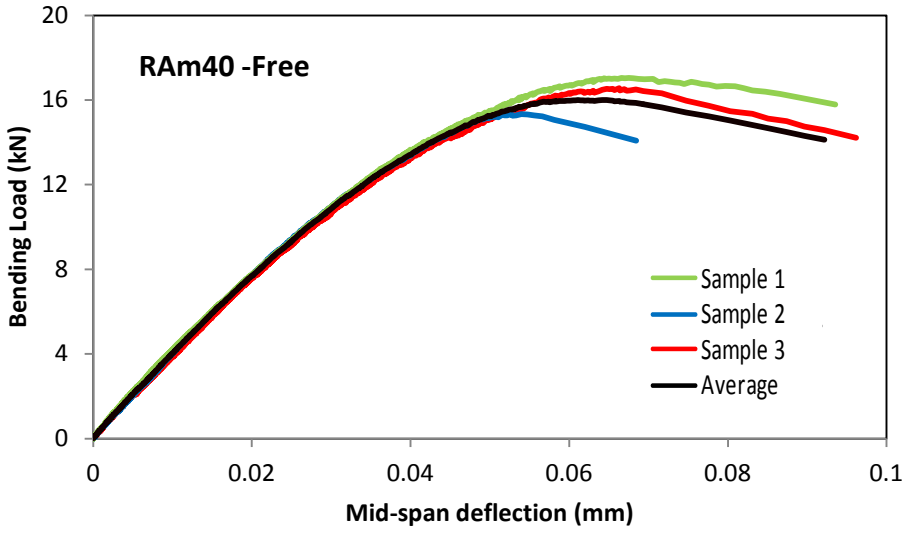

Figure G. 64 Load-deflection curve of free specimens (mix RAm40).

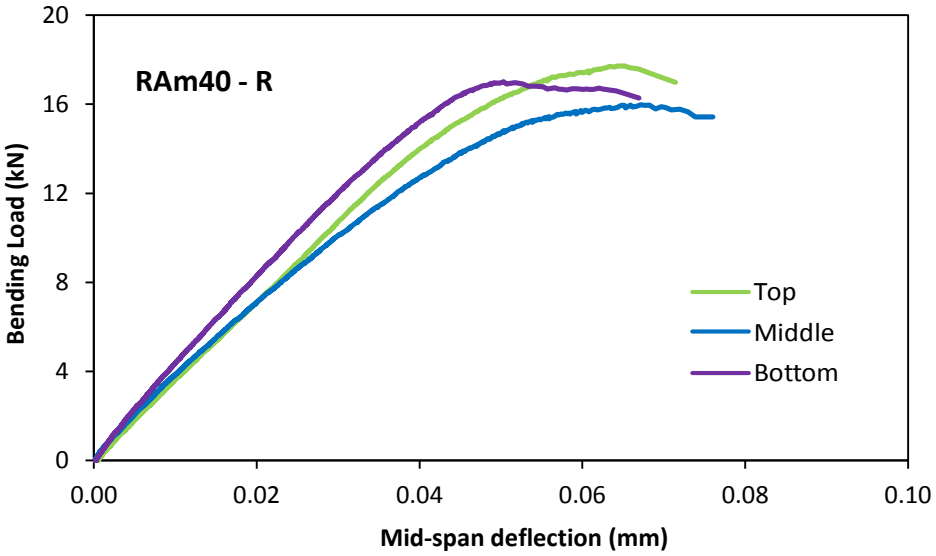

Figure G. 65 Load-deflection curve of restrained specimens (mix RAm40).

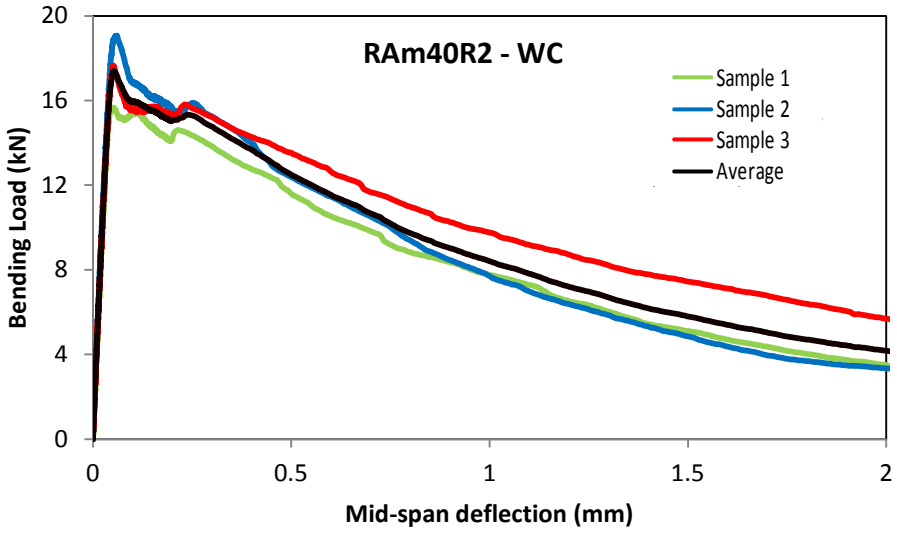

Figure G. 66 Load-deflection curve of water cured specimens (mix RAm40R2).

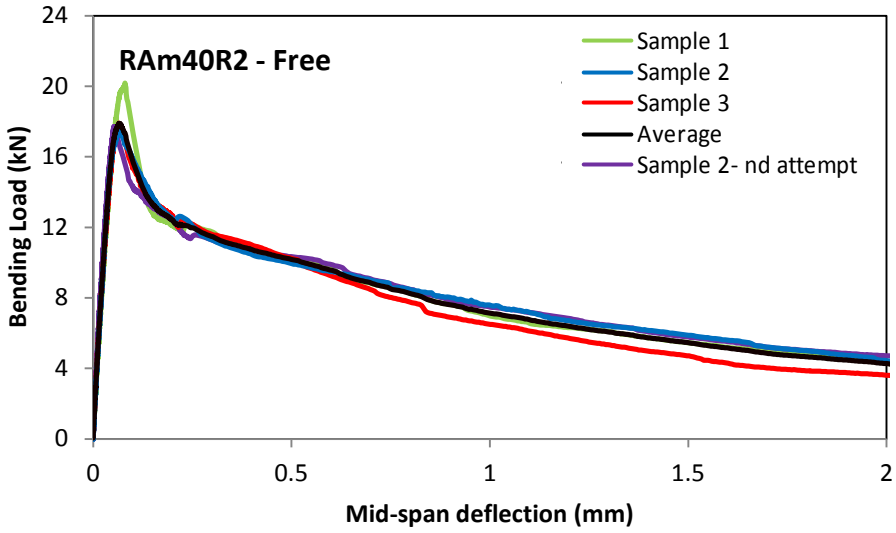

Figure G. 67 Load-deflection curve of free specimens (mix RAm40R2).

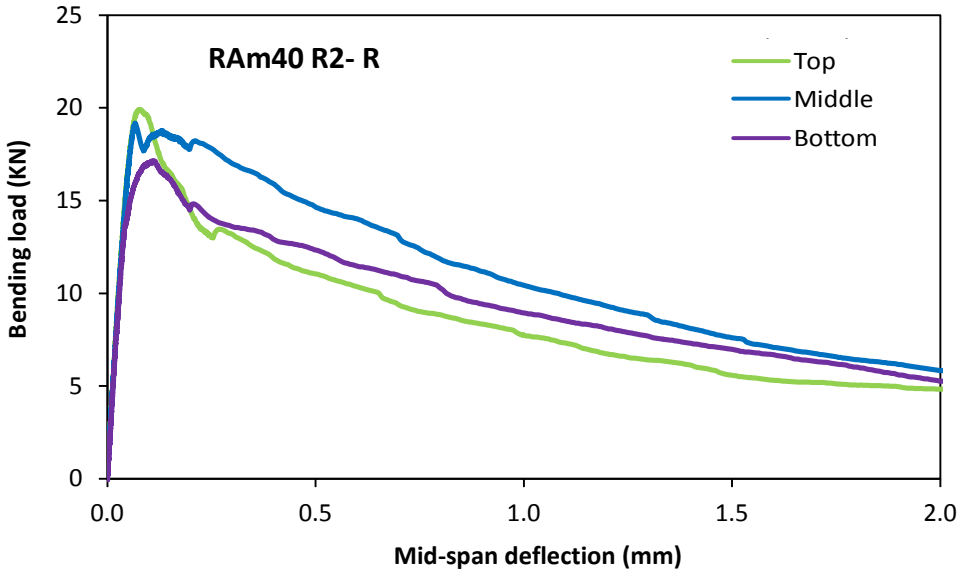

Figure G. 68 Load-deflection curve of restrained specimens (mix RAm40R2).

G.6 Flexural elastic modulus - bending load curves

G.6.1 Mixes with Natural Aggregate

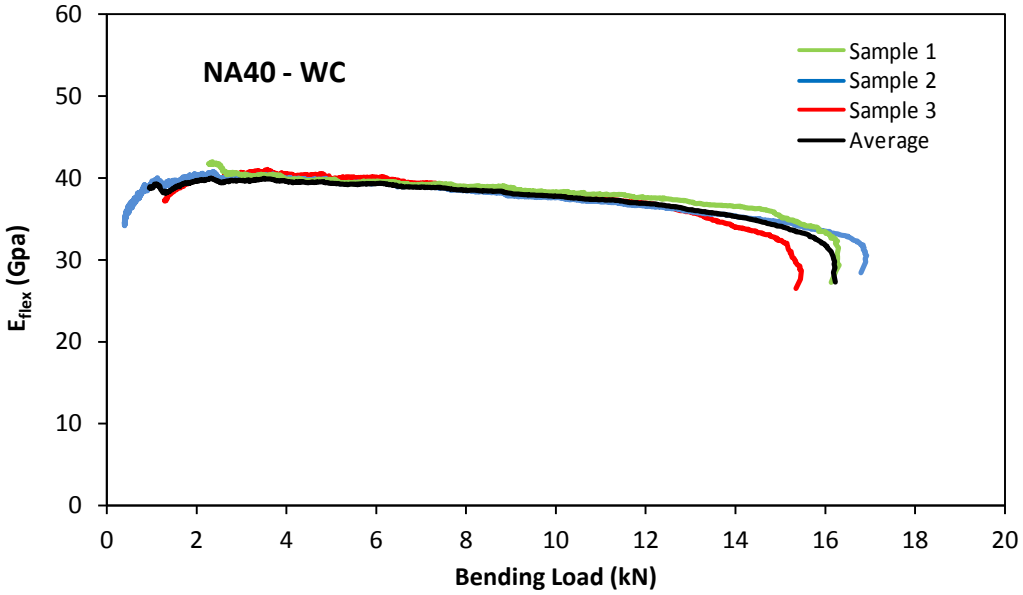

Figure G.69 Flexural elastic modulus - bending load curve of water cured specimens (mix NA40).

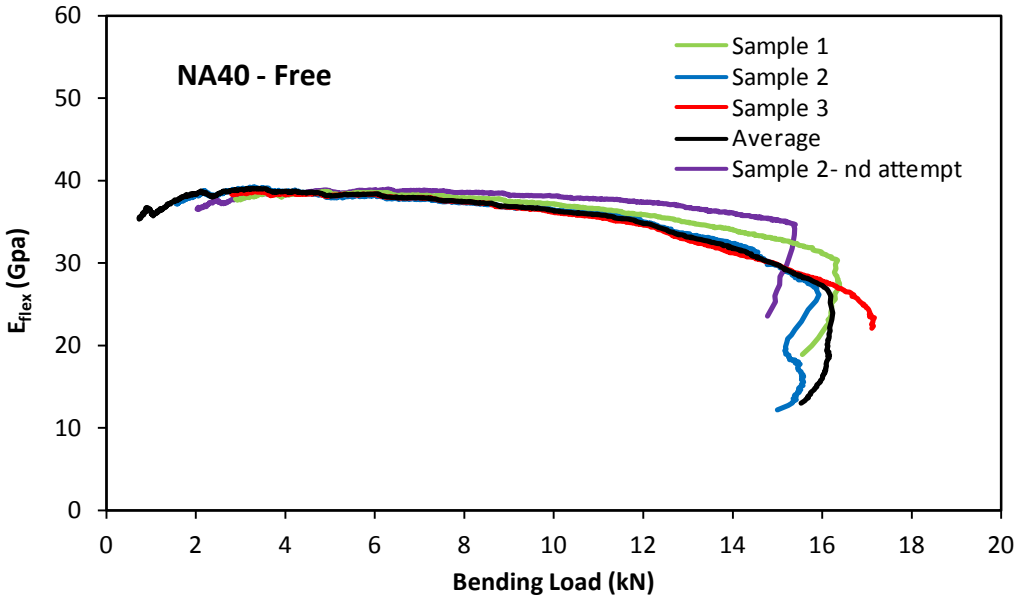

Figure G.70 Flexural elastic modulus - bending load curve of free specimens (mix NA40).

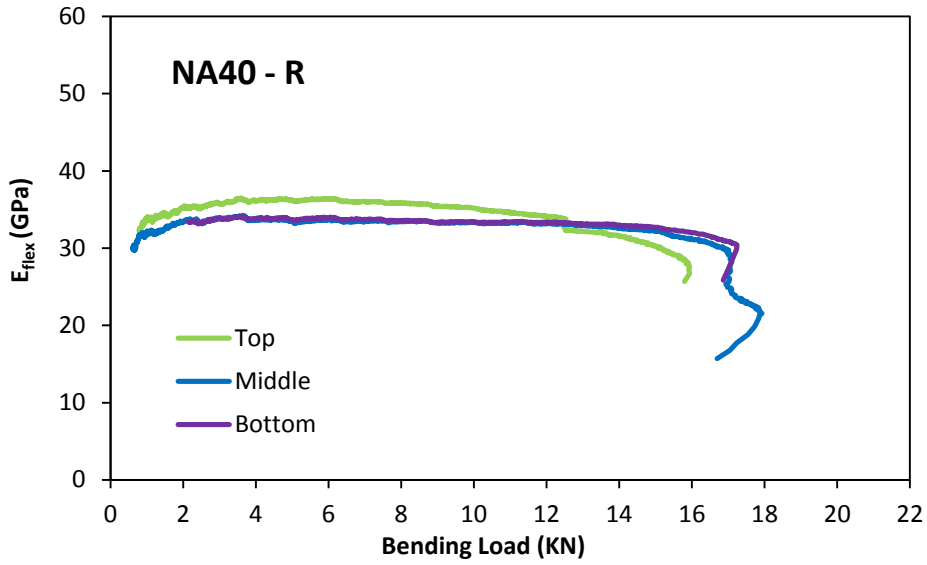

Figure G.71 Flexural elastic modulus - bending load curve of restrained specimens (mix NA40).

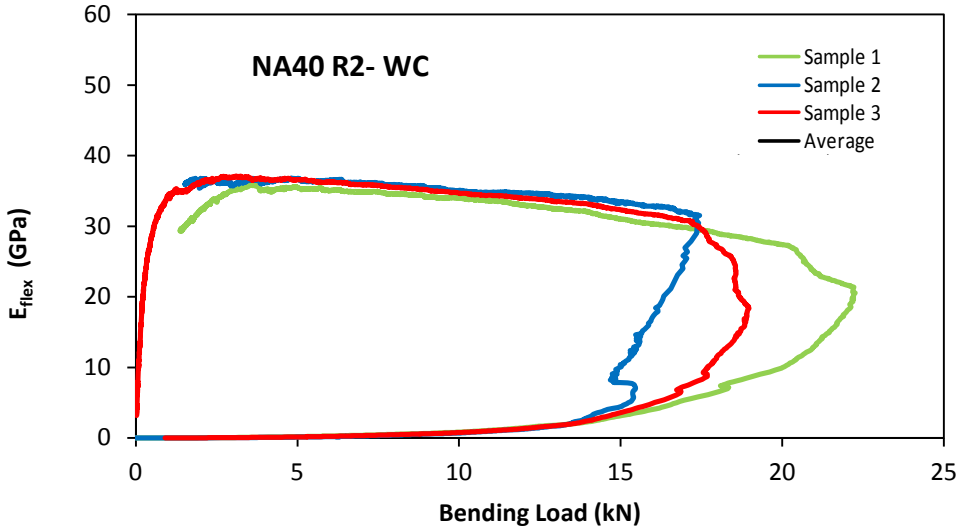

Figure G.72 Flexural elastic modulus - bending load curve of water cured specimens (mix NA40R2).

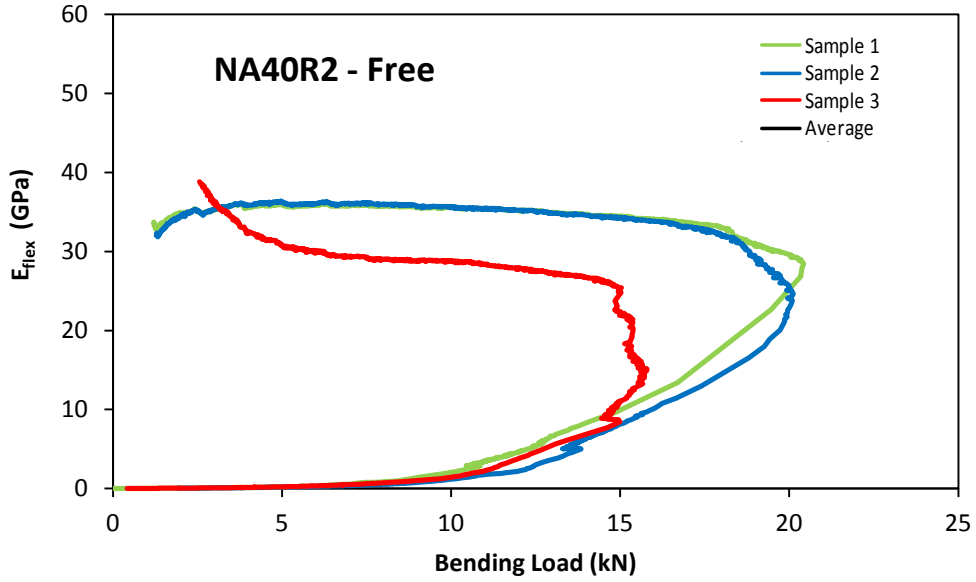

Figure G.73 Flexural elastic modulus - bending load curve of free specimens (mix NA40R2).

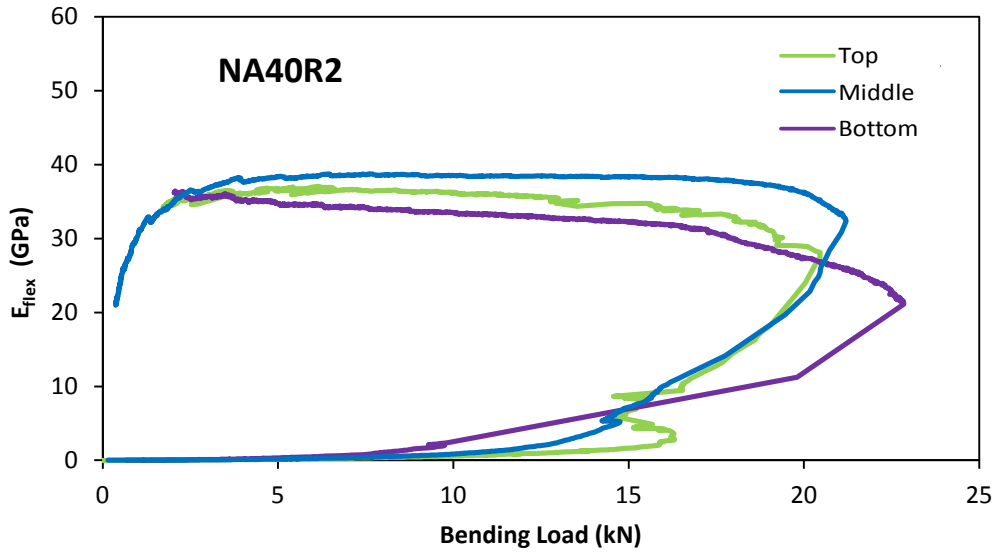

Figure G.74 Flexural elastic modulus - bending load curve of restrained specimens (mix NA40R2).

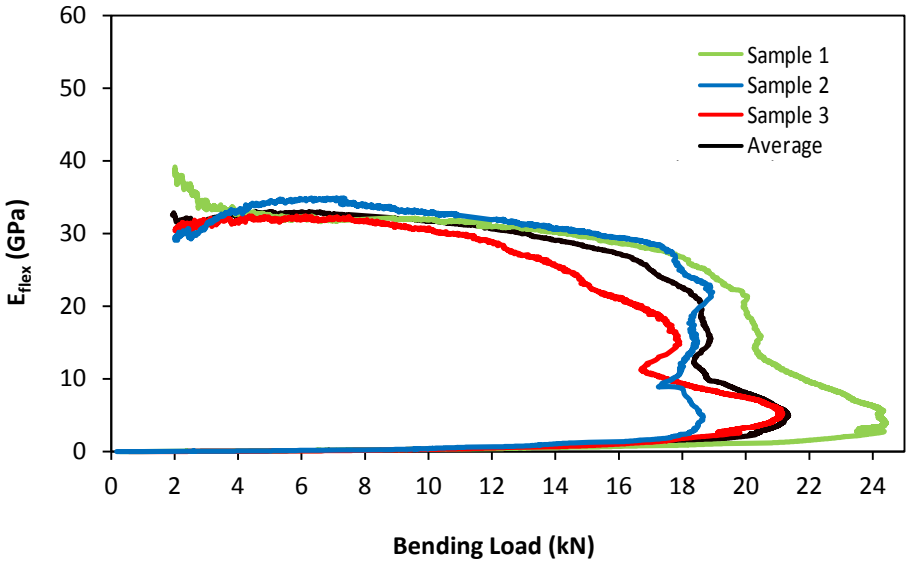

Figure G.75 Flexural elastic modulus - bending load curve of water cured specimens (mix NA40R+I).

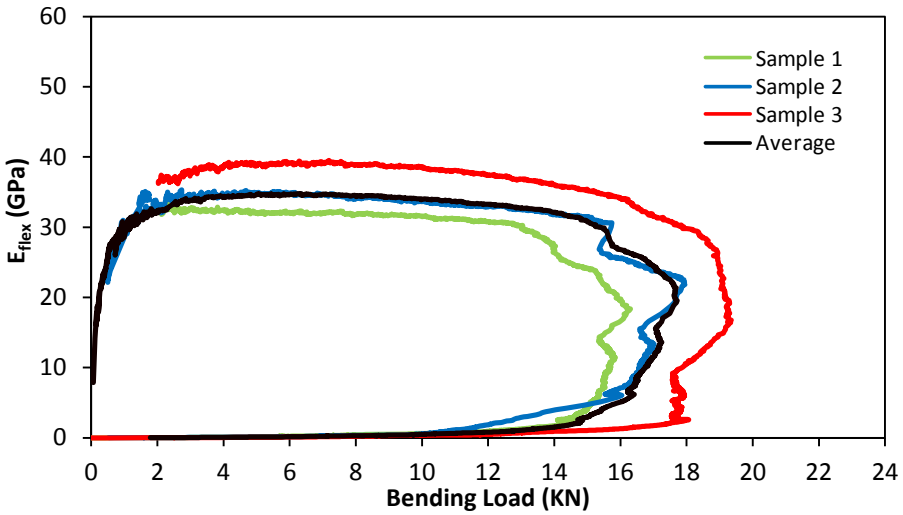

Figure G.76 Flexural elastic modulus - bending load curve of free specimens (mix NA40R+I).

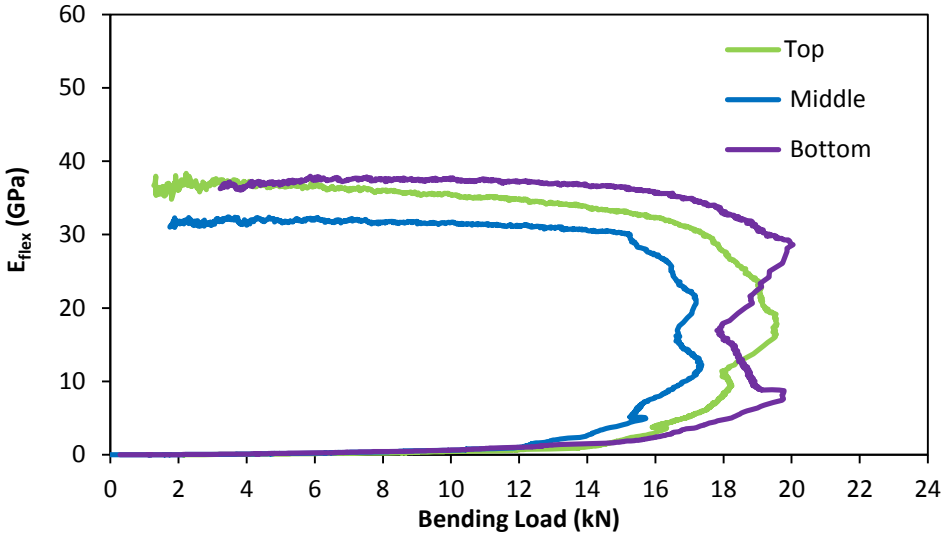

Figure G.77 Flexural elastic modulus - bending load curve of restrained specimens (mix NA40R+I).

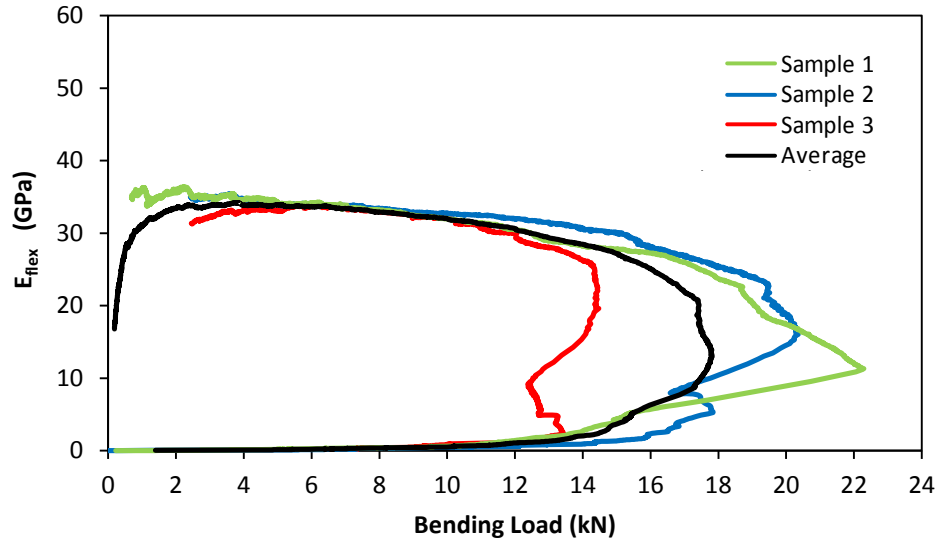

Figure G.78 Flexural elastic modulus - bending load curve of water cured specimens (mix NA40I2).

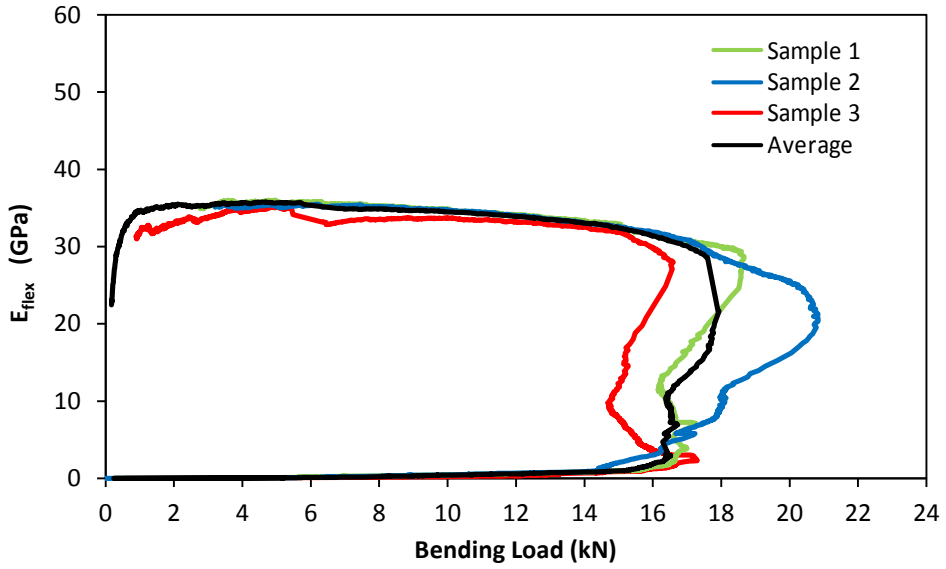

Figure G.79 Flexural elastic modulus - bending load curve of free specimens (mix NA40I2).

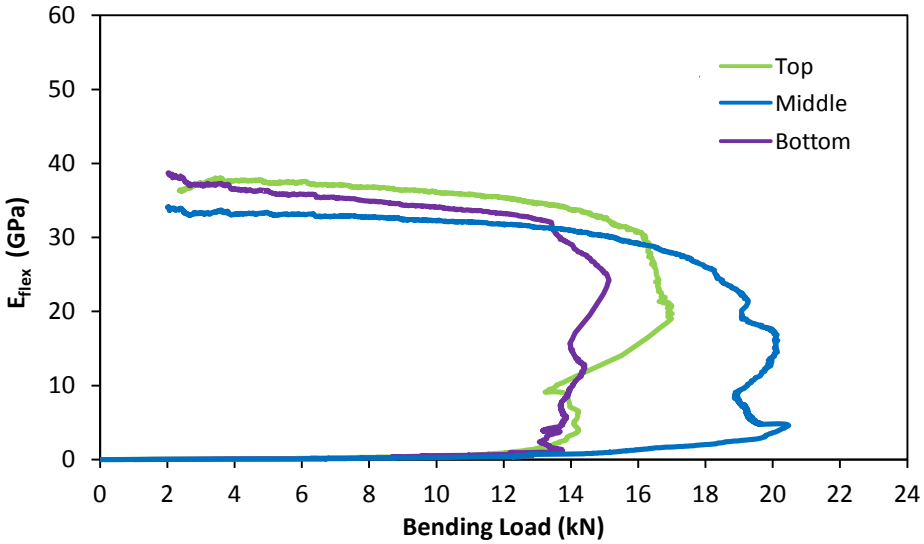

Figure G.80 Flexural elastic modulus - bending load curve of restrained specimens (mix NA40RI2).

G.6.2 Mixes with Recycled Aggregate

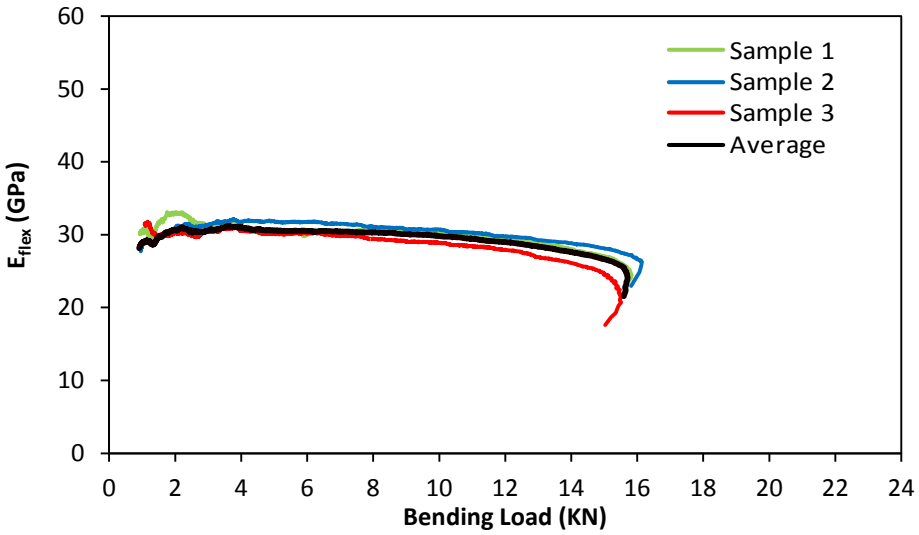

Figure G.81 Flexural elastic modulus - bending load curve of water cured specimens (mix RAm40).

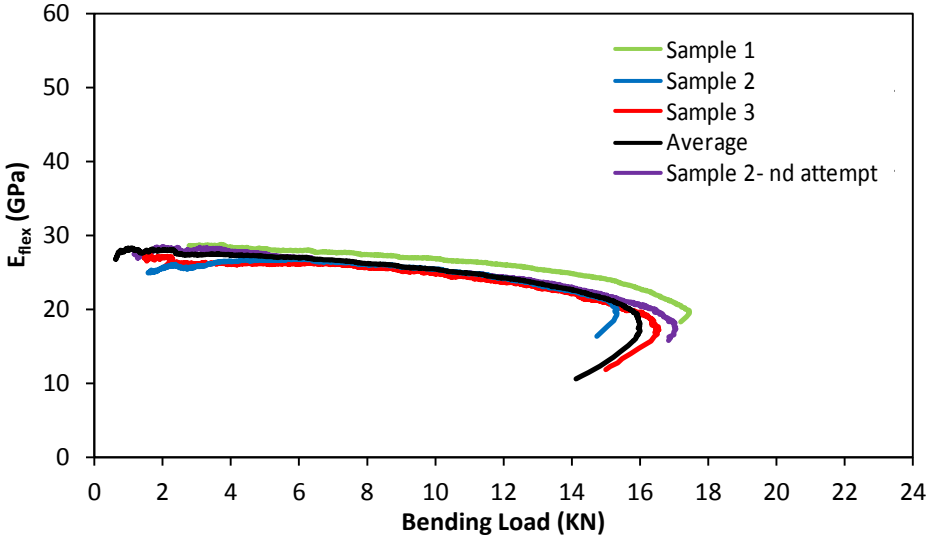

Figure G.82 Flexural elastic modulus - bending load curve of free specimens (mix RAm40).

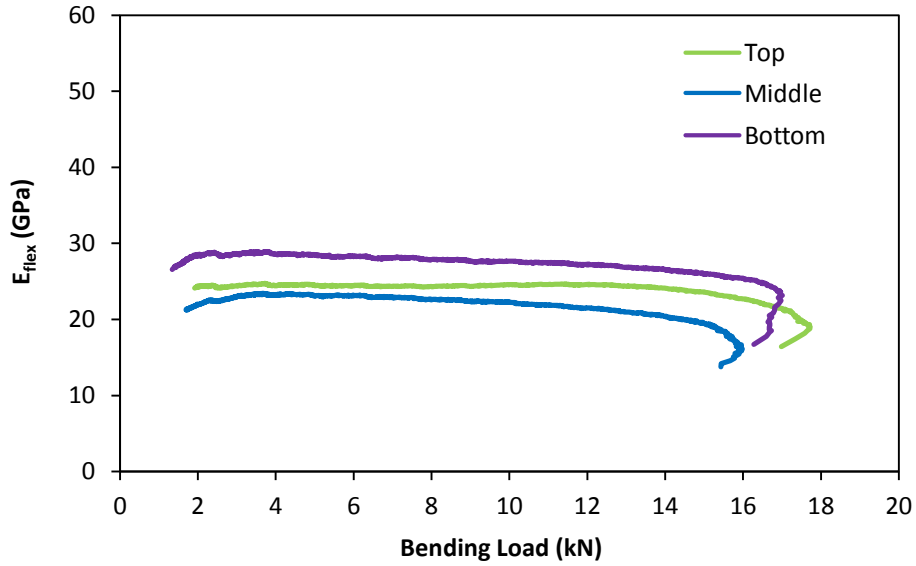

Figure G.83 Flexural elastic modulus - bending load curve of restrained specimens (mix RAm40).

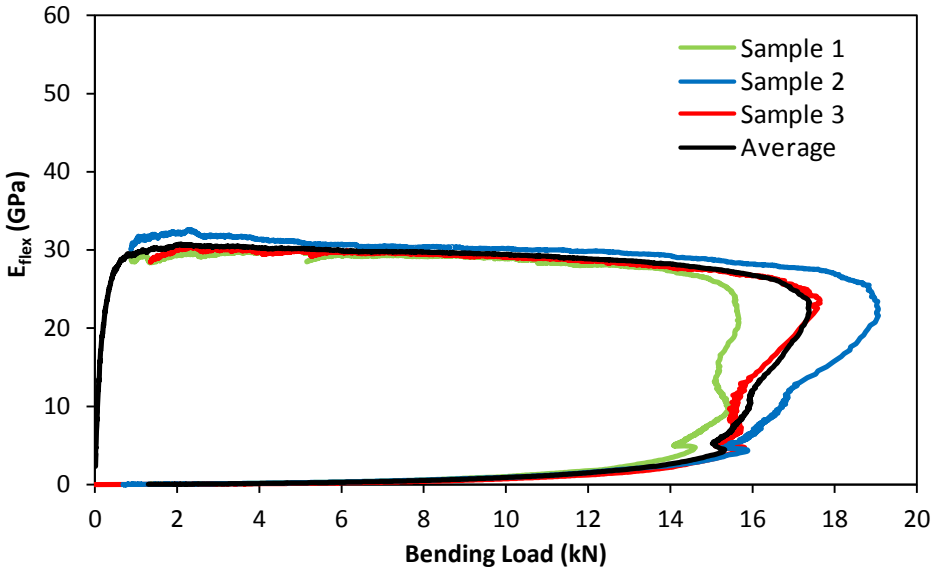

Figure G.84 Flexural elastic modulus - bending load curve of water cured specimens (mix RAm40R2).

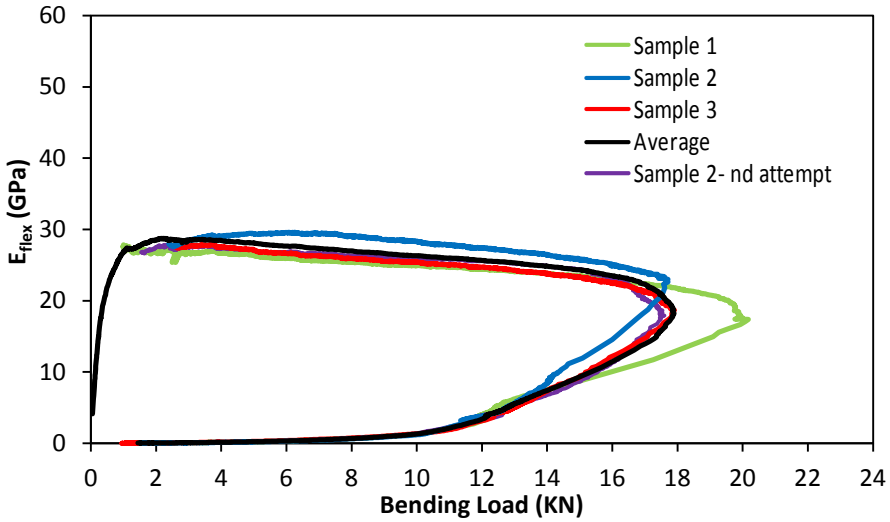

Figure G.85 Flexural elastic modulus - bending load curve of free specimens (mix RA40mR2).

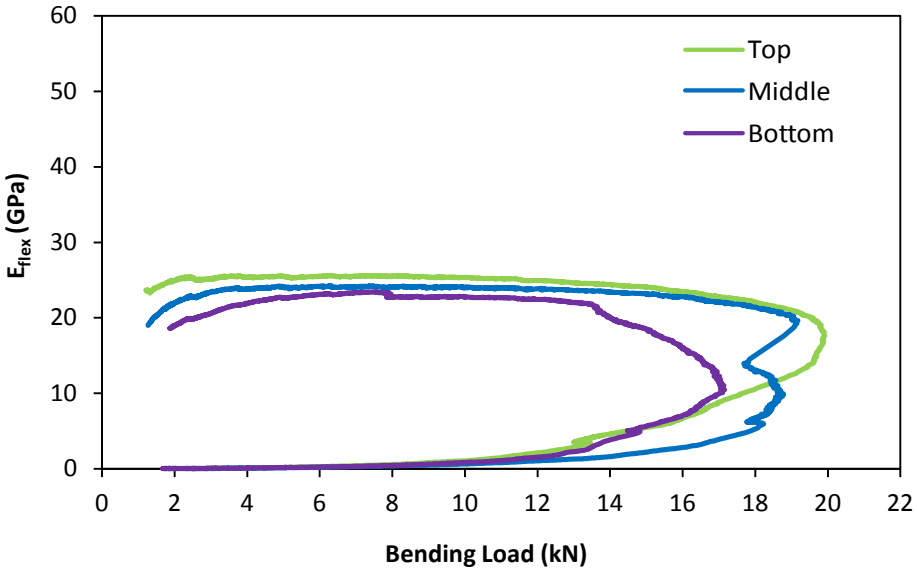

Figure G.86 Flexural elastic modulus - bending load curve of restrained specimens (mix RA40mR2).

G.7 Results of compressive strength

G.7.1 Mixes with Natural Aggregate

Table G.1 Compressive strength of cubes and portions of prisms under WC, F and R conditions- mix NA40.

Type and time	Compressive strength MPa	Average	Normalized strength	SD*
Cubes at 1 day	32.04	32.7	55	0.6
	32.98			
	33.09			
Cubes at 3 days	46.8	46.5	78	0.7
	45.65			
	46.99			
Cubes at 7 days	49.48	49.3	83	1.2
	50.38			
	48.01			
Cubes at 28days	59.43	59.4	100	0.3
	59.05			
	59.71			
Free at 28 days	50.42	51.5	87	1.0
	51.5			
	52.5			
Restrained	48.65	51.2	86	2.6
	51.1			
	53.76			
WC specimens	59.77	58.8	99	1.3
	57.4			
	59.31			

*Standard Deviation

Table G.2 Compressive strength of cubes and portions of prisms under WC, F and R conditions- mix NA40R2.

Type and time	Compressive strength Mpa	Average	Normalized strength	SD*
Cubes at 1 day	36.1	36.1	55	1.8
	37.9			
	34.3			
Cubes at 3 day	50.1	50.8	77	1.1
	52.1			
	50.3			
Cubes at 7 day	58.33	57.4	87	0.9
	57.51			
	56.44			
Cubes at 28day	65.6	66.0	100	1.7
	67.9			
	64.5			
Free at 28 days	64.2	61.9	94	2.1
	61.5			
	60.1			
Restrained	61.4	60.7	92	2.6
	57.8			
	62.9			
WC specimens	70.1	70.8	107	1.8
	49.04			
	51.73			

*Standard Deviation

Table G.3 Compressive strength of cubes and portions of prisms under WC, F and R conditions- mix NA40I2.

Type and time	Compressive strength MPa	Average	Normalized strength	SD*
Cubes at 1 day	34.31	33.8	56	0.6
	33.9			
	33.15			
Cubes at 3 day	45.76	45.3	75	1.7
	46.67			
	43.36			
Cubes at 7 day	50.38	51.3	85	1.8
	50.08			
	53.35			
Cubes at 28day	61.9	60.2	100	2.0
	60.64			
	58			
Free	60.5	57.8	96	3.0
	58.3			
	54.6			
Restrained	53.4	53.9	90	0.8
	54.8			
	53.5			
WC specimens	59.5	59.9	99	2.9
	62.9			
	57.2			

*Standard Deviation

Table G.4 Compressive strength of cubes and portions of prisms under WC, F and R conditions- mix NA40R+I.

Type and time	Compressive strength MPa	Average	Normalized strength	SD*
Cubes at 1 day	37.25	35.6	57	1.4
	34.88			
	34.69			
Cubes at 3 day	47.99	47.5	76	1.2
	46.08			
	48.34			
Cubes at 7 day	51.24	51.5	83	3.6
	48.03			
	55.22			
Cubes at 28day	64.42	62.2	100	1.9
	61.52			
	60.77			
Free	54.84	56.7	91	1.6
	57.8			
	57.55			
Restrained	49.97	53.9	87	3.6
	56.89			
	54.81			
WC specimens	60.55	61.2	98	0.6
	61.2			
	61.73			

*Standard Deviation

G.7.2 Mixes with Recycled Aggregate

Table G.5 Compressive strength of cubes and portions of prisms under WC, F and R conditions- mix RAm40.

Type and time	Compressive strength MPa	Average	Normalized strength	SD*
Cubes at 1 day	26.65	27.6	63	1.0
	28.55			
	27.57			
Cubes at 3 day	34.72	34.4	79	0.3
	34.32			
	34.25			
Cubes at 7 day	40.15	39.3	90	0.7
	39.02			
	38.81			
Cubes at 28day	43.82	43.5	100	1.4
	42.02			
	44.72			
Free	39.75	40.1	92	0.4
	40.52			
	39.89			
Restrained	39.91	39.8	91	0.6
	39.11			
	40.36			
WC specimens	46.58	45.2	104	1.3
	45.07			
	43.95			

*Standard Deviation

Table G.6 Compressive strength of cubes and portions of prisms under WC, F and R conditions- mix RAm40.

Type and time	Compressive strength MPa	Average	Normalized strength	SD*
Cubes at 1 day	27.71	28.1	52	1.1
	27.32			
	29.35			
Cubes at 3 day	36.25	36.5	67	0.7
	35.92			
	37.21			
Cubes at 7 day	42.15	43.1	79	0.9
	43.63			
	43.65			
Cubes at 28day	56.65	54.4	100	2.0
	53.82			
	52.74			
Free	49.01	49.7	91	0.6
	49.89			
	50.17			
Restrained	48.96	49.0	90	0.7
	48.29			
	49.63			
WC specimens	53.83	55.0	101	1.2
	56.18			
	55.05			

*Standard Deviation